UNIVERSITY OF SOUTHAMPTON

The Electro-Optic Properties of Liquid Crystalline Materials for Optical Device Applications

CHRISTOPHER DAVID JOHN NOOT

A thesis submitted for the degree of Doctor of Philosophy
Department of Physics and Astronomy

Faculty of Science
April 2003

UNIVERSITY OF SOUTHAMPTON

ABSTRACT

FACULTY OF SCIENCE
DEPARTMENT OF PHYSICS AND ASTRONOMY

Doctor of Philosophy

THE ELECTRO-OPTIC PROPERTIES OF LIQUID CRYSTALLINE MATERIALS FOR OPTICAL DEVICE APPLICATIONS

Christopher David John Noot

A detailed study has been made of the electro-optic properties of a number of liquid crystalline materials. The nematic, chiral nematic and ferro- and anti-ferroelectric compounds studied exhibit fast electro-optic response times and high optical tilt angles making them particularly useful for display and optical communication devices. A range of techniques were employed to fully characterise both the phase behaviour and the electro-optic properties of the materials. The design and operation of new apparatus to facilitate high resolution, fast and continuous optical tilt angle measurements is discussed.

In the present work two series of low molar mass organosiloxane liquid crystals, which combine the high tilt and wide phase range properties of laterally substituted biphenyl benzoate mesogens with the polymer ruggedness of siloxane head groups, were investigated. The mono-mesogens exhibit a 50°C wide ferroelectric SmC* phase and a P_s of ~100nC/cm^2. Temperature independent, near 45° or 45° tilt angles were measured for all three compounds. Response time measurements revealed that switching as fast as 30μs was achievable. It was found that the phase behaviour of the bi-mesogenic compounds was strongly influenced by the length of the siloxane group. The tri-siloxane and penta-siloxane bi-mesogenic compounds were antiferroelectric over 70°C wide ranges, whilst Cl11-4-11Cl displayed ferroelectric behaviour. The spontaneous polarisation was enhanced to 100-140 nCcm^{-2} whilst the other electro-optic properties had similar magnitudes and broadly followed similar trends to the mono-siloxane compounds.

A series of mixtures, of achiral nematic bimesogens and small concentrations of chiral dopants, designed to exhibit enhanced flexoelectric switching were studied. All the mixtures exhibited a single chiral nematic phase on cooling from the isotropic phase. The uniformly lying helix texture, necessary to observe flexoelectric switching was achieved through a combination of turbulent flow induced by an applied electric field and suitably treated surfaces. Exceptional room temperature tilt angles of 45° and switching times of the order of 500μs were measured.

A series of mixtures, of a proprietary dual frequency nematic compound and a low viscosity host were characterised. The temperature dependent behaviour of the crossover frequency was characterised, along with the frequency dependence of $\Delta\varepsilon$ and V_{TH}. Response times of ~5ms were achieved for an applied field of ±2V/μm. Dual frequency addressing was shown to be advantageous at temperatures far below T_{NI}, with response times decreasing by a factor of two.

DECLARATION

This thesis is the result of work done by the author whilst in registered postgraduate candidature at the University of Southampton. The work is entirely original except where due reference is made and no portion of the work referred to in this thesis has been submitted in support of an application for another degree or qualification at this or any other university or institute of learning. Results obtained in collaboration with others are clearly indicated and may be submitted by them for another degree.

Acknowledgements

There are many people without whom this thesis would not have been possible. Particular thanks to:

Harry for creating a great group, a fantastic lab and for providing me with the opportunity to write this thesis.

Dr. Graham Street of Surgical Vision Limited for the financial support and illuminating discussions on novel uses of liquid crystal devices.

Professors Luckhurst and Raynes for the 'enjoyable' the viva. Particular thanks must go to Professor Geoffrey Luckhurst for the time spent in finalising the corrections to this thesis.

Steve, Petra and Doina for providing the materials on which the work in this thesis is based.

Wendy & Carlo for the early days when everything was new and questions needed to be answered. Marcus & Seb for continuing that tradition and keeping things on track.

Bronje for leading the way with the flexoelectric materials and her support and time when proof reading.

Dean for providing the opportunity to keep fit on the squash court and the odd drink in the pub. For being a great friend and keeping in touch.

All the other members of the group for making the lab an enjoyable place to be, and especially Cecille for providing the dielectric measurements.

Special thanks must go to:
All my friends and family for their encouragement and support over the years.

Hiranthi, Gamini, Sujatha and Gehan for all their love and support.

Rhian for never asking if the thesis was finished, and finally Mum and Dad for their love and patience.

Publications & Conference Presentations

Poster P-36 & Proceedings of 14th British Liquid Crystal Society Conference, Durham (1999)
Tilt Angle and Optical Anisotropy Measurements of Organosiloxane Liquid Crystals
C.Noot, S.P.Perkins, P.Lehman and H.J.Coles

Tech. Digest 7th International Conference on Ferroelectric Liquid Crystals, Darmstadt University of Technology, Germany (29August – 3 Sept 1999)
Tilt Angle and Optical Anisotropy Measurements of Organosiloxane Liquid Crystals
C.Noot, W.K.Robinson, S.P.Perkins and H.J.Coles

Poster P-30 & Proceedings of 15th British Liquid Crystal Society Conference, Strathclyde (April 17-19 2000)
A Study of the flexoelectric switching behaviour of a hypertwisted chiral nematic liquid crystal produced using a time resolved Raman microspectrometer and the rotating analyser technique
M.J.Clarke, C.Noot, S.C.Meyer and H.J.Coles

Proceedings of 18th International Liquid Crystal Conference, Sendai, Japan (2000)
Flexoelectric Switching Angle and Optical Anisotropy Measurement of Novel Chiral Nematic Liquid Crystals
C.Noot, B.Musgrave, M.J.Coles and H.J.Coles

Tilt Angle Measurement of Low Molar Mass Organosiloxane Liquid Crystals
C.Noot, S.P.Perkins, and H.J.Coles
Ferroelectrics **244**, 331 (2000)

CONTENTS

Chapter One

INTRODUCTION

1.1 INTRODUCTION

This chapter provides the reader with a general introduction to the work presented in this thesis and introduces the notion of the liquid crystal phase. The chapter begins with a discussion of how we distinguish the liquid crystalline phases (or mesophases) from other states of matter, namely the partial degree of molecular order. This is followed by a brief description of the two basic liquid crystalline groups, thermotropes and lyotropes. The work presented in this thesis concentrates on thermotropic liquid crystals and an overview of the structures formed by these mesomorphic molecules is presented in §1.3 and §1.4.

1.2 OVERVIEW

Display systems have been at the forefront of thermotropic liquid crystal technology for almost 30 years and are understandably one of the most important liquid crystal applications at the present time. However, there is great potential and opportunity for the use of liquid crystalline materials in other optical components such as modulators and wave plates or guides. With this work we are interested in utilising both the physical and optical properties of numerous liquid crystal (i.e. nematic, ferroelectric and polymer) materials in order to develop and produce specific devices that can then be incorporated into various optical systems. The response of some liquid crystalline materials to an electric field is also of interest for developing switchable devices.

This thesis presents the results of the experimental analysis of a number of fast response, and high optical tilt angle, liquid crystalline materials for use in optical devices and displays. This chapter provides a general introduction to the subject matter of this thesis, namely liquid crystalline materials. The topic of liquid crystals is a vast area of research and study, and as such, only the aspects of liquid crystal science that are relevant to this work are discussed.

Chapter 2 builds on the brief introduction given in Chapter 1 and provides the reader with a detailed discussion of the theoretical aspects of the liquid crystalline properties discussed

in later chapters. Their bulk optical, electrical or magnetic properties may be rapidly altered by the application of moderate external fields – allowing them to be utilised in display devices. The electro-optic switching properties of a liquid crystal are the key to its use in display devices.

Before the materials can be used in such applications a number of studies need to be carried out to assess their suitability. Chapter 3 introduces the experimental techniques required to characterise the materials. Many liquid crystals possess a number of these mesophases and various complimentary procedures are employed, for example differential scanning calorimetry and optical microscopy, in order to identify and categorise the mesophases and phase transitions. Electro-optic studies concentrate on the switching properties which are key to the use of liquid crystal materials in display devices. Typical parameters such as V_{th}, the threshold field required for switching, and response times are measured as a function of applied voltage, frequency, waveform and temperature.

Chapter 4 introduces ferroelectric and antiferroelectric low molar mass organosiloxane compounds. These compounds combine a fast response time and high tilt angle with the ruggedness associated with polymers. The materials exhibit ferreoelectric and antiferroelectric mesophases, the spontaneous polarisation, tilt angle and response times of which are characterised.

Chapter 5 focuses on flexoelectric systems. The flexoelectro-optic effect is an electro-optic response two orders of magnitude faster than conventional twisted nematic systems but, until recently, applications have been limited by the lack of contrast between the switched states as a result of the low tilt angles observed. It is shown that the asymmetric chiral nematic bimesogens studied in this chapter possess the highest tilt angles seen in any flexoelectric system to date. These materials also have room temperature nematic phases, allowing the flexoelectro-optic effect to be observed at room temperature, with response times of the order of a 100μs.

Chapter 6 presents a new nematic material for use in dual frequency addressed applications. Sign inversion of the dielectric anisotropy allows the liquid crystal director to be driven between the planar and homeotropic alignments by changing the frequency of the applied field, thus producing a faster response time than conventional operation, where surface forces are utilised to return the director back to the planar configuration. A proprietary material, synthesised in house, is characterised with a view to utilising the improved response times obtained by the dual frequency addressing scheme.

Finally, Chapter 7 concludes this thesis with a summary of the main observations and discoveries made during the course of these studies and provides some avenues and suggestions for future work.

1.3 THE LIQUID CRYSTALLINE PHASE

Normally, matter is considered to exist in three well-defined states; solid, liquid and gas, each being characterised by a certain degree of atomic or molecular order. The molecules in crystalline solids exhibit both positional and orientational order (i.e. the molecules are constrained to only be in certain positions with respect to each other and to only align in fixed directions), whilst the molecules in liquids do not have any positional or orientational order. The liquid crystal phase exists between the solid and the liquid states (i.e. liquid crystals have structures or phases intermediate to conventional solids or liquids).

The first intermediate state was discovered in 1888 by the Austrian botanist Friederich Reinitzer[1]. Reinitzer noticed that cholesteryl benzoate melted at 145.5°C into a cloudy brown fluid and then became clear at 178.5°C. When the brown liquid was studied under a polarising microscope it was found to possess some distinguishable crystalline structure and anisotropic optical properties. Since optical anisotropy was undiscovered in liquids but had been detected in certain crystals the term *'liquid crystals'* was coined by Otto Lehmann[2] in 1889. In 1922, Friedel[3] referred to it as a *mesomorphic state of matter* (or

[1] F.Reinitzer, *Monatsh.Chem*, **9**, 421 (1888)
[2] O.Lehmann, *Z.Phys.Chem IV*, **4**, 462 (1889)
[3] M.G.Friedel, *Ann.Phys.*, **18**, 273 (1922)

mesophase) reflecting the intermediate nature of the phases between the crystalline solid and isotropic liquid states. From this designation the term mesogen has been derived to describe a material that is able to form mesophases. Friedel also classified the different mesophases into broad groups, nematic, cholesteric and smectic, according to the inherent molecular ordering. Today, the cholesteric mesophase is referred to as being chiral nematic, since compounds with this ordering do not need to be derived solely from cholesterol.

The preferred orientational alignment combined with the anisotropy of the individual molecules results in the macroscopic observation of anisotropy of the mesophase. This macroscopic anisotropy is most commonly observed in the physical characteristics such as refractive indicies, dielectric permittivity and the mechanical properties. The degree of anisotropy observed in these properties is governed by the anisotropy of the individual molecules and the order parameter. It is the macroscopic anisotropy combined with the fact that the director orientation can be constrained by physical boundaries and reoriented by applying electric or magnetic fields that gives the mesophases a wide variety of applications.

1.4 CLASSIFICATION OF LIQUID CRYSTALLINE PHASES

1.4.1 Introduction

The liquid crystalline state, or *mesophase*, is an intermediate state of matter that exists between the crystalline solid and the isotropic liquid phases. Consequently, the physical structure of this state is intermediate between the three-dimensional long range molecular ordering of a solid and the complete randomness of an isotropic liquid. A mesophase is a fluid state characterised by a unique combination of degrees of translational and orientational order.

Liquid crystal materials can be split into two fundamental categories. *Thermotropic* liquid crystals have properties that are dependant on temperature whilst *lyotropic* liquid crystals

are formed as a function of concentration[4]. Lyotropics are important for their use in soaps and surfactants as well as for their biological significance. It is thermotropic liquid crystals that are of primary interest and relevance to this work.

1.4.2 Thermotropic Liquid Crystals and the Order Parameter

Thermotropic liquid crystal molecules are geometrically anisotropic, they can be disk shaped (forming *discotic* mesophases) but generally tend to be rod shaped (forming *calamitic* mesophases), as shown in Figure 1.1, possessing a high length to breadth ratio with a rigid central core and flexible ends. It is the ordering of these constituent molecules within the mesophase that results in the anisotropy of the physical characteristics of the material. All the thermotropic materials discussed in this work are calamitic.

These mesophase-forming units can be incorporated into larger molecular systems without the loss of liquid crystalline behaviour. Examples include main chain and side chain liquid crystal polymers[5] (mesogens included within the polymer backbone or pendantly substituted via a linkage group respectively).

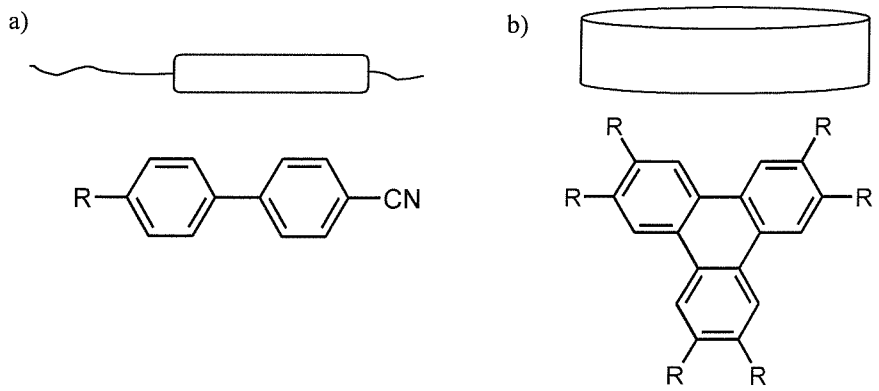

Figure 1.1 Schematic representation and typical molecular structures of liquid crystalline materials: a) calamitic mesogen, b) discotic mesogen. The substituents, R, are typically alkyl chains.

[4] I.C.Khoo and F.Simoni eds., 'Physics of Liquid Crystalline Materials', Gordon & Breach (1991)
[5] A.Cifferri, W.G.Krigbaum and R.B.Meyer eds., 'Polymer Liquid Crystals', Academic Press

Monomesogenic and bimesogenic compounds incorporating small quantities of rigid backbone material have also been the subjects of much study as it is possible to gain a certain degree of control over the phase behaviour and physical properties by altering the structure of the backbone. Figure 1.2 shows the main components of mono- and bimesogenic structures in comparison to a side chain liquid crystal polymer (SCLCP).

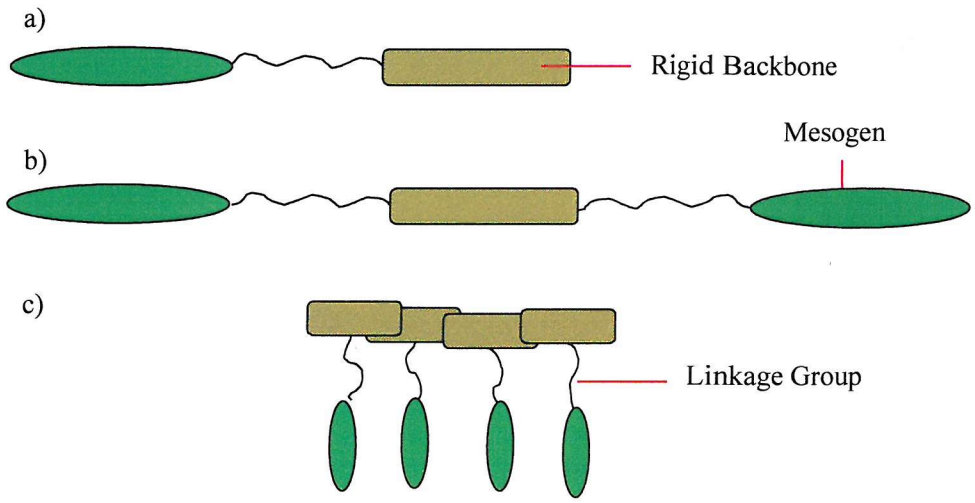

Figure 1.2 Schematic representation of a variety of mesogenic structures: a) monomesogen, b) bimesogen and c) side chain liquid crystal polymer.

Each mesophase is characterised by a unique combination of the degree of orientational and positional (translational) ordering of the molecules. The attractive inter-molecular forces are usually stronger when the molecules are aligned parallel to one another, such that an energetically favourable molecular orientation exists within the mesophase. This preferred orientation is referred to as the director, $\underline{\mathbf{n}}$. The director in a bulk sample is not necessarily uniform, it may vary depending on boundary conditions such that it maintains an equilibrium energy condition. As the molecules are free to move, the director only describes the preferred orientation of the molecules in the mesophase. The director, $\underline{\mathbf{n}}$, is a unit vector and satisfies the condition $\underline{\mathbf{n}} \equiv -\underline{\mathbf{n}}$. Due to the shape anisotropy, the material properties are different in the directions parallel and perpendicular to this statistically determined direction. To quantify the degree of orientational order in the phase another measure is required.

An order parameter, a variable that characterises this ordering, is defined such that it is non-zero in the liquid crystalline phase but zero, for symmetry reasons, in the isotropic phase. Thus, the orientational order is quantified by the order parameter [6], S, defined by

$$S = \frac{1}{2}\left\langle 3\cos^2\theta - 1 \right\rangle, \qquad (1\text{-}1)$$

where the brackets < > denote a thermal average taken over the whole sample, (due to the molecules constant motion), and θ is the angle between the long axis of an individual molecule and the director of the liquid crystal sample, as shown in Figure 1.3.

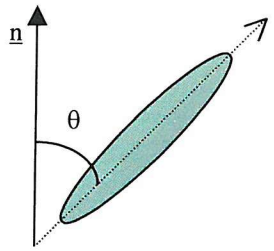

Figure 1.3 The angle, θ, between the orientation of an individual molecule and the director, n, of the whole sample.

If all the molecules in a sample are perfectly aligned then S=1, whilst S=0 in an isotropic liquid. Typically, a liquid crystal sample will have a value of S between 0.4 and 0.8, as shown in Figure 1.4.

[6] V.Tsvetkov, *Acta Physiochim (USSR)*, **16**, 132 (1942)

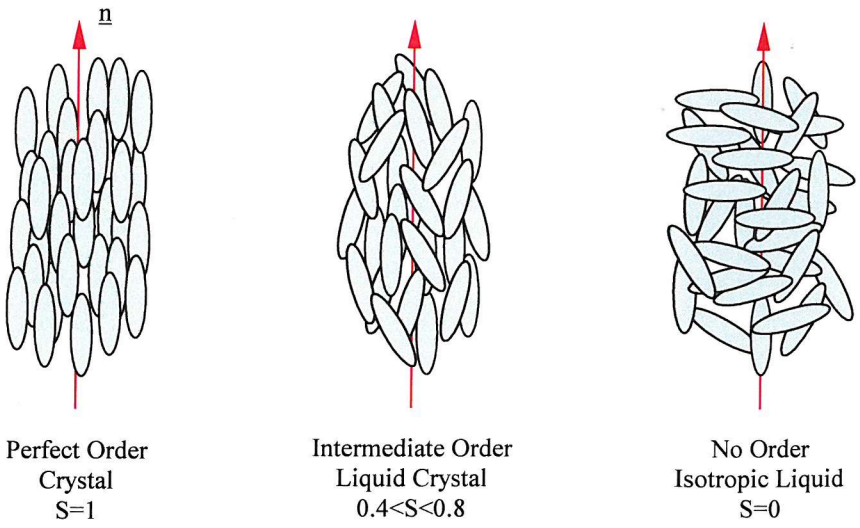

Figure 1.4 Variation of the degree of ordering, as a function of the order parameter, S, within a material exhibiting the crystal, liquid crystal and liquid phases.

In general, the liquid crystalline state consists of a number of partially ordered mesophases that occur between the three-dimensional ordering of molecules in a crystal and the complete disorder of molecules within a liquid. On cooling a fluid from the isotropic phase, one or more mesophases may be formed before the material solidifies. Classification of thermotropic liquid crystals is divided into two basic groups, nematic and smectic, designated according to the degree of order and their inter-molecular alignments. If only orientational order is present, the phase is termed *nematic*. If, in addition to the orientational order, positional (or translational) order also develops, the phase is termed *smectic*.

1.4.3 The Nematic Phase

Nematics are the least ordered of all liquid crystal structures (S=0.4 to 0.7) and generally appear in the form of droplets upon cooling from the isotropic phase, see Figure 1.6. The nematic phase (N) only differs from isotropic liquids in the tendency of the molecules to align along a particular direction. The nematic phase is therefore characterised by long range orientational ordering, (i.e. a molecular director), and the random location of the molecular centres of gravity; there is no positional order. Due to the random distribution

of the molecules the viscosity is of the same magnitude as that of an isotropic liquid. The molecules are free to move in any direction but their long axes are, on average, oriented parallel to each other. The nematic phase therefore behaves as a uniaxial medium with its optical axis along the director, $\underline{\mathbf{n}}$. If the constituent molecules do possess a permanent electric dipole, the condition $\underline{\mathbf{n}}=-\underline{\mathbf{n}}$ is still satisfied as there are just as many 'up' dipoles as 'down'; no macroscopic dipole is observed. The direction of $\underline{\mathbf{n}}$ is arbitrary in space, although, in practice, it is governed by the weak forces imparted by the constricting surfaces of the container.

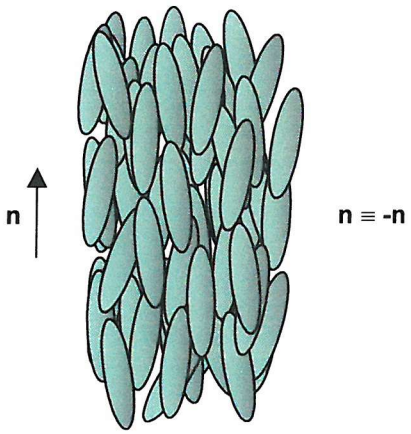

Figure 1.5 Schematic representation of the molecular arrangement in the Nematic mesophase.

One of the most common textures observed is the Schlieren pattern, shown in Figure 1.6, consisting of a network of disclination points. The disclination is a discontinuity in the director pattern and the 'brushes' are simply a macroscopic view of how the director varies in space. The intersections of the brushes form at the disclination and can occur between two or four 'brushes' (referred to S = ± ½ or ± 1 junctions respectively).

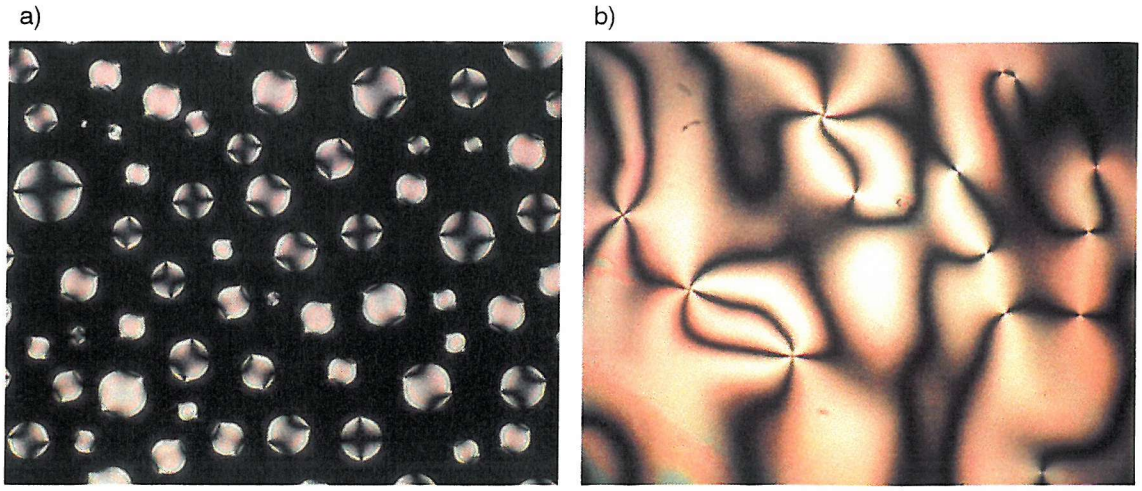

Figure 1.6 Typical textures exibited by the nematic liquid crystal 5CB; a) nematic droplets forming on cooling from the isotropic phase and b) the Schlieren texture demonstrating two- and four-point defects.

The inclusion of chiral mesogenic units or a chiral dopant can induce a helical twist into the nematic structure. This results in a major subset of the nematic group, the chiral nematic, N^*, phase.

1.4.4 The Chiral Nematic Phase

The chiral nematic, or N*, phase is similar to the nematic phase but is most commonly formed from chiral molecules causing a helical rotation of the long axes of the mesogen around an axis perpendicular to the director throughout the sample. The chiral nematic mesophase used to be referred to as 'cholesteric' as the properties exhibited by these materials were originally found in cholesterol esters[7]. The helical pitch, P, is defined as the distance over which the molecular axis rotates by 360°. The spatial period of the helix is equal to half the pitch, due to the symmetry condition $n \equiv -n$, and the helix can be either left- or right-handed. If P is of the order of the wavelength of incident light reflection can occur with $\lambda_{max}=P.n$.

[7] F.Reinitzer, Monatsh.Chem., **9**, 421 (1888)

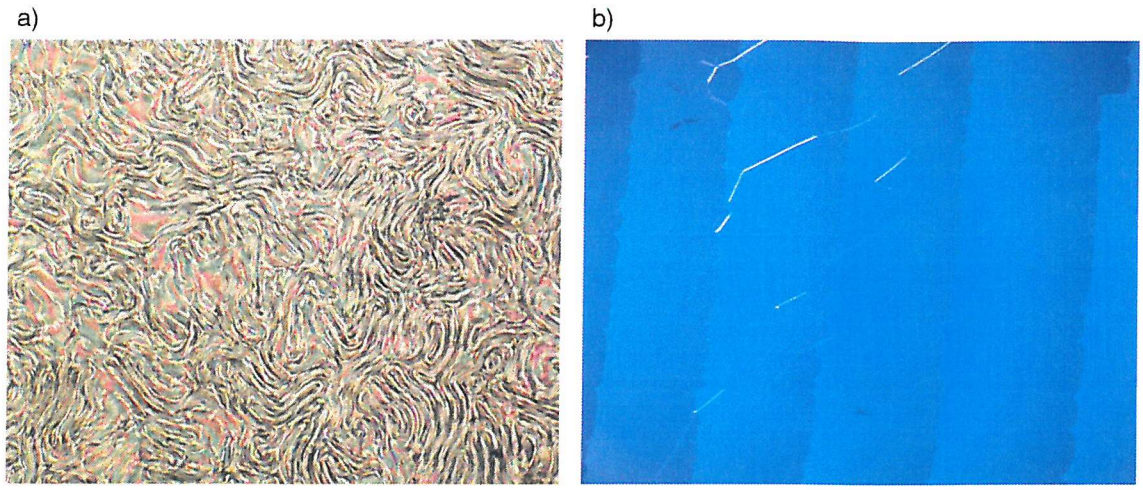

Figure 1.7 Typical chiral nemtic textures exhibited by a) SCE13 and b) nematic 7CB doped with chiral additive; a) fingerprint texture and b) Granjean texture.

1.4.5 The Smectic Phase

The term smectic is derived from the Greek σμηγμα (smegma), a reference to the soaplike mechanical properties of the materials. The smectic phase (Sm) exists at lower temperatures than the nematic phase and, as a result, possesses more order. The molecules possess short-range positional order, manifesting itself as a diffuse layered structure, in addition to long range orientational order. The layer thickness remains constant throughout the sample and is approximately equal to the length of the molecules. The layer spacing can be measured by X-ray diffraction analysis[8]. There is no long range order of the centres of gravity within the layers. The molecules can tilt or orient within the layers and the resulting varying degrees of positional and orientational ordering leads to the subdivision of the smectic phase into classes labelled from A to K (the notation being based purely on chronological discovery). The long axis of molecules within these layers can essentially be either normal (e.g. Smectic A) or tilted (e.g. Smectic C) with respect to the layer plane.

[8] P.S.Pershan, 'Structure of Liquid Crystal Phases', World Scientific (1988)

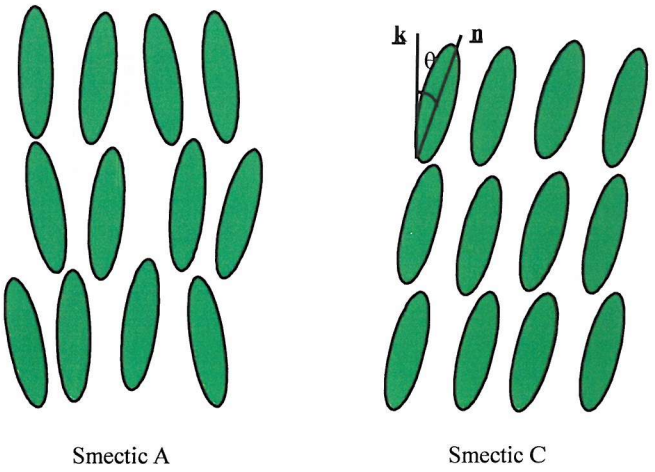

Figure 1.8 Schematic representation of the molecular order in the Smectic A and C phases.

The Smectic A phase (SmA) is the least ordered and therefore the simplest smectic phase. The mesophase is characterised by the one-dimensional positional order of the centrosymmetric and optically uniaxial molecules. On average the molecules in the SmA phase lie parallel to the layer normal and the optical axis of the phase is therefore also normal to the layer plane. If the constituent molecules possess a dipole, the layer structure is slightly modified to minimise the dipole interaction energy. The resulting antiparallel ordering of the dipoles can result in a bilayer structure, schematically depicted in Figure 1.9.

If the molecules comprising the SmA phase are chiral we denote the mesophase as SmA*, where the asterisk represents the chiral nature of the phase. It is also possible to dope the achiral molecules with a chiral additive and observe the SmA* phase. Structurally this chiral form is identical to the non-chiral SmA phase[9] but it does exhibit different optical properties (optical rotary power) as a result of the inclusion of chiral molecules. An electro-optic effect known as the electroclinic effect can also be observed, and this will be discussed in §2.4.1.1.

[9] S.Chandrasekhar, 'Liquid Crystals', Camb.Univ.Press, Second Edition, Chapter 1, (1992)

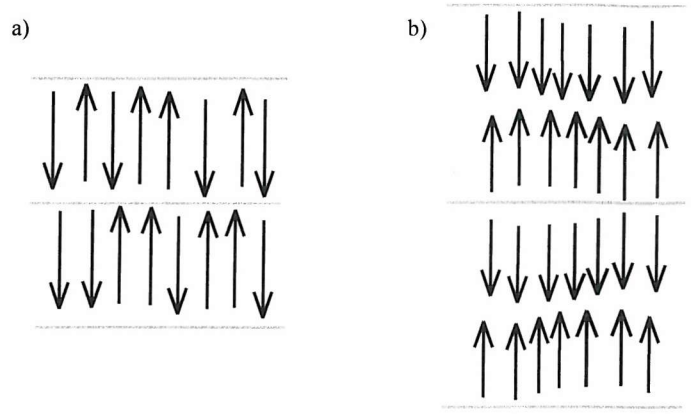

Figure 1.9 Schematic representation of the different layer structures of the Smectic A phase: a) monolayer structure formed by either polar or non-polar molecules and b) bilayer structure formed only by polar molecules.

The next simplest spatial ordering occurs in the SmC phase where the molecules tilt away from the layer normal. The SmC phase is often formed on cooling from the SmA phase. As the transition occurs the molecules tilt, breaking the symmetry about the director, n, and as a result changing the layer spacing. At the transition the focal conic texture of the SmA phase becomes distorted, or 'broken'. Formation of the SmC phase directly from the isotropic generates an unblemished focal conic texture so other methods of identification must be employed.

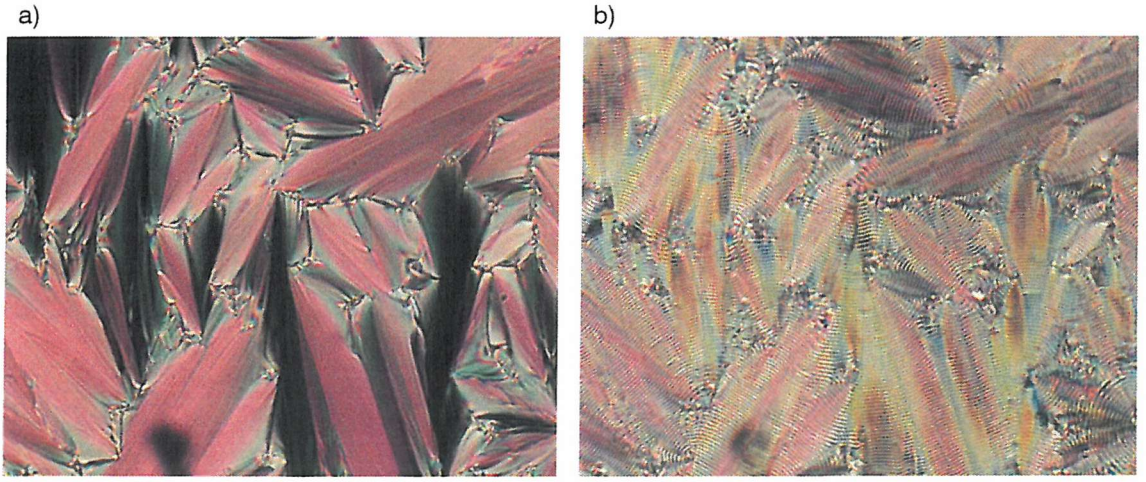

Figure 1.10 Photomicrographs demonstrating the change of the focal conic texture between a) SmA and b) SmC mesophases.

The Smectic C phase (SmC) possesses the same one-dimensional positional order as the SmA mesophase but 'on average' the molecular director $\underline{\mathbf{n}}$ is tilted by an angle θ to the layer normal k.

1.5 SUMMARY

This chapter has provided the reader with a brief introduction to the liquid crystalline phase. The classification of thermotropic liquid crystals into nematic, chiral nematic and smectic mesophases was described in terms of the order parameter. The motivation for the experimental work presented in later chapters has been discussed with respect to the current market for liquid crystal displays and optical devices. The theory of individual mesophases and the properties of particular relevance to this work will now be developed further.

Chapter Two

THE THEORY OF LIQUID CRYSTALS

2.1 INTRODUCTION

This chapter aims to build on the introduction to the concept and physics of the liquid crystalline phase given in Chapter 1. The subject of liquid crystals is a huge area of research and study so the following sections will only present the theoretical aspects most relevant to the work presented later in this thesis.

This chapter begins with a discussion of the Landau theory of phase transitions. Landau theory utilises the definition of the order parameter, introduced in the previous chapter, to describe the change of symmetry associated with the transition between two states.

The anisotropic physical properties of liquid crystalline molecules are discussed in Section 2.3. Mesomorphic molecules are geometrically anisotropic and generally, as a result of the molecular ordering, anisotropy of the physical properties is observed.

In the previous chapter, factors important to the formation of tilted smectic mesophases were discussed in terms of achiral systems. Section 2.4 introduces chiral systems as a precursor to a detailed study of ferroelectric and flexoelectric liquid crystalline systems.

A review of the display technologies that employ the classes of materials studied in this work concludes this chapter.

2.2 THE THEORY OF PHASE TRANSITIONS

Although the order parameter, discussed in §1.4.2, has been defined with respect to the orientational order of the system, it is in reality a much more general term. Every phase transition can be characterised by a parameter that describes the alteration in symmetry. The only requirement is that its value is zero in the high temperature phase and nonzero in the low temperature phase. With this definition in mind, the N-SmA transition requires an order parameter other than S, since S is nonzero in both mesophases. An appropriate order

parameter in this example would be a density distribution function, which would account for the uniform distribution of molecular centres in the nematic phase (i.e. order parameter of zero) and the layer structuring of the molecular centres in the smectic phase (i.e. non-zero order parameter).

2.2.1 Characterisation of Phase Transitions

A phase transition can be thought of as the transition between a disordered high temperature phase and an ordered low temperature phase.

In §1.4.2 an order parameter, S, was introduced to quantify the degree of orientational order in a mesophase. This was defined such that; $S=0$ in the high temperature disordered phase and $S\neq0$ in the low temperature ordered phase.

The behaviour of the system depends on the symmetry of the disordered phase. The temperature dependence of the order parameter is therefore connected to the temperature dependence of numerous material properties. The nature of the phase transitions occurring on heating and cooling can be determined by the behaviour of these temperature dependent properties. They can be broadly classified into two types.

A first order phase transition is identified by a discontinuity in the temperature dependent values of the order parameter. Figure 2.1(a), shows a first order phase transition, such as that which occurs when water is frozen into ice. Second order transitions are characterised by the continuous behaviour of the material properties, see Figure 2.1(b). The value, X, of some material property exhibited in the initial phase tends asymptotically to the value in the second phase as the temperature tends towards the transition. An example of a second order phase transition is that of the magnetic orientation below the Curie temperature.

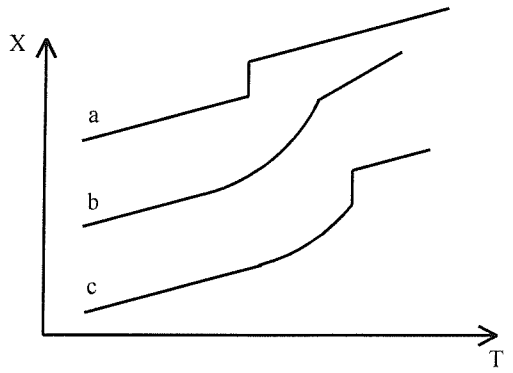

Figure 2.1 Behaviour of temperature dependent material property X through a phase transition; a) first order transition, b) second order and c) combination of first and second order

A discontinuity in the first derivative of the free energy, F, with respect to temperature results in the transition being classified as first order. Likewise a transition in which there is a discontinuity in the second derivative of F with respect to temperature is classified as second order. This 'picture' of phase transitions by Ehrenfest[1] was given a theoretical underpinning by Landau[2,3]. Landau's theory was based on reasonable models of the behaviour of F as a function of a general order parameter, ξ, in addition to considering F as a function of temperature.

2.2.2 Landau Theory of Phase Transitions

A material may undergo a phase transition due to a change in its free energy, F, as a result of a change in temperature and pressure. At constant temperature and volume, i.e. equilibrium, this free energy will be a minimum,

$$F = U - TS, \qquad (2\text{-}1)$$

where F is the Helmholtz free energy, U is the internal energy, T is the temperature and S is the entropy of the system. A thermodynamically stable equilibrium is defined as the absolute minimum of F. Metastable states are represented by other minima $\delta F/\delta\xi=0$.

---

[1] P.Ehrenfest, *Proc.Acad.Sci.Amsterdam*, **36**,153 (1933)
[2] L.D.Landau, E.M.Lifshitz, 'Statistical Physics', Pergamon Press (1958)
[3] C.Kittel, H.Kroemer, 'Thermal Physics' Second Edition, W.H. Freeman (1980)

Landau considered a model material that undergoes transitions depending on F as a function of the degree of order of the material as well as on the temperature and pressure of the system. In this case

$$F_L(\xi,T) = U(\xi,T) - TS(\xi,T), \tag{2-2}$$

where F_L is the Landau free energy and ξ quantifies the degree of order.

$F_L(\xi,T)$ can be constructed as an expansion of a power series in ξ,

$$F_L(\xi,T) = g_0(T) + g_1(T)\xi + \frac{1}{2}g_2(T)\xi^2 + \frac{1}{3}g_3(T)\xi^3 + \frac{1}{4}g_4(T)\xi^4 + \ldots . \tag{2-3}$$

where coefficients g_i describe the system and are functions of pressure and temperature.

If the assumption that the phases have a centre of inversion symmetry is made, the expansion will only be in even powers of the order parameter,

$$F_L(\xi,T) = g_o(T) + \frac{1}{2}g_2(T)\xi^2 + \frac{1}{4}g_4(T)\xi^4 + \frac{1}{6}g_6(T)\xi^6 + \ldots . \tag{2-4}$$

The simplest phase transition model is one in which the coefficient g_2 changes sign at the transition temperature T_0. If this is so, g_2 must be zero at T_0. Consequently, close to the transition we can represent g_2 as

$$g_2(T) = \alpha(T - T_0), \tag{2-5}$$

where α is a positive constant. The nature of the transition will be determined by the higher order coefficients.

2.2.2.1 First Order Transitions

A first order transition occurs if g_4 is negative, g_6 must then be positive to prevent F tending to minus infinity. Substituting this condition and equation 2.5 into equation 2.4, and differentiating with respect to ξ, yields the free energy minima

$$\left(\frac{\partial F_L}{\partial \xi}\right)_T = \alpha(T - T_o)\xi - g_4\xi^3 + g_6\xi^5 = 0, \tag{2-6}$$

which gives two solutions:

$$\xi = 0 \tag{2-7}$$

and

$$\alpha(T - T_o) - g_4\xi^2 + g_6\xi^4 = 0. \tag{2-8}$$

The temperature dependence of the resulting free energy equations, illustrated in Figure 2.2, shows that at temperatures above the phase transition temperature, T_o, only one minimum is found, at $\xi=0$. At T_o two minima exist, indicating the coexistence of the two phases, the free energy value corresponding to $\xi=0$ equals the value at the minimum given by 2.8. Below T_o only a single minima exists for non-zero order parameter.

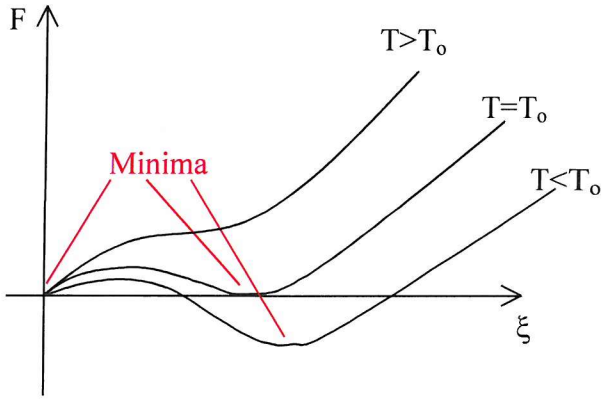

Figure 2.2 The variation of the Free Energy with the order parameter at different temperatures.

2.2.2.2 Second Order Transitions

If g_4 is positive the higher order terms may be ignored, as they do not affect the behaviour of the function significantly. Again, differentiation of F as a function of ξ,

$$\left(\frac{\partial F_L}{\partial \xi}\right)_T = \alpha(T - T_o)\xi + g_4\xi^3 = 0, \tag{2-9}$$

produces two solutions:

$$\xi = 0 \tag{2-10}$$

and

$$\xi^2 = \left(\frac{\alpha}{g_4}\right)(T_o - T). \tag{2-11}$$

For temperatures above T_o the only real solution is 2.10, since α and g_4 are both positive. At temperatures below T_o, the equilibrium order parameter varies as

$$\xi \propto (T_o - T)^{\frac{1}{2}}. \tag{2-12}$$

Thus as T_o is approached from lower temperatures, the order parameter tends continuously towards zero. The phase transition is therefore classified as being of second order.

A comparison of the temperature dependence of the order parameter in materials undergoing a series of first and second order phase transitions is shown in Figure 2.3.

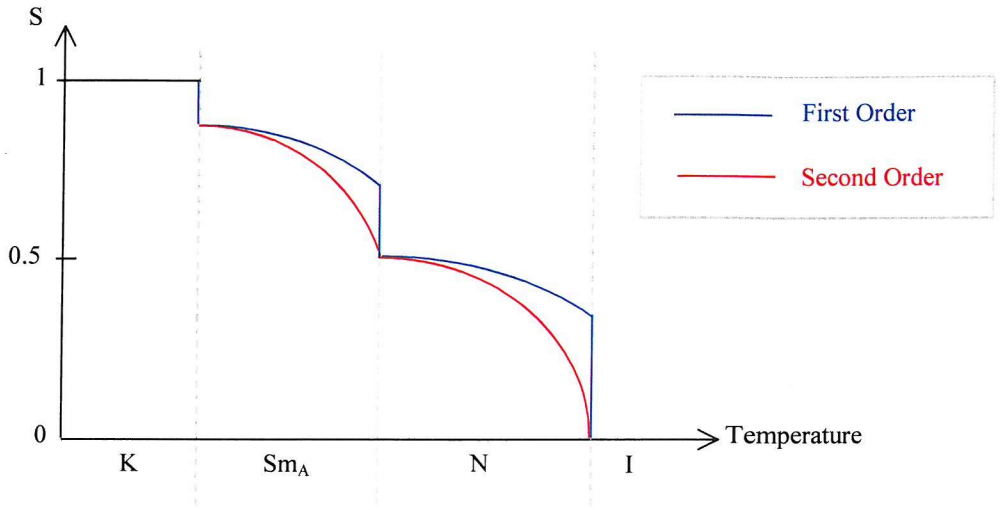

Figure 2.3 The variation of the order parameter with temperature for first and second order phase transitions.

2.2.2.3 Landau Theory of Smectic A-Smectic C Phase Transition

SmA to SmC phase transitions are second order and can be described by Landau theory.

Since the SmC phase is tilted and there is zero tilt in the SmA phase it is convenient to define the primary order parameter of this phase transition as the tilt angle,θ. In a similar manner to that discussed in §2.2.2 the Landau free energy of the system can be written as

$$F_L = g_0(T) + \frac{1}{2}g_2\theta^2 + \frac{1}{4}g_4\theta^4 + \frac{1}{6}g_6\theta^6 + \ldots \qquad (2\text{-}13)$$

As before, odd terms in θ do not occur since $F_L(\theta) = F_L(-\theta)$, and $g_2(T) = \alpha(T - T_o)$. For the purpose of this work it is sufficient to assume that g_6 is negligible. Consequently, minimising equation 2.13 with respect to θ gives two solution minima:

$$\theta = 0 \qquad T>T_o \qquad (2\text{-}14)$$

and

$$\theta = \sqrt{\frac{\alpha}{g_4}}\sqrt{(T_o - T)} \qquad T<T_o. \qquad (2\text{-}15)$$

This application of Landau's theory to a real example of a phase transition provides information on the temperature dependence of the tilt angle. This $\sqrt{T}$ relationship is observed in experimental results discussed in Chapter 3.

2.3 PHYSICAL PROPERTIES OF LIQUID CRYSTALS

Anisotropy of the physical properties is observed on a macroscopic scale as a result of the geometric anisotropy of the mesomorphic molecules and the molecular ordering in the mesophase. It is this macroscopic manifestation of anisotropy that leads to the use of liquid crystal materials in many display applications.

2.3.1 Dielectric Properties

Dielectric studies are concerned with the behaviour of a material under the application of an electric field. Unlike conductors, dielectrics posses no carriers of free charge. The charges are all bound to their atoms or molecules and thus, can only move very short distances. The application of an electric field will result in the separation of the positive and negative charges and the dielectric material becoming polarised. Molecules that possess a permanent dipole moment are said to be polar, and those that do not, are said to be nonpolar. There are three basic polarisation processes.

1) Displacement polarisation - displacement of the electrons in an atom relative to the centre of charge of the nucleus, under the influence of an electric field
2) Orientational polarisation - dipole moments of polar molecules align themselves with, and become further polarised in, the applied field
3) Atomic/ionic polarisation - oppositely charged ions in a solid move in different directions when subjected to an electric field.

For low electric fields applied across an isotropic dielectric medium, the polarisation (dipole moment per unit volume), **P**, is proportional to the applied electric field, **E**, such that

$$\mathbf{P} = \varepsilon_o \chi_e \mathbf{E}, \tag{2-16}$$

where χ_e is the electric susceptibility of the medium and ε_o is the permittivity of free space. The electric field vector **E** and the electric induction or displacement vector **D** are related by

$$\mathbf{D} = \varepsilon_o \mathbf{E} + \mathbf{P} = \varepsilon_o (1 + \chi_e)\mathbf{E} = \varepsilon_o \varepsilon \mathbf{E}, \tag{2-17}$$

where $\varepsilon = (1 + \chi_e)$ is the relative permittivity, or dielectric constant.

However, the equations above only strictly apply for isotropic media. In an anisotropic material **P** does not necessarily lie in the same direction as **E** so the susceptibility and dielectric constant then become tensor quantities.

The anisotropic dielectrical properties of liquid crystals are exploited in devices as changes in the orientation and organisation of the anisotropic molecules, to minimise the potential energy in an applied field, result in changes in the macroscopic optical characteristics of the liquid crystal phase. Dielectric anisotropy is defined as

$$\Delta\varepsilon = \varepsilon_{\parallel} - \varepsilon_{\perp} \tag{2-18}$$

since the electric susceptibility is different parallel ($\varepsilon_{\parallel}$) and perpendicular ($\varepsilon_{\perp}$) to the director.

The orientational free energy, F_E, of a liquid crystal subjected to an electric field, **E**, is given by

$$F_E = -\frac{1}{2}\varepsilon_o \Delta\varepsilon (\mathbf{n}.\mathbf{E})^2. \tag{2-19}$$

Under the application of an electric field, the free energy is minimised by molecular rotation such that for $\Delta\varepsilon > 0$, the director, **n**, is parallel to **E**, and for $\Delta\varepsilon < 0$ **n** is perpendicular to **E**.

The dielectric properties of liquid crystals are dependent on the collective response of the mesogens as well as their molecular properties. Coupling between the macroscopic polarisation and the molecular response through the internal field also occurs and, as such a full description of the dielectric properties requires the internal electric field in anisotropic media to be specified. This is not trivial so isotropic systems will be considered in the following discussion. The Debye equation for an isotropic fluid relates the permittivity to the scalar polarisability ($\bar{\alpha} = (\alpha_{\parallel} + 2\alpha_{\perp})/3$ where $\alpha_{\parallel}$ and $\alpha_{\perp}$ are the polarisability parallel and perpendicular to the molecular axis respectively) and the molecular dipole moment (μ):

$$(\varepsilon - 1) = \frac{NFh}{\varepsilon_o}\left[\bar{\alpha} + \frac{\mu^2 F}{3k_B T}\right], \tag{2-20}$$

where F and h are reaction field and cavity field factors which account for the field dependent interaction of a molecule with its environment and N is the number density. The internal field factors for isotropic fluids are given by:

$$F = \left(1 - \bar{\alpha} f\right)^{-1}, \text{ where } f = \frac{2(\varepsilon - 1)}{4\pi\varepsilon_0 a^3 (2\varepsilon + 1)}, \text{ and } h = \frac{3\varepsilon}{2\varepsilon + 1}, \tag{2-21}$$

where a is the radius of the spherical cavity that accommodates the molecule, i.e the rotation of the molecule is assumed to be spherical. Dunmur and Munn[4] have shown that shape anisotropy of the local field can be neglected in liquid crystal systems and the assumption of isotropic internal field factors is justified.

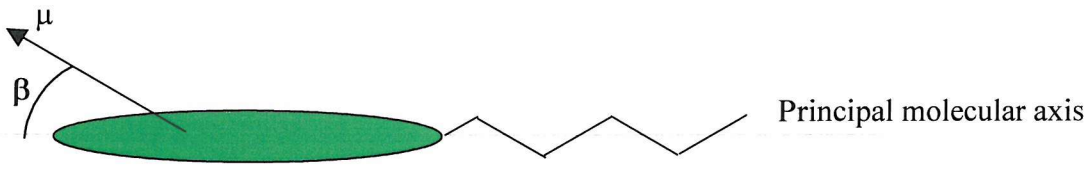

Figure 2.4 Schematic representation of a mesogenic molecule with an off-axis dipole moment, μ, making an angle β with the molecular long axis.

[4] D.A.Dunmur, R.W.Munn, *Chem. Phys*, **76** 249 (1983)

Static values of the dielectric constants, $\varepsilon_{\parallel}$ and $\varepsilon_{\perp}$, were first predicted by Maier and Meier[5] as a function of the orientational order parameter, S, the angle β between the molecular dipole moment, μ, and the principal molecular axis (as illustrated in Figure 2.4), the mean polarisability, $\bar{\alpha}$, and its anisotropy, $\Delta\alpha$

$$\varepsilon_{\parallel} = 1 + 4\pi NhF\left\{\bar{\alpha} + \frac{2}{3}\Delta\alpha S + F\frac{\mu^2}{3k_B T}\left[1 - \left(1 - 3\cos^2\beta\right)S\right]\right\}$$

$$\varepsilon_{\perp} = 1 + 4\pi NhF\left\{\bar{\alpha} - \frac{1}{3}\Delta\alpha S + F\frac{\mu^2}{3k_B T}\left[1 + \frac{1}{2}\left(1 - 3\cos^2\beta\right)S\right]\right\}. \qquad (2\text{-}22)$$

The dielectric anisotropy is then given by

$$\Delta\varepsilon = 4\pi NhF\left[\Delta\alpha - F\frac{\mu^2}{2k_B T}\left(1 - 3\cos^2\beta\right)\right]S. \qquad (2\text{-}23)$$

The first term represents the contribution of the molecular polarisability (displacement polarisation) and is always positive for rod-like molecules whereas the second term originates from the permanent dipole moment (orientation polarisation) and is positive or negative depending on whether β is smaller or larger than 54.7°. Control of the sign and magnitude of $\Delta\varepsilon$ can, therefore, be attained by varying the position and constituents of the terminal and laterally substituted groups. For a particular combination of molecular properties, the polarisability anisotropy and dipolar terms in equation 2.23 may cancel at a particular temperature[6].

2.3.1.1 Frequency Dependence of the Dielectric Permittivity

As given by equation 2.16, the permittivity determines the polarisation (dipole moment per unit volume) induced in a material by an electric field. If the applied field varies with time, the frequency dependence of the permittivity is an additional property of the material. In general the dipole moment will not be along the long axis of the molecule, and there is likely to be a complicated relationship between the motion of the dipole,

[5] W.Maier, G.Meier, *Z. Naturforsch*, **16A**, 262 (1961)
[6] D.A.Dunmur, D.A.Hitchen, Xi-Jun Hong, *Mol.Cryst. Liq.Cryst.*, **140**, 303 (1986)

which determines the frequency dependence of the permittivity, and the rotational motion of the molecule as the response may not be in phase with the applied field. The frequency dependent dielectric constant, $\varepsilon(\omega)$, then becomes complex,

$$\varepsilon(\omega) = \varepsilon'(\omega) + i\varepsilon''(\omega), \tag{2-24}$$

where the real component represents the polarisation in phase with the applied field and the imaginary part corresponds to the dielectric loss inherent in a mechanism lagging behind the applied field frequency. Assuming a single molecular dipole relaxation with Debye-like behaviour, the response of a molecule to an alternating field of frequency ω can be described by the complex permittivity:

$$\varepsilon(\omega) - 1 = (1 + i\omega\tau)^{-1} \frac{N\mu^2}{3\varepsilon_0 k_B T} \tag{2-25}$$

which gives:

$$\varepsilon'(\omega) - 1 = (1 + \omega^2\tau^2)^{-1} \frac{N\mu^2}{3\varepsilon_0 k_B T} \qquad \text{and}$$

$$\varepsilon''(\omega) = \omega\tau(1 + \omega^2\tau^2)^{-1} \frac{N\mu^2}{3\varepsilon_0 k_B T}. \tag{2-26}$$

The time τ is the relaxation time for the dipole reorientation. In real systems there may be a number of contributions to the permittivity, each relaxing at a different frequency. At low frequencies ($\omega \to 0$) the orientational polarisation contribution to the permittivity is $\frac{N\mu^2}{3\varepsilon_0 k_B T}$, neglecting any field effects, while at higher frequencies ($\omega \to \infty$) the molecular dipoles do not rotate fast enough to contribute to the dielectric response. More generally the real and imaginary parts of the permittivity can be written as:

$$\varepsilon(\omega) - \varepsilon'(\infty) = \frac{[\varepsilon'(0) - \varepsilon'(\infty)]}{1 + i\omega\tau}$$

$$\varepsilon'(\omega) - \varepsilon'(\infty) = \frac{[\varepsilon'(0) - \varepsilon'(\infty)]}{1 + \omega^2\tau^2};$$

$$\varepsilon''(\omega) = \omega\tau \frac{[\varepsilon'(0) - \varepsilon'(\infty)]}{1 + i\omega^2\tau^2}, \tag{2-27}$$

where $\frac{N\mu^2}{3\varepsilon_0 k_B T} = [\varepsilon'(0) - \varepsilon'(\infty)]$.

In the case of a liquid crystal, $\varepsilon(\omega)$ contains contributions from the molecular susceptibility and permanent dipole moments. Other effects include: a) conductivity due to ionic impurities and charge injection, b) electrode polarisation due to accumulation of electrolysis products and imperfect sample contact and c) interfacial polarisation due to sample inhomogenity.

The frequency dependence of $\varepsilon(\omega)$ results from reorientations and, to a lesser degree, internal rotations of the molecules constituting the sample and ionic or charge mobilities. The theory of Nordio *et al.*[7,8] provides a useful model for the dielectric relaxation in a homeotropically aligned nematic liquid crystal. The intensities of the two relaxation processes observed for measurements made with the applied field parallel to the director are given by

$$A_{00} = \left(\frac{\mu_l^{\,2}}{3}\right)(1+2S),$$

$$A_{10} = \left(\frac{\mu_t^{\,2}}{3}\right)(1-S), \qquad (2\text{-}28)$$

where

$$\mu_l^2 = \mu_z^2,$$

$$\mu_t^2 = (\mu_x^2 + \mu_y^2). \qquad (2\text{-}29)$$

The relaxation times for these two processes are τ_{00} and τ_{10} respectively. Similarly the intensities of the two processes observed in measurements made with the electric field perpendicular to the director are

$$A_{01} = \left(\frac{\mu_l^{\,2}}{3}\right)(1-S),$$

$$A_{11} = \left(\frac{\mu_t^{\,2}}{3}\right)\left(1+\frac{1}{2}S\right). \qquad (2\text{-}30)$$

---

[7] P.L.Nordio, G.Rigatti, U.Segre, *Molec.Phys.*, **25**, 129 (1973)

[8] P.L.Nordio, U.Segre, *The Molecular Physics of Liquid Crystals*, edited by G.R. Luckhurst and G.W. Gray, p.411, 1979 (Academic Press)

The relaxation times for these two processes are τ_{01} and τ_{11} respectively. The τ_{ii} depend on the strength of the nematic potential and so on S, and on the magnitude and isotropy of the microscopic diffusion tensor. The relative magnitudes of the frequencies of maximum loss ω_{ii}, are predicted by the theory of Nordio *et al.* to satisfy the relation

$$\omega_{00} < \omega_{01} \leq \omega_{11} \leq \omega_{10}\,. \tag{2-31}$$

Schematic representations of these fundamental motions are shown in Figure 2.5.

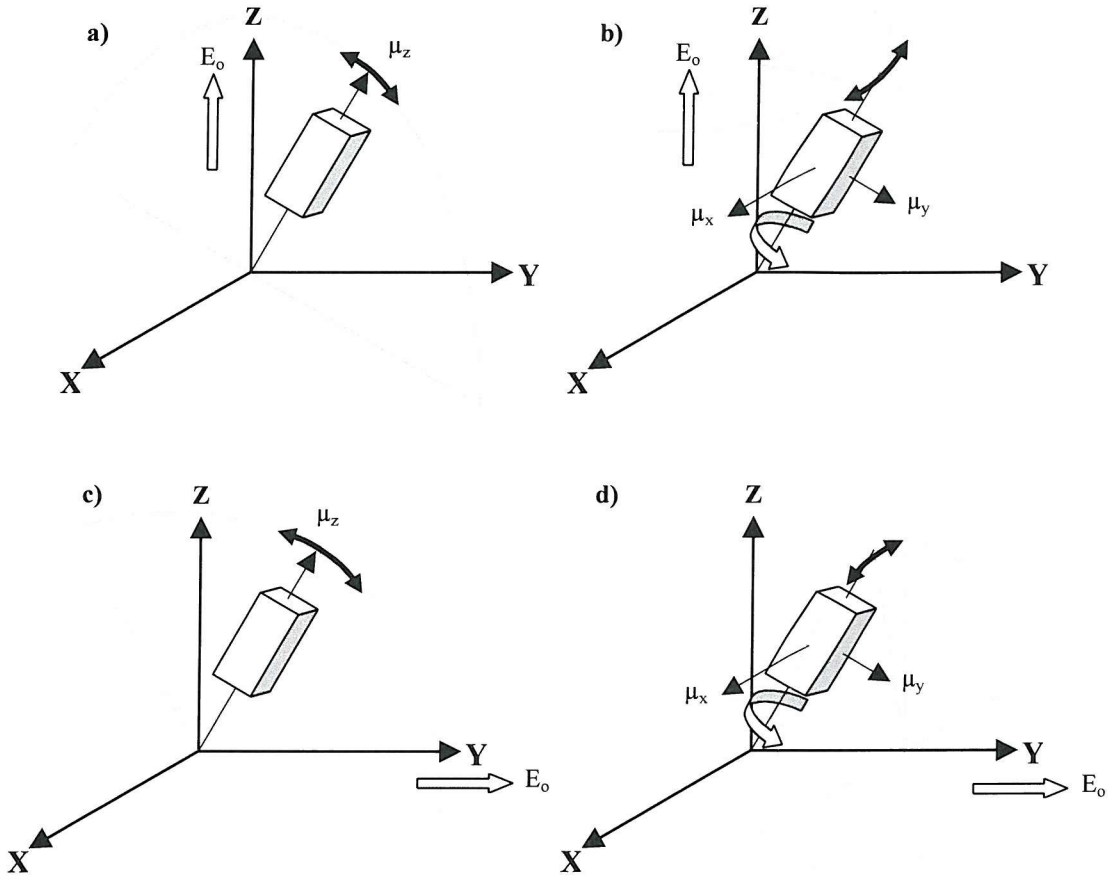

Figure 2.5 Schematic representaion of the fundamental molecular rotational modes that contribute to the dielectric relaxation. For measurements with the electric field, E_o, parallel to the director: a) relaxation process with relaxation time τ_{00}, b) process with relaxation time τ_{10}. For measurements with the electric field, E_o, perpendicular to the director: c) relaxation process with relaxation time τ_{01}, d) process with relaxation time τ_{11}.[9]

The dynamics of the molecular rotation, with the field applied parallel to the director (which is of primary interest in this work), can therefore be described by two rotational

[9] G.S.Attard, *Molec.Phys.*, **58**, 1087 (1986)

modes; end-over-end rotation (relaxation frequency ω_{00}) and rotation about the long molecular axis (ω_{10}). End-over-end rotation of the molecule is characterised by a relatively long relaxation time due to the rotation of the longitudinal component of the dipole moment around a transverse axis being strongly hindered by the barrier resulting from the long-range orientational order, as explained by the theory of Maier and Saupe[10]. The orientational polarisation perpendicular to the director experiences a much faster relaxation, as the axis of rotation is the molecular long axis. In a homeotropically aligned nematic sample the dielectric loss spectrum should consist of a low frequency dispersion centred on ω_{00} and a high frequency dispersion centred on ω_{10}.

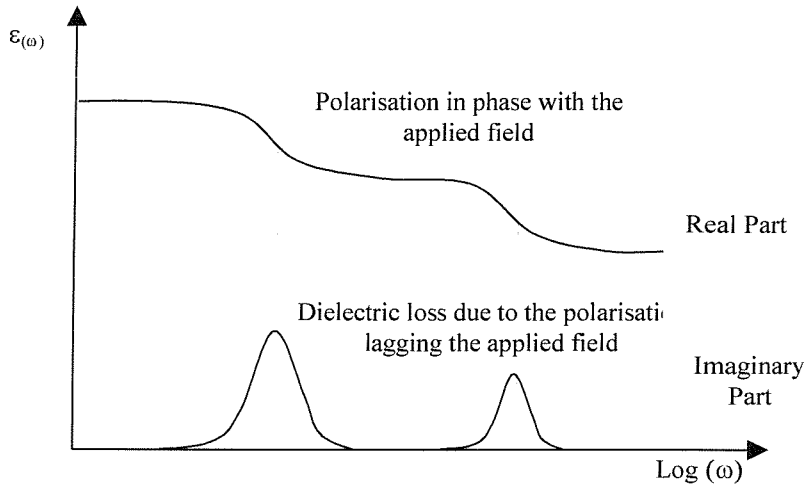

Figure 2.6 A plot of $\varepsilon_{(\omega)}$ versus frequency can show several relaxation regions.

Figure 2.6 illustrates the frequency dependent nature of $\varepsilon(\omega)$. Each reorientation mode has a fundamental frequency above which the relevant dipole moment cannot follow the rapid alternations of the field and the dipole moment contribution completely disappears. When the frequency of the AC field corresponds to the fundamental frequency of one of these dynamic processes, a change is observed in $\varepsilon(\omega)$. As the frequency is increased ε undergoes relaxation processes where its magnitude decreases as the reorientation modes are frozen out. In the same frequency bands the imaginary part is non-zero, i.e. there is a significant dielectric loss factor, since the dipoles attempt to respond but their motion lags in phase behind the applied field.

[10] W.Maier, A.Saupe, *Z.Naturforsch*, **14A**, 882 (1959)

As described by Equation 2.23, two factors determine the low frequency dielectric anisotropy; 1) the polarisability anisotropy, $\Delta\alpha$, of the molecule (a positive contribution in calamitic molecules) and 2) the dipole orientation effect, this is positive if the dipole moment is almost parallel to long molecular axis, and negative if the angle between the permanent dipole moment of the molecule and its long axis is larger than 54.74°. Thus the sign of the net dielectric anisotropy will depend on the magnitude of the two contributions.

When the static value of $\varepsilon_{\parallel}$ exceeds that of $\varepsilon_{\perp}$, the low frequency relaxation of $\varepsilon_{\parallel}$ can result in a change in sign of the dielectric anisotropy[11] of the material at the so-called dispersion or critical frequency ω_c, this is illustrated in Figure 2.7. Liquid crystals exhibiting this behaviour are known as dual-frequency materials because of potential applications in fast-switched liquid crystal devices, which are addressed by both low frequency ($\Delta\varepsilon$ positive) and high frequency ($\Delta\varepsilon$ negative) electric fields.

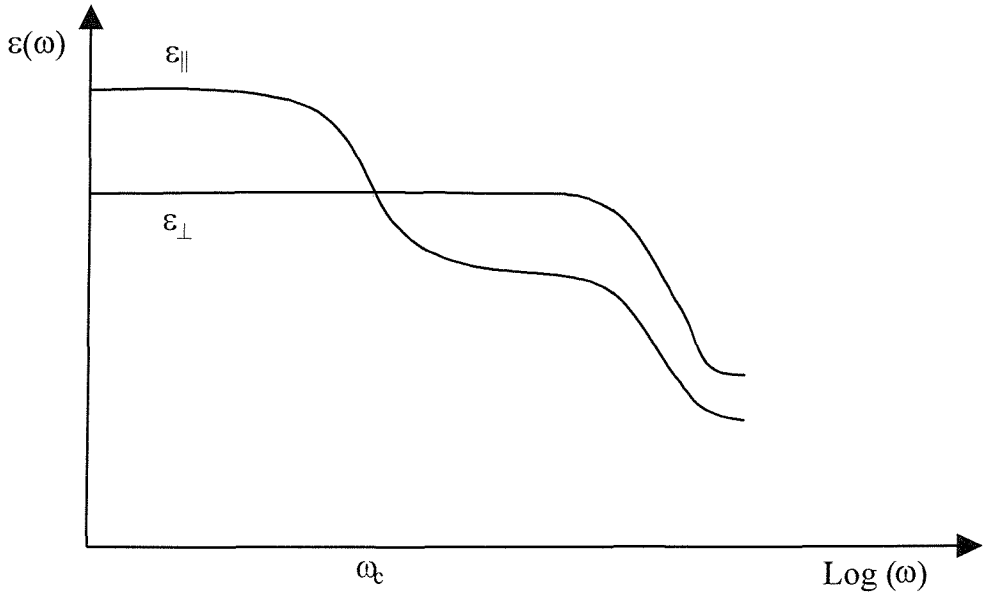

Figure 2.7 The frequency dependence of the dielectric permittivity, illustrating the critical frequency at which the dielectric anisotropy changes sign.

[11] M.F.Bone, A.H.Price, M.G.Clark, D.G.McDonnell, *Liquid Crystals and Ordered Fluids Vol.4*, Plenum, p.799 (1989)

The critical frequency can be low, particularly in nematic liquid crystals formed by long three-ring molecules[12], as barriers to the rotation of the molecules around the short axis are particularly high. The dielectric anisotropy, $\Delta\varepsilon$, of such nematics can be increased by the addition of a permanent electric dipole oriented parallel or perpendicular to the long axis of the molecule.

2.3.2 Refractive Indices

The interaction of light with the liquid crystal molecules depends on its direction of polarisation relative to the director. Due to their anisotropic nature liquid crystals possess two different refractive indices i.e they are birefringent.

If a uniaxial nematic sample is uniformly aligned, two different refractive indices can be observed; n_o corresponding to the ordinary wave (electric vector oscillating normal to the optic axis) and n_e relating to the extraordinary wave oscillating parallel to the optic axis. The velocity of light travelling along these directions will differ since the refractive indices are different.

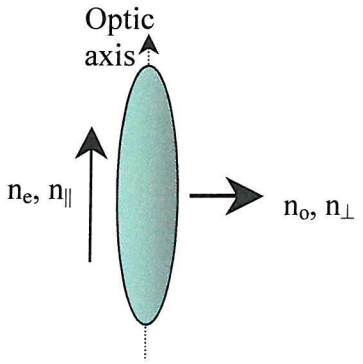

Figure 2.8 The two principal refractive indices in an uniaxial liquid crystal.

Let us consider plane polarised light incident on the aligned uniaxial liquid crystal sample (uniaxial waveplate). Unless the angle between the optic axis and the plane of polarisation is 0 or 90° the two different refractive indices contrive to split the beam into two components which subsequently propagate at different speeds. Generally, on leaving the

[12] W.H.de Jeu, Th.M.Lathowers, *Mol.Cryst.Liq.Cryst*, **26**, 225 (1974)

sample the two beams will be out of phase and polarised with their planes of oscillation normal to each other, resulting in elliptically polarised light.

The birefringence, Δn, of the material is characterised by the difference between the extraordinary and ordinary refractive indices, given by

$$\Delta n = n_e - n_o = n_{\parallel} - n_{\perp}, \tag{2-32}$$

where $n_{\parallel}$ and $n_{\perp}$ are the refractive indices measured parallel and perpendicular to the director.

At optical frequencies the orientation polarisation component can be neglected. The electric polarisability of the liquid crystal molecules therefore consists solely of contributions by the electronic and atomic parts.

$$\Delta n = n_{\parallel} - n_{\perp} \tag{2-33}$$

$$\Delta \varepsilon = n_{\parallel}^{\,2} - n_{\perp}^{\,2} \tag{2-34}$$

In an isotropic material the refractive index ellipsoid is spherical, i.e. $n_e = n_o = \bar{n}$. The unique axis of the ellipsoid defines the single optical axis of a uniaxial system, this usually corresponds to orientation of director. The condition $n_e > n_o$ describes a positive uniaxial material, such as a nematic material. Chiral nematic materials have a negative birefringence.

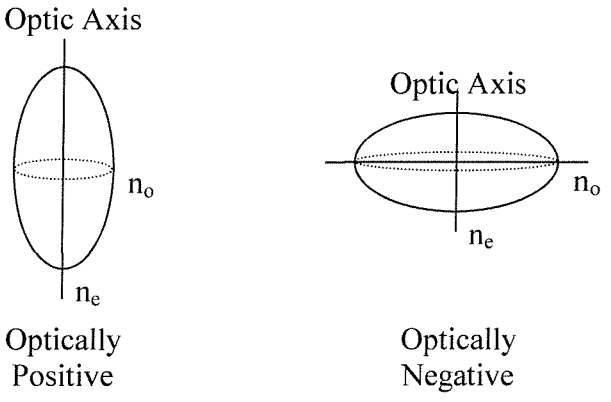

Figure 2.9 The refractive index ellipsoids for uniaxial structures with positive and negative birefringence.

As the phase difference between the ordinary and extraordinary waves accumulates along the path length in the birefringent material, the length of the sample has an important role in determining the exit polarisation state. The difference in optical paths will change the polarisation state of the light as it propagates through the medium. The optical path length of a wave is defined as the product of the refractive index, n, and the distance travelled, d.

Thus, the path length difference between the two components mentioned above will be

$$d(n_e - n_o) = \Delta nd . \tag{2-35}$$

Hence, the phase difference, δ, between the ordinary and extraordinary components is

$$\delta = \frac{2\pi\Delta nd}{\lambda}, \tag{2-36}$$

where λ is the wavelength of the incident light.

When positioned between crossed polarisers, optically anisotropic materials exhibit azimuthally dependent variations in the transmitted intensity. Isotropic media appears dark at all orientations relative to the transmitted beam whereas anisotropic media only possess distinct directions of isotropy if the transmitted beam propagates parallel to an optic axis. In all other cases of incidence the cross section of the indicatrix where the beam is incident yields an ellipse which results in the splitting of the propagating waves into different velocities and polarisation modes (birefringence) now vibrating in perpendicular polarisation planes. On passing the analyser, both rays recombine by superimposing the path difference and vibration directions of wave vectors. Only one component is transmitted, producing plane polarised light of different wavelengths and amplitude to the incident beam. The intensity of the transmitted component is given by

$$I = I_o \sin^2 2\psi_o \sin^2 \frac{\delta}{2}, \tag{2-37}$$

where I_o is the incident intensity and ψ_o is the angle between the polarisation axis of the initial polariser and the optical axis of the liquid crystal sample.

Variations in the optical birefringence across a sample of liquid crystal material can occur due to changes in the director orientation. These characteristic patterns, or textures, can be

used to identify the mesophase. Similarly, field-induced changes of the molecular alignment also cause the birefringence to vary, and are the basis for the majority of display applications.

2.3.3 Elastic Constants

As liquid crystals are anisotropic fluids the mechanical properties are not necessarily the same if measured in different directions. The elastic constants of a liquid crystal material are the restoring torques that govern its elastic, or mechanical, behaviour. Uniaxially aligned liquid crystals can be deformed in a defined manner by external mechanical forces or by magnetic or electric fields. Frank[13] has shown that it is possible to completely describe any arbitrary deformation by using a combination of just three basic mechanical deformation patterns. These are splay, twist and bend, as shown in Figure 2.10.

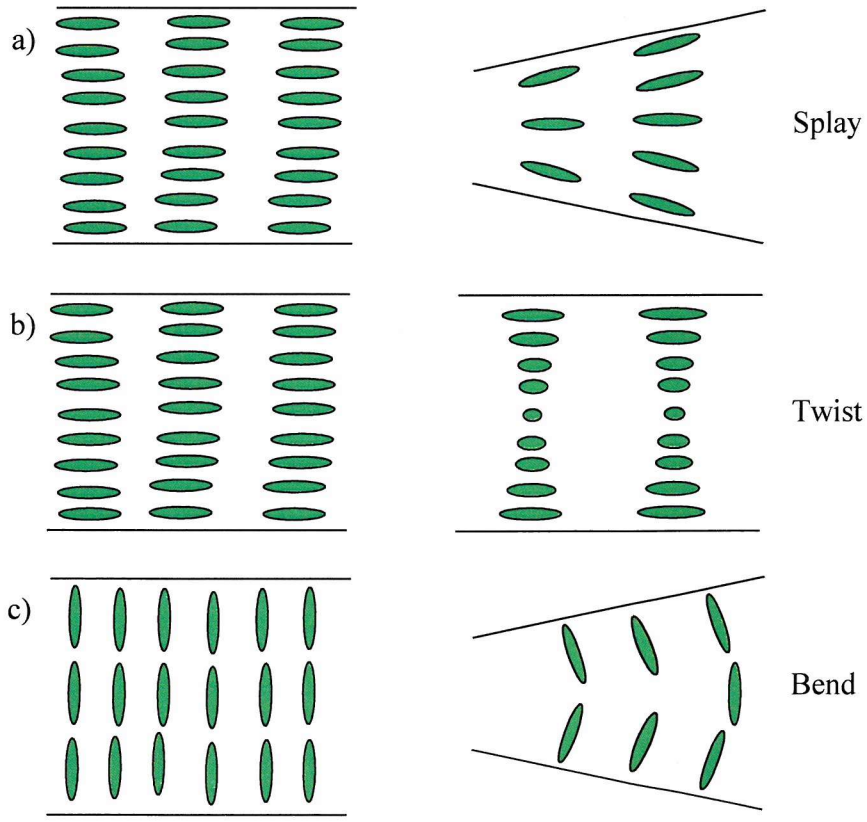

Figure 2.10 The a) splay, b) twist and c) bend deformations required to describe all the possible deformation patterns of liquid crystals.

Since the director deformations correspond to spatial changes in the director axis n(**r**), the parameters involved in the deformation energies are spatial derivatives. The free-energy densities associated with these deformations are given by;

$$\text{Splay} : F_1 = \frac{1}{2}K_{11}(\nabla \cdot n(\mathbf{r}))^2, \tag{2-38}$$

$$\text{Twist} : F_2 = \frac{1}{2}K_{22}(n(\mathbf{r}) \cdot \nabla \times n(\mathbf{r}))^2 \tag{2-39}$$

and

$$\text{Bend} : F_3 = \frac{1}{2}K_{33}(n(\mathbf{r}) \times (\nabla \times n(\mathbf{r})))^2 \tag{2-40}$$

where K_{11}, K_{22} and K_{33} are the respective Frank elastic constants.

If all three deformations occur the distortion free-energy density is given by

$$F_d = \frac{1}{2}\int d\mathbf{r}\left(K_{11}[\nabla \cdot n(\mathbf{r})]^2 + K_{22}[n(\mathbf{r}) \cdot \nabla \times n(\mathbf{r})]^2 + K_{33}[n(\mathbf{r}) \times \nabla \times n(\mathbf{r})]^2\right). \tag{2-41}$$

2.4 Ferroelectric and Antiferroelectric Liquid Crystals

The SmC structure detailed in Chapter 1 is obtained only if the molecules are optically inactive. If the constituent molecules are chiral, or a chiral dopant is introduced, the structure differs from the achiral analogue. The magnitude of the tilt away from the layer normal remains the same but on passing from layer to layer throughout the sample, we observe a precession of the molecular tilt orientation around the surface of the cone (i.e. a precession around an axis perpendicular to the layer planes). This results in a macroscopic helical arrangement that can be either left or right handed depending on the constituent molecules. The chiral smectic C phase (SmC*) is of particular importance to this work as it can exhibit ferroelectricity.

[13] F.C.Frank, *Discuss.Faraday Soc.*, **25**, 19 (1958)

2.4.1 Ferroelectric Liquid Crystals (SmC*)

It is well known that ferroelectric dielectric materials exhibit spontaneous polarisation and hysterisis when subjected to an electric field. In 1975 Meyer et al[14] used symmetry considerations to predict the existence of ferroelectricty in liquid crystals.

The allowed director orientation lies on a cone of angle 2θ, the azimuthal angle ϕ determines the position on the cone, see Figure 2.11.

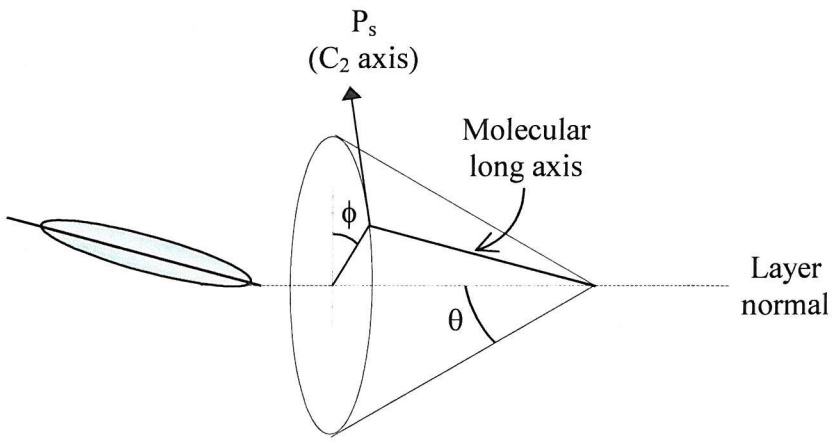

Figure 2.11 Schematic representation of the SmC phase.

In the SmC phase, schematically depicted in Figure 2.12a), the achiral molecules are arranged in diffuse layers with their long axes tilted with respect to the layer normal. There exists a centre of inversion symmetry and a mirror plane normal to the smectic layers. The "C2" symmetry axis lies parallel to the layers and perpendicular to the tilt direction, resulting in "C2h symmetry". The chiral SmC* phase, shown in Figure 2.12b), has a reduced space symmetry. The centre of symmetry and the mirror plane are lost, since the chiral molecules are asymmetric. Meyer et al theorized that a spontaneous polarisation, Ps, will develop parallel to the layer plane and along the C2 axis as a result of the dipole alignment. Each layer has a Ps associated with it, but since the layers are stacked in a helical arrangement the polarisation averages to zero, i.e. the material is helielectric. If an electric field is applied, the helix unwinds as the layer dipoles align with

[14] R.B.Meyer, L.Liebert, L.Strzelecki, P.Keller, *Le Jour de Phys. (lett.)*, **36**, 69, (1975)

the field and the phase becomes ferroelectric. Surface forces can also be used to constrain the helix and produce a macroscopic polarisation; the surface-stabilised ferroelectric liquid crystal (SSFLC) display is discussed in §2.6.3.

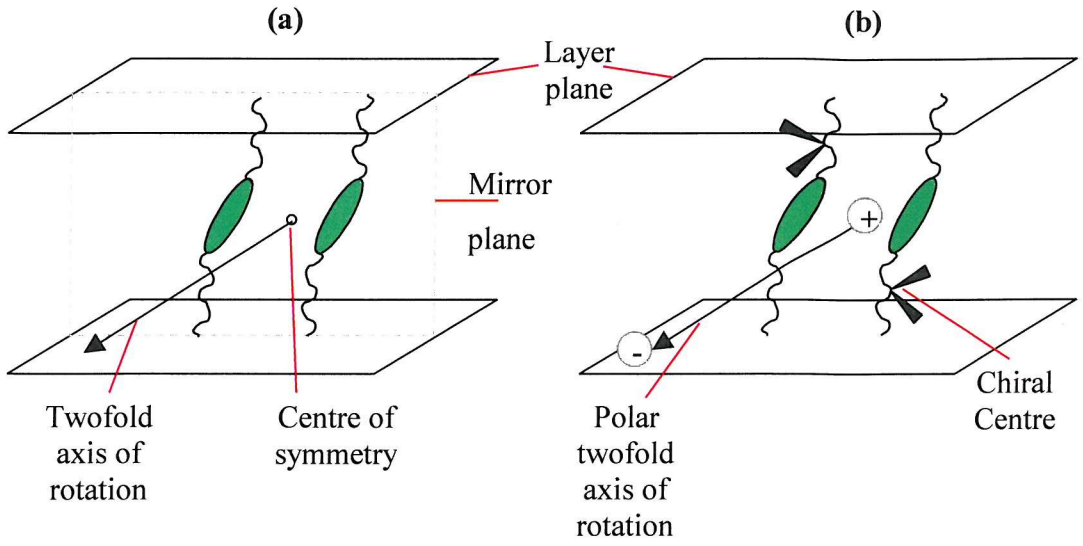

Figure 2.12 a) Non-chiral SmC mesophase; possesses a centre of symmetry and mirror plane. b) Chiral SmC* mesophase; no centre of symmetry or mirror plane.

As shown in Figure 2.13, the molecular dipoles align when the SmC* sample is subject to an applied electric field, and, as a result, the sample becomes polarised. Reversal of the applied field polarity results in the molecules rotating through an angle of 2θ around the cone (from +θ to -θ).

The local symmetry group of the SmC* phase is reduced to C_2, and since there is no mirror plane present (as the molecules are chiral) the material can be ferroelectric[15].

The P_s appears when the sample is cooled from the higher temperature phase, initially rising rapidly before tending towards a constant value if the phase transition is second order. Observation of the spontaneous polarisation property is often used to identify and characterise the SmC* mesophase, this is discussed in Section 3.5.1.

[15] R.B.Meyer, *Mol.Cryst.Liq.Cryst.*, **40**, 33, (1977)

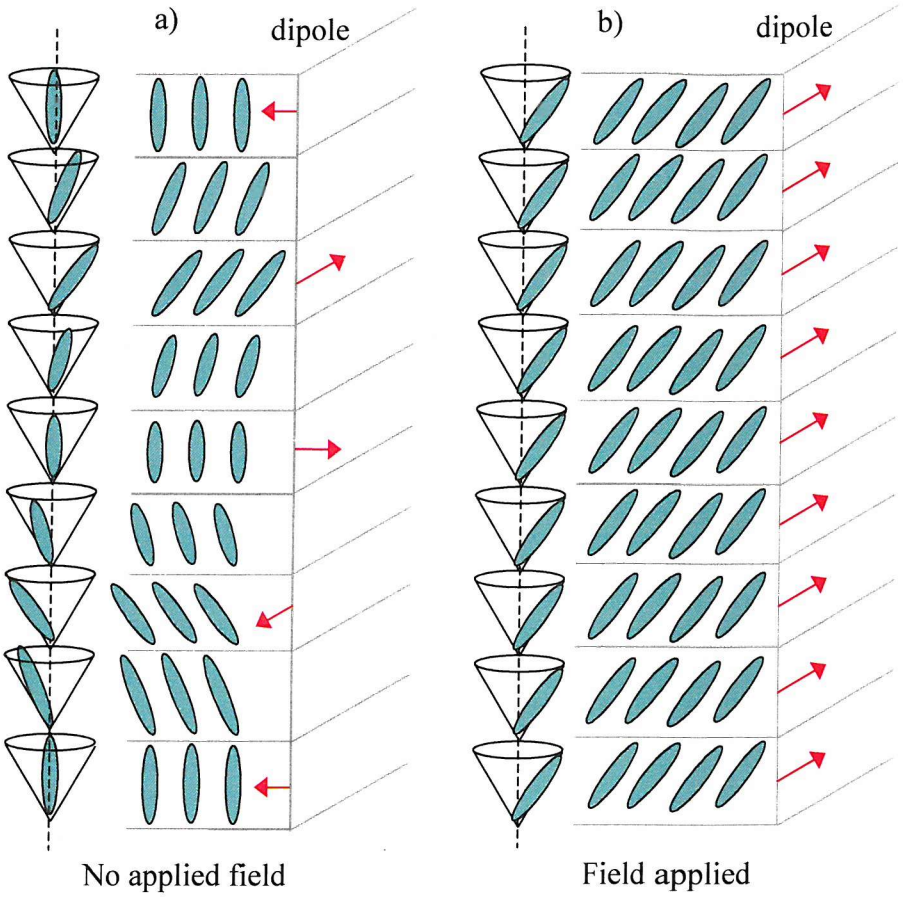

Figure 2.13 Schematic representation of the molecular arrangement in the chiral SmC (SmC*) phase in a) the absence of, and b) subject to, an applied electric field.

2.4.1.1 Electroclinic Effect

The electroclinic effect was reported for the first time by Garoff and Meyer[16]. The effect occurs in the SmA* phase near the SmA*-SmC* transition and is a field-induced tilt of the SmA* phases optic axis.

In an applied field, the optic axis rotates by angle θ, such that when the SmA* material is positioned between crossed polarisers the transmitted intensity is modified as shown:

[16] S.Garoff, R.B.Meyer, *Phys.Rev.A*, **19**, 338 (1979)

$$I = I_o \sin^2\left(2\psi_o + \theta_{(E)}\right), \tag{2-42}$$

where ψ_o is the angle between the optical axis of the liquid crystal and the transmission axis of the polariser.

The electroclinic effect can be understood in terms of the framework of Landau phase transition theory. The field dependent tilt angle, $\theta_{(E)}$, is given by

$$\theta_{(E)} \approx \frac{\mu_p \chi_\perp E}{A'} = e_c E \tag{2-43}$$

where e_c is the electroclinic coefficient and $A' = \alpha(T-T_c)$. Therefore, $e_c \rightarrow \infty$ as $T \rightarrow T_c$. The electroclinic effect also occurs for $T<T_c$ but is dominated by the Goldstone mode in the SmC* phase (which is related to the variation of the azimuthal angle, ϕ).

The switching time, τ_θ, of the director tilt angle in the electroclinic effect is independent of the applied electric field. It is defined only by the rotational viscosity, γ_θ, and the elastic modulus A'. The response time is governed by the Landau-Khalatnikov equation for the balance of viscous and elastic torques

$$\gamma_\theta \frac{\partial \theta}{\partial t} + A'\theta = 0 \tag{2-44}$$

with

$$\tau_\theta = \frac{\gamma_\theta}{A'} \tag{2-45}$$

It is the fastest of the electro-optical effects known in liquid crystals, with response times of $\tau \approx 1\mu s$ achievable at room temperature, for moderate applied fields.

2.4.2 Antiferroelectric Liquid Crystals (SmC_A^*)

Although the molecules in each smectic layer are oriented in the same way as the molecules in the SmC* phase, the chiral Smectic C antiferroelectric phase, SmC_A^*, exhibits some fundamental differences in behaviour. The molecules in any two adjacent layers are tilted in opposite directions with respect to the layer normal in the SmC_A^* state. As a result of this 'herringbone' structure[17], the macroscopic dipole of each layer is cancelled by the dipole of an adjacent layer and therefore the SmC_A^* phase possesses no intrinsic spontaneous polarisation, see Figure 2.14. Consequently, the antiferroelectric material has no net P_s in either the helicoidal or unwound structures.

Chandani et al[18] observed tristable switching between the two $\pm\theta$ states and a third stable state. In 1989 it was confirmed by Chandani et al[19] that these effects were the result of antiferroelectricity. The tristable switching is attributable to the electric field-induced transition between the antiferroelectric phase and the two equivalent states of a ferroelectric phase.

Antiferroelectric behaviour is commonly found in materials where the chiral centre is near the rigid aromatic core. Chandani postulated that strong asymmetric interactions affect the space symmetry. If the polar coupling is strong along the C_2 axis in the SmC* phase the effects can be reduced by having the direction of the polarisation alternate between the layers.

As in the SmC* mesophase, the chirality induces a slight precession in the tilt from layer to layer, leading to a helical structure with the axis perpendicular to the smectic layers.

---

[17] L.A.Beresnev, L.M.Blinov, M.A.Osipov, P.A.Pikin, *Mol.Cryst.Liq.Cryst.*, **158A**, 3 (1988)
[18] A.D.L.Chandani T.Hagiwara, Y.Suzuki, Y.Ouchi, H.Takezoe, A.Fukuda, *Jpn.J.Appl.Phys.*, **27**, L729 (1988)
[19] A.D.L.Chandani, Y.Ouchi, H.Takezoe, A.Fukuda, K.Terashima, K.Furukawa, A.Kishi, *Jpn,J.Appl.Phys*, **28**, L1261 (1989)

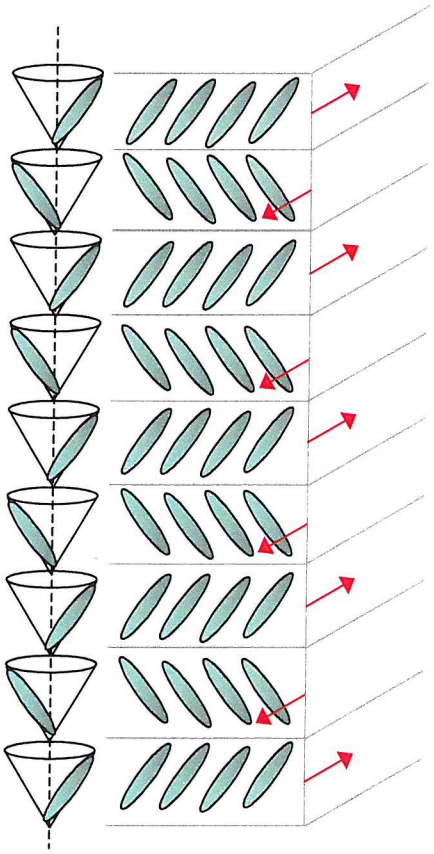

Figure 2.14 Schematic representation of the layer structure and molecular orientation in the unwound SmC_A* mesophase.

The occurrence of the SmC_A* phase can be confirmed by a number of different methods, and the reader is referred to the review article of Fukuda et al[20]. The techniques of relevance to the work in this thesis are detailed below.

[20] A.Fukuda, Y.Takanishi, T.Isozaki, K.Ishikawa, H.Takezoe, *J.Mater.Chem.*, **4**(7), 997 (1994)

2.4.3 Electro-Optic Switching in Ferroelectric and Antiferroelectric Liquid Crystals

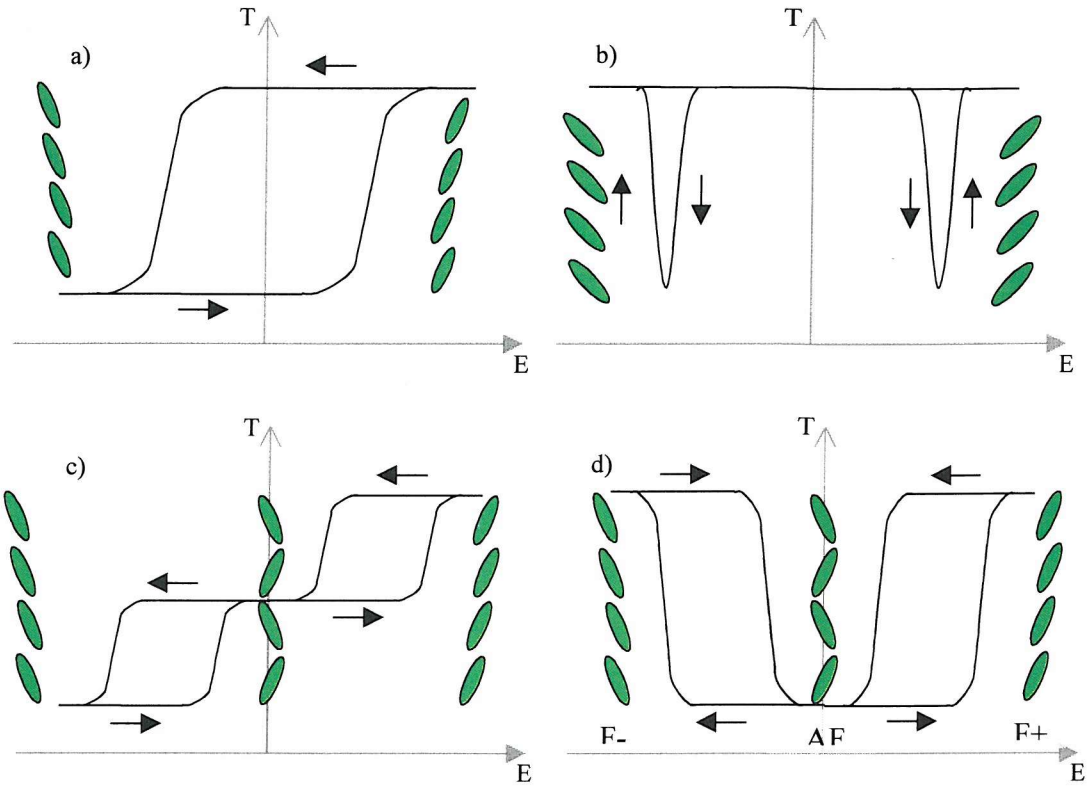

Figure 2.15 Optical hysterisis loops of the bi-stable and tri-stable switching in ferroelectric and antiferroelectric liquid crystals. a) and b) bi-stable switching in the ferroelectric state. a) The director in one switched state is parallel to the transmission axis of one of the polarisers, θ<22.5°. b) Switching is symmetric about the transmission axis of one of the polarisers. c) and d) Tri-stable switching in the antiferroelectric state. c) Antiferroelectric material aligned for maximum transmission when no field is applied, θ<22.5°. d) Antiferroelectric material aligned for minimum transmission in zero-field state, switching is symmetric about the transmission axis of one of the polarisers.

At low voltages there is no change in the tilt angle. At a critical field the antiferroelectric (AF) structure changes to ferroelectric (F) structure. The tilt angle increases dramatically and reaches a maximum in the SmC* phase. When a large electric field is applied, the layer ordering reverts back to that of the normal ferroelectric phase. Thus, when subjected to a square wave of magnitude in excess of this critical field, the AF materials exhibit the bistable switching of a ferroelectric liquid crystal, with a uniform tilting direction in the two switched states.

This switching between the antiferroelectric and ferroelectric order is also frequency dependant. At low frequencies the switching occurs via three stable states: F+, AF and F-, where the "+" and "-" states indicate the bipolar nature of the applied field. As the magnitude of the applied field is reduced, an antiferroelectric material in the F+ state relaxes back into the AF state and when the magnitude of the field reaches the critical threshold switching from the AF to F- state occurs. At high frequencies the switching is too fast for the relaxation to the AF state to occur and direct switching between the F+ and F- states is observed. At intermediate frequencies a mixture of these two processes occurs, resulting in the observation of a backward current peak[21] (see Figure 2.16 overleaf), which will be described in the following section.

The strength, or stability, of the antiferroelectricity in the SmC_A^* phase is defined as being highest for the material which has the highest critical field, i.e is able to withstand the highest applied field before the field induced transition to the ferroelectric state.

2.4.4 The Current Response of Ferroelectric and Antiferroelectric Liquid Crystals

The current response curves of SmC_A^* are more complicated than those of the SmC* phase as two peaks, not one, appear in the current response trace. The peak observed around the zero field is related to the relaxation from one ferroelectric state to the anti-ferroelectric structure. The other peak, occurring at higher fields, arises from a field-induced transition to the other ferroelectric state.

The position of this second current peak gradually shifts towards higher fields as the temperature decreases. The stronger fields required to induce the anti-ferroelectric to ferroelectric transition suggest an increase in the stability of the anti-ferroelectric structure at lower temperatures.

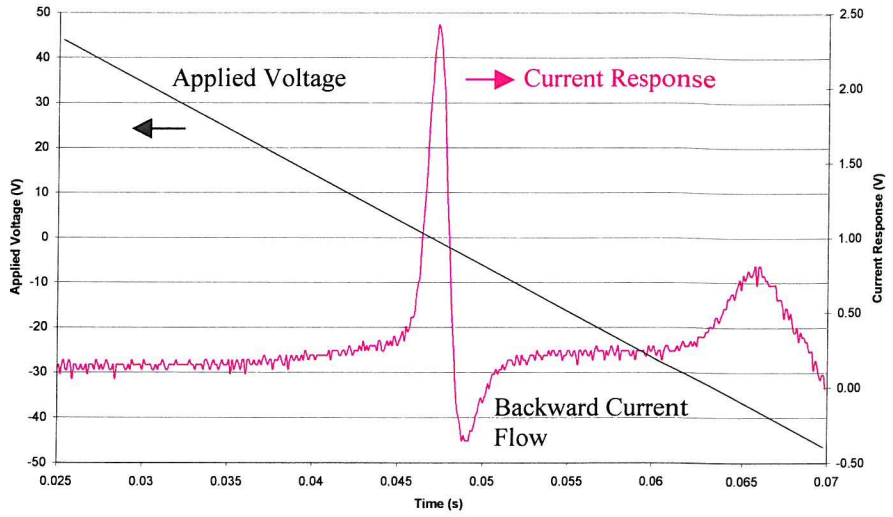

Figure 2.16 The typical current response of an antiferroelectric liquid crystal material.

The strong peak at zero field is often followed by a small backward current flow as the field is ramped. It has been proposed[21] that this peak is due to a direct switching process from one ferroelectric state to the other, followed by a backward transition to the antiferroelectric structure.

2.5 FLEXOELECTRIC LIQUID CRYSTALS

2.5.1 Flexoelectricity

When a liquid crystal possesses an electric polarisation, P, that is either spontaneous or induced, in addition to the 'quadratic in-the-field' coupling of external field with the dielectrically anisotropic medium, a 'linear in-the-field' interaction occurs, with free energy density **P.E**. This linear interaction is 'flexoelectricity'.

Molecules exhibiting dipolar flexoelectric behaviour have a strong shape anisotropy. In the absence of an applied field the molecular dipoles cancel out, resulting in no bulk polarisation. When a field is applied the permanent dipoles align with the field direction, the asymmetric molecular shape and the helical structure of chiral nematic liquid crystals causes a periodic splay-bend deformation to occur. Splay deformations are associated

with pear shaped molecules and bend deformations with banana shaped molecules, as illustrated in Figure 2.17. These orientational deformations result in the appearance of an induced bulk polarisation. The polarisation is given by the following equation[22]:

$$P_F = e_s \mathbf{n}(\nabla \cdot \mathbf{n}) - e_b (\mathbf{n} \times \nabla \times \mathbf{n}), \qquad (2\text{-}46)$$

where the flexoelectric polarisation, P_F, depends on the curvature of the director field (div**n**, curl**n**). Flexoelectricity does not arise as a result of chirality – it can occur in both chiral and achiral systems although the flexoelectro-optic effect refers explicitly to the effects of flexoelectro coupling in the N* phase.

The flexoelectric effect results in a distortion of the dielectrically stable configuration provided the director anchoring at the boundaries is weak. This differs from the Freedericksz transition[23] as the maximum angle of deformation occurs at the restricting boundary surface not in the middle of the sample. The angle of deformation is zero at the centre of a flexoelectrically-deformed sample.

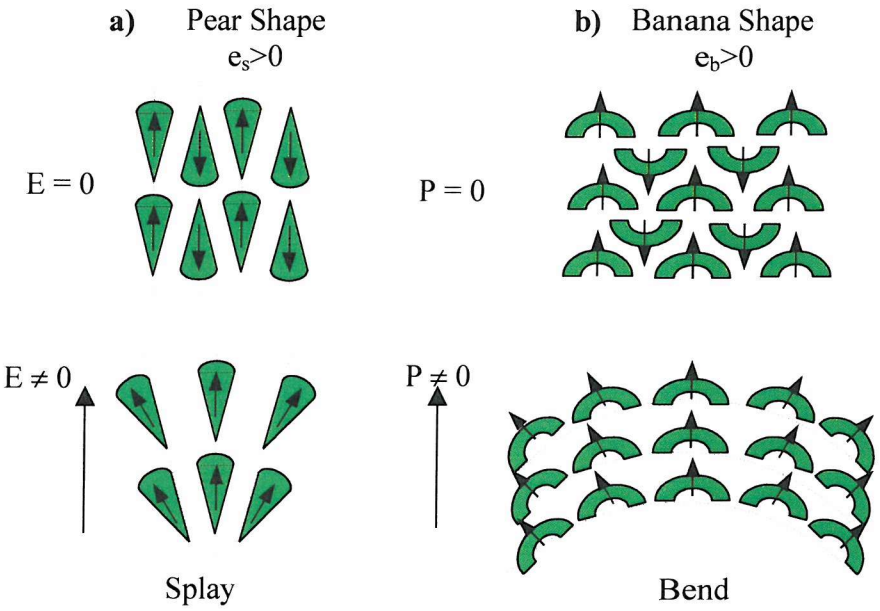

Figure 2.17 Splay and bend deformations induced by flexoelectric polarisation in a) pear and b) banana shaped molecules.

---

[21] M.Johno, K.Itoh, J.Lee, Y.Ouchi, H.Takezoe, T.Kitazume, *Jpn,J.Appl.Phys*, **29**, L107 (1990)
[22] R.B.Meyer, *Phys.Rev.Lett.* **22**, 918 (1969)
[23] V.Freedericksz, V. Zolina, *Trans.Faraday Soc.*, **29**, 919 (1933)

2.5.2 The Flexoelectro-Optic Effect

The flexoelectro-optic effect is a recently discovered phenomenon whereby a chiral nematic material switches flexoelectrically under the influence of an applied electric field. The effect is linear with amplitude of the applied field and therefore has potential applications in displays, optical switches and modulators where control of the tilt angle is of paramount importance.

The chiral nematic material is forced to adopt a uniform lying helix (ULH) texture in which the helical axis is uniformly aligned parallel to the walls of the cell. When viewed in this geometry from a direction orthogonal to the helix axis, the chiral nematic material has the appearance of a uniaxial, negatively birefringent sample. When a low amplitude alternating electric field is applied across the cell, flexoelectric coupling between the chiral nematic molecules and the field causes a rotation of the director plane of the material. As the optical axis of a short pitch chiral nematic material lies normal to the director plane, the flexoelectric coupling causes a rotation of the optic axis, as shown in Figure 2.18. If the cell is placed between crossed polarisers an optical switching effect is observed.

As the polarisation in the field occurs uniformly throughout the volume of the sample, the torque required to rotate the director through an angle, ϕ, only occurs at the surface. Hence, in order for the flexoelectric distortion to occur, it is necessary that the anchoring of the liquid crystal at the surface boundary is weak. Assume the director components parallel to the z, y plane are given by

$$\mathbf{n}_z = \cos\phi \tag{2-47}$$

and

$$\mathbf{n}_y = \sin\phi . \tag{2-48}$$

The free energy density of the system in an electric field is given by

$$g = \frac{1}{2}K\left(\frac{\partial\phi}{\partial y}\right) + \frac{1}{2}K_{22}\left(q_o - \frac{\partial\phi}{\partial x}\right)^2 - e_f E\frac{\partial\phi}{\partial y} + \frac{1}{8\pi}\Delta\varepsilon E^2\sin^2\phi , \tag{2-49}$$

where $K = K_{11} = K_{33}$.

For negligible $\Delta\varepsilon$, i.e. $\Delta\varepsilon \to 0$, minimising Equation 2.49 above results in

$$\frac{\partial\phi}{\partial x} = q_o \qquad \text{and} \qquad \frac{\partial\phi}{\partial y} = \frac{e_F E}{K}. \tag{2-50}$$

If the wavevector **k** represents the rotation of the helical axis,

$$|\mathbf{k}|\cos\phi = q_o \tag{2-51}$$

and

$$|\mathbf{k}|\sin\phi = \frac{e_F E}{K}. \tag{2-52}$$

Thus the angle of rotation is

$$\tan\phi = \frac{e_F E}{q_o K}, \tag{2-53}$$

which is linear in E for small angles.

Assuming the pitch does not change when the electric field is applied, $|\mathbf{k}| = q_o$. The free energy becomes a function of ϕ only:

$$\eta\frac{\partial\phi}{\partial t} = -Kq_o^2\phi + e_F E q_o, \tag{2-54}$$

where η is the effective viscosity coeffiecient for helix rotation.

It follows that the relaxation time is independent of the applied field;

$$\tau = \frac{\eta}{Kq_o^2}. \tag{2-55}$$

If the sample is viewed between crossed polarisers, the transmission is modulated as

$$I = I_o \sin^2(2\phi)\sin^2\left(\frac{\delta}{2}\right), \tag{2-56}$$

where $\delta = \frac{2\pi\Delta nd}{\lambda}$ is the optical phase delay of the sample.

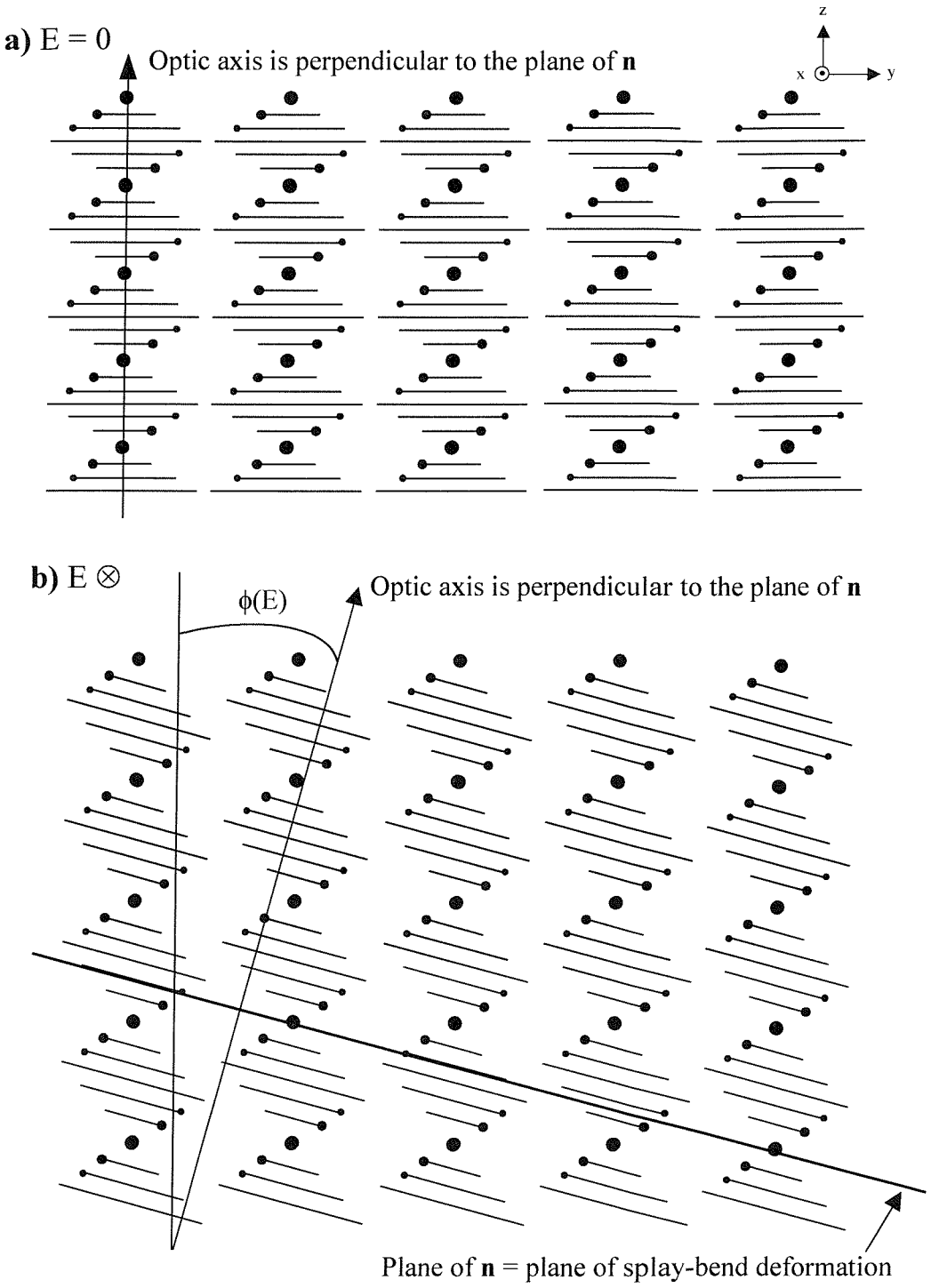

Figure 2.18 To observe the flexoelectro-optic effect the helix of the short pitch chiral nematic should lie in the plane parallel to the glass cell plates, the so-called uniform lying helix, ULH, texture. In this geometry, application of an electric field across the cell causes the layer planes to tilt – resulting in a rotation of the optic axis.

2.6 Optics of Liquid Crystal Displays (LCD's)

The anisotropy of the dielectric constant was discussed in §2.3.1. Under the influence of an applied electric field the liquid crystal director will reorient such that the maximum dielectric constant is parallel to the field. Numerous liquid crystal display devices utilise the fact that the optic axis of the material can be switched between two states of orientation.

2.6.1 The Twisted-Nematic (TN) Display

The electro-optical effect that eventually brought a breakthrough for the LCD industry was the twisted nematic (TN) cell, which was invented by Schadt and Helfrich in 1970[24].

In a TN-LCD the liquid crystal molecules lie between glass plates, which are treated with a special orientation layer (usually a 'rubbed' polyimide). Liquid crystal layers of up to several hundred microns can be aligned by anisotropic mechanical boundary forces from specially treated substrates. When a liquid crystal is in contact with a substrate that has been coated with a uniformly rubbed polymer layer, the long molecular axes of the liquid crystal molecules become aligned parallel to the substrate, and along the brushing direction. In a TN device the rubbing directions of the orientation layers on opposing substrates are aligned perpendicular to each other, such that the director is forced to point in a particular direction near one of the plates and perpendicular to that direction near the other plate. As a result, the director profile performs a 90° twist over the thickness of the liquid crystal layer, forming a helical "twisted nematic" structure.

The optics of the TN-cell in its off-state are based on an effect typical of liquid crystals observed by Mauguin[25] in 1911. The polarization of light follows any slow variation in the direction of the optical axis. Consequently a twisted director structure, such as that of the TN device, rotates the polarisation plane through the twist angle of the structure. This

[24] M.Schadt, W.Helfrich, *Appl. Phys. Lett.*, **18**, 127 (1971)
[25] C.Mauguin, *Bull.Soc.Fr.Miner.*, **34**, 71 (1911)

waveguide regime takes place when the Mauguin limit is satisfied. The Mauguin limit is defined as

$$\frac{d\Delta n}{\lambda} >> 1, \tag{2-57}$$

where Δn is the birefringence of the sample, d is the thickness of the sample and λ is the wavelength of the incident light.

This waveguiding mode is achromatic; there is no birefringence effect. Low birefringence materials are preferable due to the Mauguin limit as thicker cells are easily fabricated. High birefringence materials tend to appear coloured between crossed polarisers, resulting in a reduction of the optical contrast.

The polarisation follows the 90^{o} twist of the nematic material if the Mauguin limit is satisfied. When the film is placed between the crossed polarisers, this arrangement allows the light to pass through, yielding a bright 'field off' state. However, when an electric field is applied across the film, director coupling causes the director to align with the field and the liquid crystal will consequently lose its twisted structure, destroying the waveguiding property. Therefore, linearly-polarised light entering the crystal will not have its polarisation rotated and will not be able to penetrate through the other polariser, resulting in a dark 'field on' state. In some displays the polarisers are set parallel to each other, thus reversing the on and off states.

The 90° rotation of polarisation described here is an over-simplification and Gooch and Tarry[26] have shown that actually the linearly polarised light becomes elliptically polarised light as it propagates through the twisted nematic structure. Their work showed that the intensity of radiation transmitted through a 90° twisted liquid crystal cell between parallel polarisers, as opposed to the earlier discussion based on orthogonal polarisers, is given by

$$T = \frac{\sin^2\left[\left(\pi/2\right)\sqrt{1+u^2}\right]}{1+u^2} \qquad (2\text{-}58)$$

where $u = \frac{2d\Delta n}{\lambda}$.

The Gooch-Tarry curve, defined by equation 2.58 and shown in Figure 2.19 predicts a transmission that oscillates with the value of the general parameter , u, and increases as the wavelength decreases.

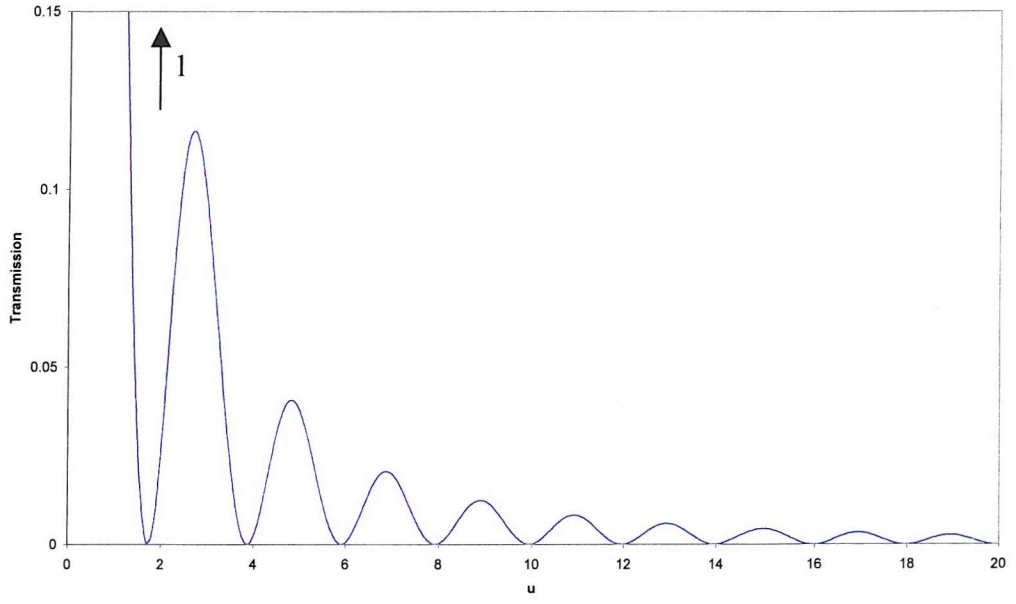

Figure 2.19 The Gooch-Tarry curve, showing off-state transmission for a 90° twisted nematic cell between parallel polarisers as a function of u=2dΔn/λ.

The important features of the rotation of light by the twisted nematic layer are a) ideal rotation of the plane of polarisation is obtained for large values of dΔn and at specific

[26] C.H.Gooch, H.A.Tarry, *Electonics Lett.*, **10**, 2 (1973)

(approximately even-integer) values of u and b) at other values of $d\Delta n$, linearly polarised light is changed into an elliptical polarisation in which the major axis of the ellipse is rotated with respect to the input polarisation.

These results can have a significant bearing on the design of specific devices in which the contrast between the two states is important. Thus, there are two ways of achieving near ideal operation; to design the twisted nematic structure for a fixed value of u and use monochromatic light, or to operate at large values of u (i.e where the Mauguin condition is fulfilled).

In the construction of the TN cell the nematic director is usually inclined to the glass plate at the '*surface tilt*' or '*pretilt*' angle, which is approximately $1^{\circ} \sim 3^{\circ}$. If a TN cell has no pretilt angle, it is not determined which molecular edge of the liquid crystal will rise to the applied voltage, resulting in viewable domains in the cell. Therefore pretilting is necessary for the TN cell to make a predetermined switch.

When an electric field is applied across the electrodes of a twist cell filled with a material with positive dielectric anisotropy a reorientation effect occurs that is a combination of the splay, bend and twist deformations[27].

The response times are usually denoted by τ_{on} and τ_{off} and they correspond to the amount of time between the application or removal of the voltage and a 90% decrease or increase in the optical response respectively. Normally τ_{off} is slightly larger than τ_{on} because, rather than being driven by the applied field the switching is driven solely by surface forces; the original planar order is restored by the elastic properties of the material, together with other intermolecular forces. Switching times can be changed by controlling the amount of orientational viscosity (or the resistance to a change in direction) in the liquid crystal and this can be seen clearly in the expressions for τ_{on} and τ_{off} of a twisted nematic display:

$$\tau_{on}^{(TN)} = \frac{\gamma_1 \cdot d^2}{\varepsilon_0 \cdot \Delta\varepsilon}(V^2 - V_{th}^2)^{-1}, \tag{2-59}$$

$$\tau_{off}^{(TN)} = \frac{\gamma_1 \cdot d^2}{K \cdot \pi^2} \quad . \tag{2-60}$$

The applied voltage, V, and the spacing of the electrodes, d, are external parameters whilst K is a function which depends on the elastic constants of the liquid crystal. V_{th} is the threshold voltage (see below). A decrease in the rotational viscosity, γ_1, will lead directly to shorter switching times and better display performance.

The voltage required to turn a pixel on in the display can be measured in two ways: the first method is to measure a simple threshold voltage, V_{th}, which is the amount of voltage across a pixel required to produce any optical response at all. V_{th} is defined by

$$V_{th} = \sqrt{\frac{\pi^2 K_{11} + \Phi^2 (K_{33} - 2K_{22})}{\varepsilon_0 (\varepsilon_{\parallel} - \varepsilon_{\perp})}} \quad , \tag{2-61}$$

where Φ is the amount of twist (e.g. $\pi/2$) before the field has been applied and K_{ii} are the Frank elastic constants.

A low V_{th} is obviously desirable and this can be achieved by using a material with a large $\Delta\varepsilon$; generally found in materials with a strong polar terminal group, (where $\Delta\varepsilon = \varepsilon_{\parallel} - \varepsilon_{\perp}$). Also, a decrease in K_{11} and K_{33} and an increase in K_{22} would lower V_{th}. The alternative method is a measure of the 'sharpness' of the optical response and is calculated by finding the difference in voltage needed to go from 10% to 90% brightness ($V_{90} - V_{10}$).

2.6.2 The Dual Frequency TN Display

In the twisted nematic (TN) display, described in the previous section, the "on" state is induced by the electric field and the off state is induced by surface effects. The "on" and

---

[27] M.Schadt, W.Helfrich, *Appl.Phys.Lett.*, **18**, 127 (1971)

"off" response times are principally governed, according to equations 2-59 and 2-60, by the magnitude of the applied field and the intrinsic viscosity of the system respectively. A variation of the TN display device that improves the "off" response time is detailed in this section.

The frequency dispersion characteristic of the dielectric anisotropy was described in §2.3.1. A decrease in the decay time can be achieved if, as a result of low frequency relaxation of $\varepsilon_{\|}$, $\Delta\varepsilon$ becomes negative at a certain frequency. Materials that possess low-frequency relaxation of $\varepsilon_{\|}$ have potential for improving the response times and modifying the threshold properties of TN devices. By switching the frequency of the applied voltage between frequencies above and below the critical frequency, ν_c, the sign reversal of $\Delta\varepsilon$ can be used to orient the liquid crystal director. If $\Delta\varepsilon$ is positive the preferred director orientation results in alignment of the optic axis normal to the electrodes. Conversely, if $\Delta\varepsilon$ is negative the optic axis will be aligned parallel to the electrodes.

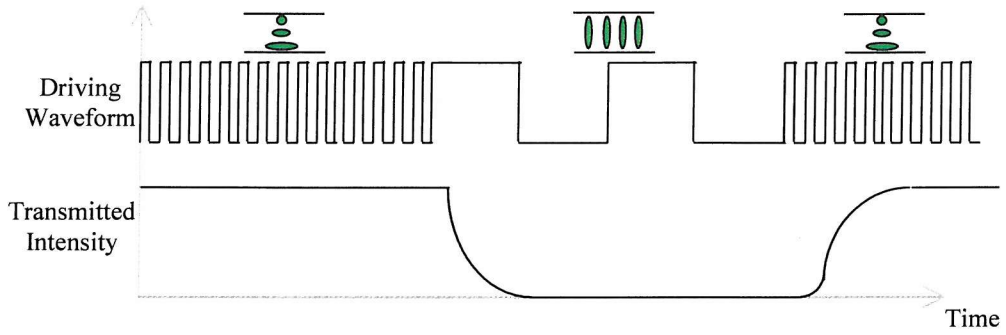

Figure 2.20 The driving scheme and molecular orientation of a typical dual frequency TN liquid crystal display.

As Figure 2.20 shows, at driving frequencies below ν_c, $\Delta\varepsilon$ is positive and the material is forced to orient with its optic axis normal to the electrodes. The reorientation process destroys the 90° twist and the transmission decreases. At driving frequencies above ν_c, $\Delta\varepsilon$ is negative and the molecules are driven back to lie parallel to the electrodes. The alignment layers subsequently confer the twisted geometry back on the nematic liquid crystal and the transmission returns to a maximum. Thus the field, rather than surface and

intermolecular forces, drives the molecules back to the planar alignment. As a result, an improvement in the response time is observed.

Figure 2.21 shows the driving scheme for a dual frequency TN display should use frequencies well above and below ν_c as this will maximise $\Delta\varepsilon$ and minimise V_{th}.

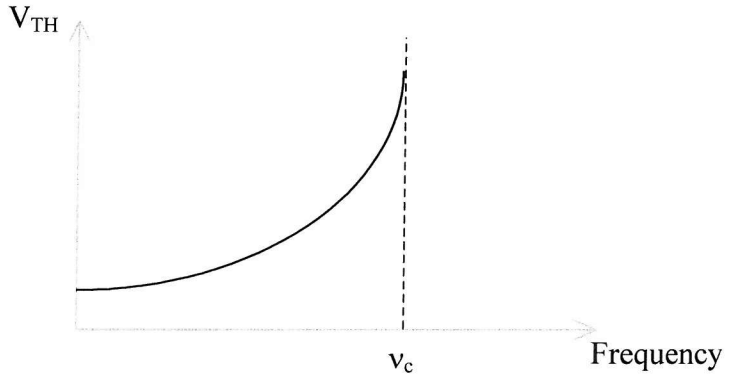

Figure 2.21 The variation of the threshold voltage V_{th} as a function of frequency of the applied field. As the frequency of the applied field approaches the critical frequency, ν_c, the dielectric anisotropy is reduced, resulting in a larger voltage being required to produce switching.

2.6.3 The Surface-Stabilised Ferroelectric Liquid Crystal Display

In order to utilise the macroscopic polarisation of ferroelectric liquid crystals, a surface stabilised cell (SSFLC)[28] is constructed from a very thin layer of SmC* liquid crystal sandwiched between two glass surfaces. The boundary conditions imposed by the surface interactions will then suppress, or unwind, the helix. If the layering is retained, two stable states, (a) and (b) as shown in Figure 2.22, exist in which the molecules align along the cone angle and parallel to the cell surfaces. The properties characteristic of a ferroelectric material such as macroscopic polarisation, hysterisis and bistability will then be observed. The application of an electric field causes the molecules to rotate so that all the dipoles lie parallel to the field.

---

[28] N.A. Clark, S.T. Lagerwall, *Appl.Phys.Lett.*, **36**(11), 899 (1980)

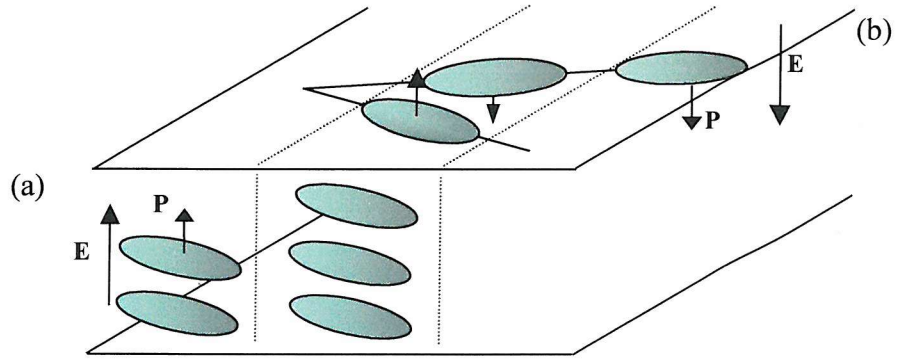

Figure 2.22 The SSFLC structure. The molecular orientation is constrained to two positions on the smectic cone. Reversal of the polarity of the applied field results in switching between these two thermodynamically stable states.

When the magnitude of the applied field is large enough to overcome the surface boundary forces the entire sample reorients uniformly, with a characteristic time

$$\tau = \frac{\gamma}{P_s E}, \tag{2-62}$$

where γ is the rotational viscosity, P_s is the spontaneous polarisation and E is the applied electric field.

Optically the SSFLC may be considered to be uniaxial, and so when placed between crossed polarisers the transmission of light, of wavelength λ, normal to the cell is given by

$$I = I_o \sin^2(2\alpha)\sin^2\left(\frac{\pi d\Delta n}{\lambda}\right) \tag{2-63}$$

where I_o is the intensity of the incident light, α is the angle of the optic axis of the SSFLC measured relative to the polarisation of the incident light, d is the thickness of the SSFLC and Δn is the birefringence of the liquid crystal material. If the SSFLC is oriented such that the optical axis in one of the states lies parallel to the polarisation direction of the incident light we obtain a minimum for I. If the cell is then switched to the other state the optic axis rotates through an angle of 2θ and the transmitted intensity is given by

$$I = I_o \sin^2(4\theta)\sin^2\left(\frac{\pi d\Delta n}{\lambda}\right). \tag{2-64}$$

2.6.4 Flexoelectro-Optic Displays

The flexoelectro-optic effect is readily observed in parallel plate cells in which the helix axis of a hypertwisted chiral nematic is uniformly aligned parallel to the glass cell plates, in the uniformly lying helix (ULH) texture, a schematic of which is given in Figure 2.23.

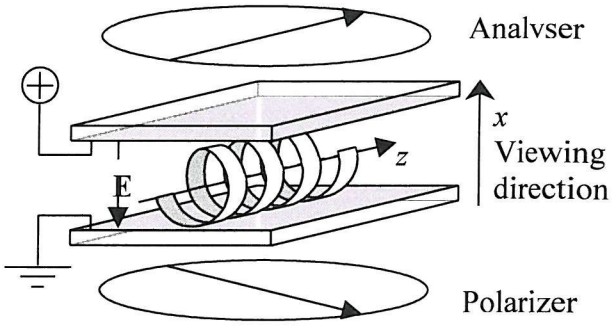

Figure 2.23 The cell geometry required in order to view the flexoelectro-optic effect.

With no external field applied this configuration behaves as a uniaxial birefringent material, with its optic axis parallel to the helix axis, see Figure 2.24(a). As described in §2.5.2 an electric field applied across the cell plates, normal to the helix axis, causes a rotation of the director plane, see Figure 2.24(b). This distortion of the helix results in a periodic splay-bend deformation perpendicular to the macroscopic optic axis. The net result of the applied field is that the system behaves as if the optic axis is rotated in a plane parallel to the glass plates, as was first shown by Meyer and Patel in 1987[29].

This affect arises due to flexoelectric coupling, which is linear in the electric field and hence results in a linear electro-optic response. The angle of rotation, ϕ, is given by the relationship[19]:

$$\tan\phi = \frac{\bar{e}}{k\kappa}E \qquad (2\text{-}65)$$

where $\bar{e}$ is an effective flexoelectric coefficient $\quad \bar{e} = (e_s + e_b)/2$,

κ is an effective elastic constant $\quad \kappa = (K_{11} + K_{33})/2$

and k is a function of the pitch length $\quad k = 2\pi$ / Pitch.

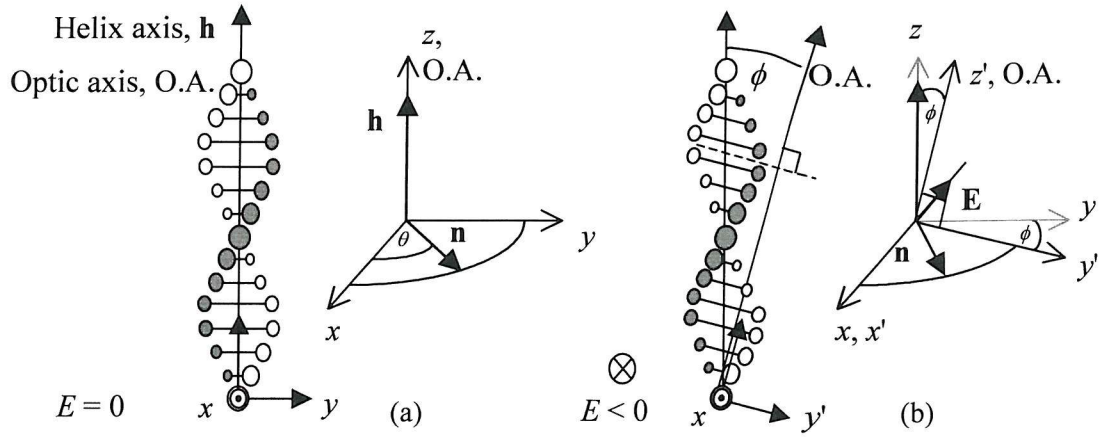

Figure 2.24 (a) An undisturbed chiral nematic material with right-handed helicity, the directors are confined to the xy-plane, orthogonal to the helix and optic axes. (b) The effect of an electric field applied along the –x direction: the director plane

Hence for small angles, where $\phi \approx \tan(\phi)$, the tilt angle is linearly proportional to the applied electric field, E. The magnitude of the tilt angle is also approximately temperature independent, providing the pitch does not change significantly with temperature. The reason for this temperature invariance is that since ϕ is proportional to $\bar{e} / \kappa$, and both $\bar{e}$ and κ vary with the square of the order parameter[30,31], S, so that $\bar{e} / \kappa$ is constant with temperature, so that ϕ is constant with temperature.

Flexoelectric switching has short response times[32], τ, often in the microsecond range. The response times are given by

$$\tau = \frac{\gamma_1}{k^2 \kappa} \quad , \tag{2-66}$$

where γ_1 is the effective viscosity related to the helix distortion.

---

[29] J.S.Patel, R.B.Meyer, *Phys. Rev. Lett.*, **58**, 1538 (1987)
[30] G.Vertogen, W.H.de Jeu, *Thermotropic Liquid Crystals, Fundamentals*, Springer series in Chemical Physics 45 (Berlin:Springer-Verlag) (1988)
[31] M.A.Osipov, 1983, *Sov. Phys. JETP*, **58**, 1167 (1983)
[32] J.S.Patel, S-D.Lee, *J. Appl. Phys.*, **66**, 1879 (1989)

2.7 SUMMARY

This chapter has built on the introduction to the liquid crystal phase given in Chapter 1. Landau theory was used to describe first and second order phase transitions and static continuum theory was introduced to discuss the anisotropy of elastic constants. The optical and dielectric properties of liquid crystal materials were then discussed. As a precursor to the work in the following chapters, a detailed description of the ferroelectric SmC* and antiferroelectric SmC_A* phases was given and the flexoelectric effect was described. Finally, the liquid crystal phases described in the preceding sections were discussed in terms of their use in display applications. The next chapter describes the experimental techniques used to identify the liquid crystal phases and characterise the properties described in this chapter.

Chapter Three

EXPERIMENTAL TECHNIQUES

3.1 INTRODUCTION

A theoretical discussion of the fundamental properties of the liquid crystalline systems relevant to this thesis was presented in Chapter 2. This chapter will discuss the experimental techniques employed to identify the mesophases and measure their properties.

The chapter begins with a discussion of the main features of the experimental assembly (§3.2). The majority of studies are carried out on a polarising microscope with the sample positioned in a heating stage so that temperature dependence could be investigated. Electro-optical investigation requires a means of applying an electric field across the liquid crystalline material to be studied.

Initial studies of a new material are solely concerned with determining the transition temperatures of the phases of interest. Several differing techniques are available for the clarification of a materials phase sequence. These are introduced in §3.3. Once the phase sequence is known, characterisation of the individual phases can commence. Sample and cell preparation procedures are discussed in §3.4

Although the basic apparatus remains the same, the full and complete characterisation of each liquid crystalline phase requires slightly different measurements to be made. A detailed description of the experimental techniques employed to characterise the nematic and ferroelectric mesophases is presented in Sections 3.5.1, 3.5.2 and 3.5.3.

New apparatus was built primarily to facilitate high resolution, fast and continuous tilt angle measurements in ferroelectric liquid crystals. In the course of the work presented in this thesis it was also found to be particularly useful for the measurement of the optic axis tilt angle in flexoelectric systems. The design and operation of this apparatus is discussed in §3.5.2.3. Finally, the chapter is summarised in §3.5.3

3.2 EXPERIMENTAL APPARATUS

3.2.1 Overview

The system to be detailed in this section enabled the study and measurement of the optical and electrical properties of the materials to be undertaken.

The majority of the optical observations and measurements undertaken in this thesis were carried out on a polarising microscope. The temperature of the specimen was controlled by a heating stage, positioned on the rotating sample stage of the microscope, and a controller. All observations and measurements were undertaken with the polariser and analyser crossed at 90° to each other, unless otherwise stated. The sample is illuminated from below, such that light passes through the polariser and sample, the analyser will then only transmit light if the sample is optically anisotropic. The birefringence textures thus observed are characteristic of the individual states of matter.

For electro-optical measurements the samples were held in specially prepared cells (described in §3.4). A function generator, in combination with a high-voltage amplifier, was used to produce a variety of electrical signals across the cell electrodes. The amplified voltage is monitored using a digitising oscilloscope. A photodiode measures the optical response of the sample and the resulting signal is amplified and subsequently displayed as a voltage on the digitising oscilloscope.

Electrical measurements also required a current-to-voltage amplifier to be connected across the cell electrodes. This enabled the electrical response of the sample to also be displayed as a voltage on the oscilloscope.

A computer was interfaced to the temperature controller, function generator and the digitising oscilloscope to allow measurements as a function of temperature, voltage or frequency to be automated.

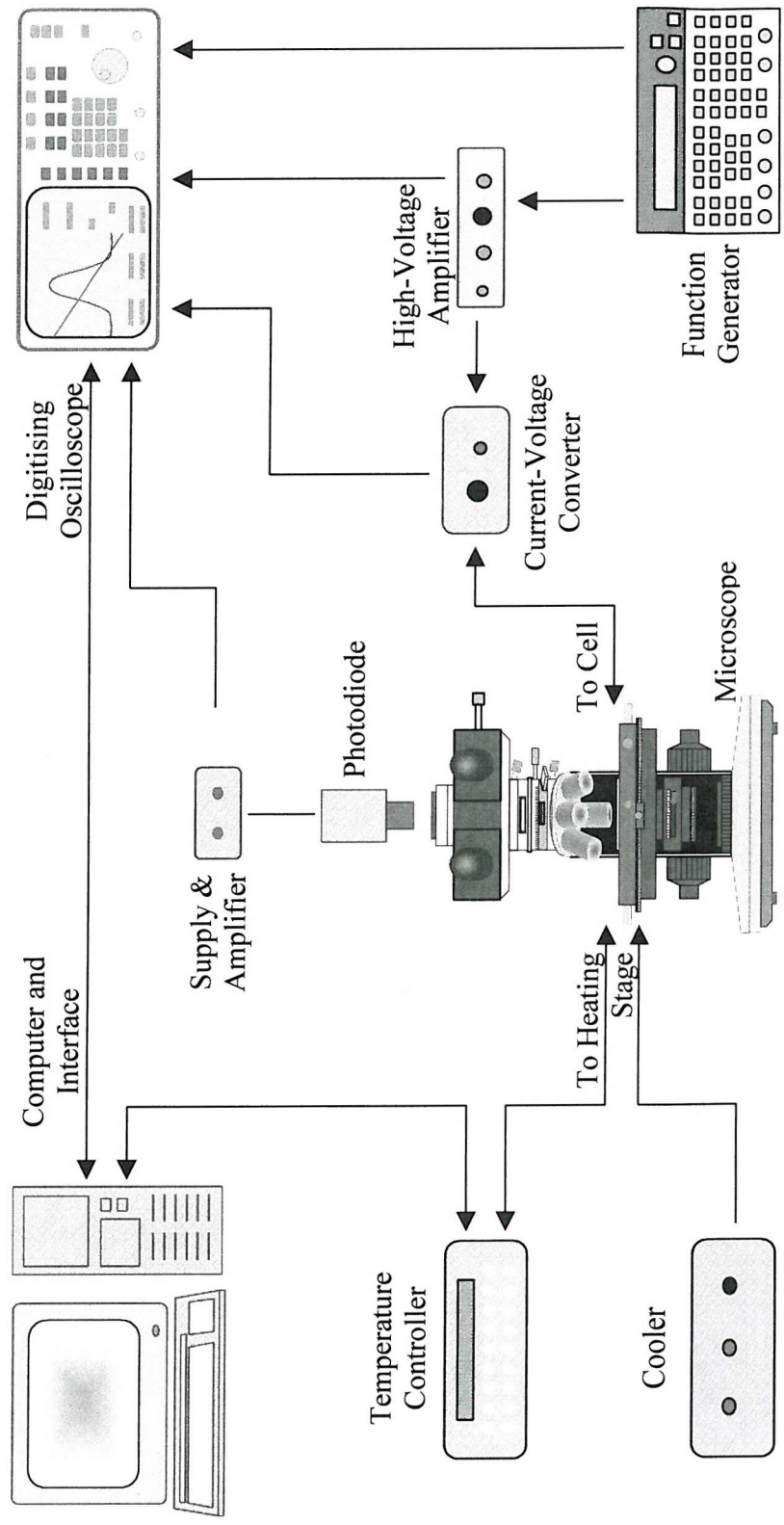

Figure 3.1 Schematic representation of the experimental apparatus used to characterise the liquid crystalline properties of a material.

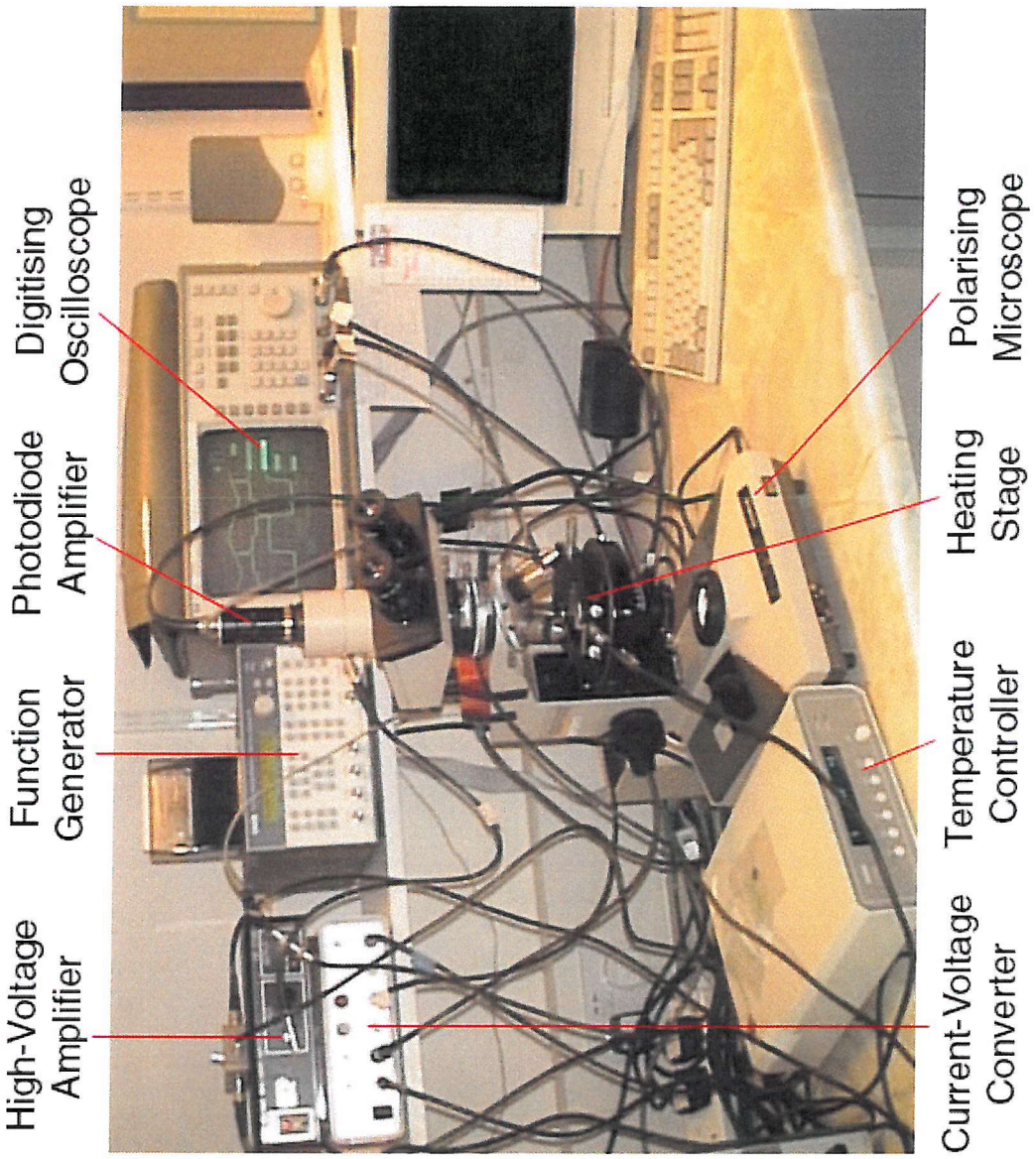

Figure 3.2 Basic electro-optical apparatus.

3.2.2 Polarising Microscope

An Olympus[1] BH-2 polarising microscope, shown in Figure 3.3, with infinity corrected optics was employed for sample observation. The use of infinity corrected objectives

[1] Olympus Optical Co. (UK) Ltd., Great Western Industrial Park, Southall, Middlesex, UK, UB2 4SB. http://www.olympus.co.uk

allows additional optical components to be inserted into the microscope tube. The 'plan' type objectives correct the field curvature and result in the image being focussed on a flat plane. The numerical aperture (N.A.) of the condenser was always matched to that of the objective in order to achieve good resolution. The objectives were held in the rotating nosepiece and had magnifying powers of 4x (N.A.=0.1), 10x (0.25), 20x (0.4) and 40x (0.65). Combined with the 10x magnification of the eyepiece, magnification of up to 400x was attainable.

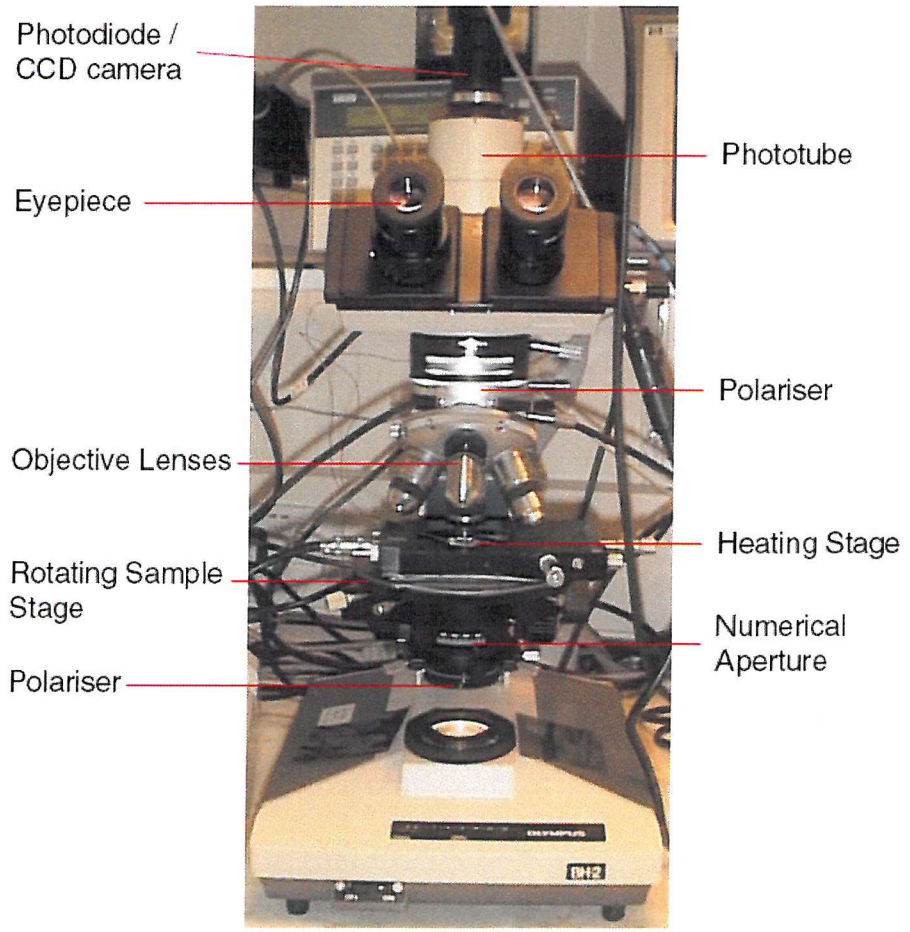

Figure 3.3 The Olympus BH-2 polarising microscope.

The majority of observations were undertaken with the polarisers crossed, i.e. with the transmission axes of the polarisers aligned perpendicularly to each other. In this situation the analyser (upper polariser) only transmits light if the sample is optically anisotropic.

The trinocular head allowed for a photodiode or camera to be attached, as well as providing two eyepieces for use during textural observations. The micrographs of textures within this thesis were obtained using a JVC CCD video camera[2] (model number KY50) and Optimas 6.5 image analysis software[3]. An NFK photo eyepiece (magnification 2.5x) is inserted into the phototube before the camera is mounted onto the microscope in order to focus the image onto the CCD array. No eyepiece was required when using the photodiode, which is also inserted in the top of the phototube.

Located between the two rotating polarisers, whose position can be known to an accuracy of $\pm 0.25^{\circ}$, is a rotating sample stage, which can also be positioned to an accuracy of $\pm 0.25^{\circ}$. Centered on the rotating stage is a heating stage to control the sample temperature.

3.2.3 Heating Stage & Temperature Controller

A silver block heating stage and LINKAM[4] TP91 temperature controller enabled the temperature of the sample to be controlled to an accuracy of $0.1^{\circ}C$ over a range of temperatures, generally from room temperature up to $150^{\circ}C$. Heating and cooling rates of between 0.1 and $5^{\circ}C$ per minute were used throughout the course of this work. A 2mm-diameter mica or quartz window in the centre of the heating block allows for the simultaneous heating and observation of the cell. The heating stage incorporates a detachable window to insulate the sample from the ambient room temperature. Without the window in place the sample cell could be directly accessed to allow concurrent heating and mechanical shearing of the sample, which was necessary to obtain good alignment in several of the materials studied in this thesis. In order to facilitate measurements below the ambient laboratory temperature it was necessary to pass a supply of nitrogen gas through the silver block in conjunction with a pump.

---

[2] Supplied by Vision Base Ltd., Vision House, 2 Toseland Way, Reading, BerkshireUK, RG6 7YA.
[3] Media Cybernetics, Optimas 6.5, http://mediacybernetics.com
[4] Linkam Scientific Instruments Ltd, 8 Epson Downs Metro Centre, Tadworth, Surrey, UK, KT20 5HT. http://www.linkam.co.uk

The temperature controller was programmable and interfaced to a PC via an RS232 cable, enabling the sample to be left to align unattended and automated measurements of physical properties versus temperature to be made.

3.2.4 Photodiode Amplifier

This was used to detect the optical signal in measurements of the electro-optical effects carried out in this thesis. The photodiode amplifier, PDA, was supplied by Thorlabs[5], model number PDA55). The silicon photodiode, model FDS100, had a spectral response from 350nm to over 1100nm with the peak spectral response occurring at 900nm. The active area was 13.7mm^2 and the response time of 10ns was sufficiently fast to follow the electro-optic response of all the materials studied in this thesis.

A specially machined holder[6] allowed for the PDA to be fitted into the photo-tube of the microscope from where changes in the light intensity could be detected. The optical response of the system, measured as a voltage by the PDA, was displayed on the oscilloscope. The PDA response to changes in the transmitted light intensity was employed in the measurement of all the electro-optic effects presented in this thesis

The linearity of the PDA's response to changes in the transmitted light intensity was confirmed by measuring the light intensity whilst rotating the analyser with respect to the polariser in conjunction with Malus' Law[7];

$$I = I_0 \sin^2 \phi, \qquad (3\text{-}1)$$

where I is the transmitted light intensity, I_0 is the light intensity incident on the first polariser and ϕ is the angle between the transmission axes of the polarisers.

The response of the PDA as a function of $\sin^2\phi$ is shown in Figure 3.4. The relationship is linear with a correlation coefficient of 0.9996. A small signal was found to exist when the

[5] Thorlabs, P.O. Box 366, Newton, NJ, USA 07860-1453. http://www.thorlabs.com
[6] Mechanical Workshop, Dept. of Physics and Astronomy, University of Southampton, Southampton, UK, SO17 1BJ

polarisers were perpendicular. This was attributed to a combination of the inability of the polarisers to extinguish all the light and a small bias in the amplified photodiode signal.

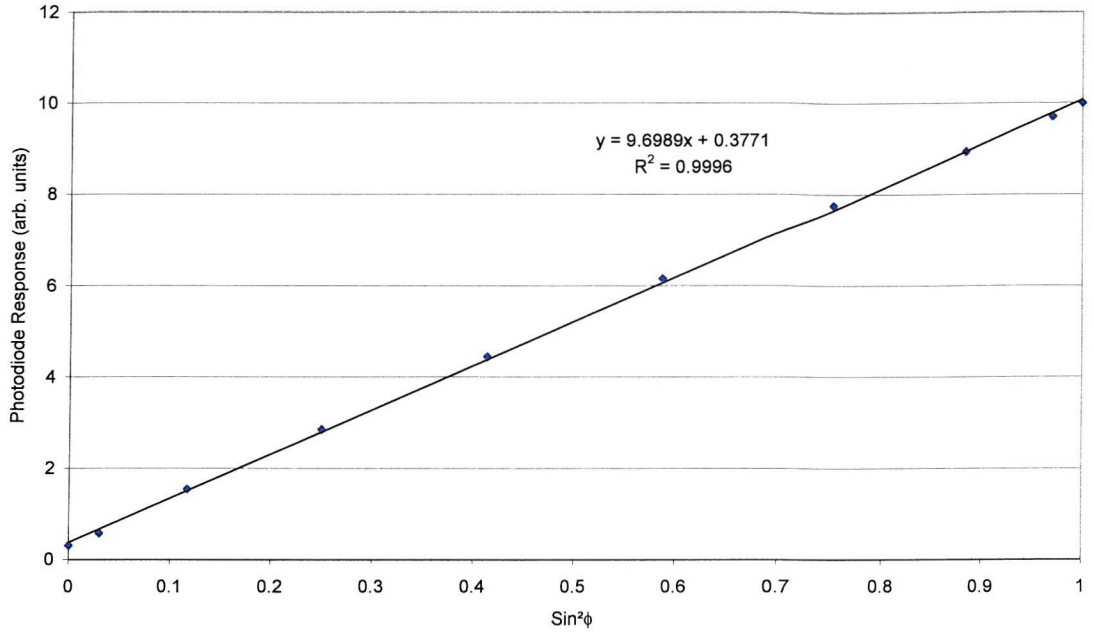

Figure 3.4 Plot of photodiode amplifier output versus Sin^2 polariser angle to demonstrate the linear response of the photodiode and amplifier.

3.2.5 Function Generator & High-Voltage Amplifier

A Thurlby-Thandar[8] TG1304 programmable function generator was used to produce a variety of electrical signals across the cell electrodes via an in-house high voltage amplifier. This system allows a maximum AC voltage of ~260V_{pp} to be applied to the cell.

The function generator can produce either DC voltages or bipolar square, triangular or sinusoidal waveforms with AC amplitudes between 2mV_{pp} and 20V_{pp} and ±10V DC offset. The frequency is variable from 10mHz to 13MHz and accurate to 0.01%.

---

[7] E.Hecht, *Optics – 2nd Edition*, **§8.2.1**, Addison Wesley (1987)

In general, due to the high fields required to align and switch some of the materials studied, it was necessary to feed the output of the function generator into a wide band high voltage amplifier (HVA). This amplifier (model number EW 1134B) was designed and manufactured in the electronic workshop of the University of Manchester Physics Department. Output signals of up to $260V_{pp}$ are achievable from the HVA-function generator combination.

3.2.6 Digitising Oscilloscope

A Hewlett-Packard[9] HP54503A 500MHz digitising oscilloscope was used in all electro-optical measurements. The signal processing capabilities of these oscilloscopes offer a distinct advantage over the use of an analogue oscilloscope. The signal averaging capability allows a waveform to be built up from up to 2048 separate traces, which greatly increases accuracy when monitoring signals with a low signal-to-noise ratio. Four channel inputs allowed simultaneous display of the applied field, current response and optical response where applicable. The oscilloscopes ability to plot two input signals on an x-y chart enabled the observation of hysterisis loops in ferroelectric switching. Manual measurements are facilitated by means of a pair of cursors on the voltage and timebase axes and automatic measurements, such as V_{pp} and frequency, can be also be made on input signals. Connection to a PC by means of RS232 cable and connections allowed waveforms and data from automatic measurements to be saved for analysis. In combination with a computer program, ScopeGrabba[10] written using HPVEE[11] enabled waveforms to be digitised and imported into spreadsheets.

---

[8] Thurlby Thandar Instruments Ltd., Glebe Road, Huntingdon, Cambridgeshire, UK, PE18 7DX, http://www.ttinst.co.uk

[9] Hewlett-Packard Ltd., Test and Measurement, Cain Road, Bracknell, Berkshire, UK, RG12 1HN. http://www.hewlett-packard.com

[10] M.Clarke, *Scopegrabba*, HPVEE program, 1999

[11] HPVEE, Hewlett-Packard Ltd., Test and Measurement, Bracknell, Berkshire, UK, RG12 1HN. http://hewlett-packard.com

3.3 CHARACTERISATION OF PHASE TRANSITION TEMPERATURES

3.3.1 Overview

It is of primary importance when studying liquid crystalline systems that one knows the phases of interest and can accurately define their respective transition temperatures. Throughout the course of this work complimentary procedures were employed to fully characterise the phase transitions of the liquid crystal samples studied. Preliminary investigations were carried out using differential scanning calorimetry in order to determine the temperature and nature of the transition between two phases. Optical studies were then undertaken. The aforementioned polarising microscope and heating stage were used to identify the exact type of liquid crystal phase. Optical phase transition measurements were also carried out on this apparatus using a thermo-optic technique.

3.3.2 Differential Scanning Calorimetry

Whenever a material undergoes a physical change of state energy is either consumed or released. Differential scanning calorimetry (DSC) reveals the presence of a phase transition by detecting the associated enthalpy change. The sample is heated (or cooled) at the same rate as a reference. The differential heat flow necessary to maintain the sample at the same temperature as the reference is measured as a function of temperature. The phase transitions show up as endotherms or exotherms, as can be seen in the DSC trace shown in Figure 3.5.

A Perkin-Elmer[12] DSC7 connected to a PC with controlling software was used during these investigations. Before each sample was studied, the temperature and enthalpy measurements were calibrated with respect to four standard metal samples (indium, gallium, lead and tin), and unless otherwise stated, heating and cooling rates of 5°C/min were used. During the heating/cooling runs 5-10mg of the sample to be studied was sealed

[12] Perkin-Elmer Ltd. Post Office Lane, Beaconsfield, Buckinghamshire, UK, HP9 1QA.
http://www.instruments.perkinelmer.com

within a specially designed aluminium pan. The use of small samples eliminates the 'temperature lag' effects often observed in larger samples. Transition temperatures were taken from the third heating and cooling runs to allow for the full relaxation of the sample; this maximises the thermal contact between the sample and the pan and ensures a consistent sample memory for comparisons. Liquid crystalline materials often show different behaviour on heating and cooling, and therefore, data is taken from both the heating and cooling runs in order to observe any monotropic phase transitions, (transitions that occur only on cooling).

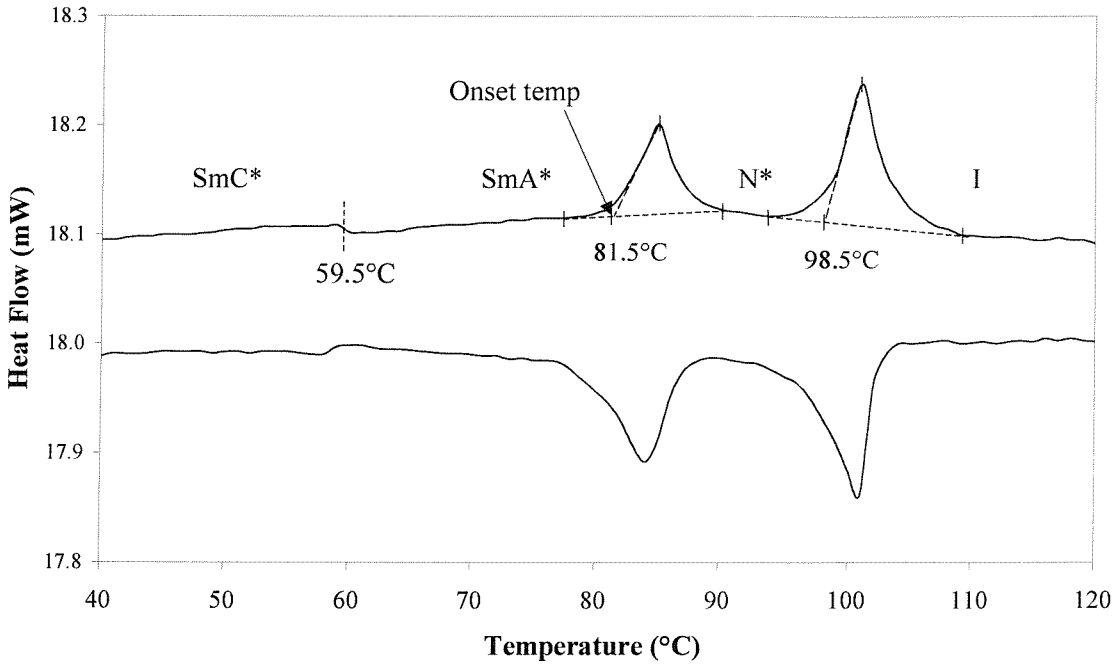

Figure 3.5 A DSC trace for the compound SCE13

First and second order transitions were discussed in Section 2.2. At a first order transition there is a discontinuity in the entropy of the system that expresses itself as a finite latent heat of transition measurable by DSC. The transition temperatures quoted from DSC data are obtained from the onset temperature of a peak by extrapolating back to the baseline with a tangent to the peak. The onset temperatures are less dependent on the sample size, whereas the peak temperatures can vary markedly depending on the sample mass and

heating rate. Glass transition temperatures were measured at the temperature at which the curve is midway between the tangents of the initial and final baselines.

Although the relative sizes of the DSC endotherms and exotherms provide an indication of the amount of structural change at the phase transition, definitive phase identification must be carried out by a different method.

3.3.3 Birefringence Methods

The varying degrees of positional and orientational order of the molecules in the individual liquid crystal phases were discussed in Section 1.4. A consequence of this is that each liquid crystal phase has a different birefringence and hence, a different appearance when viewed through crossed polarisers.

The two birefringence methods employed here utilise the distinct optical textures of each liquid crystal phase to determine the phase transition temperatures. These optically determined temperatures were then compared to those measured by the DSC. In both of the birefringence methods discussed here the sample is contained within a thin cell (see §3.4) in which surface effects can act to alter the transition temperatures.

3.3.3.1 Optical Polarising Microscopy

Optical polarising microscopy allows the specific liquid crystal phase to be identified, as well as providing information about the phase transition temperature.

Generally, the polariser and analyser are aligned with their transmission axes perpendicular to each other, extinguishing all light. If a sample, placed on the heating stage situated on the rotating stage of the microscope, is optically isotropic it appears dark. If the sample is optically anisotropic, i.e. birefringent, and suitably oriented, then light does pass through the analyser, allowing an optical texture to be observed.

In order to observe the range of each mesophase and the transition temperatures, the liquid crystal sample is heated to the isotropic state and cooled at a rate between 2 and 5°C/min. Slower cooling rates, ~0.5°C/min, are then used in the region of the phase transitions to accurately determine the transition point. Measurements can also be gathered on heating, although this leads to slightly ambiguous results since the optical textures are usually paramorphotic, i.e. they are derived from, and can exhibit features from, the preceding phase. By cooling from the isotropic phase the initial liquid crystal phase will exhibit a 'natural' texture, while on heating from a crystalline phase the texture may contain some crystalline features.

The identification of the textures was carried out by comparison with those found in standard texts[13,14]. Typical textures of some liquid crystalline phases were shown in Chapter 1.

Polarising microscopy also provides an insight into the quality of the sample alignment. Indeed, defects such as the four brush singularities observed in the Schlieren texture of the SmC* phase can be helpful in identifying the specific liquid crystal phase.

Similarities between textures often make the explicit characterisation difficult. Therefore, other techniques, primarily electro-optic measurements, were used in conjunction with optical observations for phase identification.

3.3.3.2 Thermo-Optic Analysis

Thermo-optic analysis provides information solely about phase transition temperatures. The sample is placed on the heating stage situated between the crossed polarisers of the microscope. The intensity of the transmitted light is detected by a PDA and displayed on the oscilloscope as a voltage. A computer program[15] written in HPVEE allows the heating or cooling rate and the temperature of the heating stage to be varied (1°C/min) whilst

[13] D.Demus, L.Richter, *Textures of Liquid Crystals*, Verlag Chemie (1978)
[14] G.W.Gray, J.W.Goodby, *SmecticLiquid Crystals: Textures and Structures*, Leonard Hill (1984)
[15] C. Noot, *Thermooptic*, HPVEE program (1999)

simultaneous readings are taken from the PDA trace on the oscilloscope. The transmitted light intensity is then plotted as a function of temperature. Any sharp variation in the transmitted light intensity occurs as a direct result of the birefringence changes caused by the sample undergoing a phase transition. Due to the different birefringence of each liquid crystal phase the thermo-optic trace can reveal phase transitions that the eye may miss. This aspect is particularly useful when detecting the SmA* - SmC* transition. Even without careful alignment, the transition on cooling to the SmC* phase is readily apparent as a change in transmitted intensity occurs due to the molecular tilt changing the orientation of the optical axis. Figure 3.6 shows a typical thermo-optic trace for the commercially available ferroelectric liquid crystal mixture Felix 15/30.

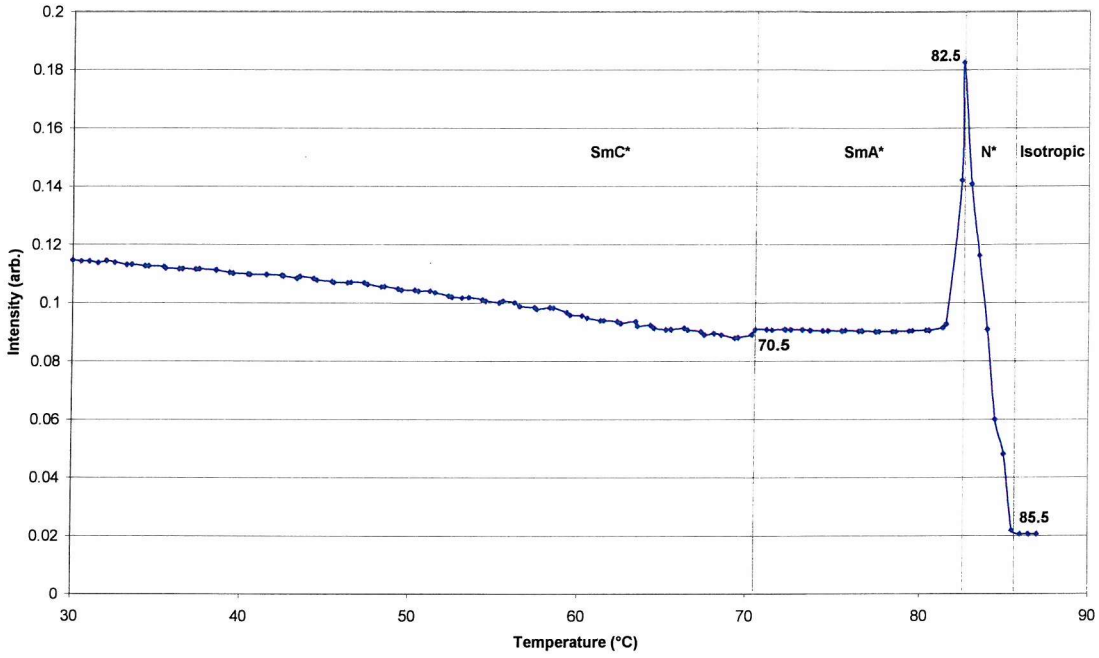

Figure 3.6 Thermo-Optic trace for ferroelectric liquid crystal Felix 15/30. (Data taken on cooling at 1°C/min).

Care must be taken when using this technique as an optical change is not always accompanied by a phase transition, and vice versa. Biphasic regions, where the liquid crystal and isotropic phases coexist, were observed over a small temperature range in a number of samples.

3.4 SAMPLE PREPARATION

In order to characterise a liquid crystalline material, a method of enclosing the sample for observation is required. The simplest method is to sandwich a small quantity of the material between a microscope slide and cover slip. The lack of macroscopic alignment in this method allows defect textures to be observed and can subsequently assist with the identification of the phases. Measurements of specific electro-optical properties require the ability to apply an electric field across the sample and often require that the sample be uniformly aligned. A variety of different cells have been used to characterise the materials and to construct device prototypes. All have the same general construction; glass walls coated with an optically transparent thin conductive layer and an alignment agent to constrain the orientation of the director. The majority of the cells used in this work were commercially available cells manufactured by Lucid EEV Ltd[16]. A schematic diagram of such a cell is shown in Figure 3.7.

3.4.1 Planar Cells

The cells are composed of two glass plates separated by a small gap (typically in the range of 3-14μm) whose thickness is determined by spherical glass beads encapsulated within an adhesive applied along two edges. The inner glass surfaces are coated with a thin layer of indium tin oxide (ITO) which act as transparent electrodes. Electrical connections to the cell are made by attaching wires to the electrodes using indium solder. The design of the ITO electrodes allows the application of an electric field across an active area of $25mm^2$. Furthermore, a rubbed polyimide alignment layer is coated onto the inner surfaces of the cell to promote planar alignment. The layer is rubbed uni-directionally, at an angle of 45^o to the sides of the cell, to ensure the pre-tilt forms along the rubbing direction. The two substrates are rubbed in opposite directions such that the pre-tilt directions favour a 'bookshelf' arrangement of ferroelectric liquid crystals.

[16] EEV Ltd., Waterhouse Lane, Chelmsford, Essex, UK, CM1 2QU, http://www.eev.com

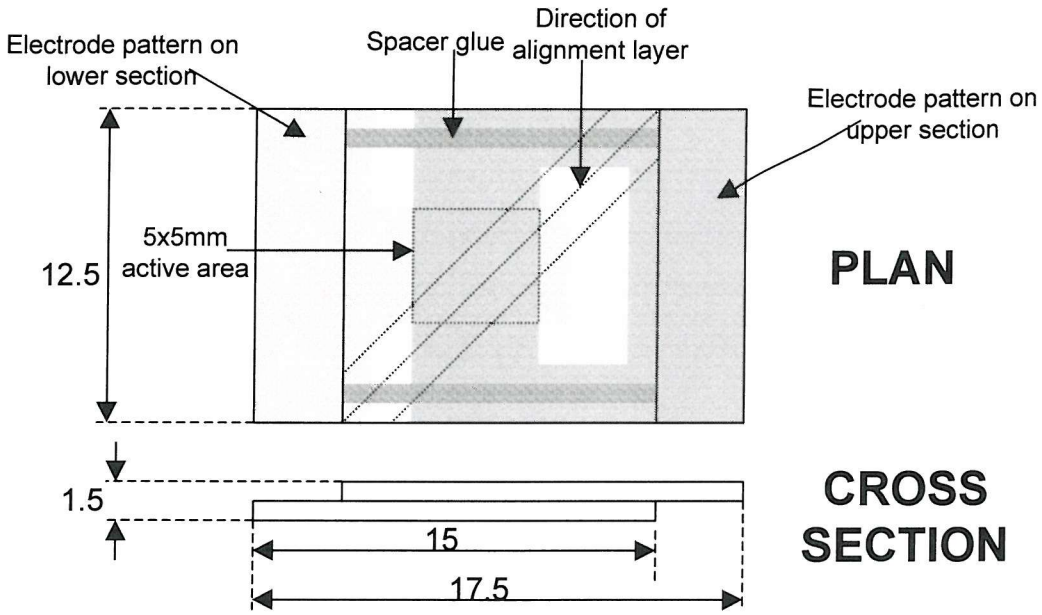

Figure 3.7 Schematic diagram of planar cell manufactured by Lucid EEV Ltd.

Twist cells were also used with some nematic materials and are referred to as twisted nematic or TN cells. When constructing TN cells, the glass plates are brought together such that the rubbing directions on each surface are perpendicular to each other, thereby inducing a 90° twist. The cells used in twisted nematic applications differ slightly in their construction from those used for planar alignment in that the cells are sealed with glue along all edges except for one small gap and thus require a different filling technique, which will be explained in §3.4.4.

3.4.2 Handmade Cell Fabrication

Handmade cells have been constructed using glass microscope slides and cover slips as well as ITO coated glass. The electrode pattern is created using photo-resist after the ITO glass has been cut to size. The ITO is subsequently etched using a 15% (w/w) hydrochloric acid solution. Before constructing the cells care must be taken to ensure the glass is clean. Removal of grease and dirt is achieved by soaking the glass in a (10% by weight) solution of potassium hydroxide (KOH) in ethanol. The glass is subsequently rinsed with distilled, deionized water and dried with clean, pressurised nitrogen. Once

clean, the glass is treated with polytetrafluoroethane (PTFE) or polyvinyl-alcohol (PVA) to produce a planar alignment layer.

PTFE alignment[17] is undertaken using in-house apparatus in a clean room environment. The glass substrate is placed on a brass block heated to 300°C. A PTFE rod is then lowered onto the substrate and allowed to reach thermal equilibrium. The deposition process involves uniform pressure (approximately 5 bar) being applied to the PTFE rod as it is drawn across the glass surface.

PVA alignment layers are deposited by simply drawing a lens tissue soaked in a 1% aqueous solution of PVA. The water evaporates leaving a thin uniform film of PVA, smoothly rubbing the film with a piece of velvet produces the alignment grooves. The quality of the alignment layers can be checked, once the cell has been filled, using a microscope.

It was also found[18] that homeotropic alignment layers could be successfully and reliably produced by filling untreated (no alignment layer) manufactured cells with a 1% solution of lecithin in chloroform. After the solvent has evaporated a lecithin layer is left to induce homeotropic alignment.

The thickness of the cell gap is determined by the diameter of an optical fibre spacer. The fibres are coated with optical glue and then placed along opposite edges of one of the pieces of glass. A second piece of glass is then placed above the spacer and pressure is applied. By manipulating the cell under a sodium discharge lamp during this process a uniform thickness can be achieved by observing the interference fringe pattern that is visible when the substrates are not parallel. The monochromatic light (~600nm) from the lamp produces interference fringes corresponding to the distance between the two glass surfaces. A bright fringe is seen when the cell thickness is an integral multiple of the sodium wavelength. The fringes act as contour lines showing regions of equal thickness,

[17] S.Meyer, Ph.D. Thesis, Université Louis Pasteur, Strasbourg, France (1995)
[18] B.Musgrave, *Ph.D. Thesis*, University of Southampton, UK (1999)

so, by carefully observing their structure and applying suitable pressure, cells with few fringes can be constructed (two adjacent fringes correspond to a 0.3μm change in thickness).

3.4.3 Cell Thickness

Before filling a cell with the sample material, its thickness was measured by an interferometric method. A Hewlett Packard 8453 UV-Visible spectrometer[19] is used to analyse the spectrum of light transmitted through the empty cell. The cell is fixed to a holder and positioned normal to the light beam of the spectrometer. The internal surface of the glass cell plates act as an etalon for the light beam, producing constructive and destructive interference. The successive interference maxima and minima occur as the wavelength of the incident light is varied, in accordance with Equation 3.2, across a range of wavelengths (typically 300-600nm). The relationship between the cell thickness and the wavelength of the maxima is given by

$$m\lambda = 2nd\cos\theta, \tag{3-2}$$

where m is an integer (peak or trough number), λ is the wavelength of the incident light, n is the effective refractive index of the material in the cell gap, d is the cell thickness and θ is the angle of incidence of the light on the cell.

It is usual for the light to be normally incident and the cell to be empty, therefore a peak will occur every time the condition for constructive interference, $2d=m\lambda$, is met, thus

$$2d = (m+i)\lambda_i, \tag{3-3}$$

where i is an integer or zero. Using the initial condition, where i=0, to eliminate m yields

$$i = 2d\left(\frac{1}{\lambda_i} - \frac{1}{\lambda_o}\right). \tag{3-4}$$

It is straightforward to choose a series of consecutive peaks and obtain the cell thickness, by using the data from the spectrophotometer to plot i versus $2/\lambda_i$ and calculating the gradient. This method allows the cell thickness to be measured to an accuracy of 0.1μm.

The accuracy was checked by performing repeated measurements on a single area of a cell, whilst the uniformity of the cell thickness was checked by carrying out a series of measurements on different sections of the cell.

3.4.4 Cell Filling

Cells are filled by one of two methods depending on their construction. The prefabricated planar and handmade cells are filled by capillary action. A small amount of the sample is placed across one of the cell openings and heated to the isotropic state. Capillary action then draws the fluid into the cell. Once the filling process is complete, the cell is subsequently sealed with a UV-curing glue[20], and exposed to UV light. A mask is used to protect the materials inside the cell from the UV light and hence avoid any problems prolonged exposure might cause.

The manufactured TN cells are constructed with only one small opening. In order to completely fill the cell, the LC must replace the residual air. This is achieved by filling under vacuum. The 'vacuum filling' apparatus is shown in Figure 3.8. The liquid crystal material is placed in an aluminium sample holder within the vacuum vessel and heated until it reaches its isotropic phase. The cell is placed in a clamp that can be raised or lowered. The whole system is then evacuated (vents 1 and 3 closed, vent 2 open) to a pressure of ~10mbar to remove any residual gas from the sample and the cell. The system is allowed to reach equilibrium. The cell is then lowered into the isotropic liquid crystal and firmly pressed down to gain good thermal contact with both the sample and the aluminium holder. The cell is allowed to reach thermal equilibrium to prevent the isotropic sample from cooling into the mesophase (resulting in an increase in the viscosity before the cell is full). Vent 2 is then closed, vent 3 is opened and the pump is switched off. The vacuum is then released and slowly brought back up to atmospheric pressure (vent 1 open). The sample material is subsequently forced into the evacuated cell by the pressure difference between the interior of the cell and the atmospheric pressure inside the

---

[19] Supplied by Anachem Ltd., 20 Charles Street, Luton, Bedforshire, UK, LU2 0EB.
http://www/anachem.co.uk

[20] Norland Optical Adhesive 81, Norland Products, 695 Joyce Kilmer Av., New Brunswick, N.J., USA.
http://www.norlandprod.com

vacuum jar. The time taken to complete this process depends on the viscosity of the sample - it was necessary to leave viscous polymeric samples to fill overnight, whilst nematic compounds filled the cells within a minute. When the filling process is complete the cell is sealed with the UV curing glue.

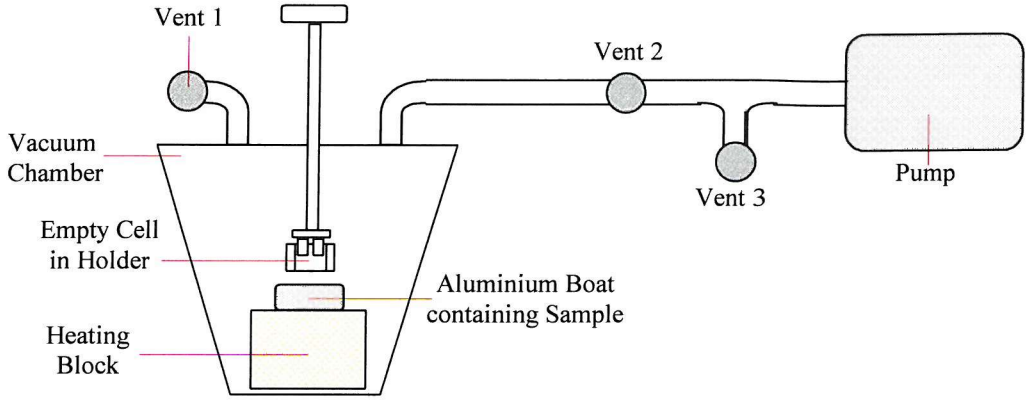

Figure 3.8 Schematic representation of the apparatus used for 'vacuum filling' twisted nematic (TN) cells.

3.4.5 Alignment

Sample alignment can often be achieved by simply heating the sample within the cell to its isotropic state and cooling slowly, allowing the alignment layer to impose the ordering on the liquid crystal molecules. Alternatively, the application of an electric field can be used to induce alignment. The coupling of the field to the molecular dipole forces the molecule to adopt some alignment. Mechanical shearing techniques, in which the liquid crystal material is subjected to physical force, can also be used.

3.5 SAMPLE CHARACTERISATION

This section discusses the different experimental techniques employed to measure the fundamental electro-optic parameters, namely the spontaneous polarisation, tilt angle and response time, of a liquid crystalline material.

3.5.1 Measurement Of Spontaneous Polarisation

3.5.1.1 Introduction

A number of different techniques can be used to measure the spontaneous polarisation (P_s) of ferroelectric liquid crystals and the majority of these techniques are direct measurements. The P_s may also be inferred indirectly by measuring either the critical field required to unwind the helix[21] or the electric field dependence of the dielectric constant[22]. The direct measurement techniques fall into one of two groups. The first group is of techniques that do not require the application of an electric field to the sample, such as the pyroelectric[23] (using the temperature dependence of the pyroelectric coefficient $\gamma = dP_s/dT$) and shear[24] techniques. The second group is of techniques that do require the direct application of an electric field. The P_s measurements reported in this work were made using the direct application of an electric field, as described below.

An AC field is applied to the sample, which is contained within an electro-optic cell, in order to reverse the orientation of the ferroelectric dipoles. This polarisation realignment gives rise to a pulse of current that can be subsequently measured. However when an electric field is applied across the cell, other effects also contribute to the total cell current. The inherent finite resistance and capacitance of the liquid crystal cell result in additional components to the current, which make it difficult to obtain accurate measurements of the polarisation current and hence, the P_s.

---

[21] Ph.Martinot-Lagarde, J.de Phys. **38**, L17 (1977)
[22] T.Uemoto, K.Yoshino, Y.Inuishi, Jpn. J.Appl.Phys. **18**, 1261 (1979)
[23] L.M.Blinov, L.A.Beresnev, N.M.Shtykov, Z.M.Elashvili, J.Phys (Paris), **40**, C3-269 (1979)
[24] P.Pieranski, P.Keller, E.Guyon, J.Phys (Paris), **36**, 67 (1976)

The current I(t) induced in a ferroelectric liquid crystal cell by an applied field V(t) can be expressed as a sum of three contributions: I_c due to charge accumulation, I_p due to the polarisation realignment and I_i due to ohmic ion flow,

$$I = I_c + I_p + I_i = C\frac{dV}{dt} + \frac{dP}{dt} + \frac{V}{R}, \tag{3-5}$$

where P is the amount of charge induced by the polarisation realignment. The current response of these components is shown in Figure 3.9.

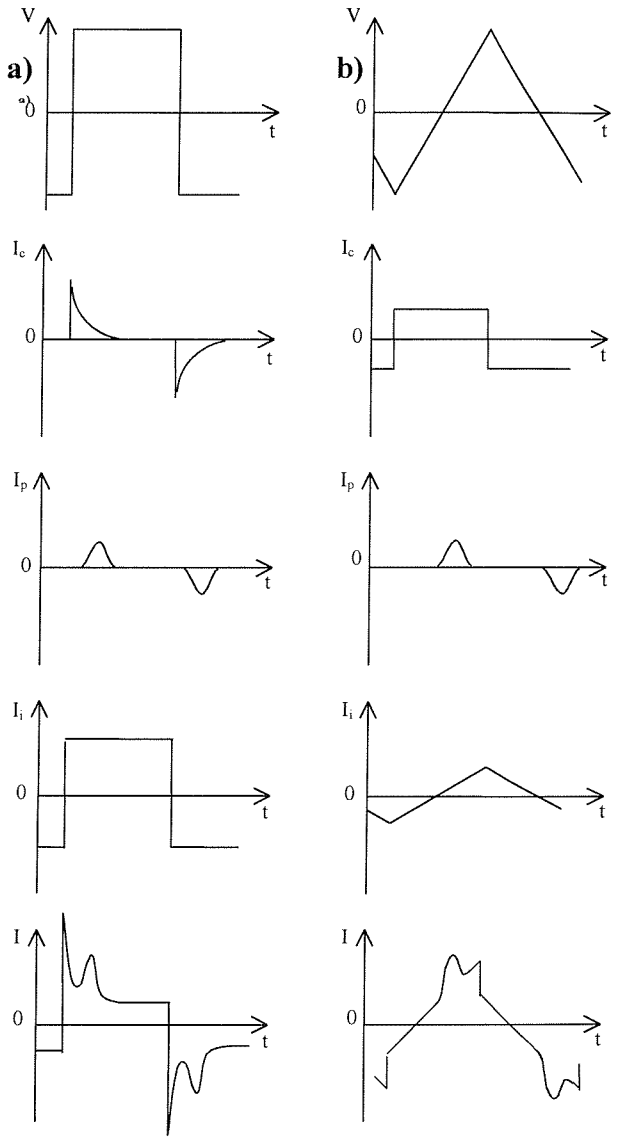

Figure 3.9 The current response of a ferroelectric liquid crystal material to an applied electric field - a) square wave and b) triangular wave driving voltages. I_c , I_p and I_i are the capacitive, dipolar polarisation and resistive components respectively, I is the net electrical response. The use of a triangular wave driving field results in a straight baseline.

The method employed to measure the P_s must therefore allow I_p to be extracted accurately from the total current, I, as given by Equation 3.4.

The Sawyer-Tower[25] method is commonly used to measure the polarisation of solid ferroelectric crystals and has also been successfully applied to the measurement of the P_s in ferroelectric liquid crystals. However, the P_s in ferroelectric liquid crystals is smaller than that measured in solid ferroelectrics by two or three orders of magnitude. This fact, combined with the higher conductivity of liquid crystals, makes it difficult to make accurate measurements by the Sawyer-Tower method. A variation on the Saywer-Tower method is the Diamant Bridge[26] method. This technique includes an additional circuit to compensate for the spurious conductive and capacitive currents. The direct electric field application method used to measure the P_s of the FLC's described in this thesis is the current reversal technique, which is explained below.

3.5.1.2 The Current Reversal Technique

The basis of this method to determine the P_s of an FLC is the measurement of the transient current induced when a polarisation reversal occurs in the sample because of a change in the polarity of the applied field. The current reversal method has the advantage that it allows for the simultaneous study of the electrical and optical properties during switching. The current is measured as the voltage drop over a series resistor and the voltage change is measured using an oscilloscope. The technique uses 'shape separation' to separate the polarisation current from that due to the capacitance and resistance. The P_s is found by setting a suitable baseline and integrating the area under the peak.

[25] C.B.Sawyer, C.H.Tower, Phys.Rev. **35**, 269 (1930)
[26] H.Diamant, K.Drenck, R.Pepinsky, Rev.Sci.Inst. **28**, 30 (1957)

By calculating the area under the polarisation current peak, the spontaneous polarisation can be found directly from the equation,

$$P_s = \int \frac{i}{2A} dt \quad = \frac{Q_t}{2A}, \tag{3-6}$$

where P_s is the spontaneous polarisation, i is the transient current, A is the switching area and Q_t is the total charge that flows when the switch occurs.

In Equation 3.5 the total charge that flows must be divided by two because the polarity of the field is reversed, not just returned to zero. Equation 3.5 also shows that there is no thickness dependence. This implies that the magnitude of the P_s will not vary with the applied field (V/μm). However, it is important that an applied field high enough to induce complete switching is used when measuring the P_s. This ensures that the P_s is saturated and independent of the applied field. The switching will be incomplete at lower applied fields, leading to spurious results.

Martinot-Lagarde[27] applied a square wave voltage across the cell but found that the conductive and capacitive current obscured the polarisation peak, as shown in Figure 3.9(a). This lead to difficulties when drawing an accurate baseline and choosing the start and end points for the integration. Skarp et al.[28] again applied a square wave voltage across the cell but constructed equivalent circuits for the liquid crystal cell in an attempt to isolate the polarisation peak. As Figure 3.9(b) shows, the dipole reversal appears as a peak, the capacitive component, I_c, appears as a discontinuous change in the baseline following field reversal and the ionic conductive component, I_i, appears as a baseline slope. In the work reported by Skarp et al., a feedback circuit was added to remove this ohmic current component and obtain a flat baseline.

The modified method proposed by Miyasato et al.[29] utilises a triangular applied field. It is clear from Figure 3.9(b) that the baseline in this case is expected to be a straight line (and confirmed by the experimental data in Figure 3.11). Thus, by applying a triangular wave

[27] Ph.Martinot-Lagarde *J.Physique(Lett)*, **38**, 17 (1977)
[28] K.Skarp, I.Dahl, S.T.Lagerwall, B.Stebler, *Mol.Cryst.Liq.Cryst.*, **114**, 283 (1984)
[29] K.Miyasato, S.Abe, H.Takezoe, A.Fukuda, E.Kuze, Jpn.J.Appl.Phys. **22**, L661 (1983)

voltage we can easily and accurately determine the baseline and the contribution of I_p to the overall current I. Figure 3.10 and Figure 3.11 illustrate the form of the current response of a ferroelectric liquid crystal when subjected to a triangular wave electric field.

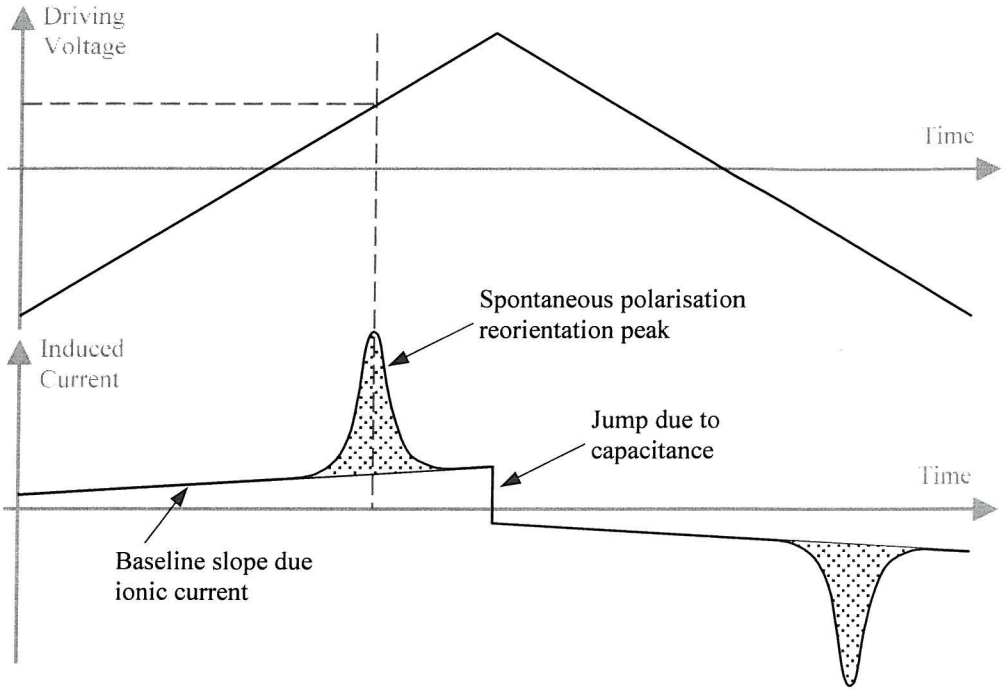

Figure 3.10 Schematic illustration of the spontaneous polarisation response of a ferroelectric liquid crystal under the application of a triangular wave driving field.

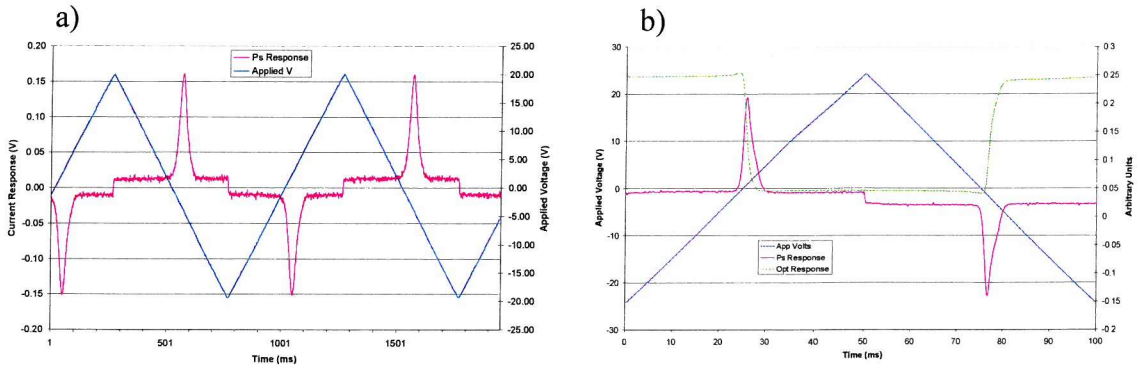

Figure 3.11 The current response of ferroelectric liquid crystals. a) SCE 13 (24°C, 40Vpp, 40Hz) and b) Felix 15/30 (40°C, 50Vpp, 10Hz)

The use of a four channel digital oscilloscope facilitates the simultaneous observation of both the optical and electrical responses of the sample. Figure 3.11(b) illustrates the

latched square wave optical response of ferroelectric liquid crystalline materials. Using this technique, it is also possible to probe the dynamics of the polarisation reversal.

The driving voltage produced by the signal generator triggers the oscilloscope. The time-base is adjusted so that a single polarisation peak is observed in the oscilloscope trace and the signal to noise ratio is maximised by adjusting the I-V amplifier gain whilst avoiding saturation. The signal averaging facility of the oscilloscope is also employed to further improve the signal quality. Computer software written by M.Clarke[30] reads the oscilloscope settings and both the current response and driving voltage waveforms and the oscilloscope settings before performing the integration of the time dependent current. Typically, this is performed 10 times before an average value of the spontaneous polarisation is produced. The control software also allows for the Linkam temperature controller to be interfaced allowing a series of measurements at different temperatures, as shown in Figure 3.12, to be automated.

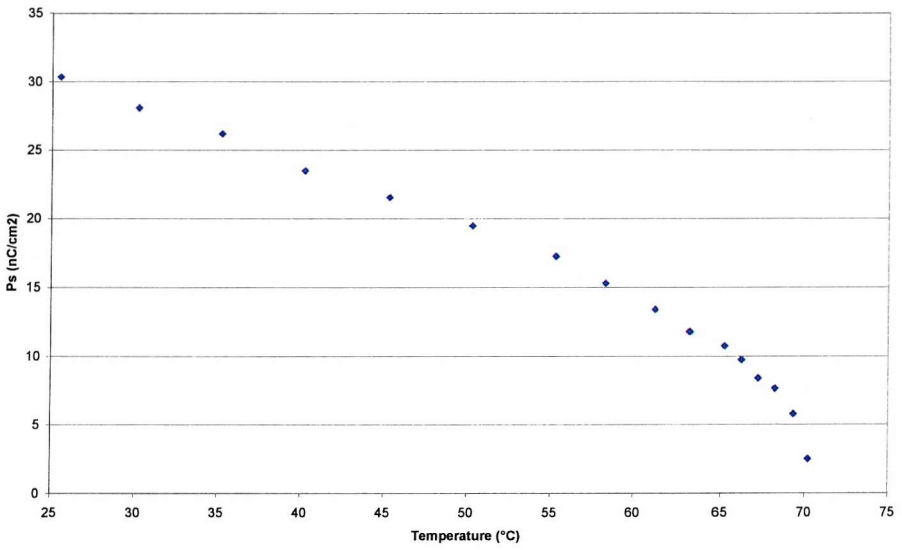

Figure 3.12 The temperature dependence of the spontaneous polarisation of the ferroelectric liquid crystal Felix 15/30. An AC triangular wave of 40Hz and 8V/μm was applied.

[30] M.Clarke, *Ph.D. Thesis (in preparation)*, University of Southampton, UK (2003)

3.5.2 Measurement Of Tilt Angle

3.5.2.1 Introduction

As discussed in Chapter 2, applying an electric field to either ferroelectric or flexoelectric liquid crystalline systems causes a molecular re-orientation and a rotation of the optical axis and results in the ability to control the direction of the optical axis. There are several methods that may be used for measuring tilt angles. The tilt angle, ϕ, is a fundamental parameter (primary order parameter) of the SmC* phase. Its magnitude can be determined from either X-ray[31] or electro-optical measurements. $\phi_{X\text{-ray}}$ is calculated from the interlayer distance and is effectively a measure of the tilt angle away from the smectic layer normal of the whole molecule. ϕ_{opt} of the mesophase is generally determined by the polarisable rigid core of the molecule, i.e. the direction of the optical axis. Thus, the optical measurement gives an indication of the angle between the direction of the molecular core and the direction of the layer normal. The tilt angle data presented in this thesis are all measured optically. It is important to note that the tilt angles derived using these two methods may differ. In general, liquid crystal molecules do not have a linear shape, and the result is that the long axis of the molecule does not coincide with the optic axis, as shown in Figure 3.13.

A number of possible optical methods can be employed to obtain the tilt angle, ϕ_{opt}. All of which are applicable to both ferroelectric and flexoelectric systems and all of which have to address the experimental problem of measuring the direction of the optic axis of a uniaxial birefringent medium as a perturbing field is applied to it.

[31] R.Bartolino, J.Doucet, G.Durand, *Ann.Phys.*, **3**, 389 (1978)

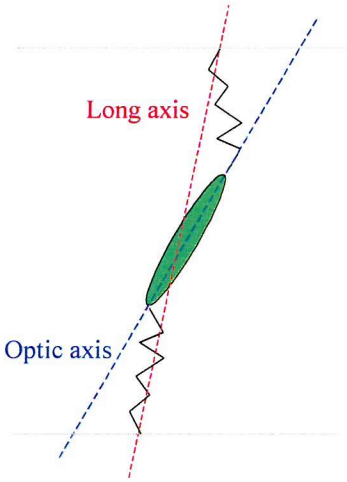

Figure 3.13 Schematic illustration of the optic axis (long axis of core) not coinciding with the long axis of the molecule.

3.5.2.2 Microscope

The most commonly used method[32] to measure optical tilt angles can be carried out using a polarising microscope and is based on the measurement of the transmission of a liquid crystal cell when viewed between crossed polarisers. The transmitted intensity is given by:

$$I = I_o \sin^2(2\alpha)\sin^2\left(\frac{\Delta n d\pi}{\lambda}\right), \qquad (3\text{-}7)$$

where I_o is the intensity incident on the cell, α is the angle the optic axis makes with the polariser, Δn is the birefringence of the sample, d is the cell thickness and λ is the wavelength of light at which the measurement is made. In order to limit the dispersion effect of birefringence it is necessary to introduce a narrow bandwidth filter.

The cell is placed in the heating stage on the microscope sample stage, allowing measurements of tilt angle versus temperature. A bipolar square wave voltage is applied to the sample causing the director to switch between the $+\phi$ and $-\phi$ states, where ϕ is the electric field induced tilt angle. If the cell is oriented such that the optical axis in, for

[32] Ph.Martinot-Lagarde, *J. Phys. (Paris)*, **37,** C3-129 (1976)

example, the +ϕ state lies parallel to one of the polarisers, the transmission of the -ϕ state is given by the equation

$$I = I_o \sin^2(4\phi)\sin^2\left(\frac{\Delta n d\pi}{\lambda}\right), \qquad (3\text{-}8)$$

as the optic axis has rotated through an angle of 2ϕ. For this state to have maximum transmission, and hence optimise the device contrast, it is clear that ϕ should equal 22.5°

To measure the tilt angle, the sample stage is simply rotated and the angular position of the cell is noted at which the light transmission is minimised for one switched state. In turn, the field polarity is reversed and the sample rotated so that the angular position of the cell at minimum transmission is recorded for the second switched state. The angle between these two positions corresponds to the switching angle, 2ϕ (or 90-2ϕ). With use of a Vernier scale on the microscope sample stage to determine its angular position, measurements taken using this method are accurate to 0.5°.

In principle, a DC field can be applied to the cell when making optical tilt angle measurements. However, the application of a square wave AC field is beneficial as this limits the effects of ionic conduction (charge build up at the electrode surface can screen the electric field and result in spurious measurements). Visual measurements of the optical tilt angle require a frequency of ~1Hz to be used, whereas the application of an AC field of high frequency (~100Hz) requires the use of a photodiode and oscilloscope to detect the transmission minima.

More accurate measurements can be obtained using the photodiode and same apparatus[33]. In this method the sample is oriented at 22.5° to the polariser as in Figure 3.14c) and d). A cursor on the voltage axis of the oscilloscope is positioned halfway between the maximum and minimum of the photodiode signal. As in the previous method the sample is rotated so that, in turn, the minima and maxima of the intensity signal are level with the cursor. Again, the angle between these two readings corresponds to the switching angle, 2ϕ. This technique is more accurate as the transmitted light intensity is more sensitive to small

angles of rotation in this geometry. Measurements accurate to 0.3° are achievable, limited by the resolution of the Vernier scale on the hotstage.

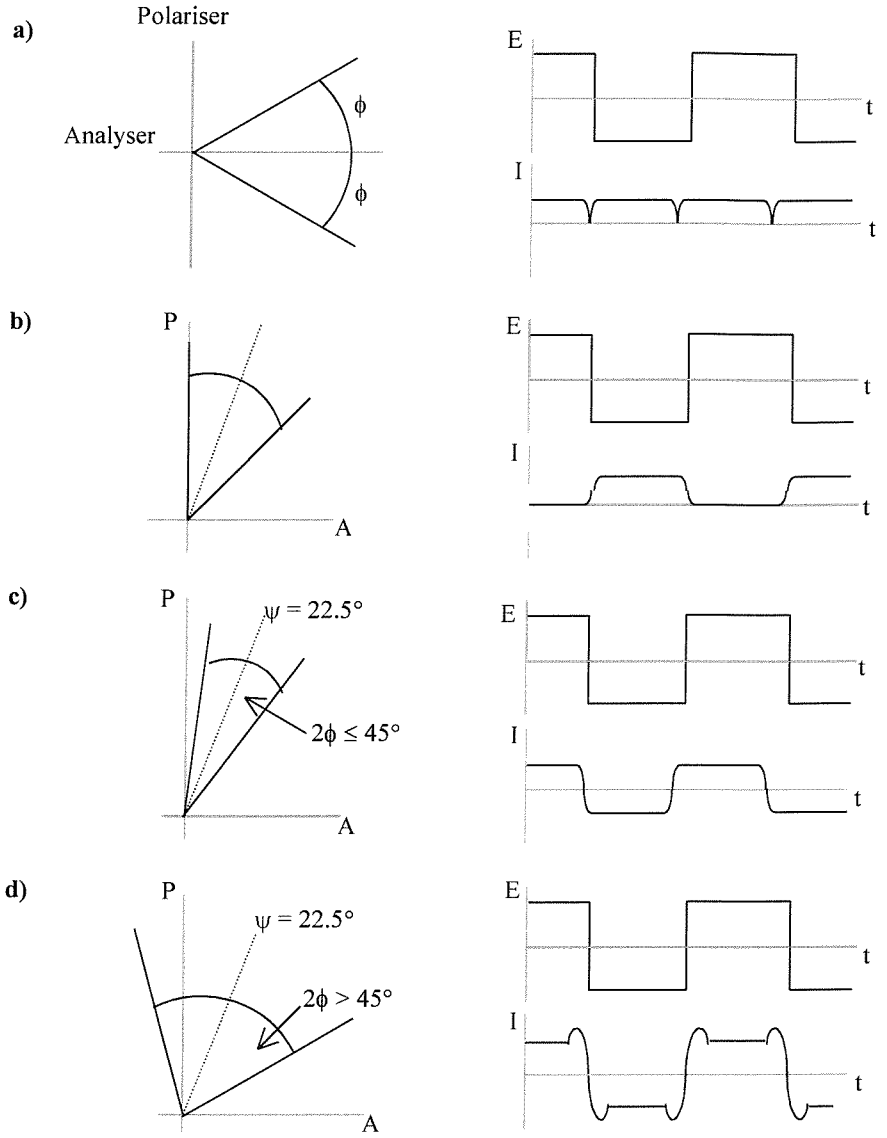

Figure 3.14 The switching geometry and optical response of a ferro- or flexoelectric material under the application of a bipolar square wave electric field. The switching material is positioned between crossed polarisers with the undisturbed optical axis aligned at an angle, ψ, to the transmission axis one of the polarisers; a) $\psi=0^{o}$, switching is symmetric about one of the polarisers, b) $\psi=\phi$, one of the switched states coincides with the transmission axis, c) $\psi=22.5^{o}$ and $\phi\leq22.5^{o}$ and d) $\psi=22.5^{o}$ and $\phi>22.5^{o}$

[33] B.Musgrave, *Ph.D.Thesis*, University of Southampton, UK (1999)

The primary advantage of these techniques is that they do not require any complicated optics to be set up and the sample alignment can be observed as measurements are carried out. However, both techniques are slow, only allowing point by point measurements to be made, and therefore unsuitable for rapid characterisation. An automated "Rotating Analyser" method based on that of Etxebarria et al[34] was employed extensively throughout this work.

3.5.2.3 Rotating Analyser Technique

This technique enables high resolution, fast and continuous in situ measurements of the optical tilt angle to be made as a function of voltage and temperature. Measurements are obtained under the application of an AC field, limiting ionic conduction and avoiding degradation of the materials. Birefringence effects are kept to a minimum by using collimated monochromatic light to illuminate the sample.

The rotating analyser experiment that was designed and built for this work is described below and can be seen in the photograph in Figure 3.15. Linearly polarised light from a 10mW He-Ne laser is incident on a quarter-wave plate orientated at 45° to the polarisation direction of the light, to produce a perfectly circularly polarised beam on the sample. This is confirmed by the observation of uniform light intensity after passing through the rotating analyser, with no sample in place. The sample is situated on a Linkam[4] heating stage to enable temperature dependent measurements to be made. On passing through the homogenously aligned sample, the beam is transformed back towards linearly polarised light, the intensity of which is measured, after passing through the rotating analyser (frequency ~100Hz), by a photodiode. The frequency of rotation of the analyser is controlled by varying the output of the stabilised DC supply that powers the 12V DC motor. The rotating analyser is mounted at a slight angle to the laser beam in order to avoid contamination of the optical signal at the photodiode as a result of back reflection. The photodiode output is displayed on the digitising oscilloscope. A reference signal,

[34] J.Etxebarria, A.Remon, M.J.Tello, A.Ezcurra, M.A..Perez-Jubindo, T.Sierra, *Mol. Cryst. Liq. Cryst.*, **150b**, 257 (1987)

derived from the rotating analyser, is also displayed as a voltage on the oscilloscope, as explained below.

An LED is used to produce a signal that is used as a reference during the measurements. The light emitted by the LED passes through the rotating analyser and another fixed linear polariser before being detected by a photodiode. The reference signal intensity therefore varies sinusoidally with the same frequency as the signal that passes through the sample. Since the signal and reference are both controlled by the rotating analyser, any effect of slight frequency variations emanating from this source is removed.

The laser intensity transmitted through the rotating analyser is given by[35]:

$$I = \frac{I_o}{4}\left[1 - \sin^2\left(\frac{2\pi d\Delta n}{\lambda}\right)\sin^2(2wt - 2\alpha)\right], \qquad (3\text{-}9)$$

where I_o is the incident light intensity, d is the cell thickness, Δn is the sample birefringence, w is the angular frequency of the rotating analyser and α is the angle of the optic axis relative to the first polarisers transmission axis.

It is shown in Equation 3.8 that the signal detected by the photodiode is sinusoidal and has a frequency 2w. The $\sin^2\left(\frac{2\pi d\Delta n}{\lambda}\right)$ term determines the signal amplitude whilst the $\sin^2(2wt - 2\alpha)$ term provides the signal frequency and phase.

For tilt angle measurements, a square wave AC electric field (1-10Hz) is applied to the sample causing the molecular director to switch between the $+\phi$ and $-\phi$ states, i.e. the optic axis moves through 2ϕ. Hence α changes by 2ϕ. The tilt angle is then obtained directly from the oscilloscope by measuring the phase shift between the two output waveforms relative to the reference signal.

[35] I.G.Wood, A.M.Glazer, *J.Appl.Cryst.*, **13**, 217, (1980)

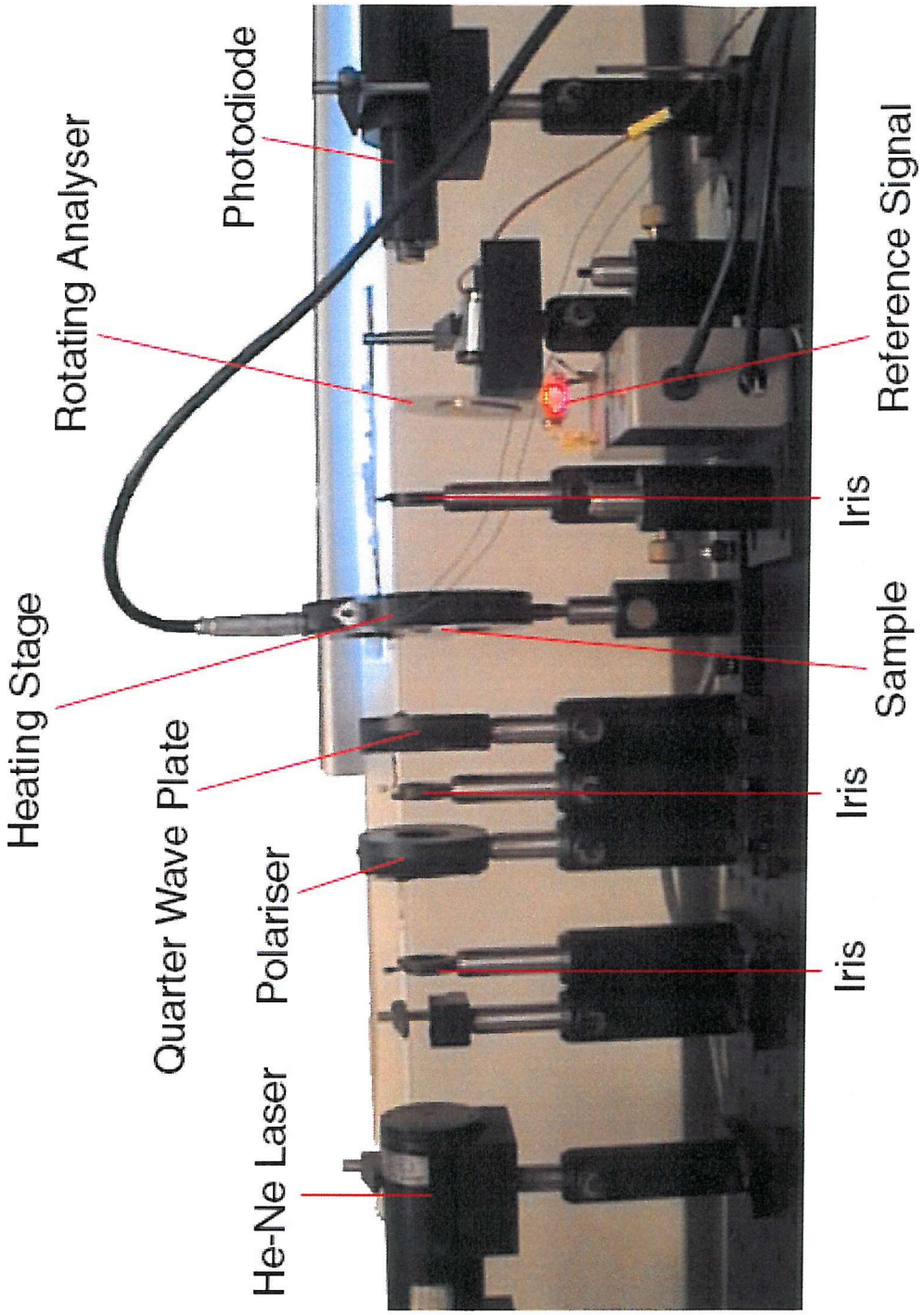

Figure 3.15 The experimental setup used for measurement of the optical tilt angle using the 'rotating analyser' technique.

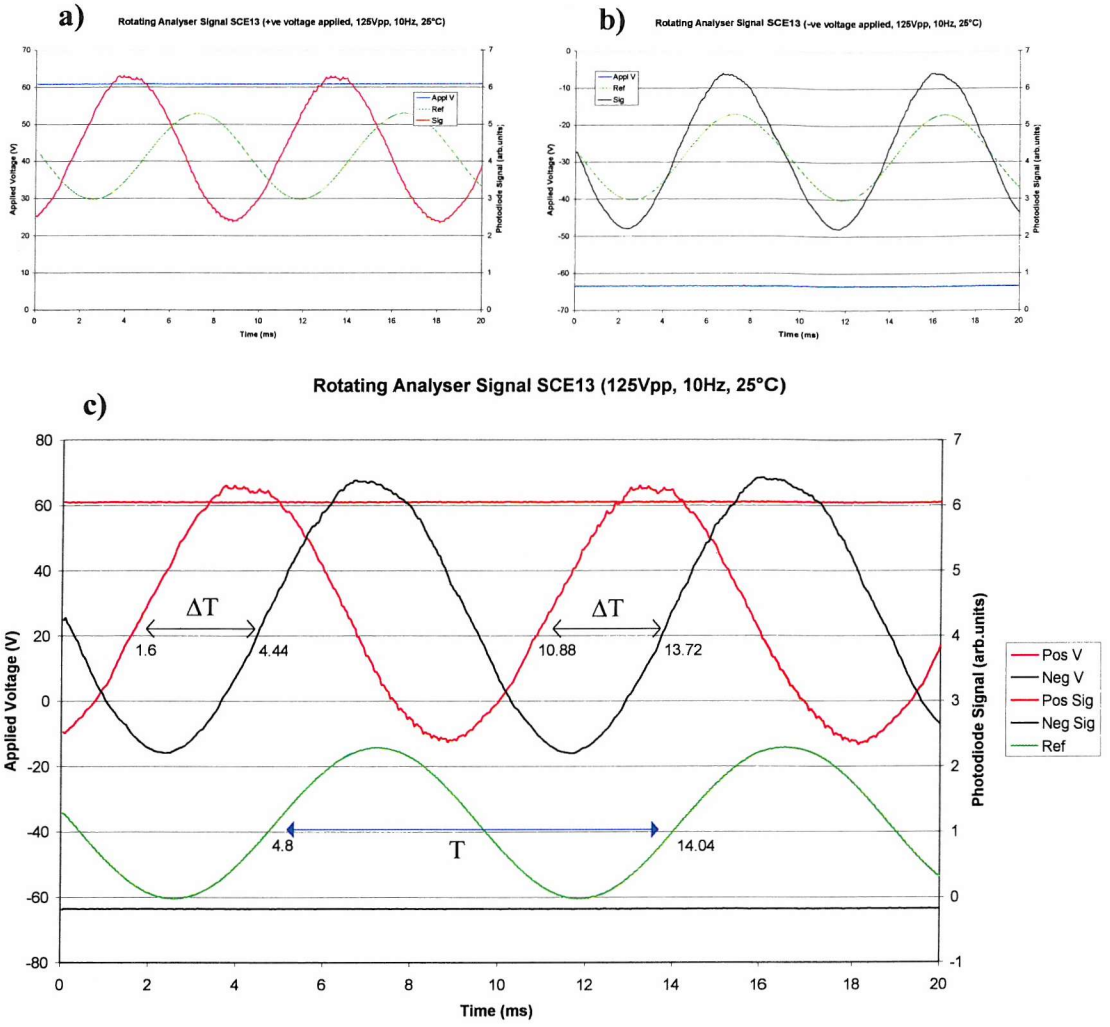

Figure 3.16 Experimental results of SCE13 using rotating analyser technique. a) oscilloscope trace - positive applied field, b) oscilloscope trace - negative applied field and c) illustration of phase shift between the two switched states (±12.5V/μm, 10Hz, 25°C).

The data shown in Figure 3.16 was obtained for the ferroelectric liquid crystal SCE13 on the rotating analyser apparatus. This data illustrates how the signal phase (relative to the reference) changes during switching. In practice, only the waveform from one switched state is displayed on the oscilloscope at any one time, as shown in Figure 3.16 a) and b), due to the complex triggering conditions required for a steady trace. The time delay between the signal and the reference is measured for each switched state, thereby enabling the time delay between the signals of the two switched states to be calculated. The angular

phase shift between the signals is equal to the switching angle, i.e. twice the tilt angle. The tilt angle is subsequently determined using the equation

$$\phi = \frac{\Delta T}{T} \times \frac{180^{\circ}}{2}, \tag{3-10}$$

where ΔT is the time delay between the signals from the two switched states and T is the signal period.

A comparison of the data obtained by the manual microscope and the automated rotating analyser methods is given in Figure 3.17. The error in the rotating analyser measurements was estimated to be ±0.3°. This compares favourably with the accuracy of the two microscopy methods, ±0.5° and ±0.3°.

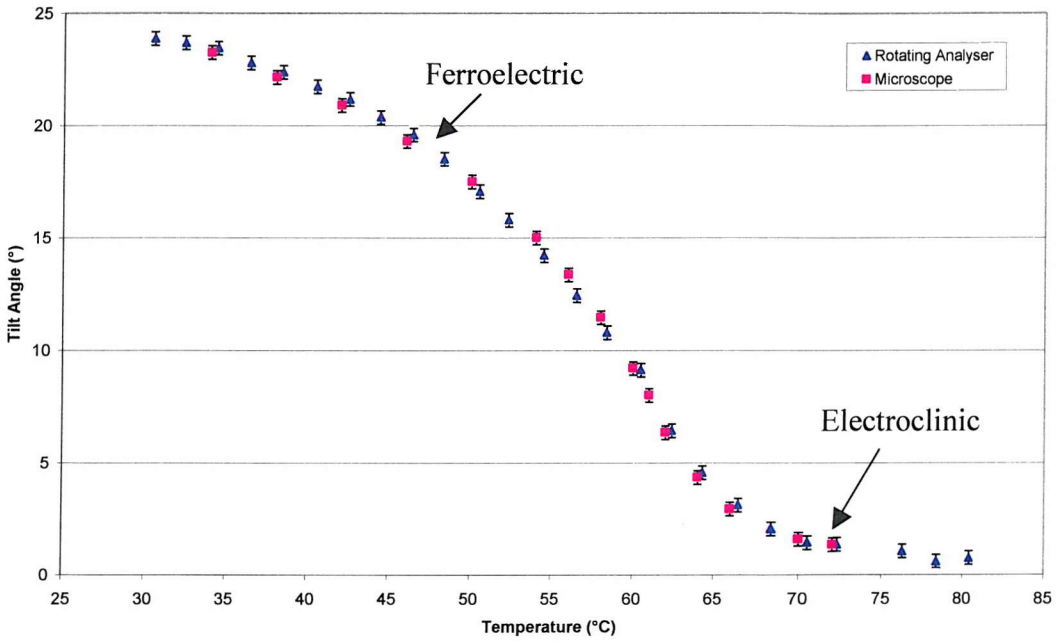

Figure 3.17 Comparison of the optical tilt angle of SCE13 measured using optical microscopy and rotating analyser methods. (10Hz, 13V/μm).

Unlike the method employed by Qui, Ho and Hark[36], the ability to measure both large (~45°) and small (<3°) tilt angles permits the continuous study of tilt angle across phase transitions, I-S_C^* or S_A-S_C^*, and therefore enables the easy study of the electroclinic effect, as shown in Figure 3.18 and Figure 3.19.

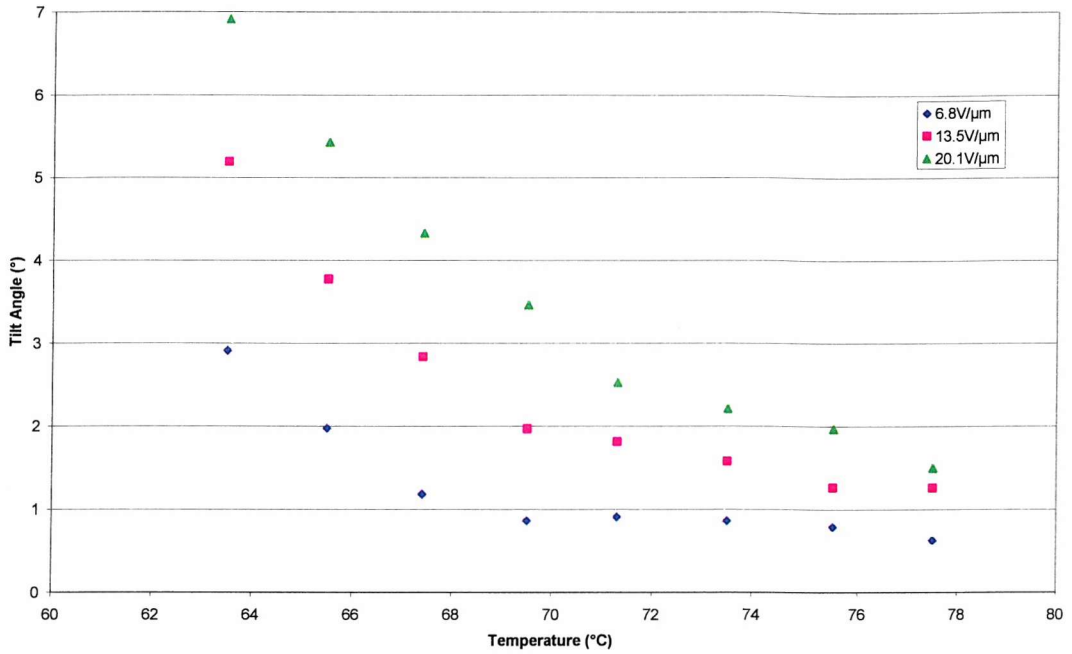

Figure 3.18 The Electroclinic Effect in SCE13

The data shown in the inset of Figure 3.19, taken at a temperature of 70°C, shows the electroclinic switching of SCE13 in the SmA phase. The linear dependence of the tilt angle on the applied field is maintained to ~20V/µm. Comparing this with the behaviour of SCE13 at 50 and 60°C, when the material is in the SmC* phase, illustrates the differences between the electroclinic and ferroelectric switching mechanisms. In the SmC* phase the tilt angle rapidly saturates at 15 to 20° under the application of a 0.2V/µm electric field; the tilt angle of the SmC* phase is much higher than the 8° tilt angle observed in the SmA phase.

[36] R.Qui, J.T.Ho, S.K.Hark, *Phys.Rev.A*, **38**, 1653 (1988)

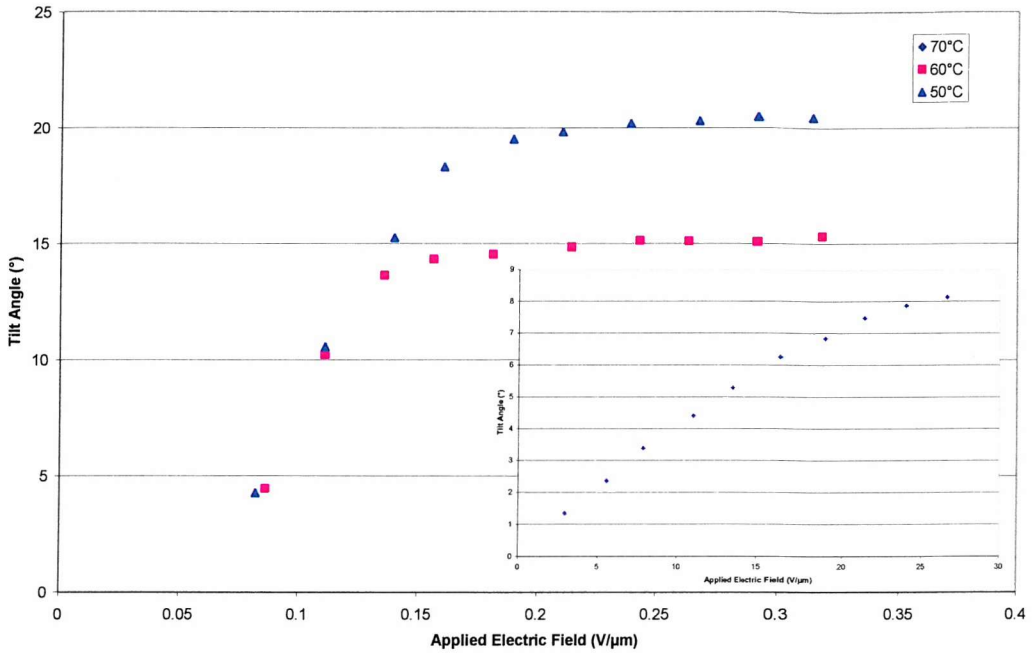

Figure 3.19 Variation of the optical tilt angle of SCE13 as a function of the applied electric field and temperature.

The limitation of the rotating analyser method is the requirement that the frequency of the applied field is ~10Hz. This can be a problem for measurements using materials where the quality of the alignment is frequency dependent.

3.5.3 Response Time Measurement

The characteristic response time of a liquid crystalline material is related to the time taken to switch between two states on the application of an electric field. The response time can be measured optically or, in the case of ferroelectric liquid crystals, electrically.

3.5.3.1 Optical Response Time

In this work the optical response time, τ, is defined as the time taken for the transmittance of the material to change from 10% to 90% of the maximum signal amplitude. The experiment used to measure τ is the same as that used to obtain tilt angle measurements using the polarising microscope and is illustrated schematically in Figure 3.20.

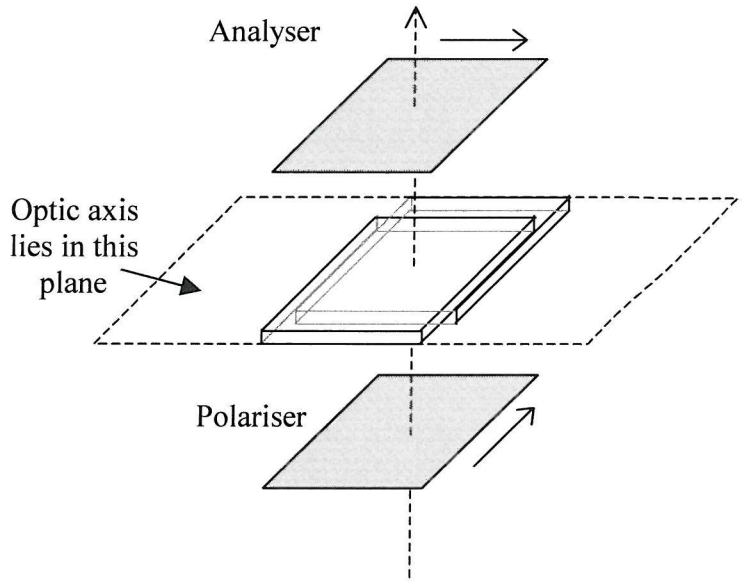

Figure 3.20 Schematic illustration of the geometry employed in the experimental determination of the optical response time of ferro- and flexoelectric liquid crystal systems.

The liquid crystal sample is contained in a cell so that the optical axis is perpendicular to both the applied field and the direction of the light beam. A square wave is applied across the sample and the transmitted intensity detected by the photodiode is displayed as a voltage on the digitising oscilloscope via the PDA.

3.5.3.2 Optical Response Time in Nematic Systems

The response time of the Freedericksz Transition in the TN geometry was measured. Application of an electric field causes the director to align with the field, destroying the twist and resulting in a dark state if the TN cell is viewed between crossed polarisers. This geometry allows for optimum contrast between the two switched states, as described in Section 2.6.1. Thus, the optical rise, τ_{rise}, and fall, τ_{fall}, times are measured as the time elapsed between the signal undergoing change from 10-90% and 90-10% respectively.

3.5.3.3 Optical Response Time in Ferroelectric and Flexoelectric Systems

The sample is oriented such that the contrast between the two switched states is maximised, i.e. the optical axis of one of the states coincides with the transmission axis of

one of the polarisers. This requires a ferroelectric liquid crystal material to be in a surface stabilised geometry and a flexoelectric liquid crystal to be in the uniform lying helix geometry. In contrast to the nematic materials, the transition between the two switched states in ferro- and flexoelectric systems is driven by the applied field in both directions. As with the measurement of spontaneous polarisation and optical tilt angle in ferroelectric liquid crystals, it is essential that the magnitude of the applied field is large enough to allow the sample to switch completely. Incomplete switching will result in erroneously fast response time measurements. Accurate measurements of the optical response time require good alignment, i.e. large monodomain samples.

In ferroelectric and flexoelectric systems a bipolar applied field will yield the response time relating to the switching angle. A monopolar field applied to a flexoelectric system will result in the response time relating to the tilt angle. Due to the bistability of ferroelectric systems a monopolar pulse will not cause the director to switch.

When the tilt angle of the material is greater than 22.5° the definition of 10% and 90% transmission levels becomes obscure. As the material switches through an angle of more than 45°, the optical transmission becomes complex, as shown in Figure 3.14(d).

3.5.3.4 Electrical Current Response Time

This method is favourable for ferroelectric materials where poor alignment results in a lack of contrast between the switched states or where tilt angles of more than 22.5° cause ambiguity in the definition of the 10% and 90% intensity levels measured using the optical technique.

The experiment is similar to that employed in the measurement of the spontaneous polarisation. In this case, however, a bipolar square wave (not a triangular wave) is applied across the cell. The current pulse is converted to a voltage change and detected by the digitising oscilloscope. The current response time is defined as the time elapsed between reversal of polarity of the applied field and the peak in the current response, as shown in Figure 3.21.

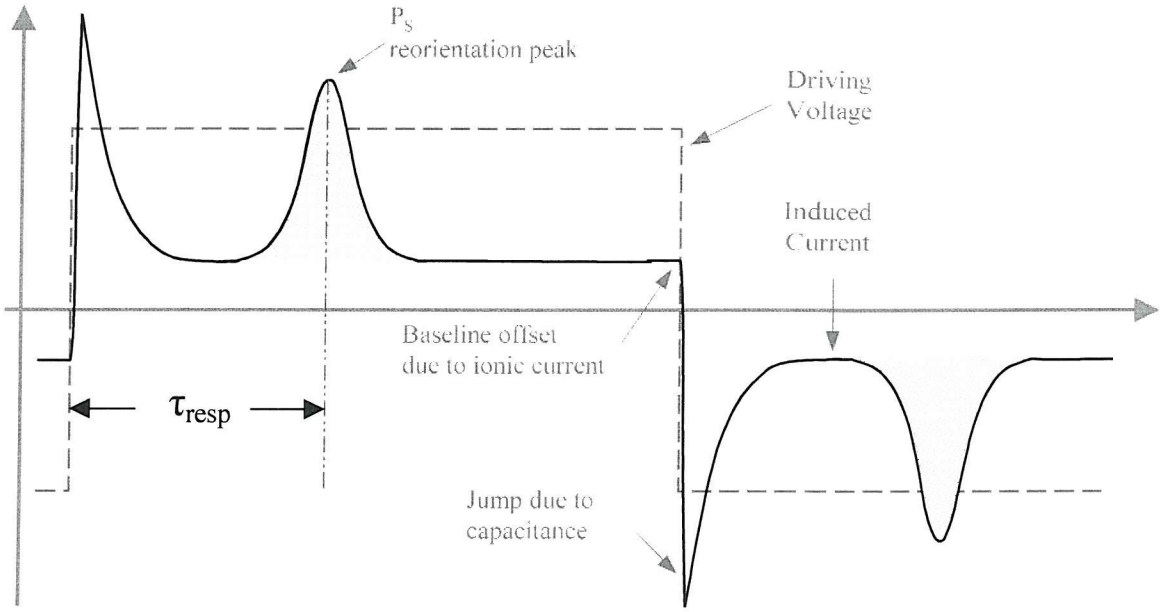

Figure 3.21 The current pulse response of a ferroelectric material to a square wave driving voltage.

The current pulse response consists of three different components as illustrated in Figure 3.21 and Figure 3.9 in the discussion on the measurement of the spontaneous polarisation. The accuracy of the current pulse method is dependent on two factors; the 'jump' in the response due to the capacitance can often have a long decay, which merges with the dipolar reorientation peak, and at lower temperatures the dipolar reorientation response becomes quite broad, making accurate identification of the peak difficult.

3.5.4 Measurement of the Dielectric Constant

Dielectric constant values were calculated from capacitance measurements carried out on a Wayne-Kerr 6425 bridge[37]. Capacitances of empty and full cells were measured as a function of voltage and frequency. Placing the cell in a Mettler Hotstage allowed measurements to be made as a function of temperature. The dielectric constant was calculated from the ratio of the full and empty values;

$$\varepsilon = \frac{C_{full}}{C_{empty}}. \qquad (3\text{-}11)$$

$\varepsilon_{\perp}$ could be obtained using planar cells whilst homeotropic cells yielded $\varepsilon_{//}$. Where homeotropic alignment was not achievable calculated values of $\varepsilon_{\perp}$ and ε_{iso} were used to estimate $\varepsilon_{//}$ via Equation 3.11:

$$\varepsilon_{iso} = \frac{\varepsilon_{//} + 2\varepsilon_{\perp}}{3}. \qquad (3\text{-}12)$$

The dielectric anisotropy $\Delta\varepsilon$ could then be estimated from $\varepsilon_{\perp}$-$\varepsilon_{//}$. For a more detailed description of this measurement, the reader is referred to the thesis of C.Schott[38].

3.6 SUMMARY

This chapter has introduced the basic experimental apparatus and procedures used for the characterisation of the liquid crystalline materials studied in this thesis. Techniques used for determining the materials' phase sequences were discussed. Details of the sample preparation and cell fabrication processes were then outlined. A detailed description of the analytical methods employed in the measurement of spontaneous polarisation, tilt angle and response time was given, with reference to the theories provided in the previous chapter. The design and operation of the 'rotating analyser' technique for measurement of

---

[37] Wayne Kerr Electronics, Vinnetrow Business Park, Runcton, Chichester, UK, PO20 1QH. http://wwwaynekerrtest.com

[38] C.Schott *Ph.D. Thesis*, University of Southampton, UK (2001)

optical tilt angles was explained. Data obtained using these techniques will be presented and discussed in the following chapters.

Chapter Four

LOW MOLAR MASS ORGANOSILOXANES

4.1 INTRODUCTION

Ferroelectric liquid crystals have been the subject of much research over the last decade principally due to their fast response to electric fields and the potential for applications in display devices. Furthermore, the antiferroelectric phase discovered in 1989, has even greater potential for displays. The application of an electric field to an antiferroelectric material will induce ferroelectric ordering which can be switched in the usual manner by reversing the field polarity. On removal of the field the antiferroelectric ordering is reformed. Effectively the antiferroelectric materials possess three stable states with well-defined electric field thresholds, allowing easier multiplexing of the display device. However, both these devices can be fragile and easily damaged by slight physical force.

Work has been carried out on polymeric liquid crystals with a view to improving the shock resistance of the ferro- and antiferroelectric phases but there are a number of inherent disadvantages to these systems, such as high viscosity, which leads to long response times and high glass transition temperatures. These disadvantages result in limited applications for polymer ferroelectric liquid crystals. A new approach to this problem has been to use organosiloxane liquid crystal systems.

The work in this chapter is based upon a new series of low molar mass (LMM) organosiloxane liquid crystal compounds, which have been shown to combine the robust properties of polymers with the fast electro-optic response times of true low molar mass systems. Low molar mass in this context refers to the size of the mesogenic unit, the chemical group associated with the formation of liquid crystal compounds.

4.2 LOW MOLAR MASS ORGANOSILOXANE LIQUID CRYSTALS

The molecules consist of one or more mesogenic moieties attached via an alkyl chain spacer to a short siloxane group. The different chemical properties of the mesogenic and siloxane moieties result in a 'microphase separation' of the siloxane groups into a polymer

'backbone'. It is due to this microphase separation that the materials possess some of the advantages of polymer systems, principally ruggedness, in combination with the aforementioned attributes of LMM liquid crystals such as low rotational viscosity of the mesogen[1] and fast response times. This structure also strongly encourages the formation of smectic phases. Thus, even when typical nematogenic moieties, such as cyanobiphenyls, form the mesogen, a layered smectic phase is usually formed[2].

In this chapter, the properties of two homologous series of organosiloxane materials are discussed. By varying the length of the siloxane group and changing the mesogenic unit a systematic study of the effect of molecular structure on phase behaviour has been carried out.

4.2.1 Materials

The typical strucutre is illustrated in Figure 4.1. The mesogens consist of a chiral moiety (A) with a laterally substituted halogen (X) grafted onto the benzoate ring closest to the chiral centre. The chiral centre, essential for ferroelectric behaviour, is marked with an asterisk. The biphenyl benzoate mesogen is associated with high spontaneous polarisation and tilt angles[1]. This chiral mesogen is attached to a siloxane group (B) by an alkyl chain spacer.

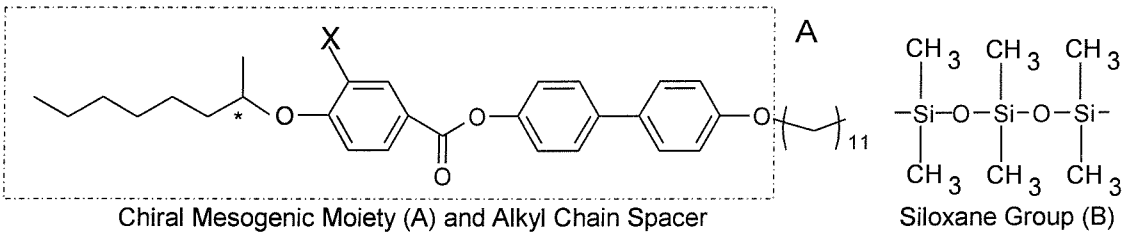

Figure 4.1 The constituents of the mono-mesogen (AB) and bi-mesogen (ABA) organosiloxane compounds.

The measurements were made on two homologous series in which the number of silicon atoms (n) in the siloxane group was varied between 2 and 5 and the halogen substituted

[1] P.Kloess, J.McComb, H.J.Coles, R.Zentel, *Ferroelectrics*, **180**, 233 (1996)

onto the mesogen was either chlorine or bromine. The length of the alkyl chain spacer was kept constant at 11 carbon atoms, previously shown to encourage high tilt angles and reduce the temperature dependence of the tilt angle and spontaneous polarisation[3]. The homologous series investigated consist of low molar mass systems with a mono-mesogenic (AB type) or bi-mesogenic (ABA type) structure[4]. In the AB molecules a single mesogen is attached to the siloxane group, whilst in the bimesogens two mesogenic units are attached symmetrically to the siloxane group. The notation **X11-n** is used to denote the mono-mesogen (AB) molecules and **X11-n-11X** is used to denote the bi-mesogen (ABA) molecules; where n indicates the number of silicon atoms in the siloxane group.

By keeping the length of the alkyl chain spacer constant (11 carbon atoms) the role of the siloxane moiety can be investigated by varying the number of silicon atoms in the end (AB) or linkage (ABA) group. The effect of substituting different halogens is also studied in a similar manner.

In this chapter the mesophase behaviour and electro-optic properties of the compounds will be presented and comparisons will be made between the monomesogenic and bimesogenic homologues.

4.3 CHARACTERISATION OF THE MONO-MESOGENIC ORGANOSILOXANE COMPOUNDS

The mono-mesogenic materials studied in this chapter are; Cl11-2, Cl11-3 and Br11-3. The samples were characterised by DSC, optical microscopy and thermo-optic analysis.

---

[2] J.Newton, H.J.Coles, P.Hodge, J.Hannington, *J. Mater. Chem.*, **4**(6), 869 (1994)
[3] P.Kloess, *Ph.D. Thesis*, University of Southampton, UK (1997)
[4] W.K.Robinson, P.Kloess, C.Carboni, H.J.Coles, *Liq.Cryst.*, **23**,309 (1997)

4.3.1 Phase Transition Temperatures

Differential scanning calorimetry was carried out at a rate of 5°C/min over the temperature range -20°C to 180°C. The DSC thermograms of all three materials exhibited two peaks on both heating and cooling. Hysteresis was observed in the low temperature peak on heating and cooling which was later attributed to the samples supercooling. The high temperature transition peaks were independent of the thermal history of the sample. The phase transition temperatures obtained (peak onset on cooling) by DSC are shown in Table 4.1. These results will be discussed in light of the thermo-optic analysis described below.

Table 4.1 Phase transition temperatures obtained by DSC (Peak Onset, Cooling at 5°C/min)

Compound	I – LC (°C)	LC - K (°C)
Cl11-2	94.5	39
Cl11-3	96	41
Br11-3	88.5	40

To complement the DSC data, thermo-optical analysis and optical microscopy studies were undertaken. These methods provide data for the materials contained in thin optical cells.

Thermo-optic analysis, carried out on heating from the crystalline state and cooling from the isotropic phase at 1°C/min, did not show any distinctive texture changes within the liquid crystalline phase, indicating that no intermediate mesophase-to-mesophase transitions occurred, see Figure 4.2. All the mono-mesogenic organosiloxanes exhibited a liquid crystalline phase over a broad, approximately 40°C temperature range. The mesophase temperature range of the chlorinated compounds is larger than that of the brominated compound by approximately 6°C. The isotropic transition temperatures of the chlorinated moieties were also higher than the brominated compound indicating that more stable, stronger anisotropic intermolecular forces exist between the chlorinated homologues compared with the brominated homologue. The chlorine atom is smaller than the bromine and therefore does not decrease the length to breadth ratio of the molecule. The weaker intermolecular forces in the brominated sample lead to reduced stability of the

mesophase and thus, lower phase transition temperatures. The liquid crystal-to-crystal transition was accompanied by a change in the transmitted light intensity (illustrated in Figure 4.4 c) and d)). This texture change is easier to observe if an electric field is applied across the sample, see Figure 4.5.

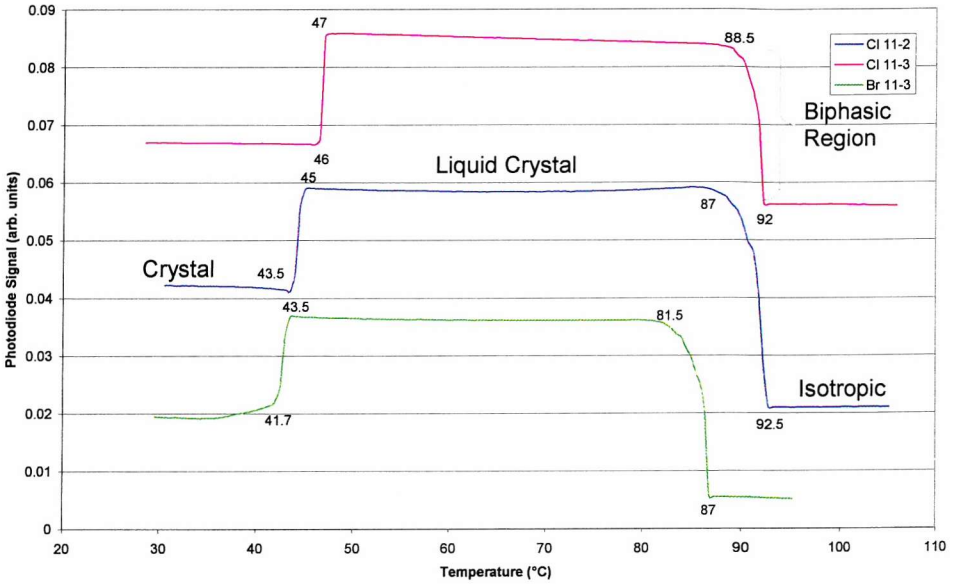

Figure 4.2 Thermo-optic response of mono-mesogenic organosiloxanes. Data taken on cooling at 1°C/min. (Curves have been offset to improve the clarity of viewing).

The transmitted intensity remains almost constant whilst the materials are within the liquid crystalline state indicating little, or no, change in the birefringence. All the compounds exhibit approximately a 5°C wide bi-phasic region on cooling from the isotropic state. Supercooling was again observed at the liquid crystal to crystal transition, as shown in Figure 4.3. The transition temperatures of Br11-3 are approximately 5°C lower than those of the chlorinated homologue Cl11-3. ratio of the molecule. The weaker intermolecular forces in the brominated sample lead to reduced stability of the mesophase and thus, lower phase transition temperatures.

The temperatures quoted in Table 4.2 are those obtained on cooling due to the effects of surface alignment noted in §3.3. The phase transition temperatures obtained optically and by DSC can differ by up to 5°C; this is primarily due to effects induced by the surface alignment of the cells.

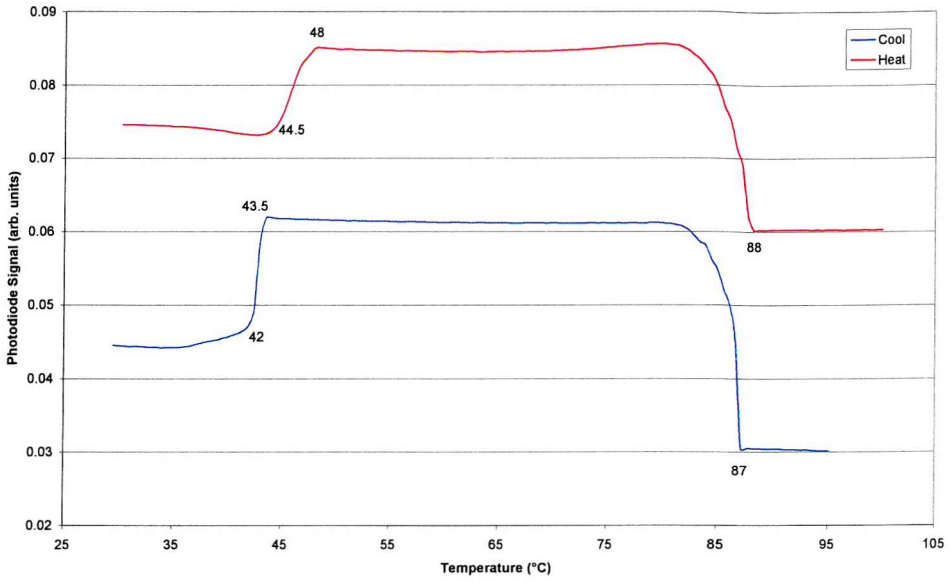

Figure 4.3 Thermo-optic response of the mono-mesogenic organosiloxane liquid crystal, Br11-3. Curves have been offset to improve the clarity of viewing. Data taken using heating/cooling rates of 1°C/min.

Table 4.2 Phase transition temperatures obtained from thermo-optic analysis on cooling at 1°C/min

Compound	I – LC (°C)	LC - K (°C)
Cl11-2	92.5	45
Cl11-3	92	47
Br11-3	87	43.5

4.3.2 Textures

Textural observations were made on the sample enclosed in a planar aligned 'Lucid' cell with a nominal thickness of 5μm. The cell was filled by capillary action, as described in §3.4.

At room temperature the materials have the appearance of a waxy solid. On heating from this crystal phase all the materials displayed a broad liquid crystal phase before clearing to the isotropic state. All three materials exhibited similar textures on cooling from the

isotropic phase in the absence of an applied field; a fine Schlieren, or sandy texture was adopted by all the materials, (see Figure 4.4).

The transition from the isotropic phase to the liquid crystalline phase occurred via the formation and growth of 'florets' of fine Schlieren texture, Figure 4.4 a). The biphasic region existed over a 2-5°C range. The fine Schlieren texture was retained over the entire liquid crystal phase range. Very little change in the texture was observed as the temperature was reduced from 85°C to 60°C, indicating the sample birefringence remains approximately constant. No further textural changes occurred until the transition into a glass. This transition was accompanied by a noticeable reduction in the transmitted intensity, although the texture remained intact, see Figure 4.1 d).

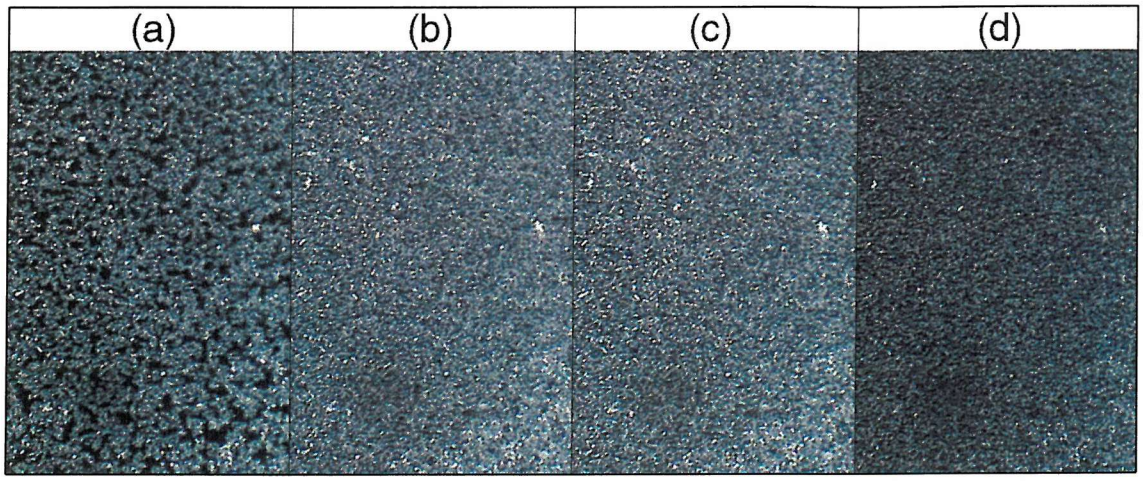

Figure 4.4 Photomicrographs of the textures exhibited by Br11-3 on cooling from the isotropic phase in the absence of an applied electric field. a) 88°C, b) 85°C, c) 60°C, d) 40°C.

On cooling from the isotropic phase in the presence of an electric field, a focal conic texture formed, which is typical of the SmC* phase, (shown in Figure 4.5). This texture remained when the field was removed. Some degree of uniform alignment was obtained by cooling very slowly from the isotropic phase in the presence of an alternating applied field. The frequency and magnitude of the applied field were varied until electrohydrodynamic (EHD) instabilities[5,6] were observed. These turbulent regimes typically appeared at applied field strengths of ~10V/μm and frequencies of ~10Hz.

[5] J.A.Guerst, W.A.Goosens, *Phys.Lett.*, **41**, 369 (1972)
[6] A.B.Davey, W.A.Crossland, *Mol.Cryst.Liq.Cryst.*, **263**, 325 (1995)

Initially, the batonnets formed on cooling from the isotropic phase are in rapid motion. On further cooling this motion slows down and the batonnets coalesce into a uniform texture.

The lack of good alignment leads to poor optical signals, making it difficult to obtain optical hysteresis curves used to characterise the nature of the switching mechanism.

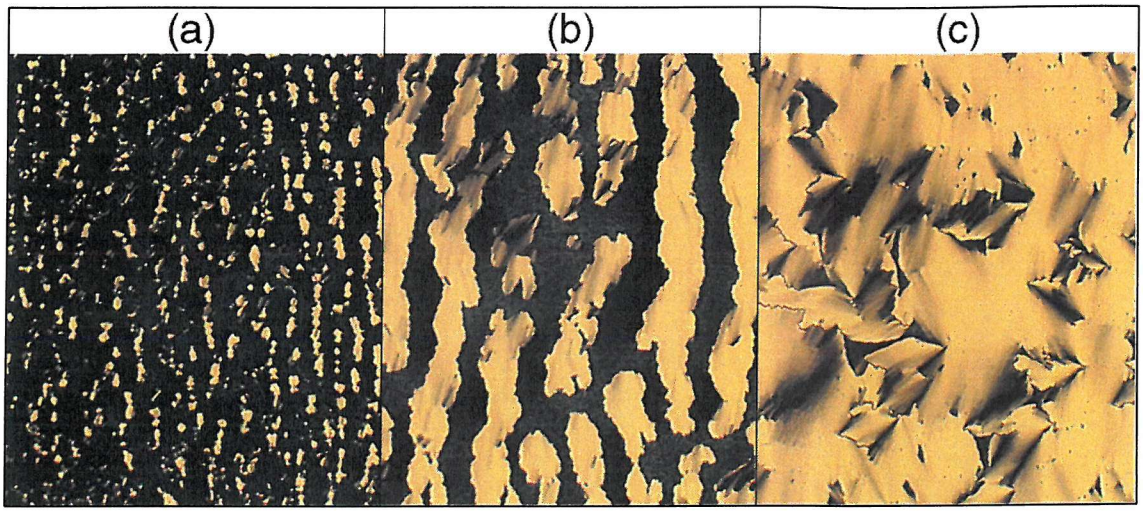

Figure 4.5 The alignment process of Br11-3 – application of 20V/μm, 30Hz triangle wave applied field whilst cooling the sample at 0.5°C/min. a) 90.5°C, b) 88°C, c) 83°C.

The application of an electric field increases the transition temperatures by approximately 4°C in all cases. This effect is due to changes in the boundary conditions and the ordering at the cell surfaces, which result in the liquid crystalline state becoming stable at higher temperatures. Switching, which is apparent from the onset of the liquid crystalline phase, is observed throughout the liquid crystal phase until the transition to a crystal phase. The switching mechanism was confirmed as Goldstone-mode (ferroelectric) switching by recording optical hysteresis curves and the electrical response. The electro-optic response of all the mono-mesogenic materials displayed the characteristic hysteretic response of the ferroelectric SmC* phase, as discussed in §2.4.3.

Under the application of an electric field the liquid crystal-to-crystal transition is accompanied by a distinct change in texture, as shown in Figure 4.6. As the sample is cooled into the crystal phase the focal conic fans break and the macroscopic birefringence

is dramatically reduced, resulting in reduced light transmission between crossed polarisers. The sample does not respond to an electric field in the low temperature state.

All the mono-mesogenic compounds were found to be ferroelectric over the whole mesophase range. The electro-optic studies are detailed in the following sections.

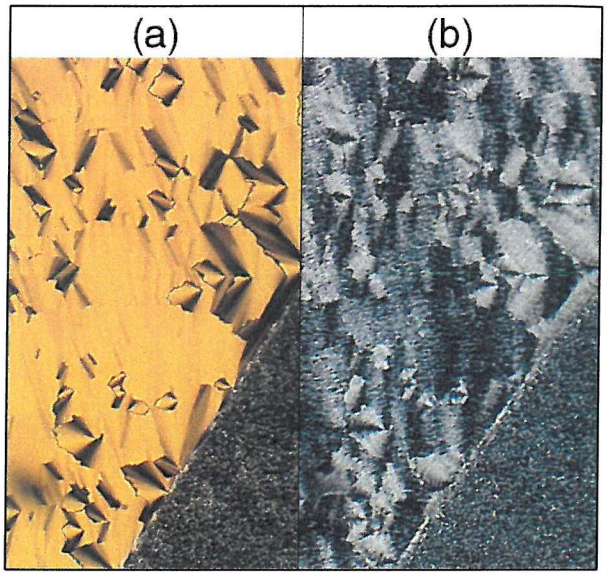

Figure 4.6 Photomicrographs of the textures exhibited by Br11-3 when subject to a 14V/μm, 30Hz triangular wave applied electric field. a) liquid crystal, 60°C and b) crystal, 40°C. Also visible are the electrode edge and the fine Schlieren texture of the material when it is not subjected to an electric field.

4.3.3 Electro-Optic Transmission Curves

The electro-optic response of Cl11-2 to a triangular wave applied field is shown in Figure 4.7. This trace was typical of that exhibited by all the mono-mesogenic organosiloxanes. The cell was rotated between crossed polarisers such that the switched states were symmetric about one polariser axis. As described in §3.5.2, the two switched states appear bright and have equal transmission. When the molecules reorient due to the reversal of the field polarity, the optic axis crosses the polariser axis, resulting in a dip in the transmission before the opposite switched state is entered. It was not possible to attain an orientation in which the material switched between light and dark states – at all times the transmission of the switched states was equal. These observations were interpreted to mean that the

material was undergoing a 90° switch. In this scenario the two switched states will always make an equal angle with one of the polariser axes, resulting in equal transmission in both states.

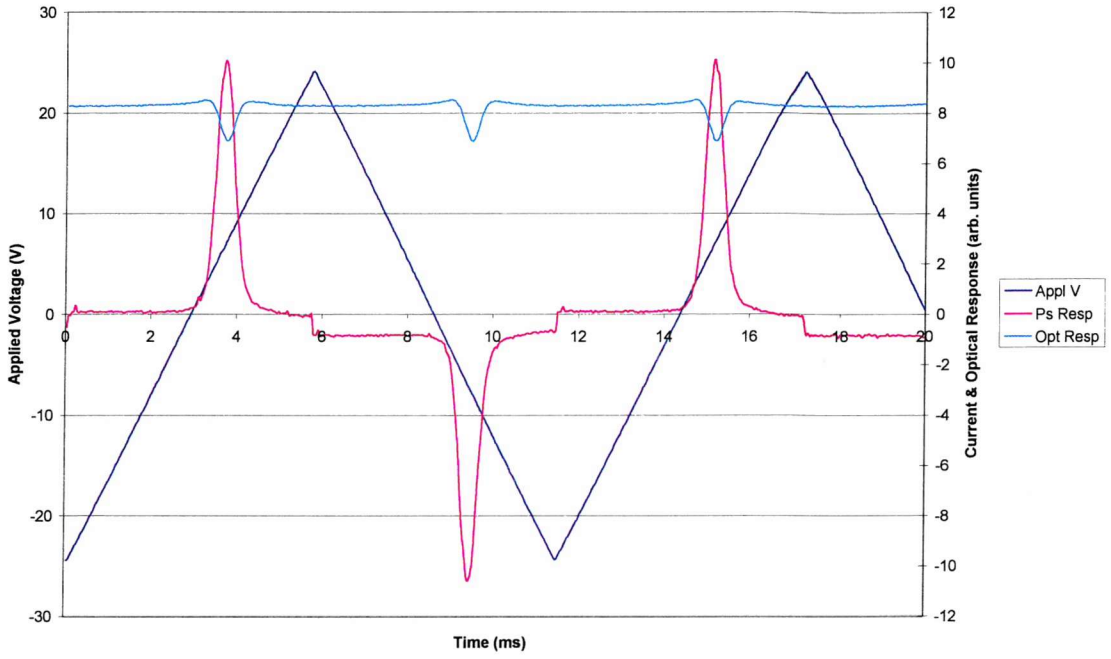

Figure 4.7. The current and optical response of Cl11-2 to a 5V/μm, 87.5Hz triangular applied electric field.

Also shown in Figure 4.7 is the current response, typical of ferroelectric materials, arising from the spontaneous polarisation of the material. The advent of a single current peak with onset just after the reversal of the field polarity is a characteristic of ferroelectric liquid crystals and has been discussed in detail in Section 3.5.1. The absence of any additional peaks in the current response verified that no higher order switching processes occurred within the mesophase.

Figure 4.8 records the optical hysteresis loop derived from the optical response of Cl11-2 to the triangular wave shown in Figure 4.7. The sample was positioned such that the light transmitted by one of the switched states was maximised. Graphs of this type illustrate the voltage dependence of the optical response. The applied field is plotted on the x-axis and the optical response plotted on the y-axis. This hysteresis loop was typical of that

expected for a 45° tilt (90° switching) material, thus confirming the earlier assumption made on the basis of the optical microscopy observations.

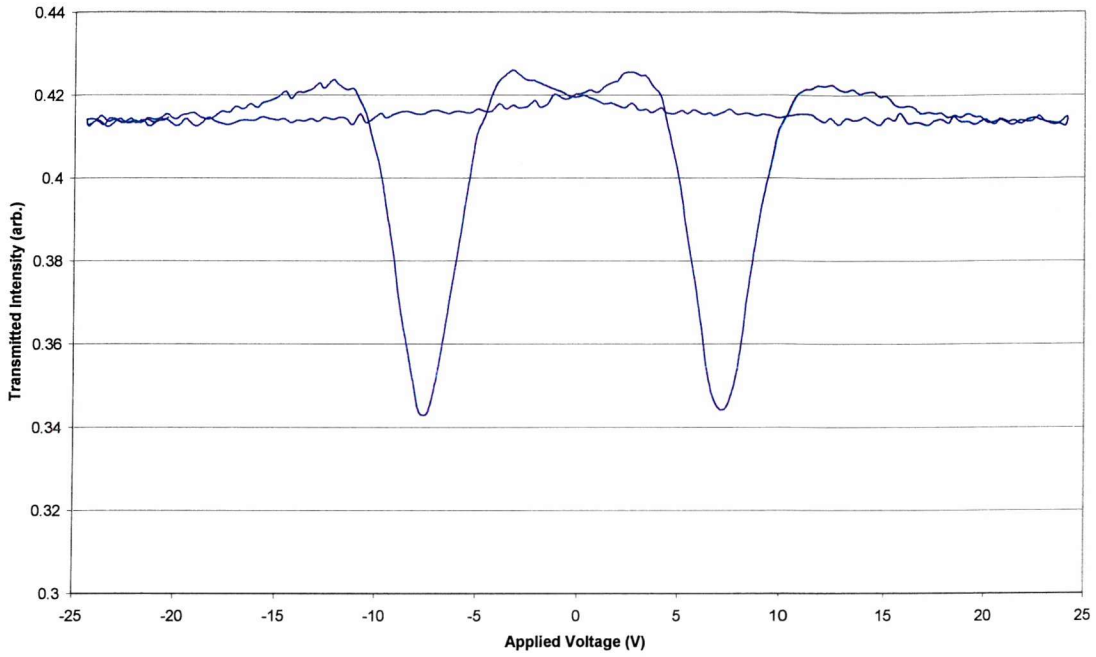

Figure 4.8 Optical hysteresis exhibited by Cl11-2 when subjected to 5V/μm, 87.5Hz triangular wave applied electric field at 70°C.

4.3.4 Spontaneous Polarisation

Measurements of spontaneous polarisation as a function of temperature were carried out using the current pulse method described in §3.5.1. A triangular wave of frequency 87.5Hz was applied across the sample. The magnitude of the applied field was increased to ensure that the switching was saturated. The results are shown in Figure 4.9.

The P_s rapidly increases on cooling into the SmC* mesophase from the isotropic state and within the mesophase has little temperature dependence. The extremely rapid saturation of the P_s may be explained by the first order nature of the I-SmC* transition. A more gradual

increase in P_s (called Curie-Weiss behaviour), typical of a second order transition[7], is not observed.

On cooling from the isotropic phase, the P_s of Cl11-2 rapidly increases to 100nC/cm². The spontaneous polarisation remains above this value for a 40°C wide temperature range, peaking at 115nC/cm² approximately 20°C below the I-SmC* transition, before crystallisation gradually occurs and the P_s decreases to zero at 40°C. On heating from the crystalline phase the P_s remains at zero until 45°C where it quickly rises above 80nC/cm² as the crystals melt before again reaching a peak of 115nC/cm² at about 20°C below the clearing point. The P_s of Cl11-3 has a temperature independent value of ~97nC/cm² across the whole mesophase range and only close to the extremities of the phase does it decrease towards zero.

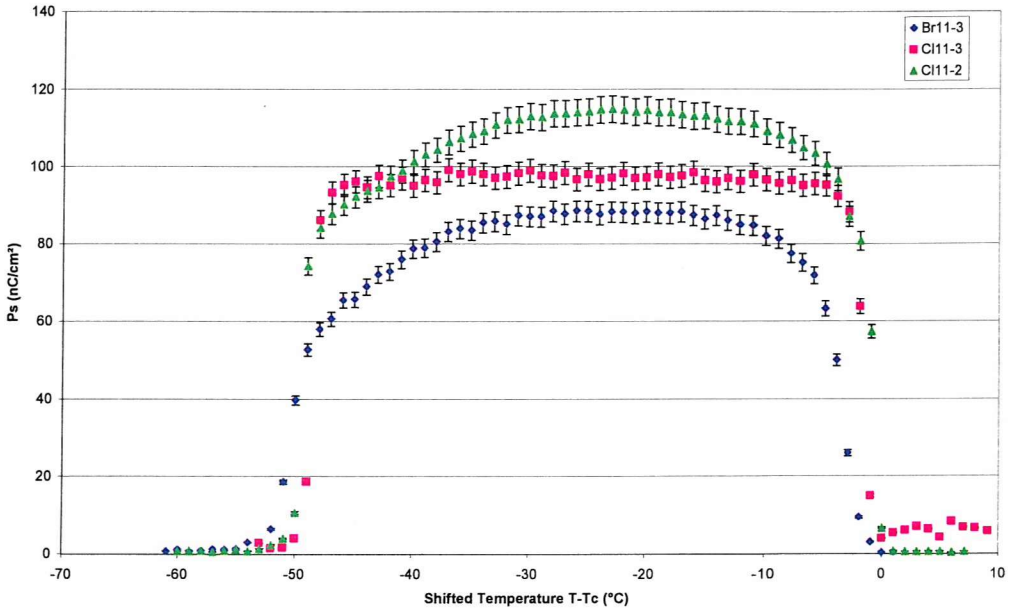

Figure 4.9 Measurements of the spontaneous polarisation of mono-mesogenic organosiloxane compounds as a function of shifted temperature. Data taken on cooling at 1°C/min.

A comparison of the data obtained for Cl11-2 and Cl11-3 indicates that Cl11-2 has a P_s approximately 10% higher than that observed in Cl11-3. As both compounds contain the same mesogen and alkyl spacer length the differences in behaviour will arise from the

[7] C.Kittel, *Introduction to Solid State Physics*, J.Wiley and Sons, p.425 (1986)

differing siloxane groups. The expected behaviour of the P_s can be modelled by the equation[8]

$$P_s = (yield\ factor)\ x\ (no.\ of\ molecules\ per\ unit\ volume)\ x\ (transverse\ dipole\ moment) \quad (4\text{-}1)$$

The longer siloxane chain of Cl11-3 results in an increase of molecular volume, and hence a decrease in the number of mesogens per unit volume. Thus if all other factors remain constant the P_s should decrease, as observed. The presence of the longer siloxane head group also seems to reduce the temperature dependence of the P_s.

Br11-3 has a smaller P_s than both the chlorinated mono-mesogens for two reasons. The difference in behaviour compared with Cl11-2 can be explained using the same argument as that just given for the P_s difference between Cl11-2 and Cl11-3, i.e. the change in behaviour is related to a change in molecular volume. However, perhaps more pertinent to this discussion is the magnitude of the respective dipoles arising from the presence of the bromine or chlorine atoms. Since the bromine atom has a lower electro-negativity than the chlorine atom, the bromo- substitution results in a smaller dipole being associated with the molecule and hence a lower Ps.

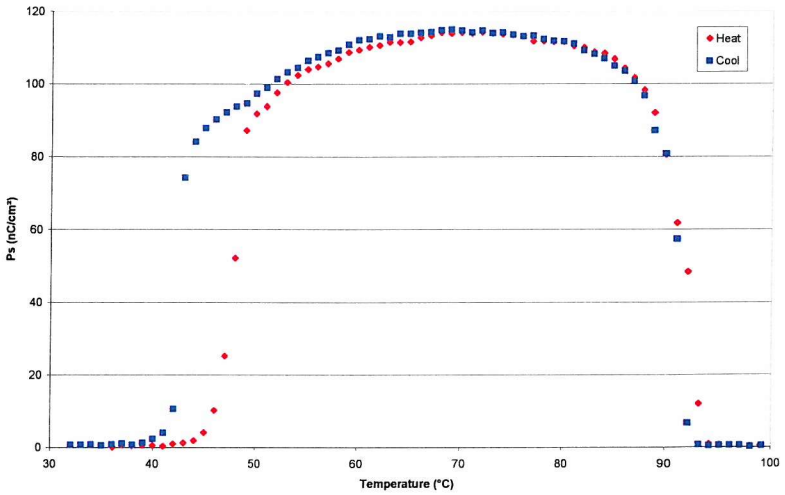

Figure 4.10 Measurements of the spontaneous polarisation of Cl11-2 illustrating the supercooling nature of the SmC*-Crystal phase transition. Error bars have been removed for clarity of viewing.

[8] P.G.de Gennes, J.Prost, *The Physics of Liquid Crystals*, Clarendon Press, p.380 (1993)

Figure 4.10 shows the hysteresis effects observed between the data taken on heating and cooling runs is a result of supercooling around the crystallisation point. This is often a feature of P_s versus temperature data and was observed in all the mono-mesogenic organosiloxane materials.

4.3.5 Current Response Time

The variation of the response time with temperature was also studied. Due to the difficulty of obtaining sufficiently good alignment in the optical cells it was deemed more accurate to measure the current response time than the optical response time. The current response times were defined as the time elapsed between field reversal and the peak current response and were measured by the method described in §3.5.3.

The current response of Cl11-2 to a triangular wave applied voltage of frequency 87.5Hz at a variety of different temperatures is shown in Figure 4.11a). The dynamics of the switching process gradually slow down as the Cl11-2 sample is cooled. It can be seen that the time elapsed between the reversal of the field polarity and the peak of the current pulse response increases as the temperature decreases. The area under the peaks remains almost constant throughout, illustrating the temperature independence of the P_s; tall thin peaks at high temperatures become shorter broader peaks at low temperatures. As the sample is cooled the peak becomes broader and the maximum peak height is significantly reduced.

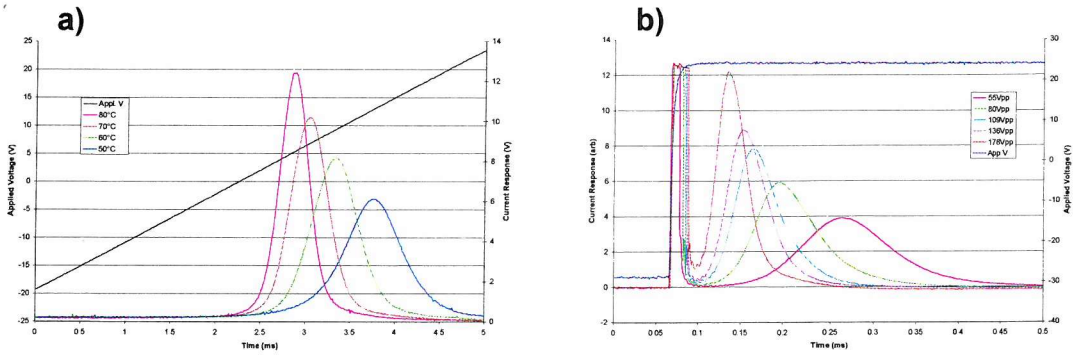

Figure 4.11 The temperature and electric field dependence of the spontaneous polarisation response of Cl11-2 to a) 5V/μm, 87.5Hz triangular wave applied field and b) 80Hz square wave applied field at 60°C.

Figure 4.11b) illustrates the field dependent behaviour of the current pulse in Cl11-2 at 60°C. The amplitude of a square wave voltage applied across the sample, held at constant temperature, was varied. For clarity of viewing only one of the applied waveforms is shown: the trigger conditions of the oscilloscope were set such that the polarity reversal of all the applied fields occurred at the same point on the time (x) axis. An increase in the applied field results in a decrease in the current response time.

The temperature dependence of the response time was measured using the current response to the application of a square wave alternating voltage of frequency 30Hz and amplitude 10V/μm. The response times are shown in Figure 4.12. The response times of all the mono-mesogenic organosiloxane compounds are of similar magnitude to other LMM systems. The response time remains under 100μs for temperatures within 30°C of T_c, with response times as fast as 30μs attainable at temperatures close to T_c. The temperature dependence of the response time increases markedly as the sample is cooled to more than 30°C below T_c.

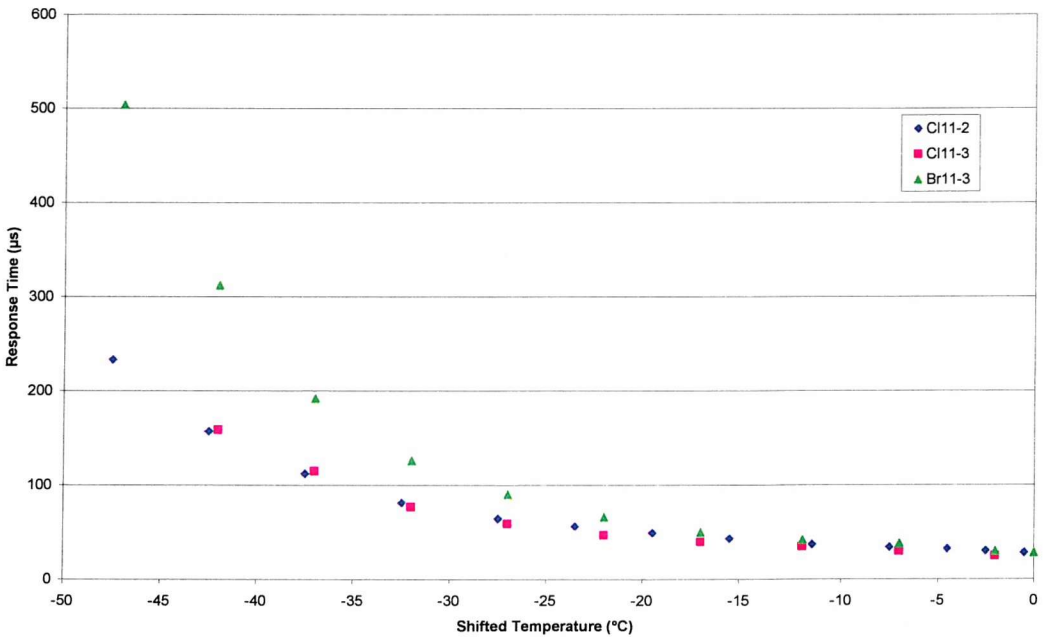

Figure 4.12 The temperature dependence of the current response time of the mono-mesgenic organosiloxanes. Data taken on cooling under the application of a 10V/μm, 30Hz square wave.

At a given reduced temperature the response time of Cl11-3 is faster than Br11-3. This is a direct result of the larger P_s of the chlorinated material. A comparison of Cl11-2 and Cl11-3 indicates that, the larger P_s and the smaller head group of Cl11-2 leads to slightly faster response times than those of Cl11-3 as a result of the reduced bulkiness of the siloxane end unit.

The slower response times observed at lower temperatures for all the materials are a result of the increased viscosity, γ. If we refer back to the equation governing the response time of ferroelectric liquid crystals, Equation 4-2, we see that the current response time, τ, measured at a given temperature, should be inversely proportional to the magnitude of the applied electric field, E.

$$\tau_{curr} \propto \frac{\gamma \sin^2 \theta}{\underline{P_s}.\underline{E}}. \qquad (4\text{-}2)$$

The dependence of the response time on the applied field for the three materials is shown in Figure 4.13a), b) and c). At high temperatures there is a small dependence on the applied field. As the sample is cooled this field dependence increases. The response time of the material also increases as the sample is cooled. It has been shown that the spontaneous polarisation and the tilt angle remain almost temperature independent throughout the phase so the increased response time is attributed to the rotational viscosity term in Equation 4-2.

It can also be seen in Figure 4.13 that as the temperature is decreased the gradient of the linear relationship between τ_{curr} and 1/E increases. The data given in this section and §4.3.6 shows that two of the variables in Equation 4-2, namely spontaneous polarisation and tilt angle, are temperature independent throughout the phase. Therefore, the steeper gradient was attributed to the rotational viscosity, γ, - the viscosity increases at lower temperatures resulting in the steeper gradient.

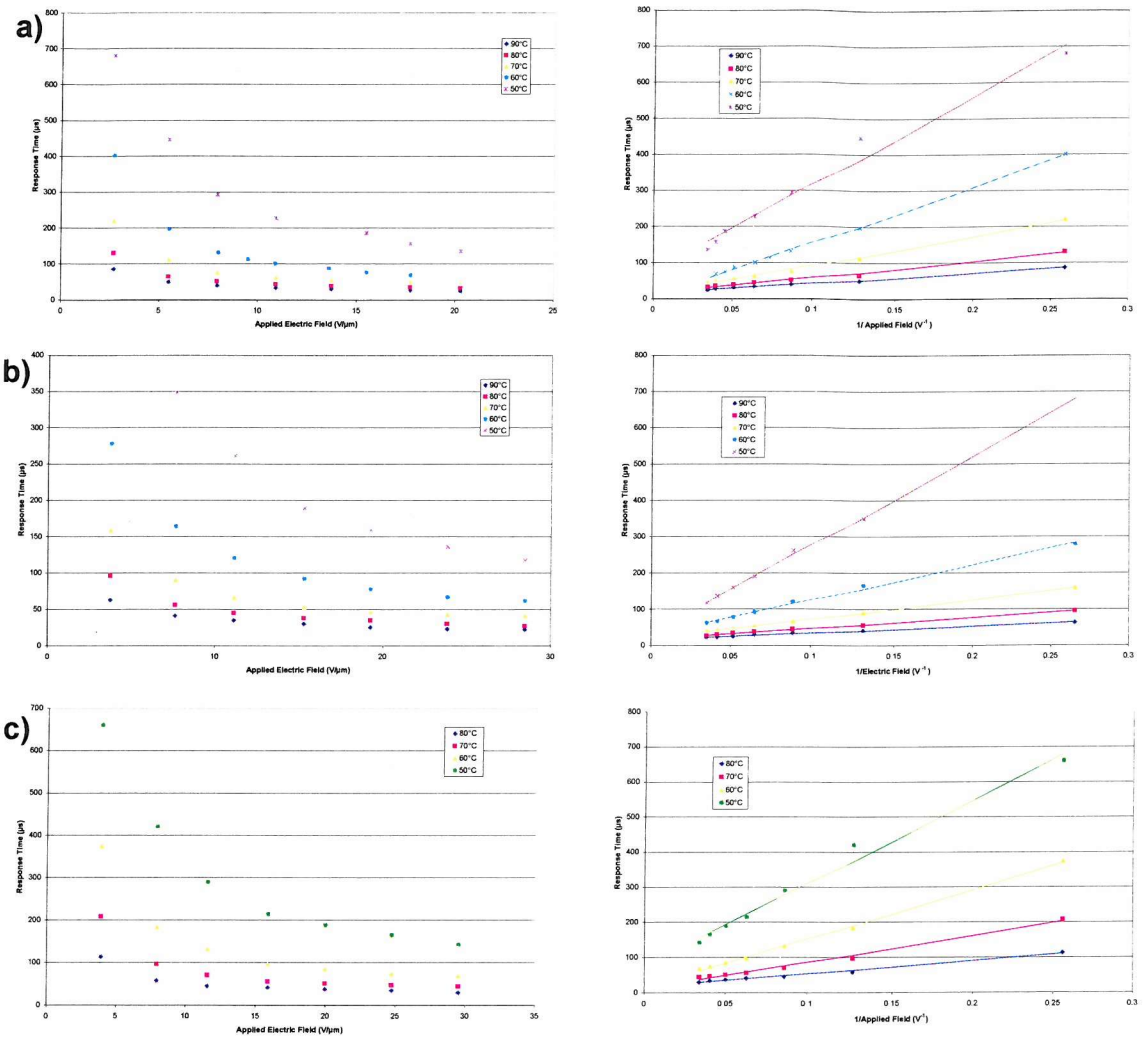

Figure 4.13 The temperature and electric field dependence of the current response time of the mono-mesogenic organosiloxane compounds, a) Cl11-2, b) Cl11-3 and c) Br11-3. The frequency of applied field was 80Hz.

4.3.6 Tilt Angle

As discussed in the previous chapter, the definition of the tilt angle is non-trivial. The direction of the average axis of the siloxane moiety can be quite different from that of the mesogenic moiety. We have defined the tilt angle as the angle between the optic axis of the mesogen and the normal to the plane of the smectic layers because it is the optic axis of the mesogen that determines the electro-optical properties of the material. Figure 4.14 shows the temperature dependence of the optical tilt angle of Cl11-2, Cl11-3 and Br11-3.

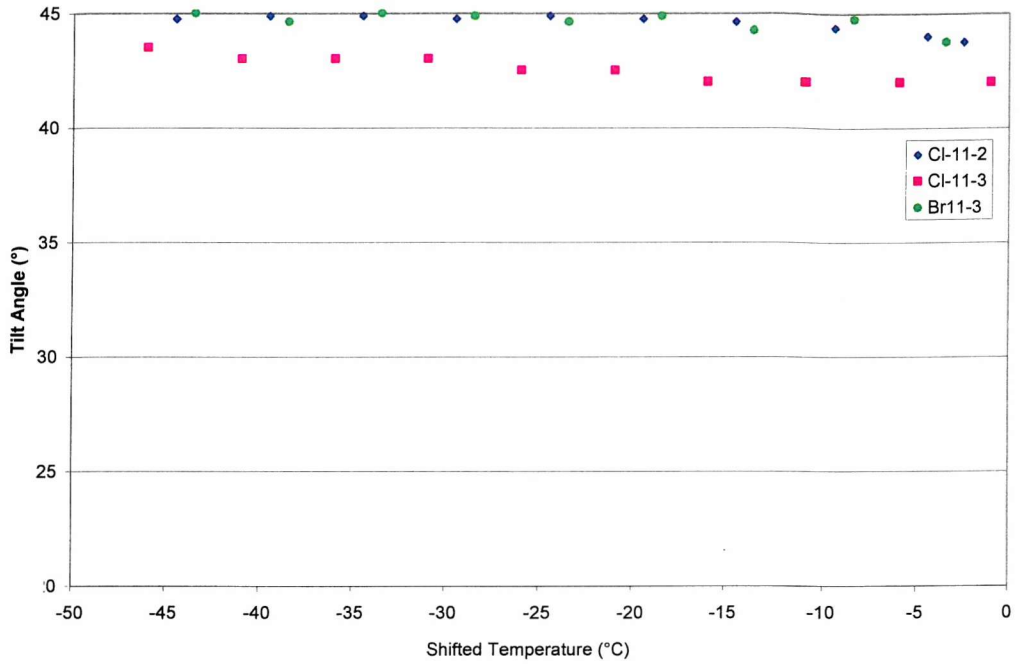

Figure 4.14 The temperature dependence of the optical tilt angle of the mono-mesogenic compounds.

The data given in Figure 4.14 was measured using the rotating analyser technique and applying ±5V/μm; the tilt angle is independent of the applied voltage above very small fields. The figure clearly shows the large range over which the tilt angle is temperature independent. The high, temperature independent tilt angle has been shown to be promoted by the presence of siloxane head groups[9]; the biphenyl benzoate mesogenic precursors do not possess these properties. These results are consistent with X-ray studies[10], which indicate constant layer spacing throughout the phase. The tilt angle is also high, 42-45°, making the materials ideal for single polariser dye guest host displays[11]. This type of device has the advantage of requiring just one polariser, thereby doubling the optical throughput of a conventional birefringence device.

The first order nature of the I - SmC* transition is again apparent. The extremely rapid saturation of the tilt angle is explained by the fact that the higher temperature phase is

[9] J.Newton, *Ph.D. Thesis*, University of Manchester, UK (1994)
[10] E.Corsellis, D.Guillon, P.Kloess, H.J.Coles, *Liq.Cryst.*,**23**(2), 235 (1997)
[11] D.E.Shoosmith, H.J.Coles, in preparation

isotropic and not SmA or nematic, as a result of the siloxane backbone strongly enhancing the smectic layer ordering. The transition from the isotropic phase to the ferroelectric SmC* phase is strongly first order and Curie-Weiss type behaviour[12] will not be observed. As is common in tilted smectic mesophases with a first order transition into the phase, the tilt angle remains constant throughout the mesophase. Indeed, the tilt angle data in Figure 4.14 will not adequately fit to the Curie-Weiss equation given in Section 2.2.2. The tilt angles of the materials are high, again this is typical of materials with a direct I-SmC* transition[13]

The bromo- substituted compound exhibits a slightly larger tilt angle than the chloro-substituted compound with the same length siloxane group. This is consistent with X-ray measurements showing the brominated material to have a smaller layer spacing than the chlorinated material[14].

The magnitude of the tilt angle is only weakly dependant on the length of the siloxane group. The grafting on of the siloxane moiety tends to impose a 45° tilt on the mesogens. As the siloxane chain is lengthened there is a small tendency for the tilt angle to decrease[15], returning towards the intrinsic tilt angle of the vinyl-terminated precursors.

4.4 CHARACTERISATION OF THE BI-MESOGENIC ORGANOSILOXANE COMPOUNDS

The bi-mesogenic organosiloxane compounds consist of two mesogenic units connected via alkyl chain spacers to the siloxane chain. In order to characterise the effect of the siloxane chain length on the system, compounds with 3, 4 and 5 siloxane units were synthesised. The length of the alkyl chain spacer was kept at a constant 11 units. This

[12] C.Kittel, *Introduction to Solid State Physics*, J.Wiley and Sons, p.425 (1986)
[13] G.W.Gray, J.W.Goodby, *Smectic Liquid Crystals-Textures and Structures*, Leonard Hill (1984)
[14] E.Corsellis, D.Guillon, P.Kloess, H.J.Coles, *Liq.Cryst.*, **23**, 235, (1997)
[15] W.K.Robinson, C.Carboni, P.Kloess, S.P.Perkins, H.J.Coles, *Liq.Cryst.*, **25**, 301, (1998)

length spacer was chosen for its favourable physical properties, these include high, temperature independent values of tilt and spontaneous polarisation[16].

The bi-mesogenic materials studied in this chapter were Br11-3-11Br, Cl11-3-11Cl, Cl11-4-11Cl and Cl11-5-11Cl. The materials were synthesised by Dr. S.P.Perkins.

4.4.1 Phase Transition Temperatures

Once again, the phase behaviour of the samples was characterised by DSC, optical microscopy and thermo-optic analysis. Again, the thermo-optic results differed slightly to those obtained by DSC due to the boundary conditions imposed in the materials within the optical cells, i.e. imposed on the sample by the alignment layers and cell thickness.

Table 4.3 Phase Transition Temperatures obtained by DSC (Peak Onset, Cooling at 5°C/min)

Compound	I – LC (°C)	LC - K (°C)
Cl11-3-11Cl	123	45
Br11-3-11Br	116	47
Cl11-4-11Cl	130	50

Table 4.4 Phase transition temperatures obtained from thermo-optic analysis on cooling at 1°C/min

Compound	I – LC (°C)	LC - K (°C)
Cl11-3-11Cl	120	47.3
Br11-3-11Br	109.5	40.5
Cl11-4-11Cl	113.8	45.5
Cl11-5-11Cl	120	50

Thermo-optic analysis was carried out on cooling at a constant rate of 1°C/min. The curves in Figure 4.15 have been offset to improve the clarity of viewing.

[16] P.Kloess, *Ph.D. Thesis – University of Southampton* (1997)

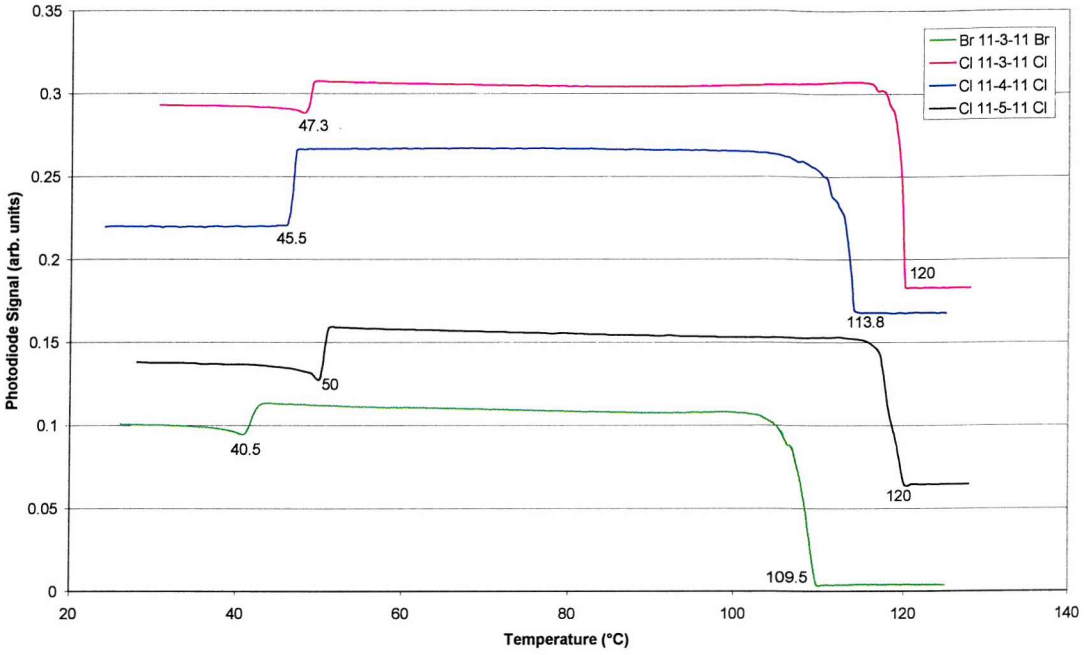

Figure 4.15 Thermo-optic traces of bimesogenic organosiloxane compounds taken on cooling at 1°C/min. (Data has been offset to improve the clarity of viewing).

All of the materials exhibit a biphasic region over ~5°C on cooling from the isotropic phase. All of the materials showed broad mesophase ranges of ~70°C. Little change in the intensity of the transmitted light across the mesophase indicated that there were no noticeable textural changes and little change in the birefringence. The transition from the mesophase to the crystal phase is accompanied by a reduction in the transmitted intensity. Cl11-4-11Cl was observed to have lower transition temperatures than the 3 and 5 siloxane chlorinated derivatives. This was attributed to the well-documented odd-even effect[17]. Cl11-4-11Cl also possesses a broader biphasic region at the transition between the isotropic phase and the mesophase. A comparison between the data obtained for Cl11-3-11Cl and Br11-3-11Br shows that the brominated derivative has lower transition temperatures. This was deemed to be a result of the presence of the bromine atoms, which are larger than chlorine atoms and affect the intermolecular forces more strongly, subsequently affecting the ordering conformation.

[17] W.K.Robinson, C.Carboni, P.Kloess, S.P.Perkins, H.J.Coles, *Liq.Cryst.*, **25**, 301, (1998)

4.4.2 Textures

Optical microscopy of the samples, contained in planar aligned 'Lucid' cells, showed all materials to exhibit similar Schlieren textures on cooling from the isotropic phase in the absence of an applied field. The monomesogenic organosiloxane compounds that were previously shown to be ferroelectric also adopted this fine Schlieren texture, as shown in Figure 4.16. The results of the thermo-optic investigations were confirmed since no textural changes were observed. The Schlieren structure remained into the crystal phase although there was a noticeable reduction in the transmitted intensity at the liquid crystal to crystal phase transition.

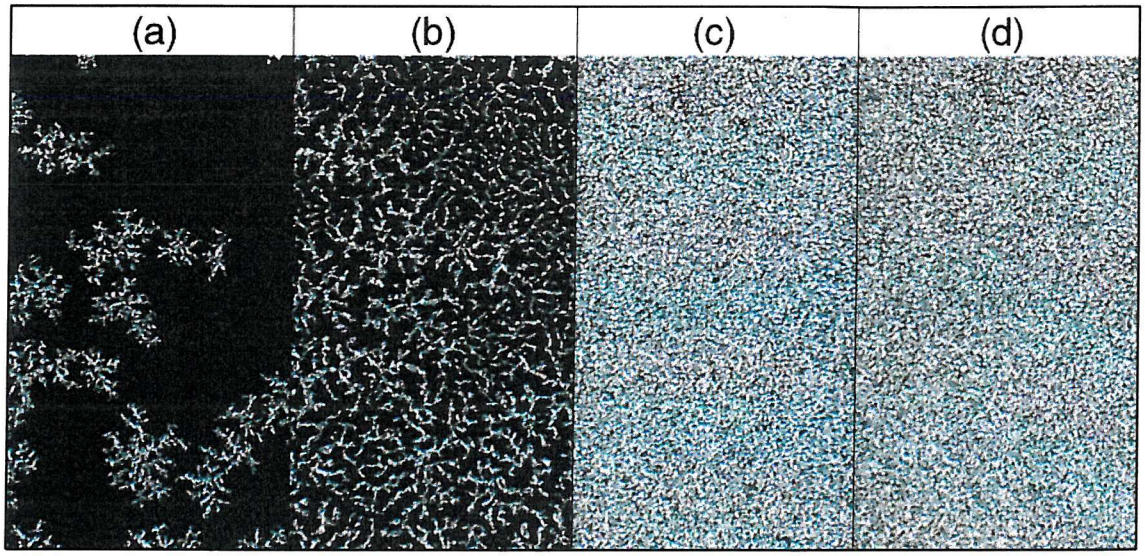

Figure 4.16 Textures of Cl11-5-11Cl whilst cooling at 1°C/min in the absence of an applied electric field. a) 118°C b) 117°C c) 112°C d) 42°C

The application of an electric field to the bimesogens whilst cooling from the isotropic phase results in the formation of a focal conic texture. In contrast to the behaviour of the mono-mesogenic compounds, a distinct change in texture is observed on removal of the applied field, as shown in Figure 4.17. The exception to this was Cl11-4-11Cl, in which the texture induced by the applied field remains after the field is removed.

Figure 4.17 Textures exhibited by the bimesogenic organosiloxane Cl11-3-11Cl, a) no applied electric field and b) electric field applied. 2- and 4-brush defects characteristic of smectic phases are observed.

As with the monomesogenic organosiloxane compounds, the materials were difficult to align. The exception to this was Cl11-4-11Cl. The textures exhibited by Cl11-4-11Cl on cooling in the absence and presence of an applied field are shown in Figure 4.18 and Figure 4.19 respectively.

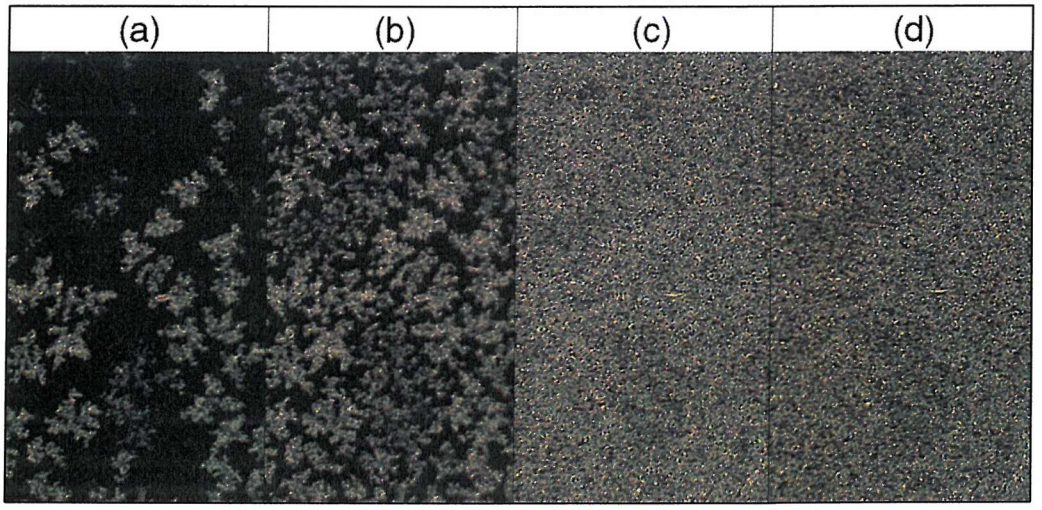

Figure 4.18 Textures of Cl11-4-11Cl on cooling with no field applied, a) 111°C, b) 110°C, c) 80°C, d) 38°C.

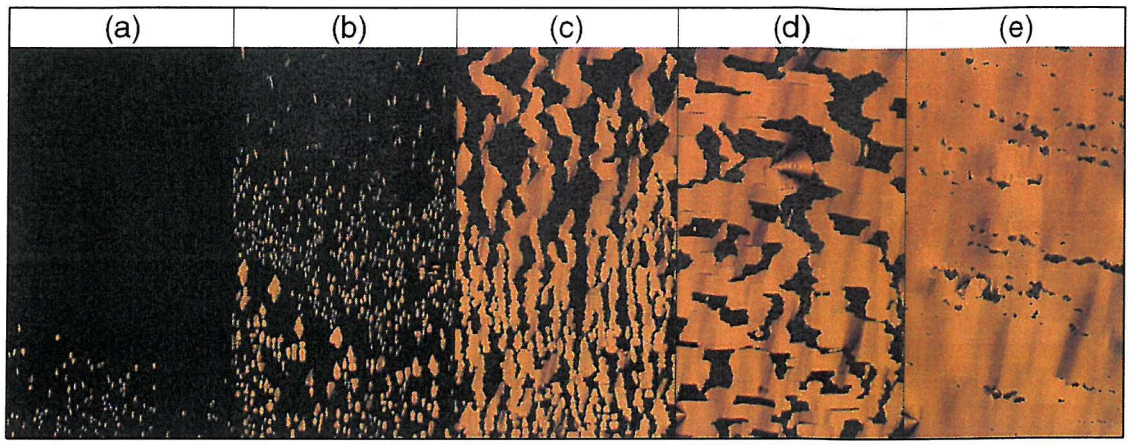

Figure 4.19 Textures of Cl11-4-11Cl on cooling under the application of 9V/μm, 87.5Hz electric field, a) 113°C, b) 112°C, c) 110°C, d) 107°C, e) 95°C.

4.4.3 Electro-Optical Properties

The 'aligned' sample was positioned on the heating stage of the microscope and oriented between crossed polarisers such that, in the absence of an applied field, the optic axis of the material coincided with one of the polariser axes, i.e. the sample was positioned for minimum transmission. Both the signal from the photodiode and the current-voltage amplifier were attached to channels on the oscilloscope to enable recording of the waveforms.

With the exception of Cl11-4-Cl the current response exhibited by all the bimesogens was dual peaked response characteristic of the SmC_A* phase. The current response of Cl11-4-11Cl showed the single peak associated with the SmC* phase, see Figure 4.20. The variation of the sample temperature and the frequency and magnitude of the applied electric field failed to change this ferroelectric response.

Typical traces of the optical and current responses of Br11-3-11Br, obtained at different temperatures under the influence of a triangular waveform, are shown in Figure 4.21. The frequency and applied field strength were kept at a constant 87.5Hz and 20V/μm, thus ensuring that the field strength was above the threshold required to induce ferroelectric switching. The traces shown in Figure 4.21 were obtained on cooling, however it is noted that the same trend is observed on heating. Once again the sample was oriented such that

the ferroelectric switching was symmetric about one of the polariser axes. The changes in transmission seen in the optical response correspond to the switching processes observed in the current response trace. The changing shape of the curves can be explained as follows.

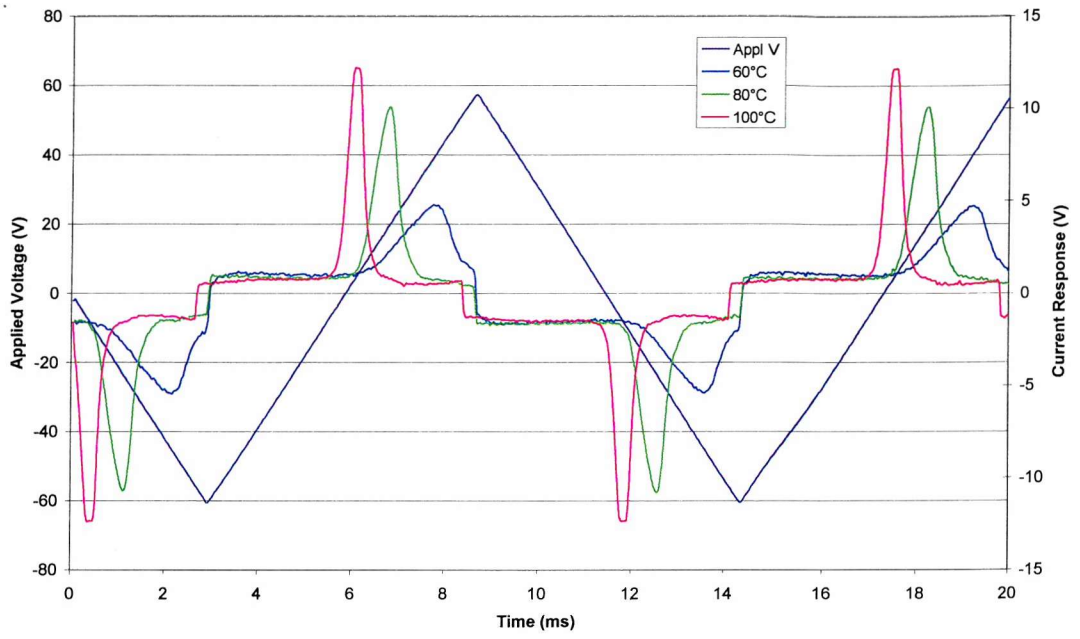

Figure 4.20 The temperature dependence of the current response of Cl11-4-11Cl to a 12V/μm 87.5Hz triangular wave applied field.

At 110°C and arguably at 100°C, a solitary peak characteristic of ferroelectric switching is seen in the current response. As the sample is cooled, the antiferroelectric state becomes increasingly stable. A second peak appears in the current response, at the expense of the original peak; the total area under the peaks remains almost constant. Between 90°C and 85°C this second peak, corresponding to the antiferroelectric (AF) to ferroelectric (F) switch, becomes larger than the F to AF relaxation peak. The threshold field required to induce the AF to F switch is seen to increase.

The AF phase is a sub-phase of the ferroelectric phase and, as it is more ordered, it appears at a lower temperature. Hence, on cooling the sample, the SmC* behaviour observed at higher temperatures gives way to the SmC_A* behaviour. Consequently, it is advantageous

to investigate materials at the low temperature end of the mesophase when looking for evidence of antiferroelectric behaviour. A comparison of the data in Figure 4.22a) and b) illustrates the increased stability of the antiferroelectric state at lower temperatures.

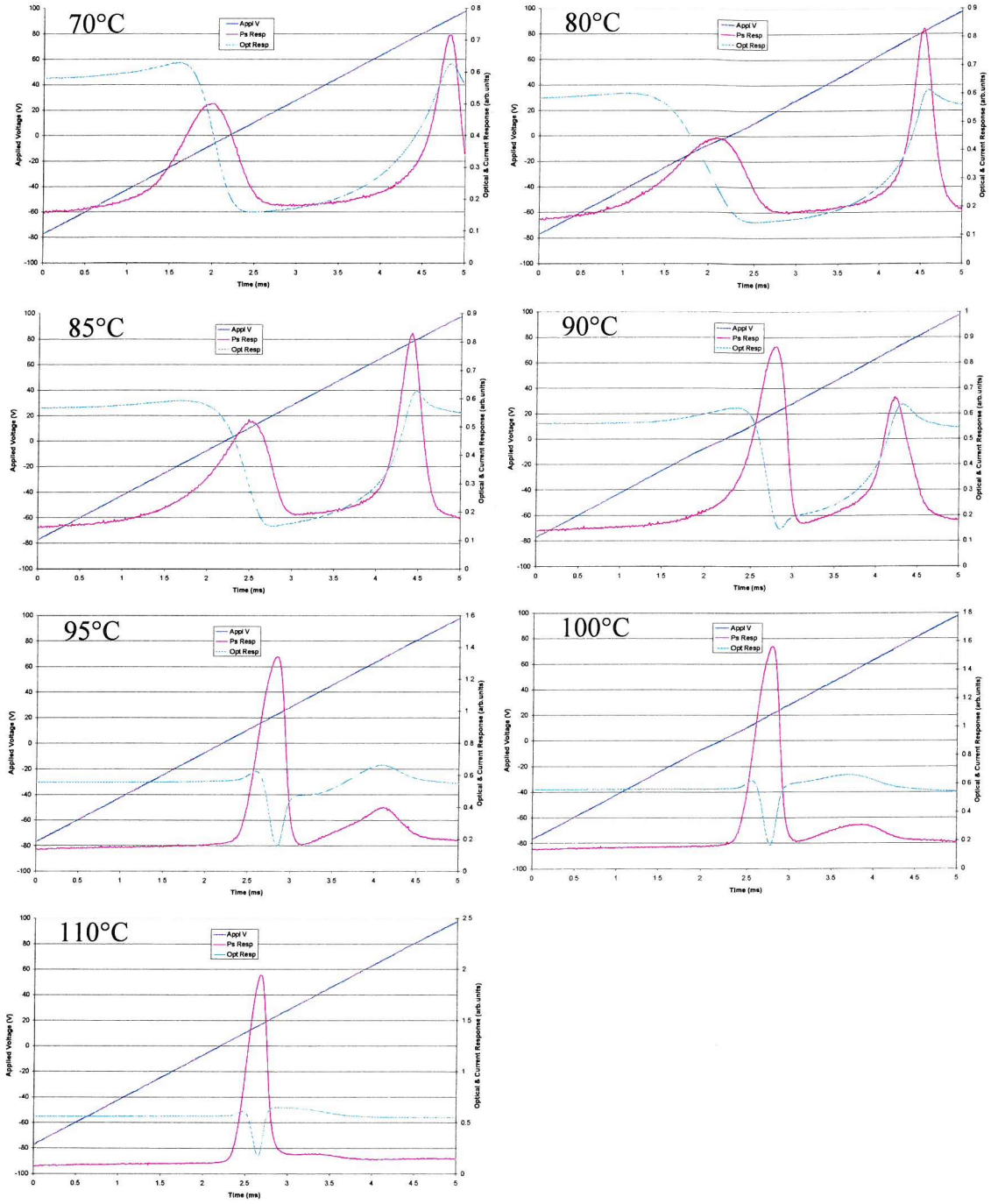

Figure 4.21 The electrical and optical response of Br11-3-11Br to an 87.5Hz, 20V/μm triangular wave applied field.

Optical hysteresis curves of Br11-3-11Br, measured at 65°C and 110°C, for various applied field amplitudes and constant frequency 20Hz, are shown in Figure 4.22. The field was increased until saturated switching was observed. At all times the transmitted light intensity of the switched states was found to be equal, this is again indicative of the molecules switching through an angle of 90°. Incomplete switching was observed at low fields. For applied fields of up to ±10V/μm the transmission, at both temperatures, is seen to increase with increasing voltage. This observation indicates that the induced tilt angle is increasing, possibly due to electroclinic effects. No hysteresis is detected. The optical hysteresis curves observed for field strengths greater than 15V/μm differ considerably at the two temperatures. At 15V/μm and 65°C the switching is not saturated, whilst at 110°C fully saturated F-F switching is recorded for the same field amplitude. In contrast to the ferroelectric switching observed at 110°C, a further increase of the applied electric field to 20V/μm at 65°C resulted in saturated stable ferroelectric switched states at maximum applied field strengths and a stable antiferroelectric state around zero applied field. This tristable switching is a characteristic feature of the antiferroelectric SmC_A^* phase.

To investigate the dynamics of the response to an applied field, the frequency of the driving wave was varied whilst the field magnitude and the sample temperature were kept constant. A definite change in the optical response was observed on varying the frequency. The optical hysteresis curves are shown in Figure 4.23. At low frequencies (less than ~1Hz) the material exhibited double hysteresis loops indicative of antiferroelectric behaviour. The hysteresis loop will now be discussed, taking one of the fully switched ferroelectric states as the starting point. As the field decreases towards 0V the material relaxes into the antiferroelectric state. This state is stable until 40V where the ferroelectric state is induced. As the frequency is increased, the stability of the ferroelectric state increases and the antiferroelectric state is not attained at 0V. The origins of a direct F- to F+ switch are observable at 5Hz, before the F to AF mechanism dominates. As the frequency is increased further, the F- to F+ switch becomes increasingly dominant until, at frequencies of 40Hz and above, no intermediate AF state is visible and the switching is completely ferroelectric.

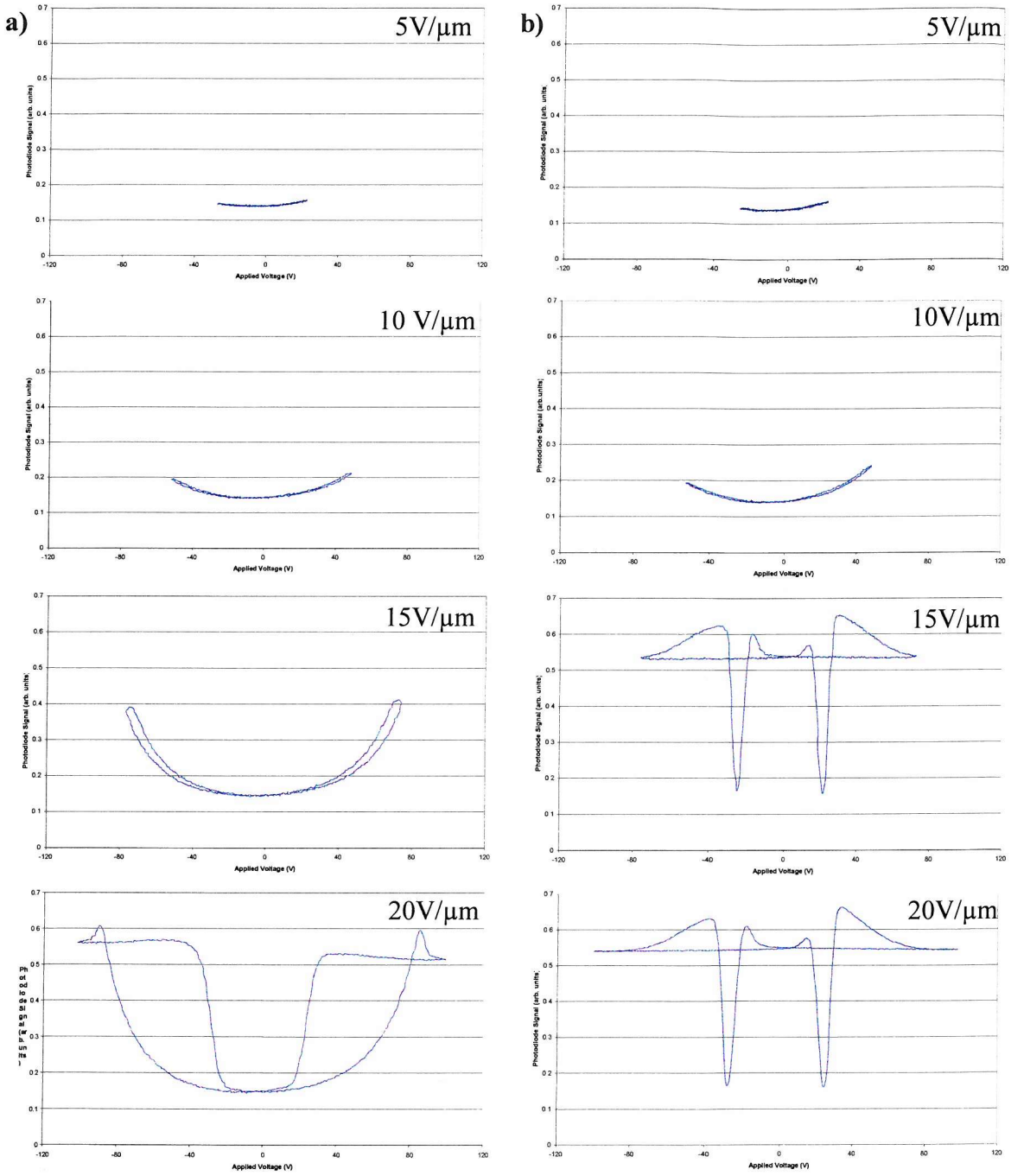

Figure 4.22 The dependence of the optical hysteresis of Br11-3-11Br on the magnitude of the applied electric field. Data taken at a) 65°C and b) 110°C, 20Hz triangular wave electric field.

A couple of conclusions can be drawn from the optical hysteresis curves of Br11-3-11Br shown in Figure 4.22 and Figure 4.23.

- At a given temperature and frequency, the ferroelectric state becomes increasingly stable as the strength of the applied field is increased.
- At a given temperature and applied field strength, the ferroelectric state becomes increasingly stable as the frequency is increased.

At 65°C the response time of the material is too long for the material to react to the rate of change of the applied field. The current response to applied field frequencies of 40Hz and 60Hz shows that the second polarisation peak occurs very close to the reversal point of the applied field – this makes the measurement of Ps difficult in Br11-3-11Br.

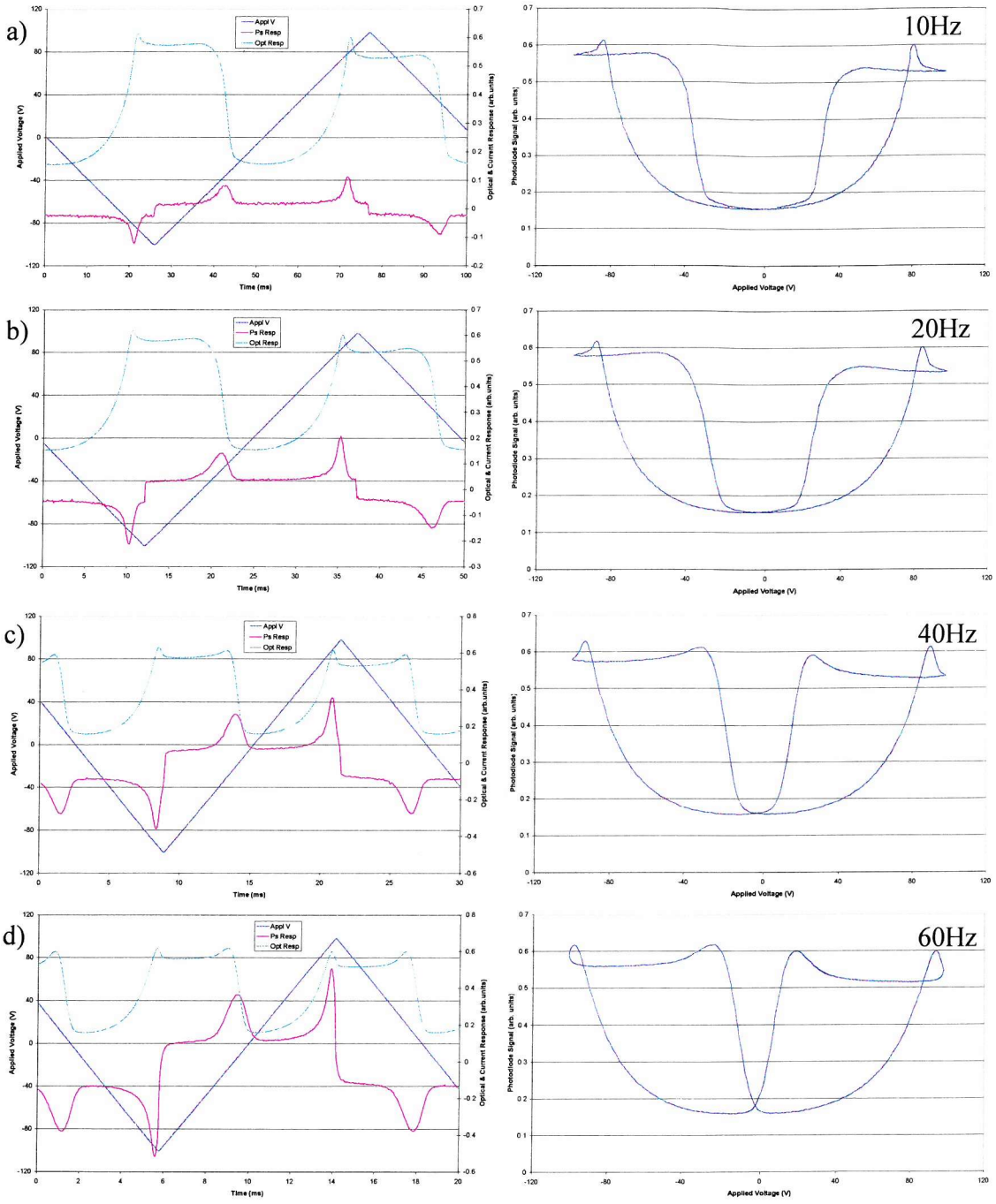

Figure 4.23 The frequency dependence of the electrical and optical response of Br11-3-11Br to a 20V/μm triangular wave applied field at 65°C.

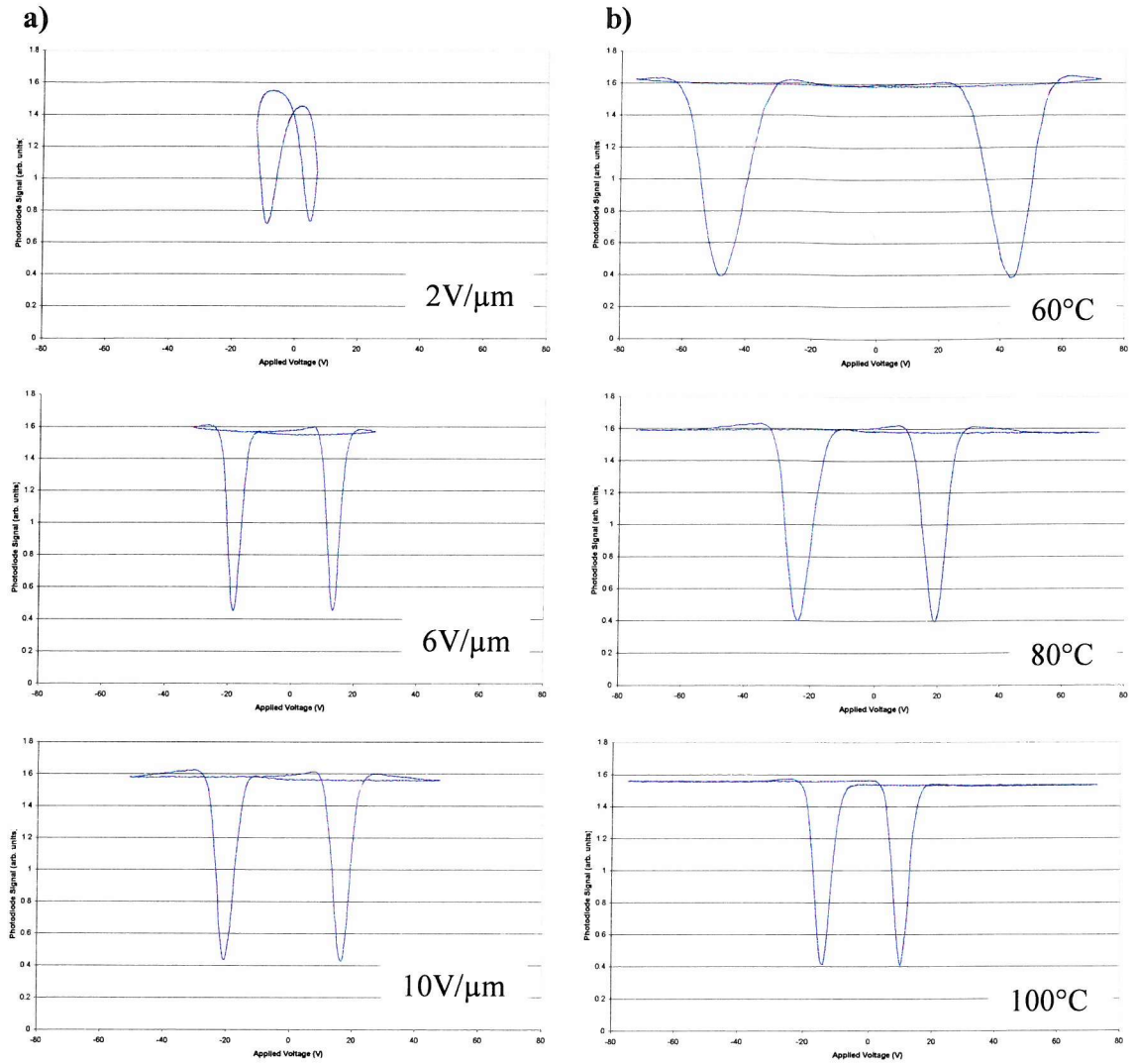

Figure 4.24 The dependence of the optical hysteresis of Cl11-4-11Cl on the magnitude of the applied electric field and sample temperature. Data taken at a) 80°C and b)15V/µm, 87.5Hz triangular wave electric field.

4.4.4 Spontaneous Polarisation

The spontaneous polarisation measurements described in this section were undertaken with a field large enough for the switching to be completely saturated, i.e for F+ to F- switching to occur. Measurements of the total induced polarisation were carried out using the current pulse technique described in §3.5.1.

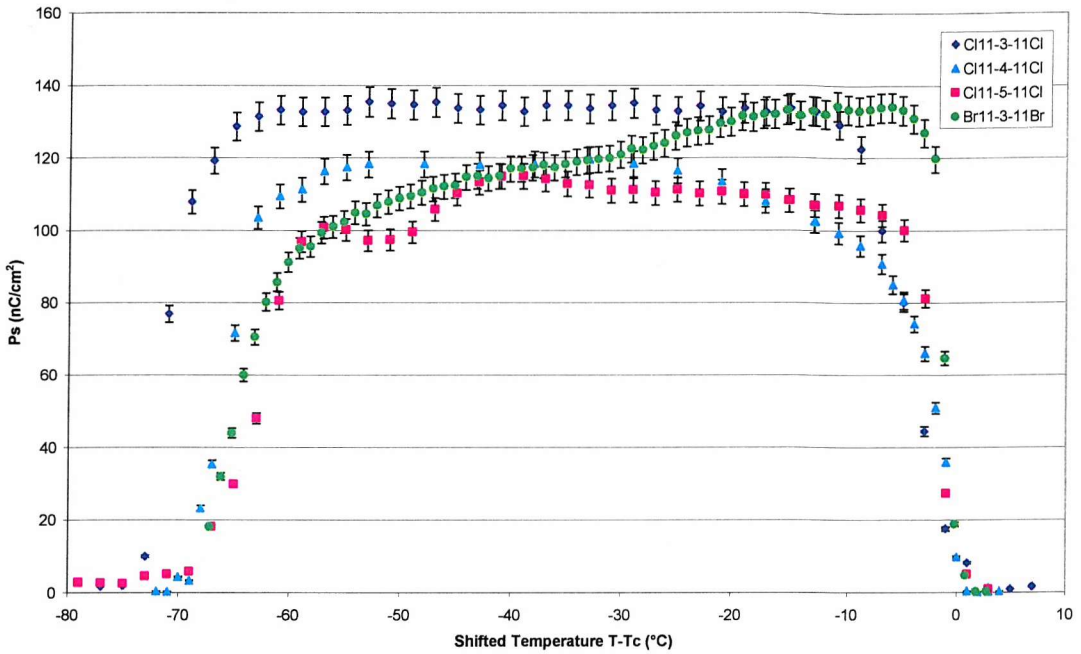

Figure 4.25 The temperature dependence of the spontaneous polarisation of the bi-mesogenic organosiloxane materials.

The magnitude of the P_s is larger than that seen in the mono-mesogens. On cooling from the isotropic phase into the mesophase, the P_s of all the materials rapidly increases and in each case saturates at a value greater than 100nC/cm². The P_s is nearly temperature independent and is only reduced when the onset of crystallisation begins to affect the switching behaviour. The P_s decreases to zero in the crystal phase.

The P_s decreases with increasing siloxane content due to the dilution effects of the longer siloxane chain. The decrease in the number of dipoles per unit volume results in a decrease of the P_s. The reduction in the P_s at lower temperatures was attributed to incomplete switching. At high temperatures, moderate fields and high frequencies allow saturated switching. As the samples are cooled, larger fields and lower frequencies are required to maintain saturated switching. Br11-3-11Br required larger fields and lower frequencies to induce saturated ferroelectric switching than the chlorinated compounds but these conditions often resulted in the chemical degradation of the sample and the electrical shorting of the cell. The P_s of Br11-3-11Br was therefore determined from the area under the two peaks of the antiferroelectric current response. From the optical hysteresis and

electro-optic data in Figure 4.22, Figure 4.23 and Figure 4.24 it is clear that the crossover is temperature and field dependent. The temperature and frequency dependence of the threshold field is investigated in §4.4.5.

4.4.5 Threshold Field for Ferroelectric Switching in Antiferroelectric Bimesogens.

The applied field at which the behaviour changes from antiferroelectric to ferroelectric was defined as the threshold field for ferroelectric switching. Measurements of the threshold field as a function of temperature were undertaken. A 7.5Hz square wave was applied across the sample cell. The magnitude of the applied field was increased until the transition to ferroelectric behaviour was observed optically.

Figure 4.26 shows a comparison of the threshold fields for complete switching of Br11-3-11Br, Cl11-3-11Cl and Cl11-5-11Cl. To aid the comparison, the data in Figure 4.26 is plotted on a reduced temperature scale. AF behaviour is observed over the whole mesophase range. The very high threshold field required to induce ferroelectric behaviour in the tri-siloxane materials indicates a very stable antiferroelectric phase. The threshold field for ferroelectric switching in all compounds displays the same temperature dependence. On decreasing the temperature through the SmC^*_A phase, the threshold field for complete switching increases in a linear fashion. Below the threshold the bimesogen exhibits a SmC^*_A phase. The SmC_A* phase becomes increasingly stable as the temperature is decreased. The field required to induce ferroelectric switching at a shifted temperature of -60°C is twice as large as that required close to T_c. At a given shifted temperature, the SmC_A* phase of Br11-3-11Br is more stable than the SmC_A* phase of Cl11-3-11Cl. The lower P_s results in reduced coupling with the field, requiring a higher field to change the conformation of the molecule. At temperatures just below the isotropic phase the field required to induce ferroelectric switching in Cl11-5-11Cl is just 1V/μm. Indeed, at first glance the material does appear to be ferroelectric. However, at lower temperatures the AF state is more stable and applied fields of ~5V/μm are required to instigate ferroelectric switching. The threshold field for ferroelectric switching is much

lower than in the tri-siloxane derivative indicating that the AF state is not as stable. Much less energy is required to change the conformation of the penta-siloxane than the tri-siloxane.

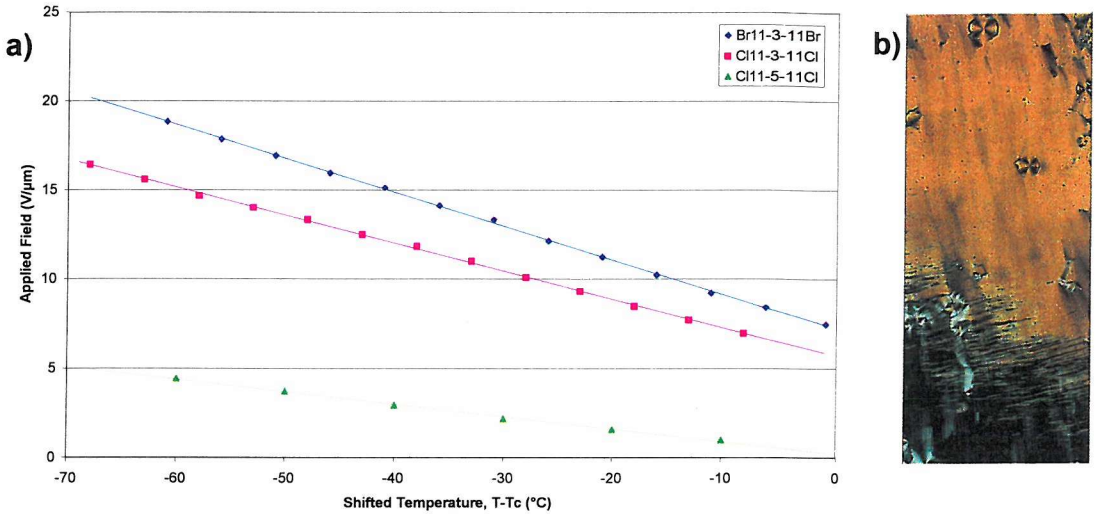

Figure 4.26 a) The temperature dependence of the threshold field for ferroelectric-antiferrolectric switching in X11-n-11X. b) Transition effects observed in Br11-3-11Br.

The textures shown in Figure 4.26b) were obtained via polarising microscopy. The AF state appears grey and is aligned for minimum transmission. Above the threshold field the compounds adopt the SmC^* phase structure. This state has a high tilt angle and appears orange. The difference in the colour between the F and AF states is attributed to birefringence (Δn) effects. The 'herringbone' organisation of the molecules in the SmC^*_A phase results in a drop in Δn. Due to the anticlinic molecular ordering in the SmC_A^* phase the average optical axis does not coincide with the optic axis of the individual molecules. Thus the birefringence of the SmC_A^* phase is smaller than in the SmC* phase where the molecular orientation coincides with the average optical axis. The rotation of the optical axis is clearly illustrated by observing the four-brush defects in Figure 4.27.

The field induced transition from SmC^*_A to the SmC^* phase occurs via the nucleation and growth of stripe shaped domains of ferroelectric SmC material along the smectic layer.

X-ray diffraction measurements[18] have shown that this transition is accompanied by reversible switching from a chevron to bookshelf geometry. On increasing the temperature it becomes increasingly easy to force the compound from AF switching to ferroelectric switching. The field required to induce the SmC_A*-SmC* transition is smaller at higher temperatures.

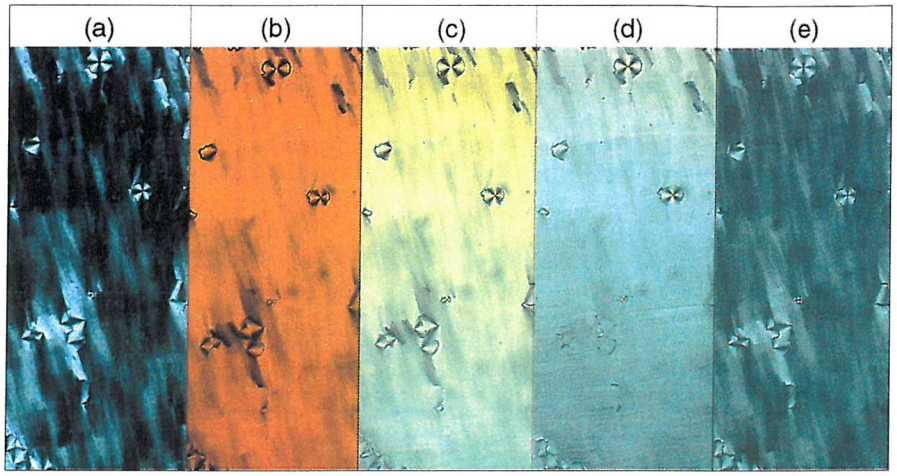

Figure 4.27 The frequency dependence of the antiferroelectric-ferroelectric transition in Br11-3-11Br. a) zero field, b) 1Hz, c) 300Hz, d) 600Hz and e) 1kHz (110°C, 15V/μm).

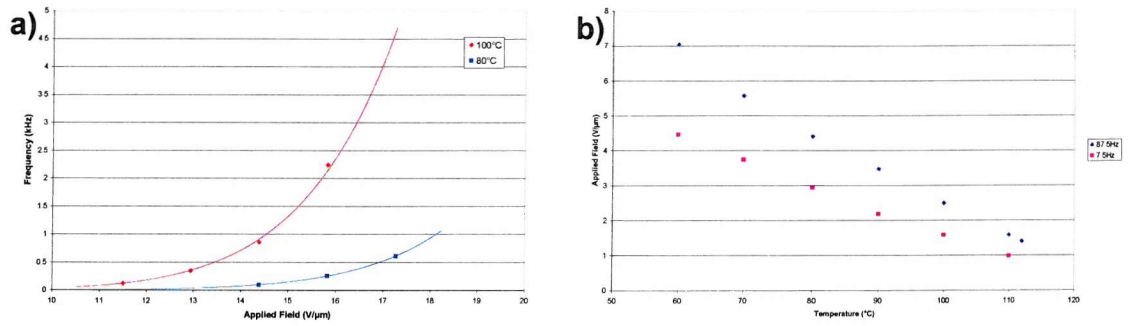

Figure 4.28 The frequency dependence of the threshold field for ferroelectric-antiferroelectric switching in a) Br11-3-11Br and b) Cl11-5-11Cl.

Figure 4.28 illustrates the frequency dependent nature of the threshold field. In the low frequency regime the threshold field has very small frequency dependence. This frequency dependence becomes more pronounced at higher temperatures and frequencies.

[18] M.Johno, Y.Ouchi, H.Takezoe, A.Fukuda, K.Terashima and K.Furukawa, *Jpn.J.Appl.Phys*, **29**, L111 (1990)

All the bimesogens showed similar dependences. The frequency dependent nature of the AF to F transition can be seen in Figure 4.27.

4.4.6 Tilt Angle

The optical tilt angle data in Figure 4.29 and Figure 4.30 were taken using the rotating analyser apparatus discussed in Section 3.5.2. Care was taken to ensure the magnitude of the applied field was strong enough to produce saturated switched states. This was necessary because the alternating layer structure of antiferroelectric compounds results in no observable macroscopic optical tilt. The optical tilt angles as a function of temperature are shown in Figure 4.29. The temperature independent nature and the first order transition from I-SmC_A* are clearly observed.

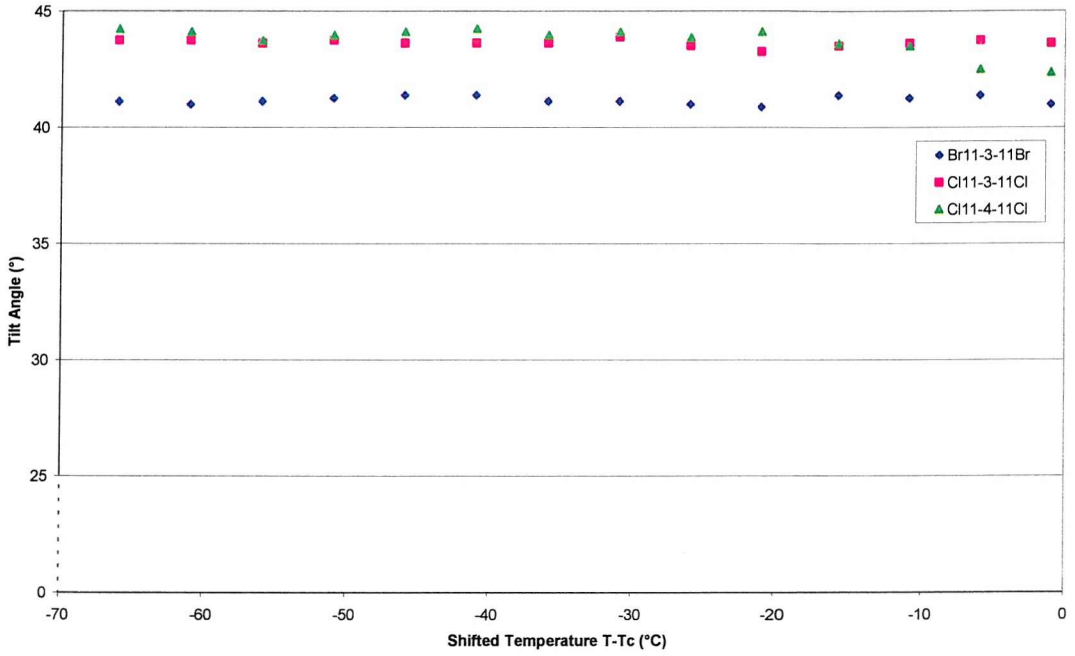

Figure 4.29 The temperature dependence of the optical tilt angle of the bi-mesogenic organosiloxane compounds.

The dependence of the tilt angle on the applied field is shown in Figure 4.30. The applied field was kept constant and the sample cooled. When the switching is saturated the tilt angle was found to be constant at ~42° across the 60°C range over which the mesophase exists. In the high tilt (SmC^*) region the tilt angle magnitude is independent of

temperature and voltage. In the low tilt (SmC^*_A) regime the magnitude of the tilt angle is, again, independent of temperature but now demonstrates a linear dependence on the applied voltage, possibly due to electroclinic effects.

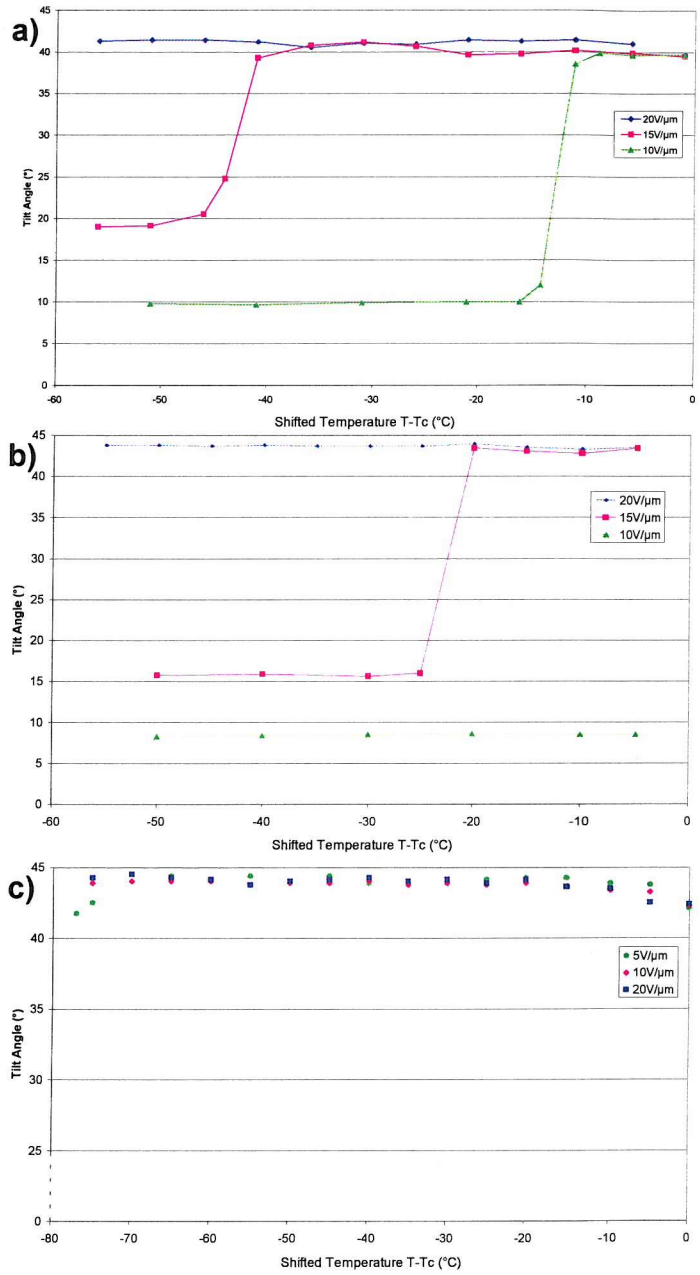

Figure 4.30 The dependence of the optical tilt angle of the bi-mesogenic compounds on the magnitude of the applied electric field. a) Cl11-3-11Cl, b) Br11-3-11Br and c) Cl11-4-11Cl.

The temperature dependence of the threshold field is clearly visible, with higher fields attaining saturated switching at lower temperatures than weaker applied fields. The tilt angle of Cl11-5-11Cl saturates at all but very low applied fields, indicating that the SmC_A* phase is not energetically stable. The tilt angle of Cl11-4-11Cl shows very little temperature or field dependence. Saturated switching occurs at much lower fields than in the bromo- and chloro- tri-siloxane bimesogens.

The tilt angle is field dependent within the unsaturated SmC_A* regime, this is illustrated in Figure 4.31.

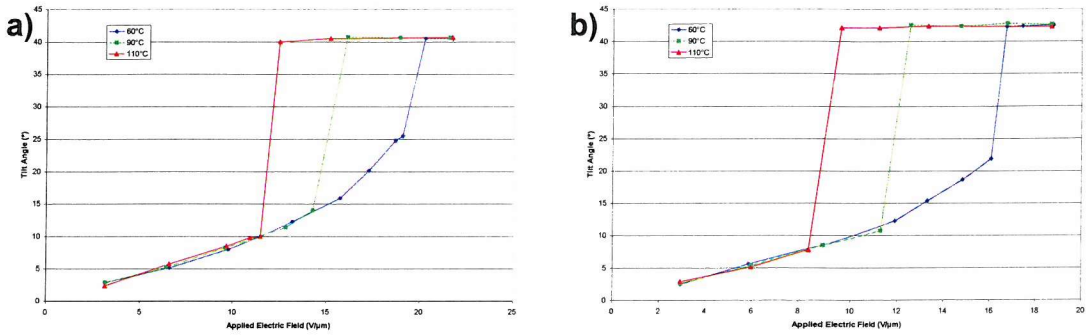

Figure 4.31 The field dependence of the optical tilt angle of a) Cl11-3-11Cl and b) Br11-3-11Br.

The field dependence has two regimes. For low applied fields there is an almost linear increase of the tilt angle with field strength; this linear response is temperature independent. At higher fields there is a temperature dependent transition to a high tilt angle state where the tilt angle is temperature and field independent as in the SmC* saturated switching regime.

4.4.7 Current Response Time

Response time measurements of the bimesogens were carried out using the current pulse technique. The response times, shown in Figure 4.32, are comparable to those of the mono-mesogenic compounds. The response times show very little temperature dependence near the clearing point. As the crystal phase is approached the response times increase in a

non-linear fashion. The length of the siloxane spacer has little impact on the response times.

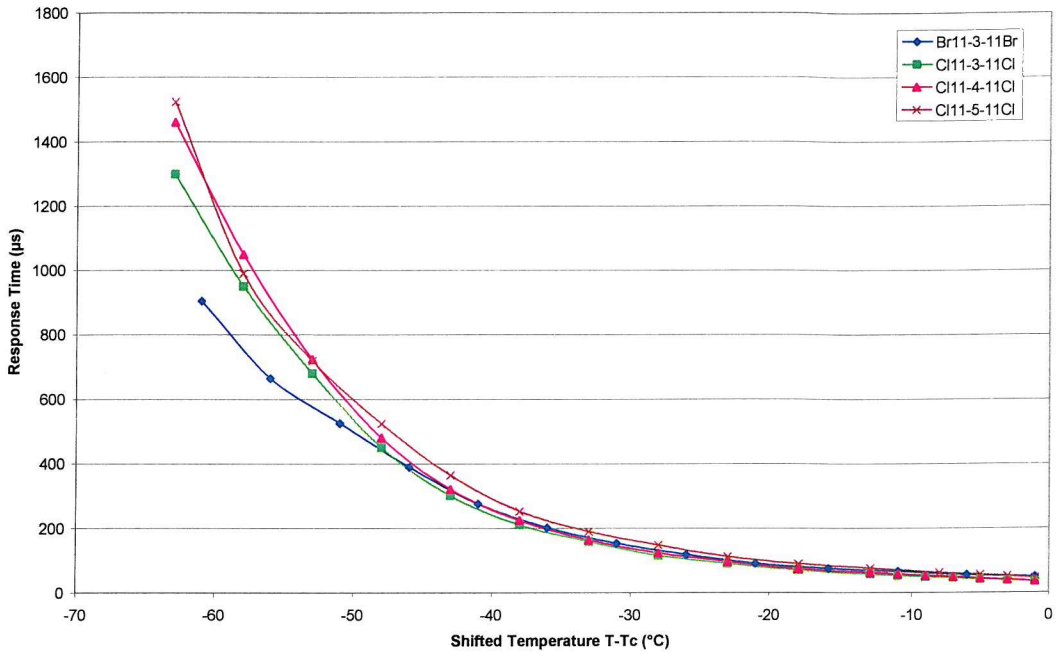

Figure 4.32 The temperature dependence of the current response time of the bi-mesgenic organosiloxanes.

Studies of the field dependence of the response time of the SmC* Cl11-4-11Cl revealed behaviour similar to that observed in the mono-mesogens, Figure 4.33. The electric field dependence is increased at lower temperatures and the same linear dependence on 1/E is also observed.

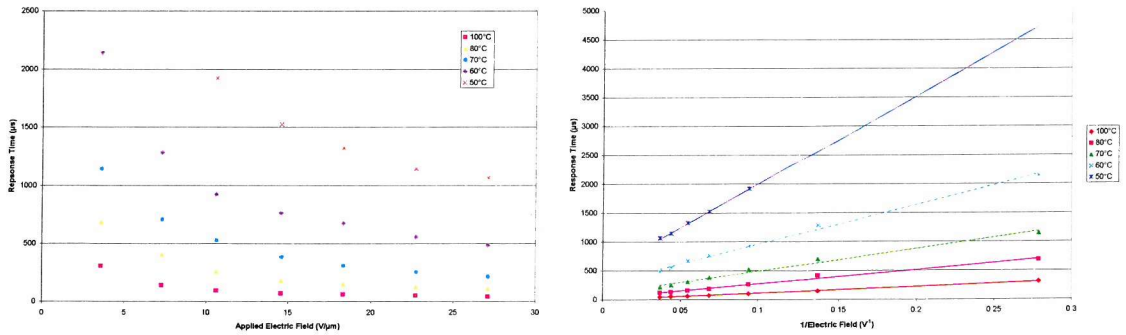

Figure 4.33 The temperature and electric field dependence of the current response time of Cl11-4-11Cl. The frequency of the applied field was 80Hz.

4.5 SUMMARY

The compounds studied in this chapter consisted of a laterally substituted halogenic biphenyl benzoate mesogen joined to an organosiloxane core by an eleven length alkyl chain. All the compounds exhibited high, and largely temperature independent, spontaneous polarisation, P_S, and optical tilt angles, θ. Response times of the order of 100μs were readily achievable.

Two series of low molar mass organosiloxane materials were investigated. The mono-mesogenic compounds exhibited the ferroelectric SmC* phase, whilst the phase behaviour of the bi-mesogens was influenced by the length of the siloxane group. The tri- and penta-siloxane bi-mesogenic compounds were antiferroelectric whilst Cl11-4-11Cl was ferroelectric. The antiferroelectric state of the penta-siloxane derivatives is not as stable as the tri-siloxane since less energy is required to change the confirmation of the longer siloxane chain.

On cooling from the isotropic phase the mono-mesogens undergo a first order phase transition to the SmC* phase and display ferroelectric properties over a 50°C temperature range. The lack of a less ordered preceding phase makes alignment difficult, although uniform alignment could be obtained by annealing the sample in the presence of an electric field. All mono-mesogenic compounds exhibit P_S of ~100nC/cm^2 with the P_S depending on the concentration and size of the dipoles. Response times of ~50μs are observed and were shown to be inversely proportional to the applied electric field. In contrast, the tilt angles, of ~45°, were shown to be field independent above very small applied electric fields.

All the bimesogenic materials possessed mesophases over a 70°C temperature range. With the exception of Cl11-4-11Cl, the bimesogenic materials exhibited the antiferroelectric behaviour of the SmC_A* phase. Cl11-4-11Cl displayed the ferroelectric behaviour of the SmC* phase. The dependence of the electrical and optical response of the SmC_A* materials to the frequency and magnitude of the applied electric field and sample

temperature was examined resulting in the conclusion that the ferroelectric state becomes increasingly stable as the magnitude and frequency of the applied field is increased. The magnitude of the P_s was larger than that observed in the monomesogens due to the increased dipole concentration.

Chapter Five

HYPERTWISTED CHIRAL NEMATIC LIQUID CRYSTALS

5.1 INTRODUCTION

Nematic liquid crystals have been utilised in display devices for many years. The electro-optical effects have been the subject of many detailed investigations[1] and are well understood. One of the main limitations of these displays is the optical response time to the applied electric field. Recently, much interest has been shown in a new, fast electro-optical effect observed in both the nematic and chiral nematic liquid crystalline phases.

The flexoelectro-optic effect[2,3], discussed in Chapter 2, has great potential for use in display applications and optical modulators due to the short optical response times and temperature independent optic axis tilt angles which are linear in the applied field. The work presented in this chapter is solely concerned with the characterisation of the flexoelectro-optic effect occurring in highly twisted nematic flexoelectric liquid crystal bimesogens[4].

Section 5.2 discusses the molecular structure of the achiral nematic bimesogens studied in this chapter. In order to observe flexoelectro-optic effects it is necessary to add a small amount of chiral dopant to the bimesogens. The phase sequences of a number of mixtures are discussed in Section 5.3. The techniques used to obtain the uniformly-lying helix texture necessary to observe flexoelectro-optic switching are described in Section 5.4. Following the discussion in Section 5.5 of the applied field dependence of the textures exhibited by the mixtures, the electro-optic properties of the flexoelectro-optic effect are detailed in Section 5.6. This section focuses on the temperature and field dependence of the response time and tilt angle, which are important considerations for any material with potential for use in electro-optical devices. Finally, Section 5.7 summarises the important findings presented in this chapter.

---

[1] L.M. Blinov and V.G. Chigrinov, Electrooptic Effects in Liquid Crystal Materials, Springer-Verlag, New York (1994)
[2] R.B. Meyer, *Phys.Rev.Lett.*, **22**, 918 (1969)
[3] J.S. Patel and R.B. Meyer, *Phys.Rev.Lett.*, **58**, 1538 (1987)
[4] B. Musgrave, P. Lehman and H.J. Coles, *Liq.Cryst*, **28**, No. 8 (1999)

5.2 MATERIALS

A series of nematic bimesogenic liquid crystals have been synthesised, the generic structure of which is shown in Figure 5.1, where X, Y, Z are functional halogenic groups and n is the number of carbon atoms in the spacer unit.

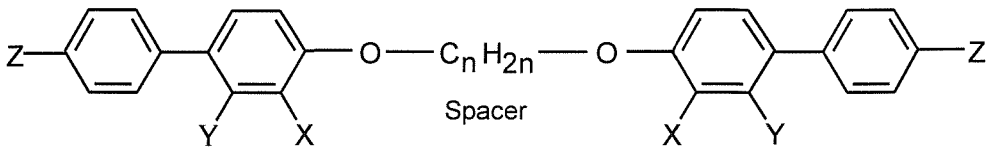

Figure 5.1 The generic structure of the achiral nematic bimesogen materials studied.

As Z and Y are Fluorine atoms the achiral nematic bimesogens[5] are referred to as $F_fB(n)B_fF$, where n is the length of the alkyl spacer unit.

5.3 MIXTURES

The flexoelectric materials studied in this work are a mixture of the achiral bimesogens with different spacer lengths. The lengths of the alkyl spacers used in this work were 7, 9 and 11 and selected eutectic mixtures have been prepared. The chiral dopants BDH1218[6], BDH1305[6] and CB15[6] were added in low percentage by weight concentrations to produce a chiral nematic phase.

5.3.1 50%-50% $F_fB(7\text{-}9)B_fF$ Mixture & 4%BDH1305

A small amount (4% wt/wt) of the chiral dopant BDH1305 was added to a 50:50 wt/wt mixture of the achiral bimesogens with 7- and 9-length alkyl spacers.

[5] H.J. Coles, M.J. Coles, S. Perkins, B. Musgrave and D. Coates, E.U. Patent filed Sept 1999
[6] BDH/Merck, Southampton, UK

5.3.1.1 Phase Characterisation

The phase sequence was determined by a combination of DSC and optical microscopy. On cooling from the isotropic phase, with no external field applied, a scattering focal conic chiral nematic texture is observed at 43.5°C, as shown in Figure 5.2. A further transition to a crystalline state occurs at 28°C.

Crystal 28°C Chiral Nematic 43.5°C Isotropic

Super-cooling is also observed in the thin optical cells, allowing room temperature flexoelectric switching to be observed. The material is generally liquid crystalline for more than 6 hours, when 8°C below the crystallisation point.

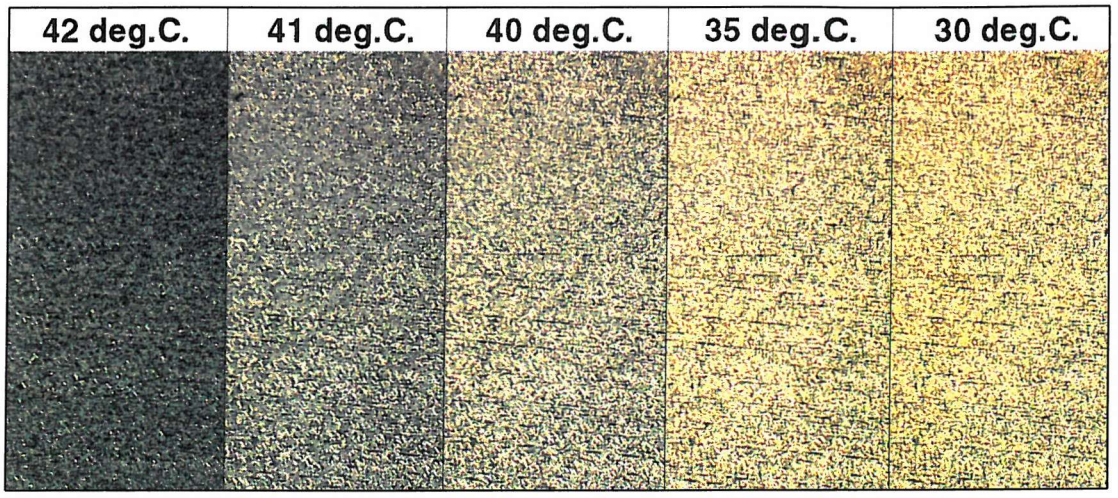

Figure 5.2 The scattering focal conic texture formed on cooling from the isotropic phase. No electric field is applied.

The textures shown in Figure 5.2 were obtained using a 'hybrid' cell[7], described in Section 5.4.3. The alignment of the mixtures will be discussed in the Section 5.4.

5.3.2 46%-44% $F_fB(7\text{-}11)B_fF$, 2% BDH1218 & 8% CB15 Mixture

The chiral dopants BDH1218 and CB15 were added to a 51%:49% wt/wt mixture of the achiral bimesogens with 7- and 11-length alkyl spacers in concentrations of 2% and 8% respectively.

[7] Supplied by Merck, Southampton, UK

5.3.2.1 Phase Characterisation

The phase sequence was determined by a combination of DSC and optical microscopy. On cooling from the isotropic phase, with no external field applied, a transition to the chiral nematic phase is observed at 47°C, as shown below in Figure 5.2. A further transition to a crystalline state occurs at 22°C.

Crystal 22°C Chiral Nematic 47°C Isotropic

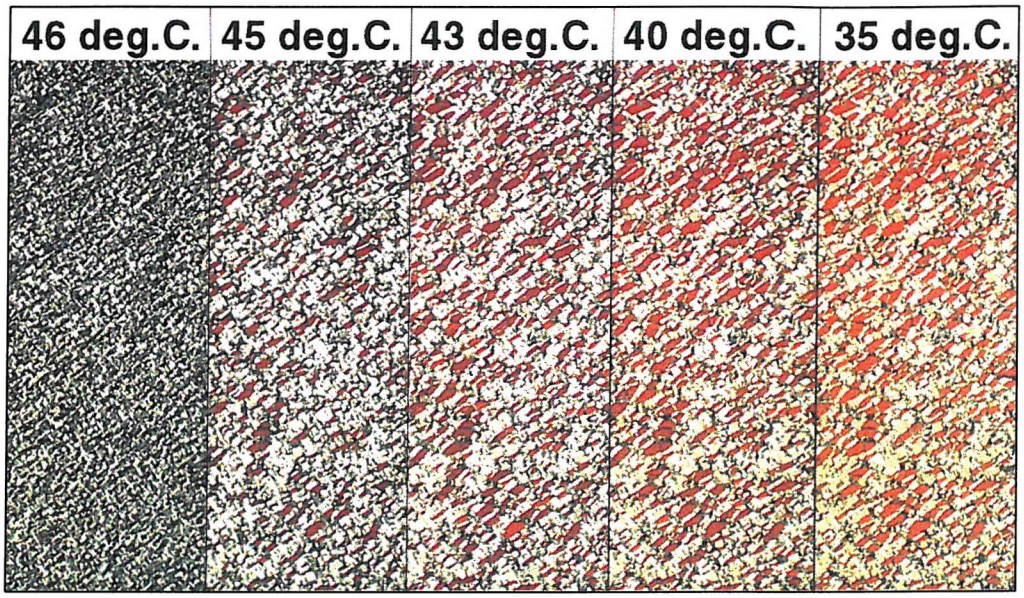

Figure 5.3 The Grandjean texture and 'oily streak' defects formed by the 46%-44% $F_fB(7-11)B_fF$, 2% BDH1218 & 8% CB15 mixture on cooling from the isotropic phase. No electric field is applied. The sample is contained within a planar cell.

The textures in Figure 5.3 were obtained on cooling the sample in a planar cell at 1°C/min from the isotropic phase in the absence of an applied electric field. At 35°C the red texture of standing helix Grandjean structures separated by oily streak defects can be seen.

5.3.3 67%-23% $F_fB(7-11)B_fF$, 8%CB15 and 2%BDH1218 Mixture

The chiral dopants BDH1218 and CB15 were added to a 67:23 mixture of the achiral bimesogens with 7- and 11-length alkyl spacers.

5.3.3.1 Phase Characterisation

The phase sequence was determined by optical microscopy. On cooling from the isotropic phase, with no external field applied, a transition to the chiral nematic phase is observed at 47.5°C. No crystallisation was observed on further cooling to 20°C.

Chiral Nematic 47.5°C Isotropic

5.3.4 20%-80% $F_fB(7\text{-}9)B_fF$ and 20% CB15 Mixture

20% wt/wt of the chiral dopant CB15 was added to a 20:80 mixture of the achiral bimesogens with 7- and 9-length alkyl spacers.

5.3.4.1 Phase Characterisation

The phase sequence was determined by optical microscopy. On cooling from the isotropic phase, with no external field applied, a transition to the chiral nematic phase is observed at 38.5°C. No crystallisation was observed on further cooling to 20°C.

Chiral Nematic 38.5°C Isotropic

5.4 ALIGNMENT

The uniformily-lying helix texture is required for the observation of the flexoelectro-optic properties of the hypertwisted chiral nematic liquid crystals. During the course of this work a number of methods have been employed to facilitate and stabilise the formation of this texture. These are detailed in the following sections. In all cases the magnitude and frequency of the applied field required for good alignment is material specific and should therefore be refined as necessary.

5.4.1 Formation of the Uniformly-Lying Helix (ULH) Texture

The alignment techniques, and the switching mechanism, of a chiral nematic flexoelectric liquid crystalline material utilise the fact that the helical structure of chiral nematics can be

modified or unwound by an applied electric field as the helix distorts to a lower free energy. Figure 5.4 illustrates the sequence of textures exhibited by a chiral nematic material under the application of an electric field.

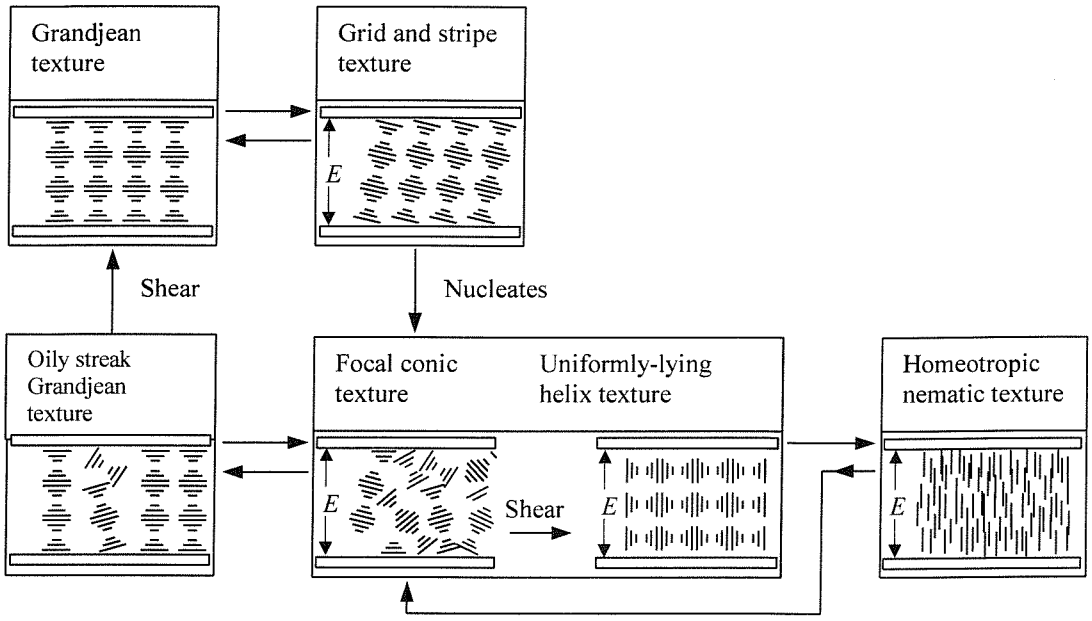

Figure 5.4 The sequence of textures observed in chiral nematic materials with positive dielectric anisotropy on increasing (→) and decreasing (←) the amplitude E of an electric field applied across the cell.

An example of this sequence is shown in Figure 5.5. 20% wt/wt of the chiral dopant CB15 was added to a 20:80 mixture of F_fB7B_fF and F_fB9B_fF and contained in a planar cell. On cooling from the isotropic phase the sample readily adopts the Grandjean texture. The application of an electric field of increasing amplitude parallel to the helix axis causes the focal conic texture to nucleate directly from the Grandjean texture, as no grid texture is observed. Further increase of the field amplitude results in the unwinding of the helix as the director aligns along the field direction and the appearance of the homeotropic texture.

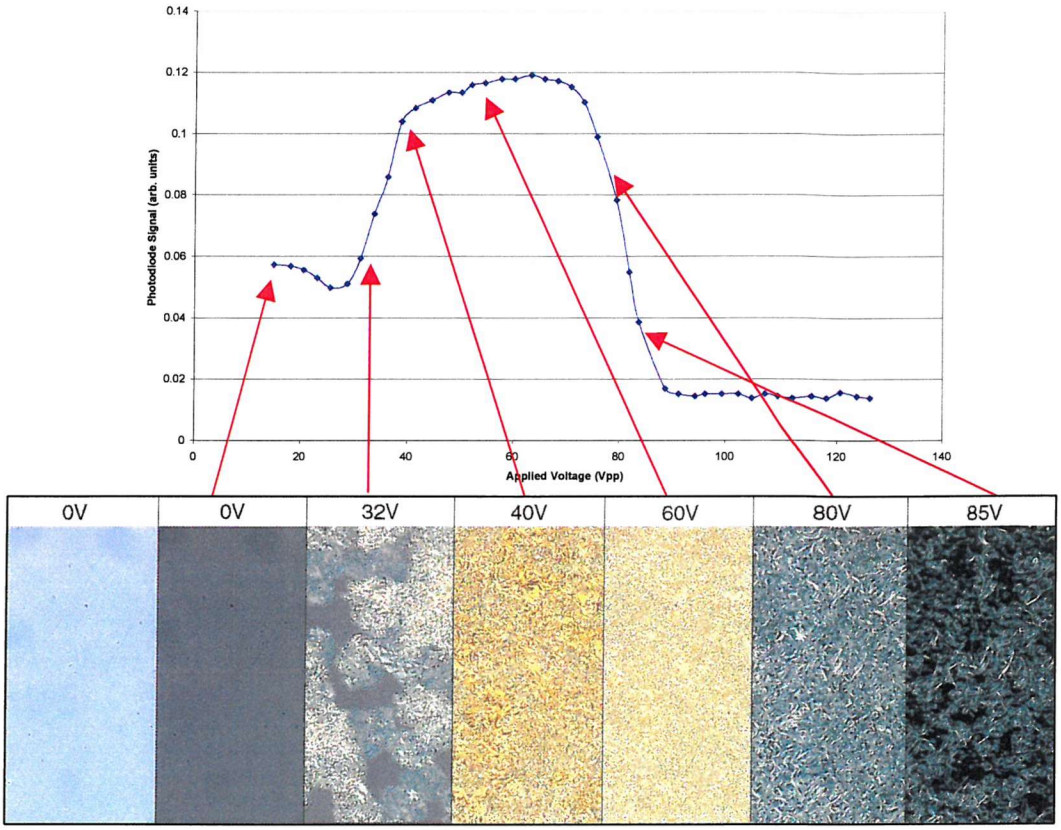

Figure 5.5 The sequence of textures exhibited by a mix of 20-80 $F_fB(7\text{-}9)B_fF$ and 20% CB15 on increasing the amplitude of an applied electric field across the sample. The Grandjean texture is exhibited in the absence of an electric field – it was necessary to reduce the light intensity to avoid saturation later in the sequence. The focal conic texture nucleates as the field magnitude is increased. Further increase of the field magnitude results in a homeotropic texture as the director aligns with the field.

5.4.2 Planar Cells

The ULH texture can be obtained by applying an electric field across the sample and pressing the edge of the cell to force the material within to flow. The combination of forces resulting from the dielectric coupling to the field and the mechanical shear provide good alignment over large areas.

The textures shown in Figure 5.6 were obtained by cooling a sample of the 46%-44% $F_fB(7\text{-}11)B_fF$, 2% BDH1218 & 8% CB15 mixture from the isotropic phase to 40°C in the presence of a 7V/μm, 80Hz square wave applied field. The uniformly-lying helix texture

only forms in the active area of the cell. The Grandjean texture and oily streak defects are visible in the unaligned area. The uniformity of the ULH texture in the active area of the cell is improved by shearing. The uniform flow field resulting from mechanical shearing causes the helix axes to lie uniformly, perpendicular to the direction of flow. The effects of the shear can also be clearly seen outside the active area where the number of oily defects has been significantly reduced. Just inside the active area a region of distorted helices can be seen, these are a result of backflow after shearing.

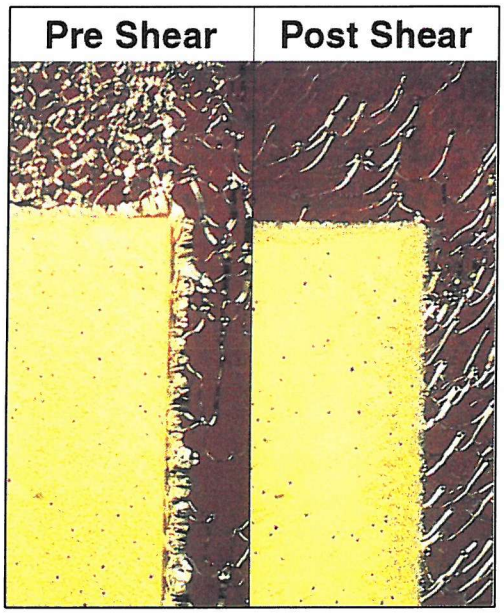

Figure 5.6 The ULH texture adopted by the 46%-44% $F_fB(7\text{-}11)B_fF$, 2% BDH1218 & 8% CB15 mixture in a planar cell on cooling to 40°C at 1°C/min in the presence of a 7V/µm, 80Hz square wave applied field.

5.4.3 Hybrid Cells

The use of hybrid aligned cells, where one surface possesses planar alignment and the other surface homeotropic alignment, results in the manifestation of an internal shear field. On cooling from the isotropic phase with a 9.5Vµm, 80Hz square wave electric field applied the 50:50 $F_fB(7\text{-}9)B_fF$ and 4%BDH1305 mixture formed an aligned focal conic, or ULH, texture, see Figure 5.7

As opposed to the planar cell alignment, no external shearing forces are required to produce this ULH texture. Uniform alignment is obtained by a combination of turbulent flow induced by the applied field and suitably treated surfaces.

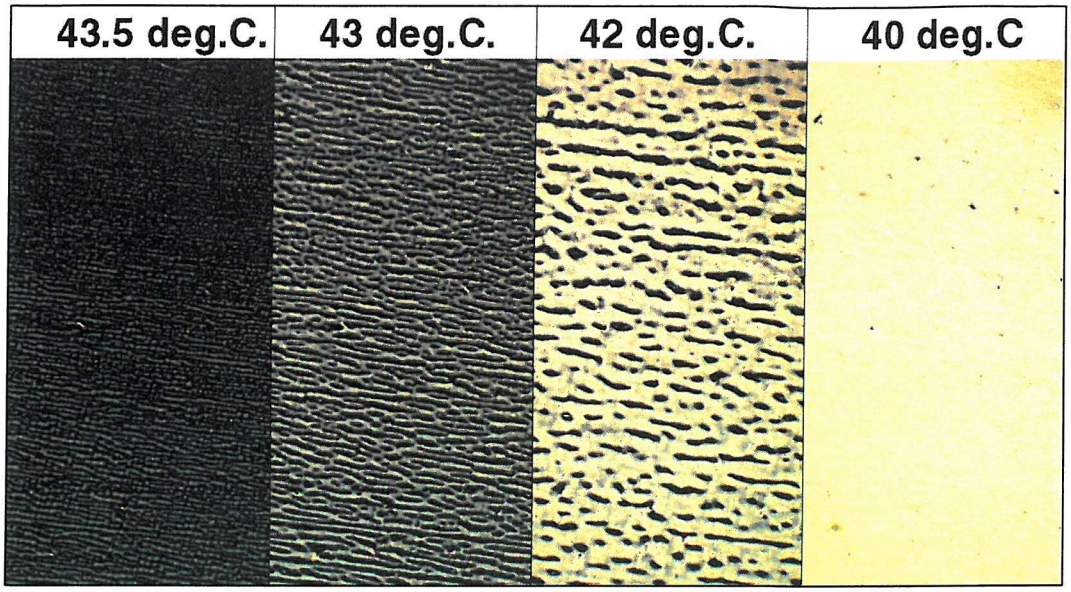

Figure 5.7 The alignment process - cool from isotropic phase whilst applying 9.5V/μm square wave at 80Hz.

5.4.4 Homeotropic Cells

The homeotropic alignment promoted by lecithin treated surfaces results in the chiral nematic liquid crystal mixtures readily adopting the ULH texture. Good quality alignment is obtained by following a similar methodology to that described for planar treated cells. However, care must be taken as the lecithin coating begins to break down at temperatures above ~80°C.

5.5 CRITICAL FIELDS FOR HELIX UNWINDING

The application of an electric field across the sample results in dielectrically-induced textural changes, as were shown in Figure 5.4. The performance of materials exhibiting strong flexoelectric switching is limited at high fields by dielectric coupling causing the helical structure to unwind[8]. Magnitudes of the critical fields required to cause texture changes were evaluated by monitoring the changes in the transmitted light intensity by a material between crossed polarisers as the amplitude of the voltage applied across the cell

was varied. Plots of the applied field versus the photodiode signal allow the temperature dependence of this behaviour to be analysed. As helix unwinding is a dynamic process, and the transmitted intensity is therefore constantly changing, automated computer software was used in these measurements to ensure that the time resolution was kept constant.

The initial texture for the measurements in Figure 5.8 was the ULH texture. The sample orientation was constant for all measurements such that transmission when the cell was placed between crossed polarisers was maximised for the alignment field, namely a 6.4V/μm 80Hz square wave, at 39°C.

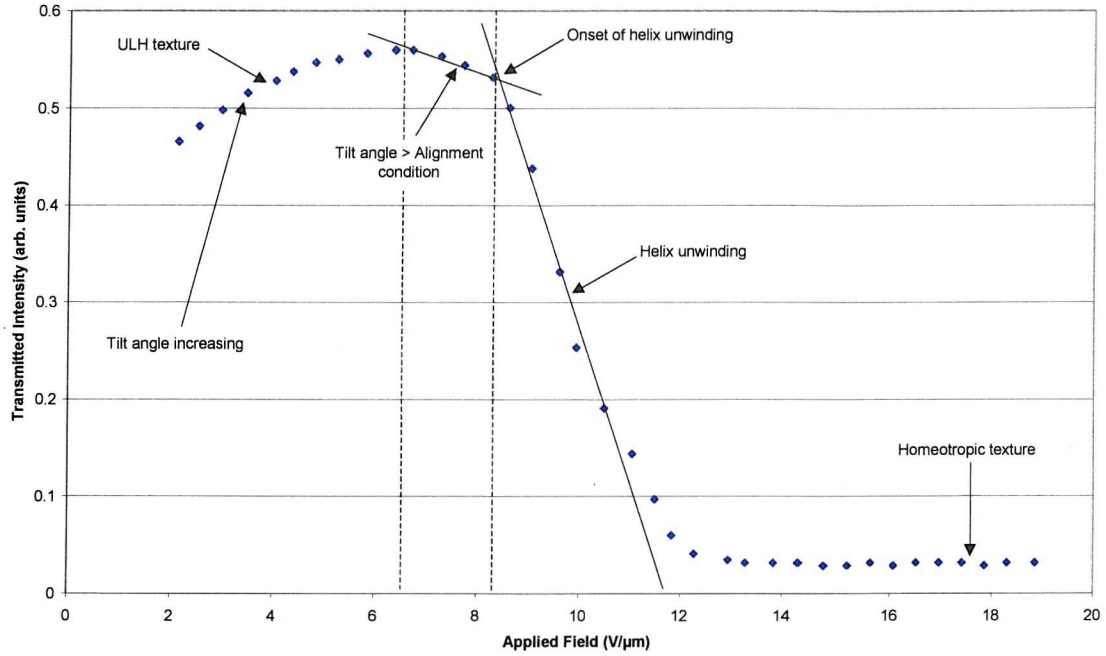

Figure 5.8 Typical form of the applied field dependence of the transmitted light intensity through the transition from the ULH to the homeotropic textures.

As the field across the sample is increased the transmitted intensity increases in a linear fashion due to the increasing tilt angle. As the tilt angle exceeds that of the initial orientation field the light reaching the photodiode begins to decrease. As the critical field for helix unwinding is approached, the light intensity at the photodiode decreases further.

[8] P.Rudquist, L.Komitov and S.T.Lagerwall, *Ferroelectrics*, **213**, 53 (1998)

This change of mechanism, from changing tilt angle to helix unwinding, results in a distinct change in the slope of the data. The gradient remains constant throughout the helix unwinding process until the texture becomes homeotropic.

The data in Figure 5.9 shows the temperature dependence of the helix unwinding behaviour in 67-23% $F_fB(7\text{-}11)B_fF$, 8% CB15 and 2% BDH1218. Clearly, as one would expect, the stability of the ULH texture increases as the sample temperature decreases.

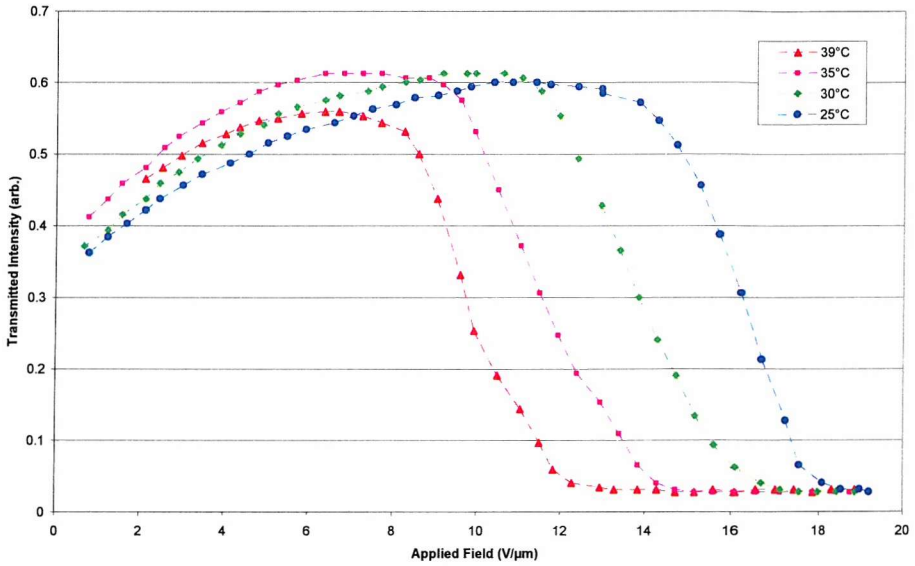

Figure 5.9 Transmitted light intensity as a function of the applied field magnitude in 67-23% $F_fB(7\text{-}11)B_fF$ 8%CB15 2%BDH1218 (80Hz square wave).

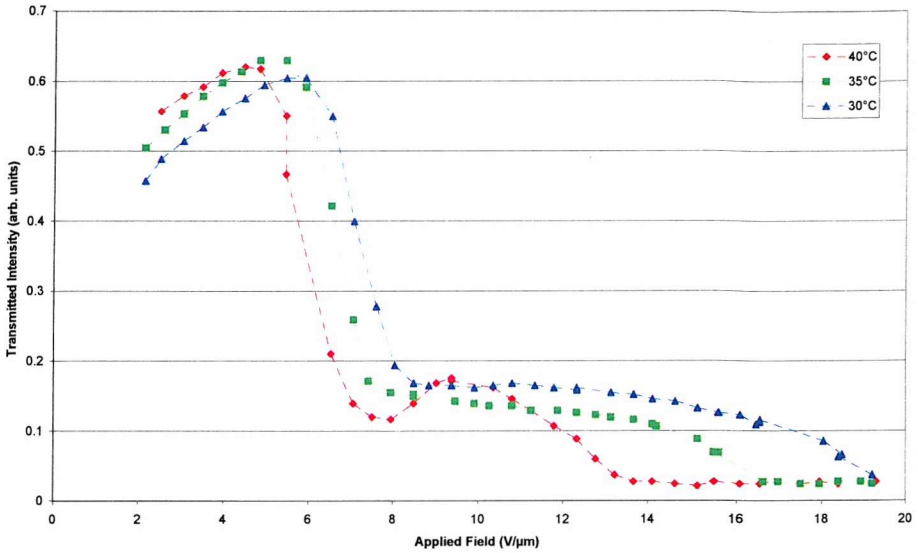

Figure 5.10 Transmitted light intensity as a function of the applied field magnitude in 67-23% $F_fB(7\text{-}11)B_fF$ 8%CB15 2%BDH1218 (10Hz square wave).

The quality of alignment and the stability of the ULH texture are strongly dependent on the frequency of the applied field. Comparisons between the data in Figure 5.9 and Figure 5.10 show that the ULH texture of the 67-23% $F_fB(7\text{-}11)B_fF$, 8% CB15 and 2% BDH1218 mixture is a lot less stable when subject to a 10Hz rather than 80Hz applied field. The 10Hz field causes very quick degradation of the alignment with the onset of helix unwinding occurring at lower fields. At 40°C, the helix unwinds into the focal conic texture, visible for fields of ~10V/µm, before adopting homeotropic alignment at higher fields. This behaviour is less pronounced at lower temperatures. The degrading effect of helix unwinding on the ULH texture is shown in Figure 5.11

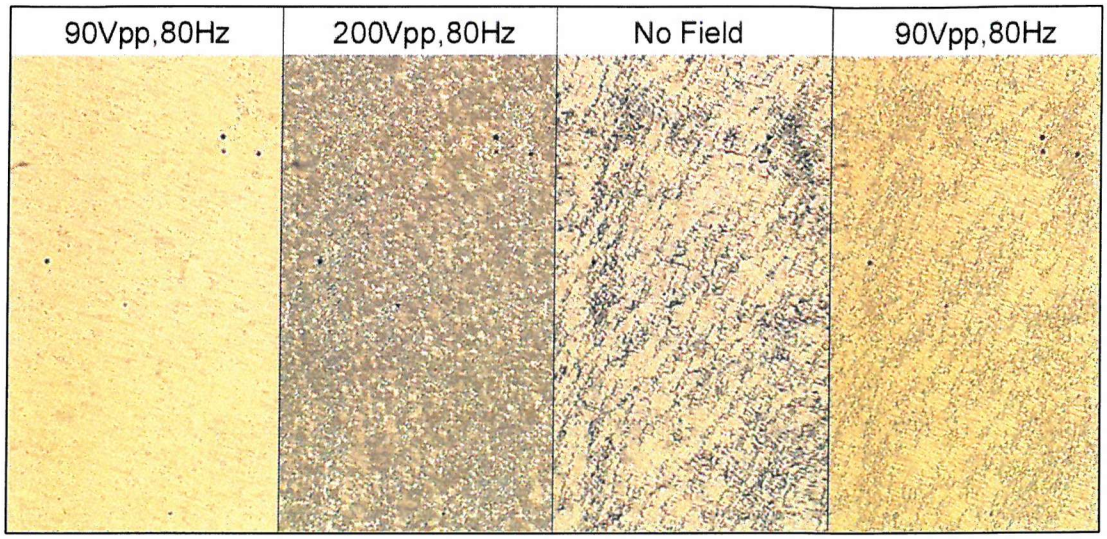

Figure 5.11 The effect of helix unwinding on the ULH texture of the 50:50 $F_fB(7\text{-}9)B_fF$ and 4%BDH1305 mixture. Initially the sample is in the ULH texture (90Vpp), the strength of the field is then increased to unwind the helix (200Vpp). The degradation in alignment quality is readily apparent when the field is removed and the initial field strength reapplied. The pictures were taken at 40°C.

5.6 FLEXOELECTRIC SWITCHING PROPERTIES

The flexoelectro-optic effect was discussed in Chapter 2. The result of the theory discussed in Section 2.5.2 is that the optic axis is rotated with respect to the electric field direction. The direction and magnitude of this rotation are directly proportional to the polarity and magnitude of the applied field. Phenomenologically, this is analagous to the electroclinic switching observed in ferroelectric liquid crystals in Chapter 4.

5.6.1 Electro-Optic Response

The transmission of light through the flexoelectric samples positioned between crossed polarisers was monitored using a photodiode connected to a digitising oscilloscope. Application of an electric field across the samples resulted in modulation of the transmitted light. Figure 5.12 shows the dynamic response of the 50%-50% $F_fB(7\text{-}9)B_fF$ mixture and 4%BDH1305 to a square wave applied electric field of magnitude 9.5V/μm

and frequency 80Hz; this response was typical of all the hypertwisted chiral nematic mixtures studied.

Unlike a conventional twisted nematic device, there is no time delay between the field application (or polarity reversal) and the electro-optic response. The rise and fall times are also approximately equal since the applied field drives the switching in both directions.

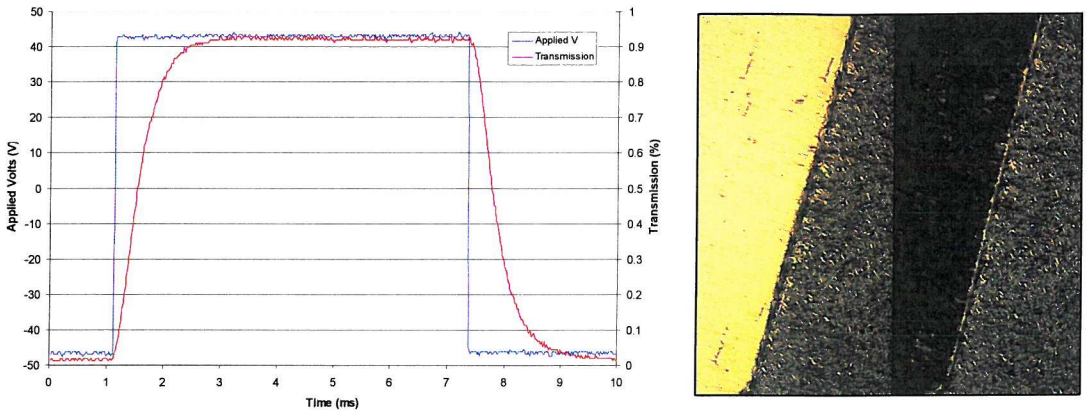

Figure 5.12 The optical response of the 50%-50% $F_fB(7\text{-}9)B_fF$ mixture and 4%BDH1305 to a 9.5V/μm 80Hz applied field and the contrast between the respective light and dark states.

Under these conditions, a contrast ratio of greater than 90:1 is achieved when the cell is positioned between crossed polarisers, satisfying one of the requirements for applications in display devices. The contrast between the switched states is dependent on the magnitude of the optic axis tilt angle, which will be discussed in Section 5.6.3. The scattering focal conic texture is clearly observable outside the active electrode area in Figure 5.12.

Figure 5.13 illustrates the optical response of the same material, 50%-50% $F_fB(7\text{-}9)B_fF$ mixture and 4%BDH1305, to a triangular wave applied electric field. The sample was positioned between crossed polarisers such that the optical axis of the undisturbed ULH texture was at 22.5° to the axis of one of the polarisers.

At low fields the electro-optic response is linear; a consequence of the linearity of the flexoelectric coupling. A nonlinear response at high fields is observed due to the helix deformation that is a result of dielectric coupling.

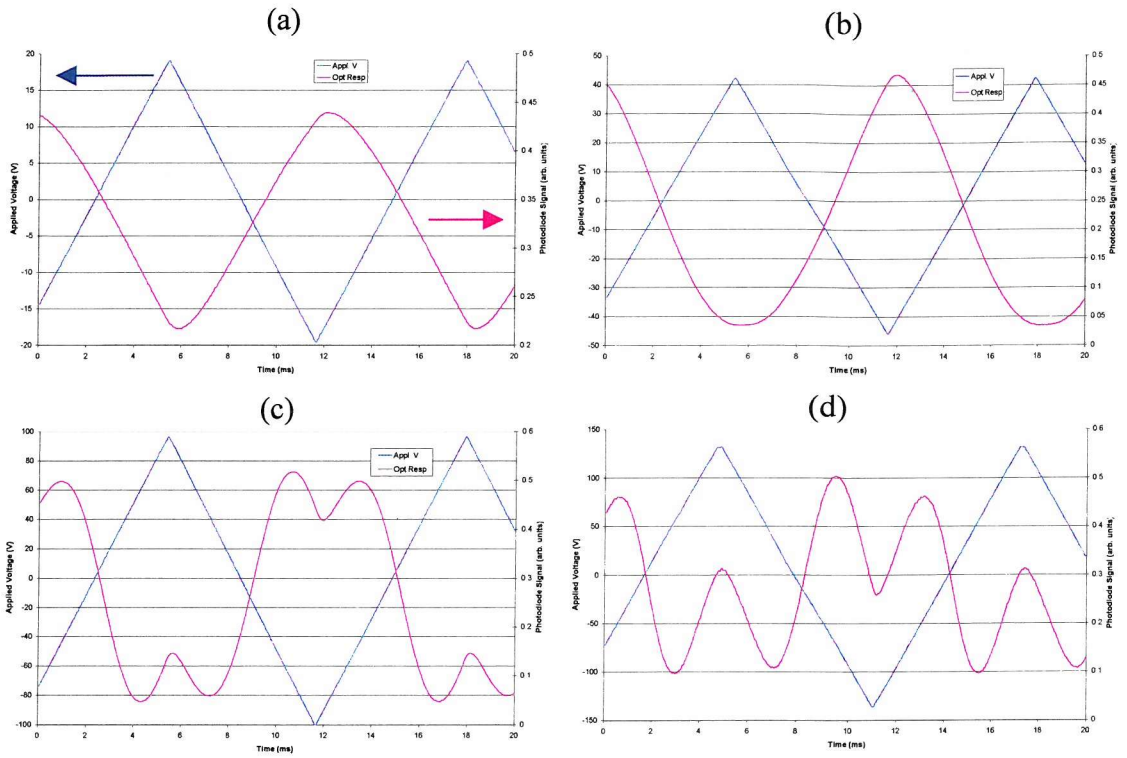

Figure 5.13 The flexoelectro-optic response of the 50%-50% $F_fB(7\text{-}9)B_fF$ mixture and 4%BDH1305. (a) linear response (4V/μm), (b) non-linear response (9V/μm), (c) switching angle > 45° (20V/μm) and (d) switching angle > 90° (27V/μm). The data was taken using a 80Hz AC triangular wave applied field at 35°C.

The magnitude of the optical axis rotation increases as the strength of the applied field increases. This increased switching angle results in the observation of double peaks, corresponding to tilt angles of more than 22.5°, in the optical response of the flexoelectric mixture for applied fields of 20V/μm or more. The dependence of the optic axis rotation on the strength of the applied field is discussed in Section 5.6.3.

5.6.2 Response Time

The optical response times were measured as the time taken for the transmitted light intensity to change from 0-90% of the peak to peak amplitude after the field polarity reversal of an 80Hz square wave.

The temperature dependence of the response times of the 50%-50% $F_fB(7\text{-}9)B_fF$ mixture and 4%BDH1305 is shown in Figure 5.14. Response times of less than 1ms are readily achieved. The magnitude decreases with increasing temperature as γ_1, the viscosity term in Equation 2.62, also varies with temperature. The response times are also approximately independent of the applied field[9]. The torque on the director is proportional to the magnitude of the applied field, hence the director rotates faster, but under higher fields the angle of rotation is greater, therefore there is effectively no change in the response time. The weak field dependence has been shown to be introduced by surface anchoring conditions[10].

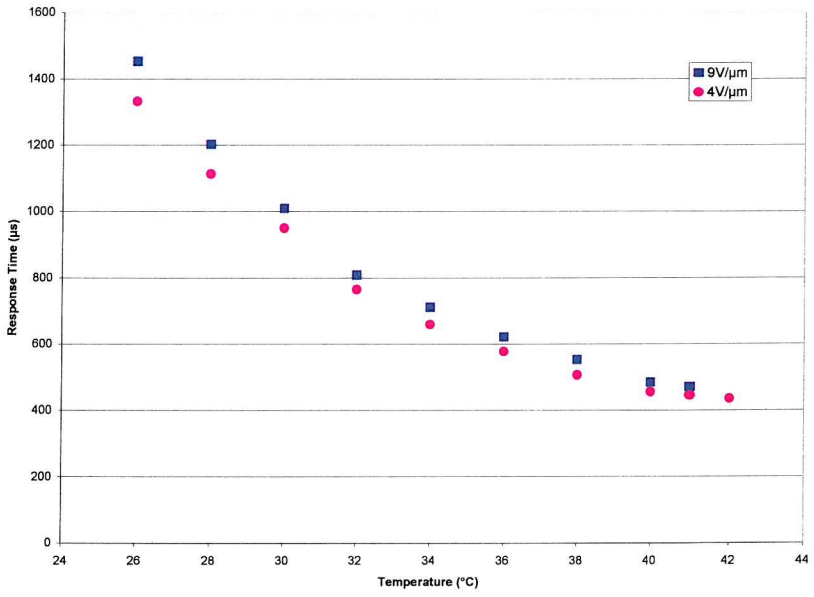

Figure 5.14 Optical response times of the 50%-50% $F_fB(7\text{-}9)B_fF$ mixture and 4%BDH1305 as a function of temperature to an 80Hz square wave.

[9] S-D. Lee, J.S. Patel, R.B. Meyer, *J. Appl. Phys.*, **67**, 1293 (1990)
[10] S-D. Lee, J.S. Patel, R.B. Meyer, *Mol.Cryst.Liq.Cryst*, **209**, 79 (1991)

High tilt angles, of more than 22.5°, precluded sensible response time measurements being made from 0-90% changes in light intensity at higher fields.

It was found that the response times of all the mixtures studied had similar temperature dependence characteristics, as shown in Figure 5.15 below.

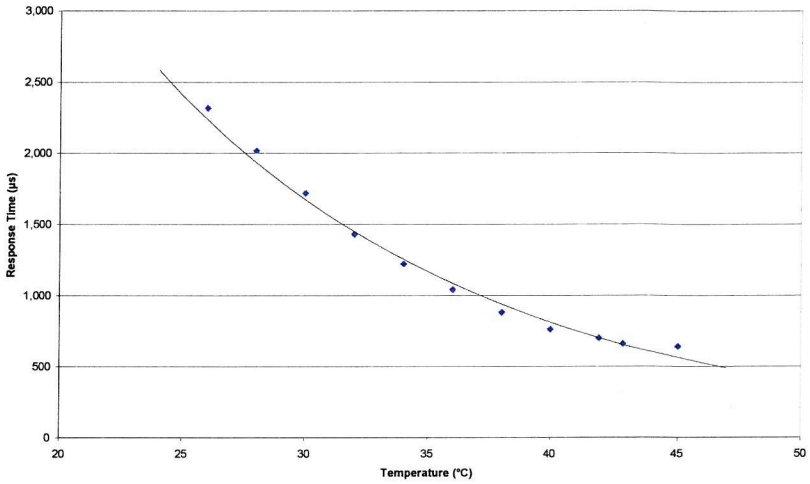

Figure 5.15 The temperature dependence of the response time of the F_fB7B_fF 67%/23% FBf11fBF, 8%CB15 and 2%BDH1218 mixture.

5.6.3 Tilt Angle

The field induced optic axis tilt angle measurements were carried out using the rotating analyser technique. The experimental setup is the same as that previously used to characterise ferroelectric materials and is described in Section 3.5.2. Tilt angle measurements were undertaken with a 10Hz square wave alternating waveform applied across the sample in the ULH texture, whilst the amplitude of the applied voltage and temperature were varied.

Figure 5.16 illustrates the applied field dependence of the tilt angle of the 50%-50% $F_fB(7\text{-}9)B_fF$ mixture and 4%BDH1305 at 40°C. The material exhibited remarkably high tilt angles per unit field of ~2.4°/Vμm^{-1} in the linear regime before dielectric coupling manifests itself in the form of helix unwinding at larger fields. Figure 5.17 illustrates the

applied field dependence of the tilt angle of the 67-23% $F_fB(7-11)B_fF$, 8% CB15 and 2% BDH128 mixture at 40°C.

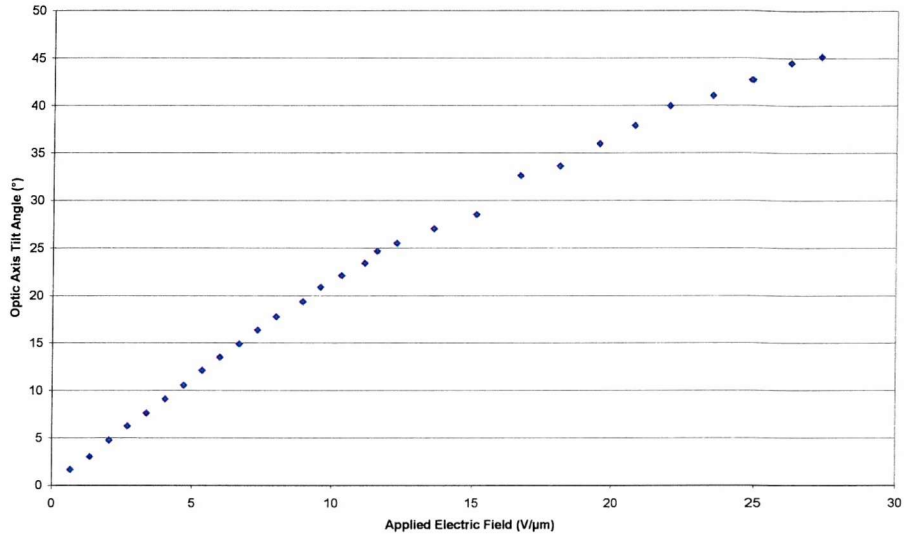

Figure 5.16 Optic axis tilt angle of the 50%-50% $F_fB(7-9)B_fF$ mixture and 4%BDH1305 as a function of applied electric field, 10Hz square waveform, 40°C.

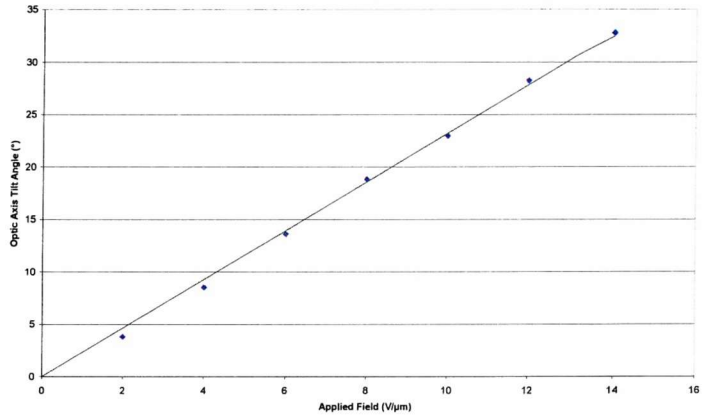

Figure 5.17 Applied electric field dependence of the optic axis tilt angle of the 67-23% $F_fB(7-11)B_fF$, 8% CB15 and 2% BDH1218 mixture, 10Hz square waveform, 40°C.

The extreme limits of achievable tilt are determined by the dielectric coupling, which is quadratic in the field. If the dielectric coupling is not suppressed by using a material with $\Delta\varepsilon\approx 0$, partial or total unwinding of the helix can occur under the application of high fields. This affects the electro-optic response and destroys the ULH structure. Limits of the tilt are set by dielectric coupling and electrical breakdown. The dependence of the tilt angle

on the magnitude of the applied field is linear up to a field at which dielectric coupling results in unwinding the helix.

The magnitude of the tilt angle was observed to be virtually temperature independent, as shown in Figure 5.18, indicating that the pitch does not change significantly with temperature.

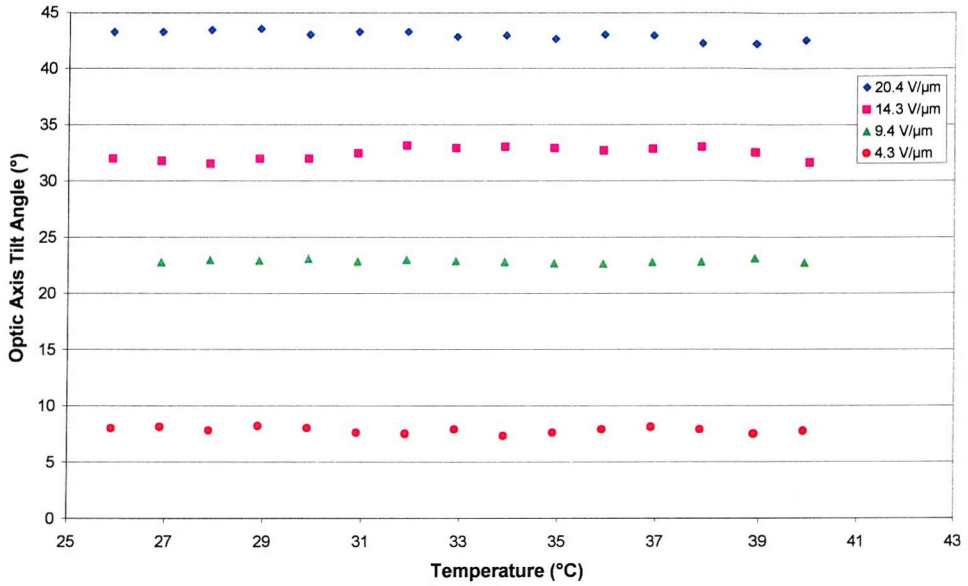

Figure 5.18 Optic axis tilt angle as a function of temperature, (10Hz square waveform).

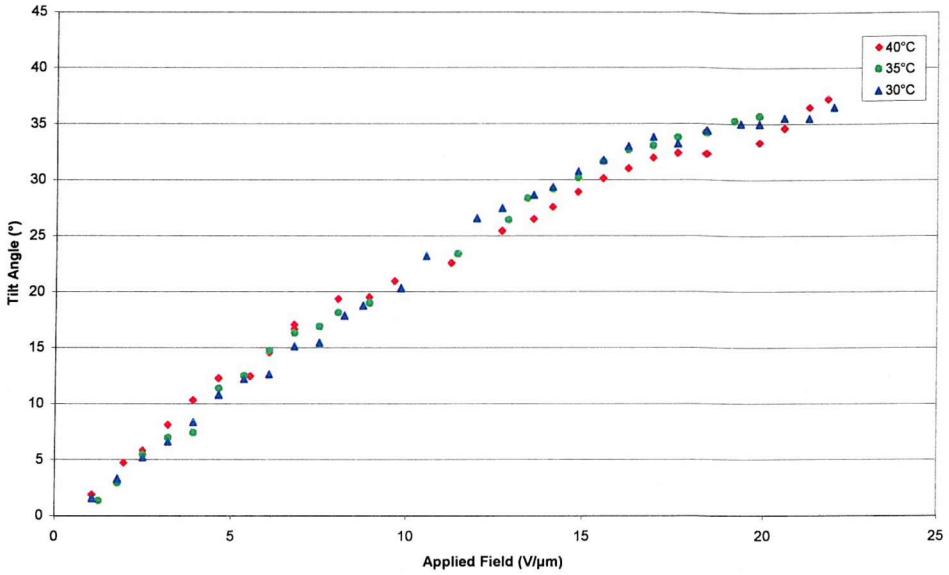

Figure 5.19 The temperature and field dependence of the tilt angle of the 46%-44% $F_fB(7-11)B_fF$, 2% BDH1218 & 8% CB15 mixture.

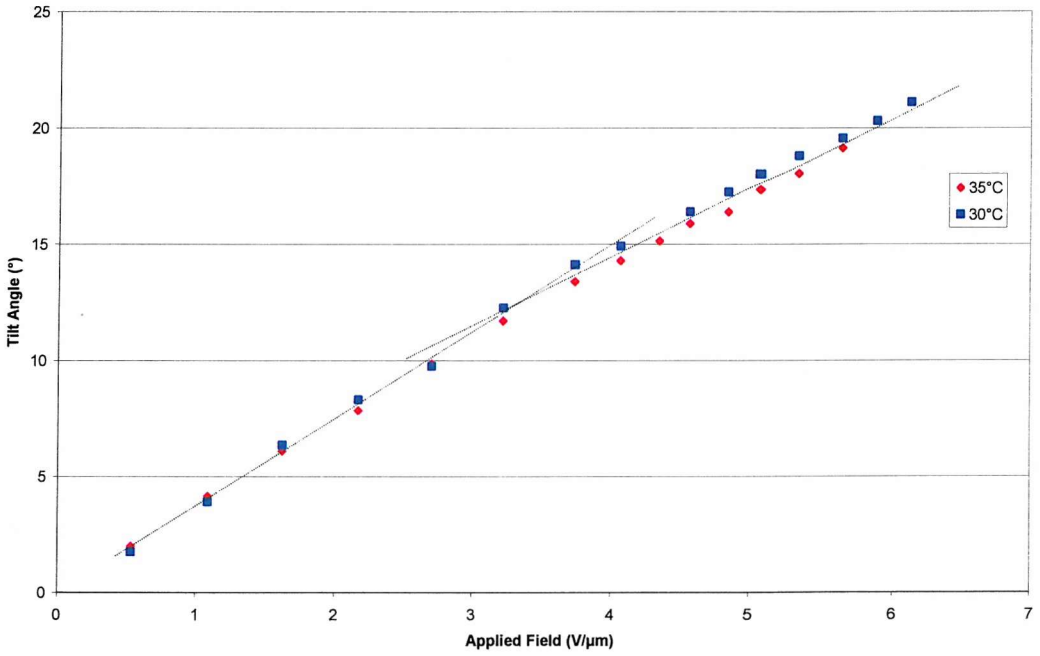

Figure 5.20 The temperature and field dependence of the tilt angle of the 20%-80% $F_fB(7-9)B_fF$ and 20% CB15 mixture.

In Figure 5.16, Figure 5.19 and Figure 5.20 a change in the linear behaviour of the optic axis rotation at 15V/µm, 10V/µm and 3V/µm respectively can be identified. It is has been

proposed[11,12] that this behaviour can be attributed to a distortion in the boundary layer. Two regimes are proposed; a low field regime in which the bulk of the sample distorts to reduce the free energy of the system and, a high field regime in which the boundary layer is modified to accommodate the distortion of the helix. It is interesting to note the temperature dependence of this distortion, particularly visible in Figure 5.19, in which the gradient of the discontinuity changes sign.

5.7 SUMMARY

The flexoelectro-optic effect in eutectic mixtures of a series of achiral nematic bimesogens and small quantities of chiral dopant has been studied. The mixtures all possess a room temperature chiral nematic phase and good alignment of the ULH texture can be achieved by combining surface forces and applied AC fields whilst cooling through the isotropic – nematic transition. The temperature dependence of the critical field for unwinding the helix has also been examined.

Investigations into the behaviour of the flexoelectro-optic properties have yielded some very promising results. Switching times of the order of 500μs and contrast ratios of 90:1 are readily achieved. For the first time a switching angle of 90° is attainable with the flexoelectro-optic effect at room temperature. The constancy of the tilt angle, indicating constant pitch, is particularly useful for fixing the optical contrast as a function of temperature as the direction of external polarisers can be optimised and fixed during device fabrication.

Tilt angles of 22.5°, the optimum for birefringence displays, can be obtained with moderate ($10V\mu m^{-1}$) applied fields and allow the material to be utilised in double polariser devices. Higher fields yielded tilt angles of 45°, providing optimal contrast ratios for single polariser devices such as dye-guest host displays.

---

[11] S-D.Lee and J.S.Patel, *Phys.Rev.A*, **42**, 997 (1990)
[12] S-D.Lee and J.S.Patel, *J.Appl.Phys*, **67**, 1293 (1990)

The gradient $\tan\phi/E$ of these materials is approximately $0.05\mu m V^{-1}$ - similar in magnitude to the gradient observed in previous work on estradiol and cyanobiphenyl bimesogens[13]. Assuming a pitch length of ~700nm (similar to the pitch estimated by Musgrave for a mixture with the same concentration of chiral dopant) implies that the ratio e_F/K is approximately $6CN^{-1}m^{-1}$, from Equation 2.53; an order of magnitude larger than those reported by Musgrave $(0.6CN^{-1}m^{-1})$[13,14]. This result can be explained by the confirmational ground state of the two materials in question, as illustrated in Figure 5.21. The odd number of carbon atoms in the spacer chain of the $F_fB(n)B_fF$ materials studied in this chapter confers a bent (or banana) shape on the molecule resulting in a transverse dipole. Thus, as e_F is dependent on the transverse dipole moment[15] a significant increase in the flexoelectric behaviour is observed.

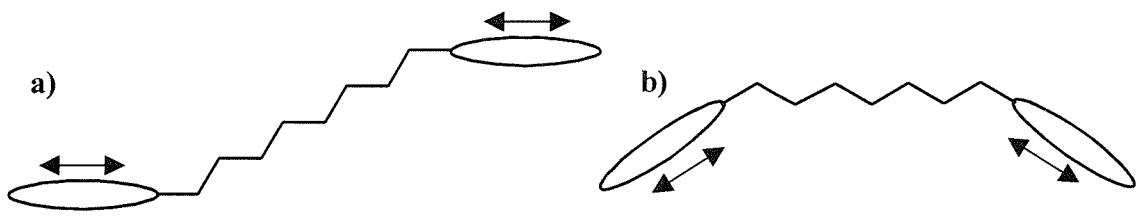

Figure 5.21 The confirmational ground states of the bimesogens; a) CBO8OCB, the material studied by Musgrave and b) $F_fB(7)B_fF$.

Dielectric coupling depends on the net dipole moment. Symmetric bimesogens tend to have a lower net dipole moment, resulting in a lower $\Delta\varepsilon$, and therefore higher critical fields for helix unwinding.

This is not a truly meaningful comparison since the measurements presented here were made under different conditions to those made by Musgrave; the cyanobiphenyl bimesogens studied by Musgrave are nematic at temperatures in the range of 180°C, considerably higher than the near room temperature measurements detailed in this thesis. In addition to lowering the temperature at which the nematic phase exists, flourination,

[13] B.Musgrave, P.Lehman and H.J.Coles, *Liq. Cryst.*, **26**, 1235 (1999)
[14] B.Musgrave, *Ph.D Thesis*, University of Southampton (1999)
[15] M.A.Osipov, *Sov. Phys. JETP*, **58(6)**, 1167 (1983)

rather than the terminal cyano unit, reduces the viscosity allowing sub millisecond switching at dramatically reduced temperatures.

Chapter Six

DUAL FREQUENCY NEMATIC LIQUID CRYSTALS

6.1 INTRODUCTION

The operation of twisted nematic devices using a 'dual frequency' driving scheme was discussed in §2.6.2. To recap, the advantage of using such a scheme over the conventional twisted nematic operation is that the director is driven both 'on' and 'off'. Since the dielectric anisotropy, $\Delta\varepsilon$, of the 'dual frequency' materials changes sign upon changing the frequency of the driving field from low frequencies, ν_L, to high frequencies, ν_H, or $\nu_{H\ to}\ \nu_L$ fast, active response times can be achieved[1]. M.Schadt[2] has shown that the active switching is 3 to 4.5 times faster than the conventional passive switching mechanism.

The work in this chapter is based upon a new nematic material exhibiting dielectric dispersion. Section 6.2 introduces the properties of dual frequency nematic liquid crystals through the characterisation of a proprietary mixture provided by Merck. Section 6.3 builds on this foundation through the characterisation of a new proprietary material synthesised within the Liquid Crystal Institute in Southampton. The frequency and temperature dependence of the dielectric anisotropy sign reversal, voltage threshold for switching and response times are investigated. The effect of mixing this material with a low viscosity host in order to reduce the response times is also undertaken and a comparison between the response times obtained with dual frequency and conventional driving schemes made. Finally, Section 6.4 summarises the key findings of the work presented in this chapter.

6.2 PRELIMINARY WORK – TX2A

Preliminary work in this direction was undertaken using the Merck mixture TX2A. This mixture is a dual frequency material that is nematic at room temperature. Dr. Doina Ionescu of Merck[3] provided a small quantity of the material in three electro-optic cells,

---

[1] W.H.de Jeu, C.J. Gerritsma, P. van Zenten, W.J.A. Goosens, *Phys.Lett.*, **39A**, 355 (1972)
[2] M. Schadt, *Appl.Phys.Lett.*, **41**, 697 (1982)
[3] Merck, Southampton, UK. `http://www.merck.com`

one planar alignment cell and two with twisted alignment geometries, all with a nominal thickness of 5μm.

6.2.1 Characterisation – TX2A

6.2.1.1 Phase Charactersation

Nematic 99°C Isotropic

The phase sequence of the mixture was characterised via thermo-optic and polarising microscopy methods. On cooling from the isotropic phase the material entered the liquid crystalline phase at 99°C. No further textural changes were observed on cooling to ambient room temperature. The decrease in the transmitted intensity as the material is cooled through the nematic phase is due to the predominant colour of the texture continuously changing throughout the phase range. The colour transmitted through the cell depends on the cell thickness and birefringence of the sample (Equation 2.24). The cell thickness is believed to remain almost constant as the temperature varies, therefore, the sample birefringence must change.

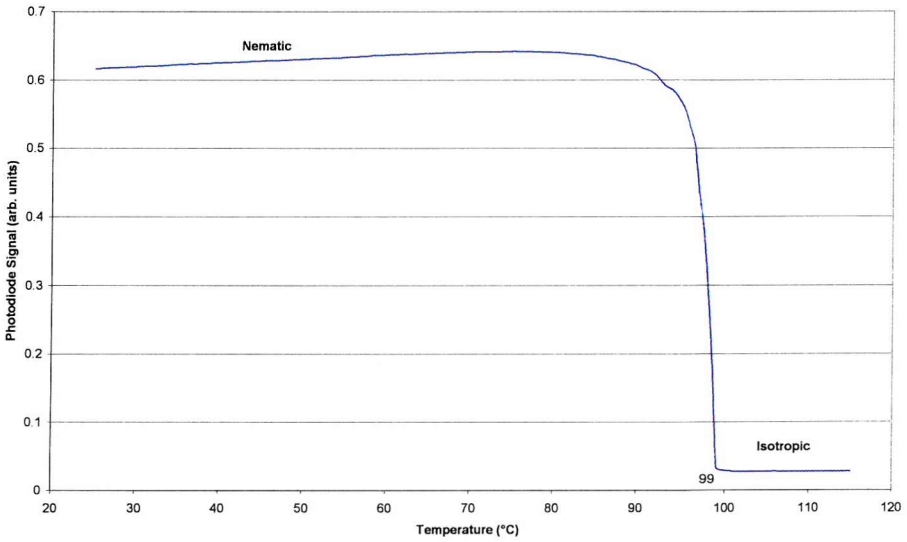

Figure 6.1 Thermo-Optic trace - TX2A. Data taken on cooling at 1°C/min.

6.2.1.2 Dielectric Properties

The method employed for dielectric characterisation of a liquid crystalline sample has been described in §3.5.4. Briefly, this method involves measuring the capacitance of an

empty cell before measuring the capacitance of the cell when filled with the liquid crystal material to be investigated. As the samples of TX2A were obtained with the material already in cells the exact determination of $\Delta\varepsilon$ could not be achieved using this method. The frequency dependent nature of the dielectric anisotropy was inferred by measuring the capacitance of the full cells, C_{full}.

Capacitance measurements were undertaken using a Wayne Kerr bridge[4]. By using two different voltages, V_H and V_L, to approximate homeotropic and homogneous alignments it was hoped to gain an understanding of the behaviour of the $\varepsilon_{||}$ and $\varepsilon_{\perp}$. Initial observations of TX2A, when subjected to a DC electric field, indicated that at low frequencies the dielectric anisotropy of TX2A was positive. Therefore, a relatively high applied voltage (5V – the maximum of the Wayne Kerr bridge) would result in homeotropic alignment and, as a result, the capacitance measured would be dependent on $\varepsilon_{||}$. A low applied voltage (0.25V – the minimum of the Wayne Kerr bridge) has little effect on the director and results in surface forces imposing homogenous alignment upon the molecules; the resulting capacitance is therefore dependent on $\varepsilon_{\perp}$. The results are shown in Figure 6.2.

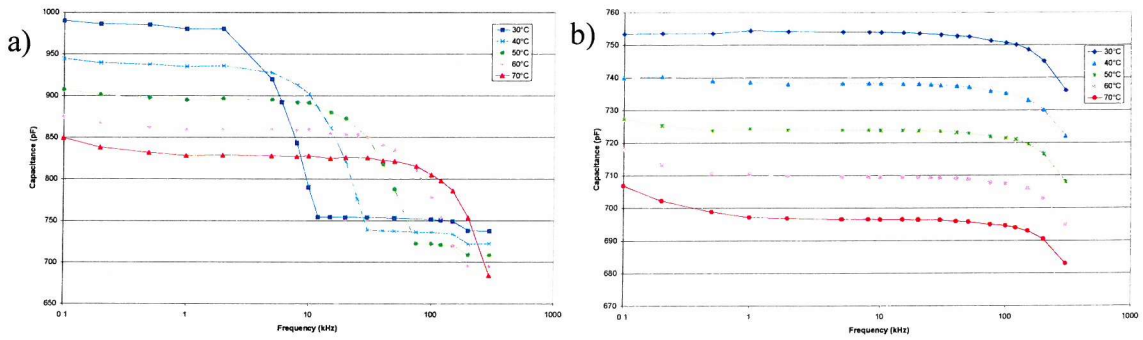

Figure 6.2 The frequency and temperature dependence of the capacitance of TX2A. a) Applied voltage V_{ac} = 5V (simulating $\varepsilon_{||}$ via homeotropic alignment) and b) Applied voltage V_{ac} = 0.25V (simulating $\varepsilon_{\perp}$ via homogenous alignment).

The data presented in Figure 6.2 and Figure 6.3 clearly shows that $\varepsilon_{||}$ has a strong frequency dependence whilst $\varepsilon_{\perp}$ remains constant over a wide range of frequencies.

[4] Wayne Kerr Electronics, Vinnetrow Business Park, Runcton, Chichester, UK, PO20 1QH. http://wwwaynekerrtest.com

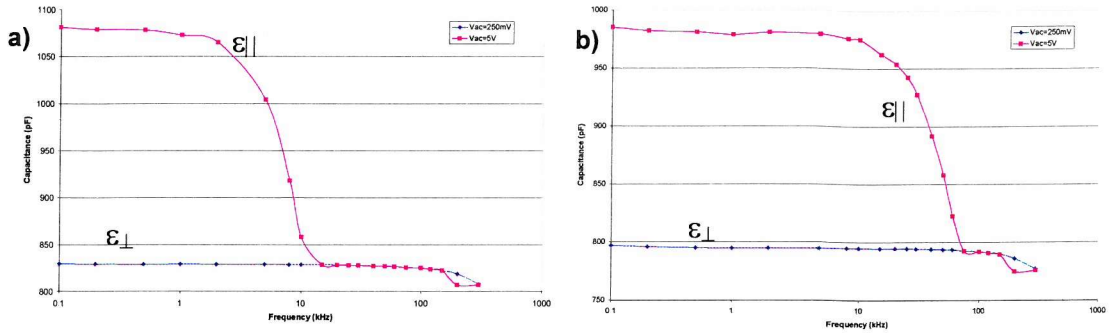

Figure 6.3 The frequency dependence of the capacitance of TX2A at a) 30°C and b) 50°C.

The dielectric anisotropy, $\Delta\varepsilon=\varepsilon_{||}-\varepsilon_{\perp}$, is positive for low frequency applied fields. The temperature dependence of the dispersion frequency, the frequency at which $\Delta\varepsilon$ becomes negative i.e. when $\varepsilon_{||}$ is less than $\varepsilon_{\perp}$, is also observable, with lower temperatures resulting in a lower dispersion frequency, f_d. In this experimental arrangement it was not possible to quantify the extent of the crossover since when this occurs the director adopts the homogenous alignment configuration. Therefore, true measurement of the change in $\varepsilon_{||}$ was not possible as when the crossover occurs the capacitance becomes dependent on $\varepsilon_{\perp}$.

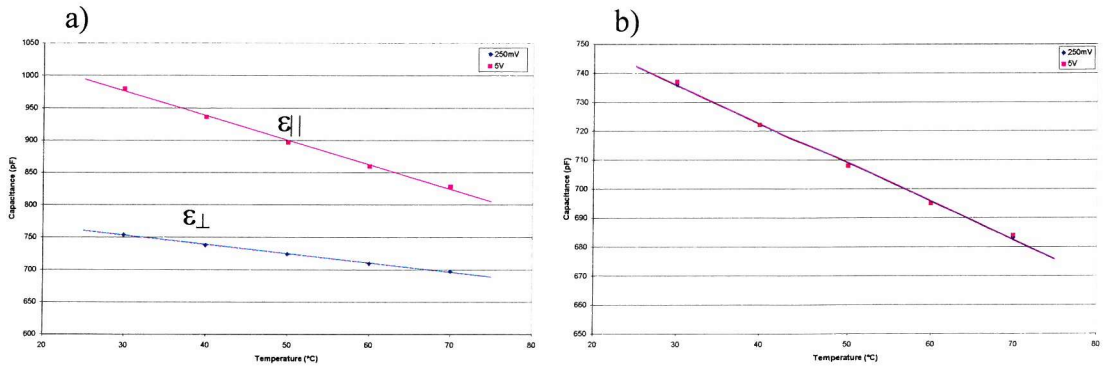

Figure 6.4 The temperature dependence of the capacitance of TX2A when subject to high and low applied voltages. a) frequency of applied field 2kHz and b) frequency of applied field 300kHz.

The data in Figure 6.4a) indicates the slight temperature dependence of $\Delta\varepsilon$, with higher temperatures resulting in a lower value of $\Delta\varepsilon$. The cutoff frequency is below 300kHz for all temperatures, therefore, the director alignment in the cell is the same for both high and low voltages as seen in Figure 6.4b).

6.2.1.3 Transmission versus Frequency

Measurements of the transmitted intensity as a function of the frequency of the applied field allow the temperature dependent nature of the dispersion frequency to be observed. All measurements were made in transmission at vertical light incidence with the cell positioned between crossed polarisers. Coupling with the applied field at low frequencies due to the positive $\Delta\varepsilon$ destroys the twisted structure, resulting in practically zero transmission. At higher frequencies, $\Delta\varepsilon$ becomes negative, the director adopts the planar orientation and the twisted structure is conferred by the alignment layers.

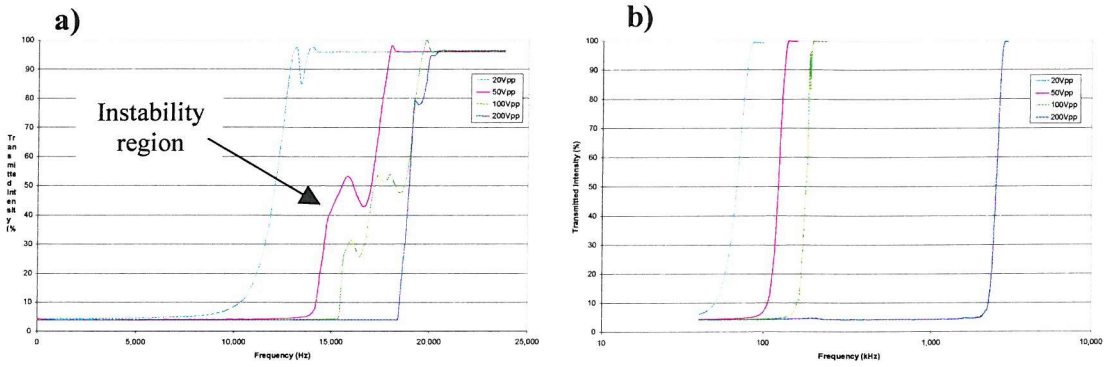

Figure 6.5 TX2A – The frequency dependence of transmission a) 30°C and b) 60°C (5µm cell).

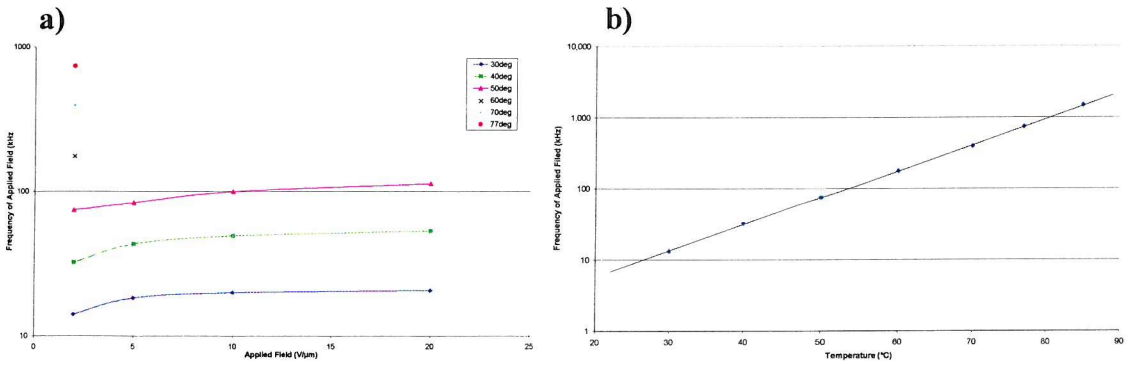

Figure 6.6 a) Dispersion frequency versus applied field (5µm cell) and b) the temperature dependence of the dispersion frequency in TX2A (±2V/µm, 5µm cell).

The transition from the dark to bright states occurs via instability growth. The intensity fluctuations observed in the region around ν_c are caused by the formation of electrohydrodynamic, EHD, instabilities[5]. Some of these textures are shown in Figure 6.7.

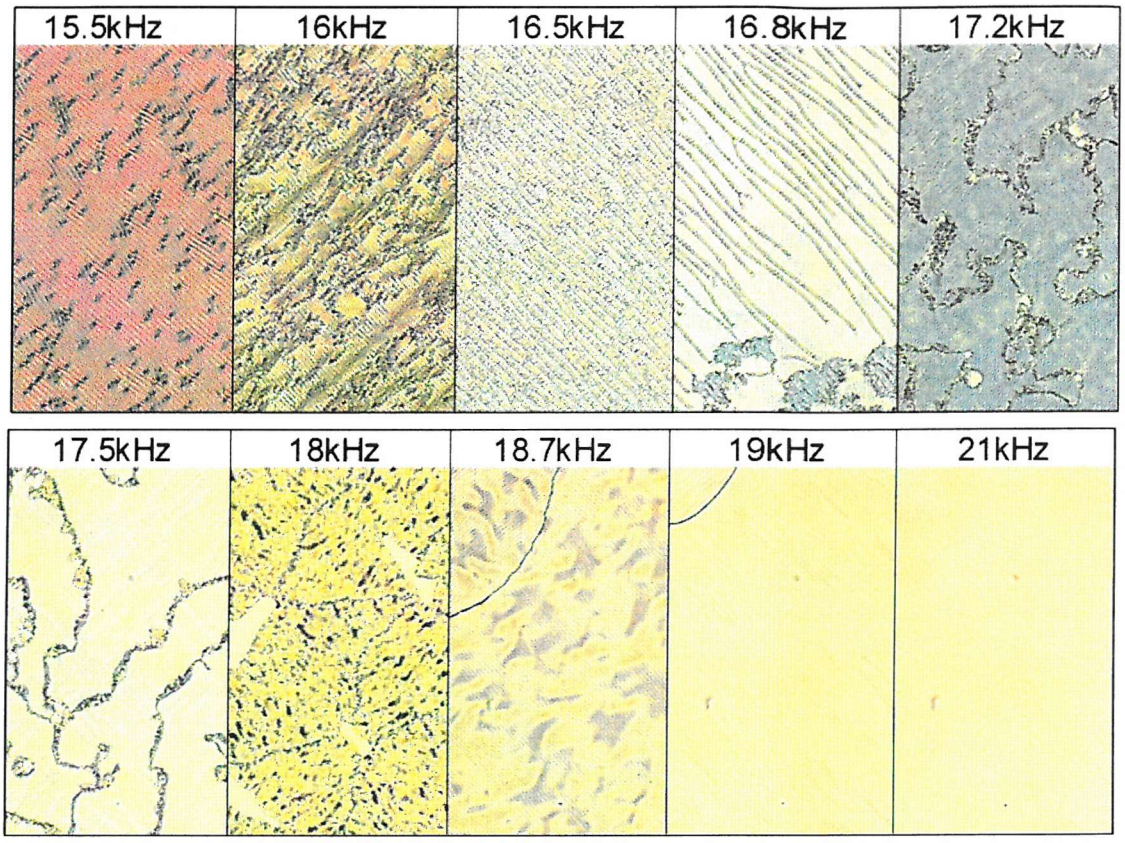

Figure 6.7 Electrohydrodynamic (EHD) instabilities observed in TX2A (5μm cell, 100Vpp, 30°C).

6.2.1.4 Threshold Voltage

Figure 6.8a) clearly illustrates the frequency dependence of the threshold voltage V_{th}. The reduction of $\Delta\varepsilon$ as the frequency is increased and ν_c is approached has been discussed in Section 2.3.1. Equation 2.61 shows that a consequence of this is that V_{th} increases. At 30°C the dispersion frequency of TX2A is ~12kHz, thus when applying a 10kHz signal a large increase in V_{th} is observed due to the reduction of $\Delta\varepsilon$. This effect is less pronounced at higher temperatures as the frequencies applied are well below ν_c, (since ν_c increases with increasing temperature), as shown in Figure 6.6b).

[5] L.M.Blinov, *J.de.Physique*, **40**, C3-247, (1979)

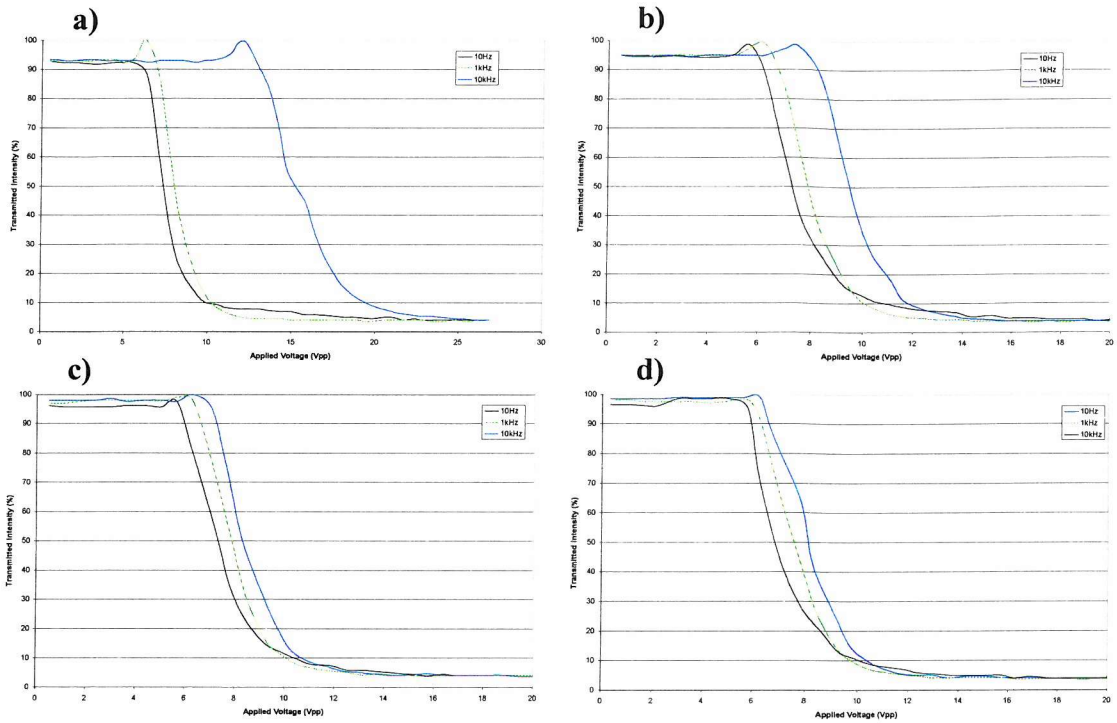

Figure 6.8 The temperature and frequency dependence of the threshold voltage of TX2A, a) 30°C, b) 40°C, c) 60°C and d) 70°C (5μm cell).

6.2.1.5 Switching Characteristics and Response Times

Figure 6.9 illustrates the difference in the switching dynamics of TX2A in a twisted nematic configuration when subjected to the a) conventional (field on – field off) and b) dual frequency (low frequency field – high frequency field) driving schemes.

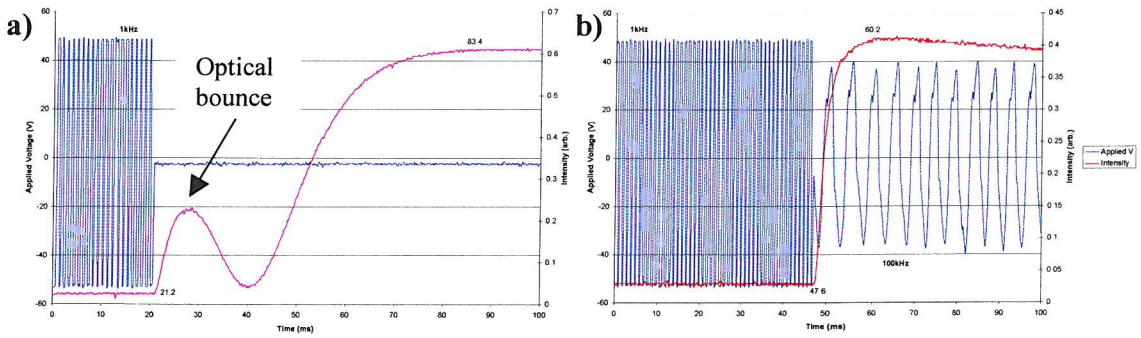

Figure 6.9 The optical response of TX2A when subject to a) conventional applied field switching scheme and b) dual frequency adressing scheme.

The response times were measured using the methodology described in Section 3.5.3. The response times shown in Figure 6.10a) clearly show that faster rise times are achievable

with a dual frequency addressing scheme. The occurrence of the 'optical bounce', seen in Figure 6.9a), complicates the rise time measurement. A small increase is observed in the fall response times due to the slightly reduced $\Delta\varepsilon$ as a result of the application of the high frequency field in the twisted configuration.

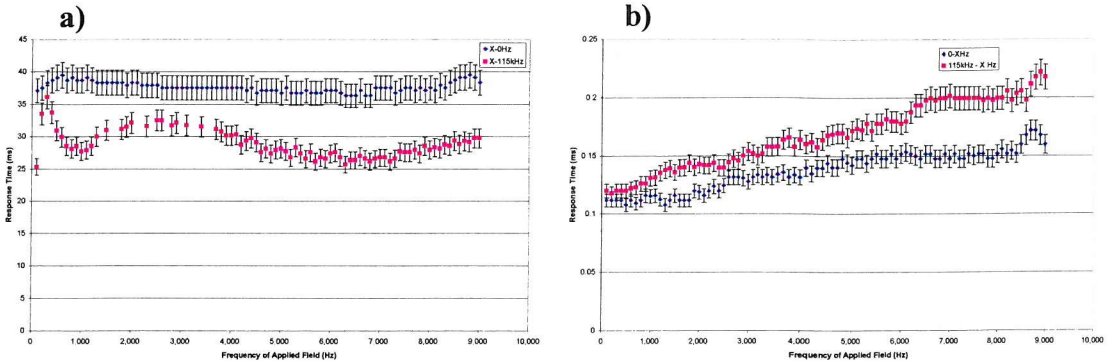

Figure 6.10 The frequency dependence of the a) rise and b) fall response times of TX2A (30°C, 20V/μm)

6.3 PROPRIETARY DUAL FREQUENCY MATERIAL - 5PFP5

6.3.1 Introduction

Frequency dependent dielectric properties can be used to decrease the response times of liquid crystalline materials. This section discusses the work undertaken to characterise a fast response nematic liquid crystal for use in display applications. The material 4-n-pentylphenyl 2-fluoro-4-(4-n-pentylbenzoyloxy) benzoate, (5PFP5), synthesised within the Southampton Liquid Crystal Institute, was based upon the chlorinated compound used by Bücher et al[6]. The fluorinated version used in this work was synthesised to possess a larger negative $\Delta\varepsilon$ above the critical frequency and hence an improvement in the response times. The 3 ring structure will have low viscosity whilst the fluorine has a small volume and large electro-negativity. The higher melting point of the 3-ring structure, in comparison to a 2-ring structure, will also be beneficial.

[6] H.K. Bücher, R.T. Klingbiel, J.P. VanMeter, Appl.Phys.Lett., **25**, 186, (1974)

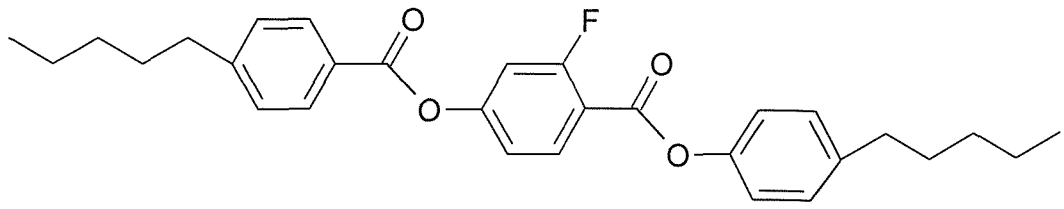

Figure 6.11 The molecular structure of the dual frequency nematic liquid crystal 5PFP5. (4-n-pentylphenyl 2-fluoro-4-(4-n-pentylbenzoyloxy) benzoate)

Liquid crystals are often fluorinated to reduce the viscosity nad bring down transition temperatures[7]. Fluorine possesses the highest electronegativity of all elements, and, attached to a phenyl ring it is still partly pushing electrons into the ring due to the positive mesomeric effect resulting from the three electron pairs. The Carbon-Fluorine (C-F) bond has a high energy and is therefore stable. Any lateral substitution will reduce the length to breadth ratio and therefore lead to a reduction in the nematic-isotropic transition (T_{NI}). Fluorine will therefore reduce the transition temperature, T_{NI}, less than chlorine. The '2' position will also reduce the conjugation of the rings. The dispersion frequency of nematic liquid crystals formed by long 3-ring molecules is lower than 2-ring molecules as the barriers to the rotation of the molecules around the short axes are particularly high[8].

A sequence of mixtures of 5PFP5, nominally 5%, 10% 20% and 50% by weight, in MDA-00-984[9] were prepared. The Merck mixture MDA-00-984 is a broad range nematic mixture with very low viscosity. In the absence of a complete data sheet a full characterisation of MDA-00-984 was also undertaken.

6.3.2 Phase Characterisation

Phase characterisation was undertaken using the DSC and optical microscopy methods discussed in Chapter 3. The transition temperatures of the mixtures and pure MDA-00-984 and 5PFP5 are shown in Figure 6.12.

---

[7] D.J.Byron, A.S Matharu, R.C.Wilson, J.W.Brown, Mol. Cryst. Liq. Cryst., **258**, 95 (1995)
[8] W.H. de Jeu, Th.M. Lathowers, Mol. Cryst. Liq. Cryst., **26**, 225 (1974)
[9] Supplied by Merck, Southampton, UK. `http://www.merck.com`

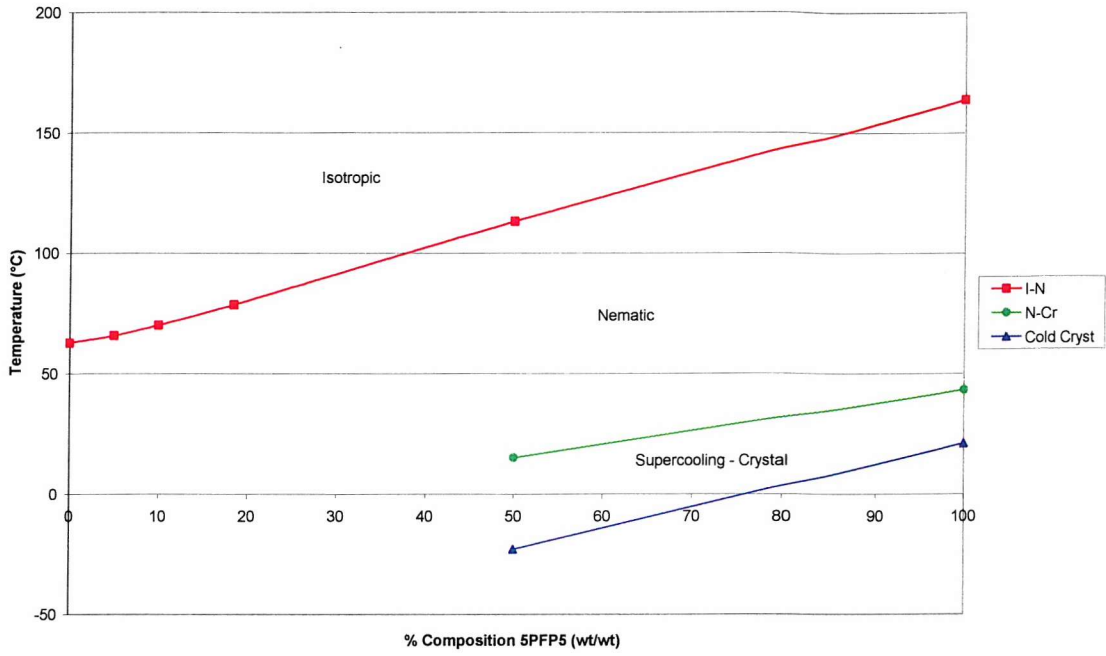

Figure 6.12 Phase diagram of mixtures consisting of 5PFP5 and MDA-00-984. Measurements taken on cooling by DSC.

The phase sequence and electro-optical characterisation of each sample will be discussed in the following sections.

6.3.3 Pure MDA-00-984

The pure compound MDA-00-984 exhibits only one liquid crystalline phase. On cooling from the isotropic phase a solitary phase transition to the nematic phase is observed at 55°C. No crystallisation was observed on cooling to –50°C.

Nematic 55°C Isotropic

Electro-optic studies revealed no apparent switching. A very small negative dielectric anisotropy[10] resulted in no observable switching in the conventional planar and twisted 'Lucid' cell geometries. Therefore no voltage threshold for switching was measurable.

[10] Data sheet, Merck, Southampton, UK. http://www.merck.com

6.3.3.1 Transmission vs Frequency

With a view to the intended dual frequency operation of the mixtures transmission versus frequency data was recorded across a range of different applied fields and temperatures. As discussed in the previous section, the application of AC and DC electric fields of up to 20V/μm did not result in observable switching, however, variation of the frequency resulted in a drop of the transmitted intensity due to the formation of electrohydrodynamic (EHD) instabilities[11] and Williams domains[12].

In all the following transmitted intensity measurements the intensity has been normalised, taking $I_{100\%}$ to be the light intensity transmitted by a parallel polariser/analyser combination. All measurements were made in transmission at vertical light incidence. The TN cell was situated on the hotstage of the polarising microscope and positioned such that the transmitted light intensity was maximised when no electric field was appplied. The maximum magnitude of the applied field was limited to 20Vpp (~±2V/μm) due to the inability of the HVA to accurately amplify the field at frequencies above 100kHz. The HVA was therefore removed from the experimental setup so the applied field was produced solely by the signal generator.

[11] L.M.Blinov, *J.de.Physique*, **40**, C3-247, (1979)
[12] R.Williams, *J.Chem.Phys*, **39**, 384, (1963)

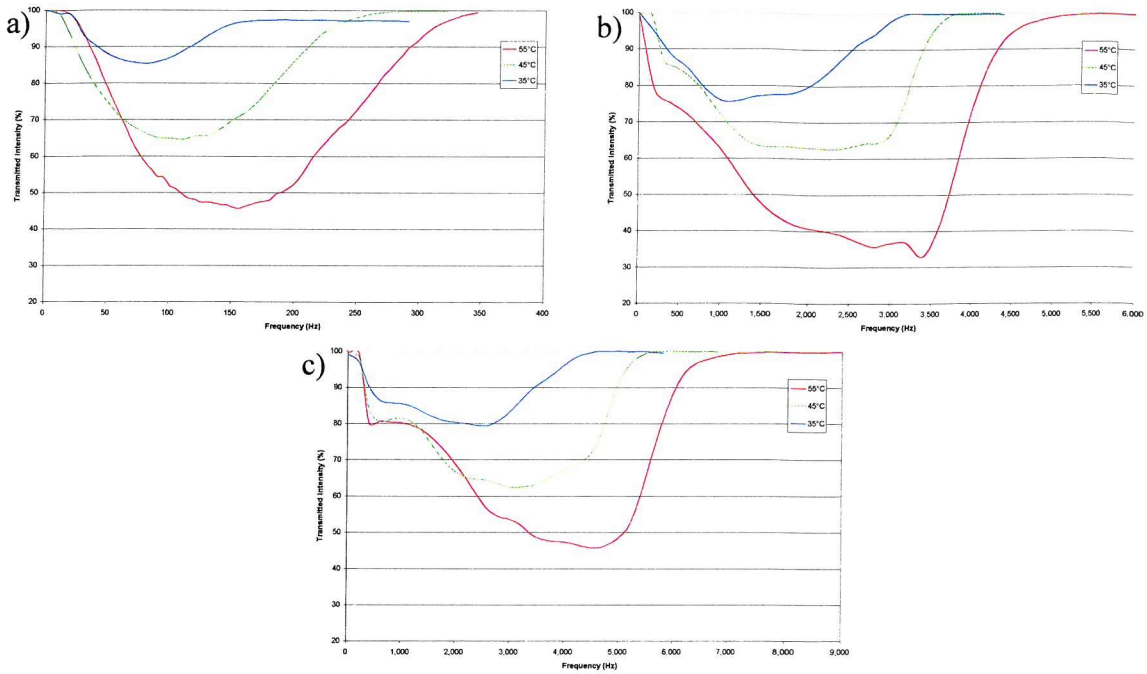

Figure 6.13 Pure MDA-00-984 : Transmitted intensity versus frequency of the applied field. (a) ±2V/µm, b) ±14V/µm and c) ±20V/µm

For small applied fields (±2V/µm) instabilities appear in the 50-300Hz frequency range. This frequency range was reduced at lower temperatures. At higher fields the instabilities were observed over a larger frequency range. For applied fields of ±14V/µm the instabilities were observed in the range 50Hz-4.5kHz, and ±20V/µm – range 200Hz-6kHz, again this range was reduced at lower temperatures.

6.3.4 Pure 5PFP5

The pure compound 5PFP5 exhibits only one liquid crystalline phase. Phase characterisation was undertaken using DSC and optical microscopy methods. On cooling from the isotropic phase a transition to the nematic phase is observed at 161°C. Crystallisation occurs at 50°C with a further 'cold crystallisation' at 20°C.

Cold Crystal 20°C Crystal 50°C Nematic 161°C Isotropic

Optical studies were carried out on the sample in a planar Lucid cell. The photomicrographs in Figure 6.15 show the isotropic to nematic transition, the variance of the birefringence and the texture of the crystallised sample.

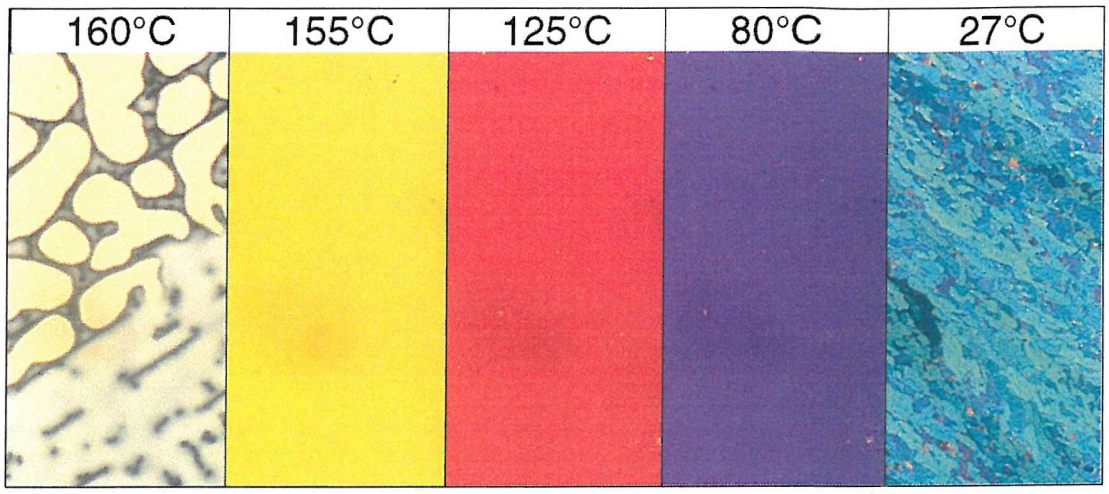

Figure 6.14 Photomicrographs of 5PFP5 taken on cooling at 2°C/min. 160°C Isotropic to nematic transition, 155-80°C colour change due to change in birefringence and 27°C crystalline structure.

6.3.4.1 Dielectric Anisotropy

Measurements performed by C. Schott[13] enabled the behaviour of the dielectric anisotropy, $\Delta\varepsilon$, to be ascertained. The data in Figure 6.15 illustrates the temperature and frequency dependence of $\Delta\varepsilon$. In order to obtain measurements of $\Delta\varepsilon$ it was necessary to mix the pure 5PFP5 with a small quantity of the chiral dopant BDH1281[14]. A mixture of 3% BDH1281 in pure 5PFP5 was made up in order to obtain the necessary alignment. The chiral sample has a uniformily-lying-helix (ULH) structure so that the experiment gives the average of the two dielectric components. The perpendicular component is measured separately using an undoped sample in a uniform planar cell. The $\Delta\varepsilon$ of the chiral dopant was low, therefore the addition of a small quantity did not significantly change the $\Delta\varepsilon$ of the sample.

[13] C.Schott, *Ph.D. Thesis*, University of Southampton (2002)
[14] BDH Chemicals, Broom Road, Poole, Dorset, BH12 4NN, UK. http://www.merck.com

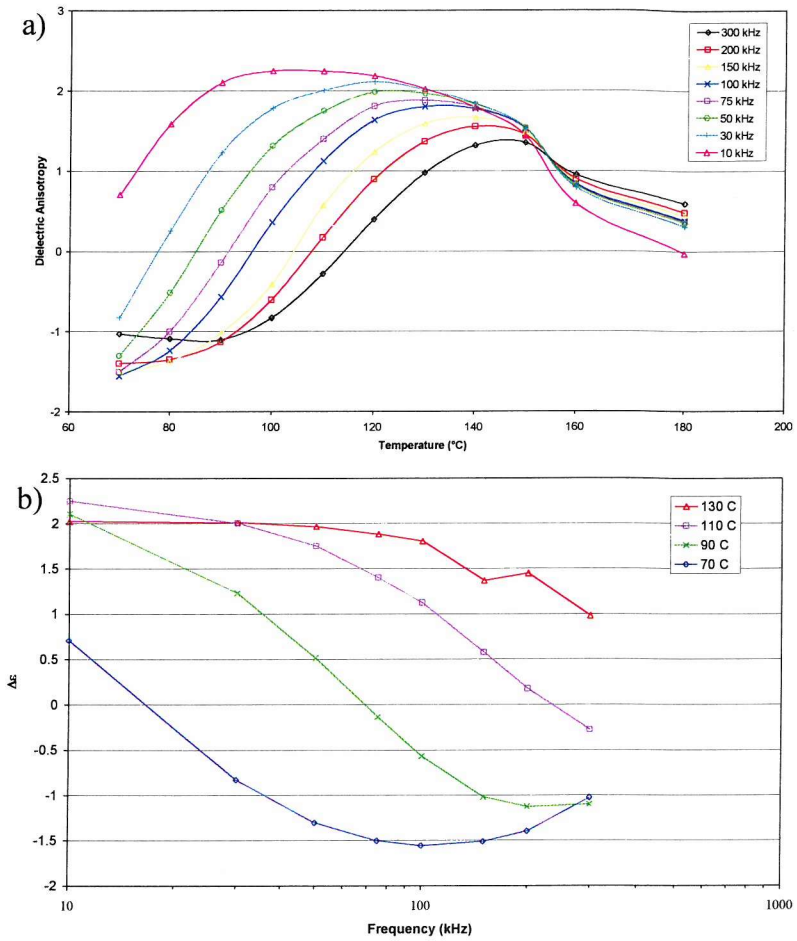

Figure 6.15 The a) temperature and b) frequency dependence of $\Delta\varepsilon$ in 5PFP5 (3% BDH1281). V_{rms}=250mV.

The dielectric anisotropy, $\Delta\varepsilon$, tends towards zero as the applied field frequency approaches ν_c, and eventually becomes negative at frequencies above ν_c, resulting in an increase in the threshold field. The data in Figure 6.15 was limited to a maximum frequency of 300kHz by the Wayne-Kerr bridge.

6.3.4.2 Threshold Voltage

It is apparent from the data in Figure 6.15 that when the frequency of the applied field is low the dielectric anisotropy is positive, the molecules therefore couple with the applied field such that the director (i.e. optic axis) is parallel to the field direction. The twist is destroyed and no waveguiding takes place, resulting in a dark state when a twisted nematic cell is placed between crossed polarisers.

Threshold voltage measurements were carried out with the TN cell oriented between crossed polarisers such that, with no field applied, the transmission is maximised. The transmitted light intensity was measured by the PDA as the magnitude of the applied field was steadily increased. The results, for applied fields of different frequencies at a number of temperatures are shown below. The frequency of the applied field is kept in the range below the crossover frequency.

The data in Figure 6.16 shows the variation of the threshold field with temperature. The frequency of the applied field is kept constant. In Figure 6.16a) the frequency is 100Hz. The frequency is 10kHz in Figure 6.16b). Little variation is seen in the threshold when the applied field frequency is 100Hz. At high temperatures the threshold field decreases, primarily due to a reduction in the elastic constants (i.e. viscosity), and an increase of $\Delta\varepsilon$, refer to Equation 2.49. No data is presented for temperatures below 60°C due to the propensity of the material to crystallise.

Greater variation with temperature is seen in the data of Figure 6.17b). A definite trend is observed with a decrease in temperature resulting in an increase in the threshold field. The variation is much more marked at low temperatures. A significant increase in the threshold field is seen between 80°C and 60°C. This will be discussed with reference to the transmission versus frequency data presented in Figure 6.18 and the dielectric data presented in Figure 6.15. Near the lower end of the nematic phase range, i.e. 60°C, 10kHz is close to the crossover frequency, ν_c, of 35kHz. The significant reduction in $\Delta\varepsilon$ results in the increase of the threshold field.

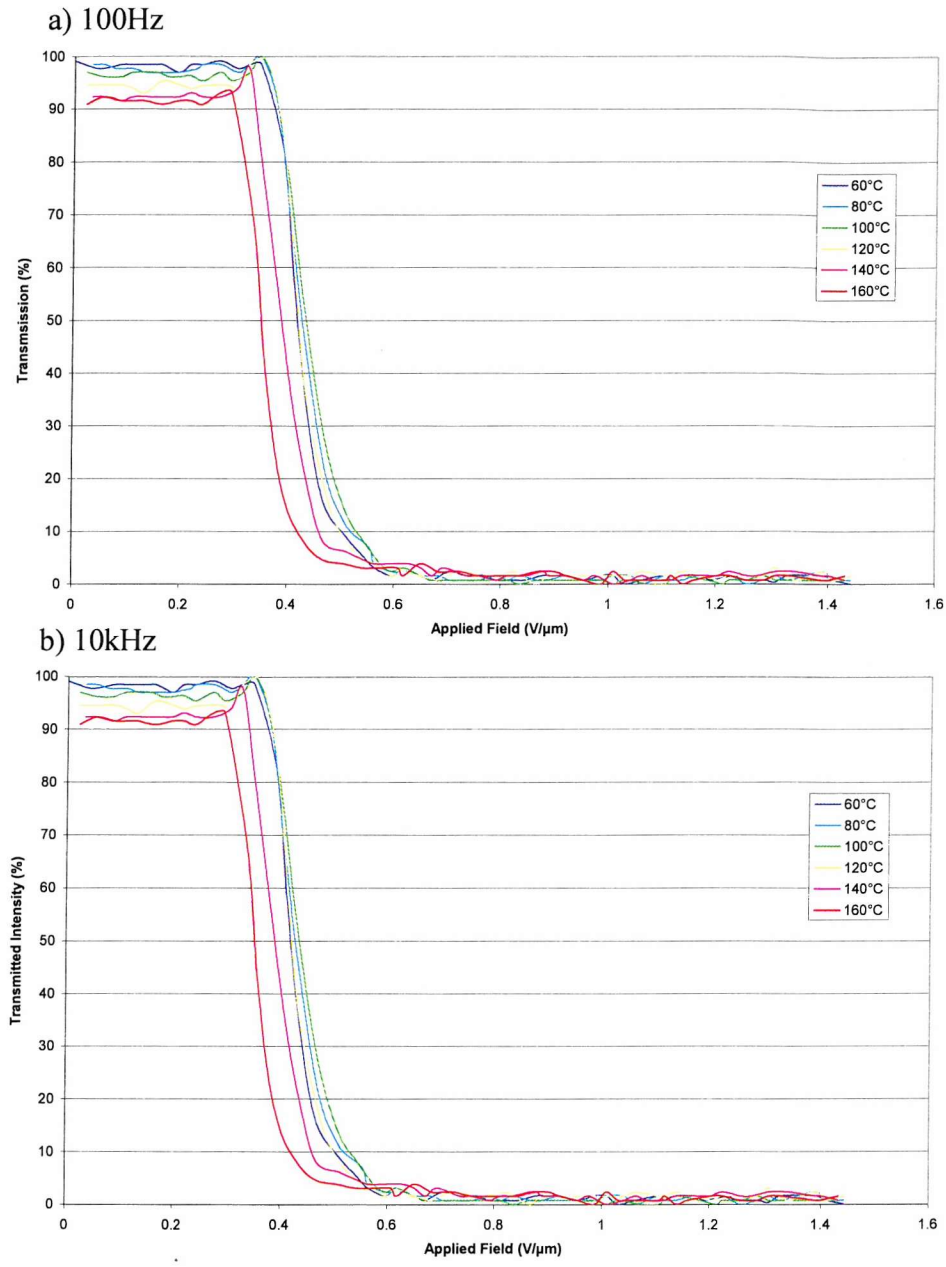

Figure 6.16 The temperature dependence of the threshold field in pure 5PFP5.

This increase of the threshold field as the crossover frequency is approached is illustrated in Figure 6.17a) and b) in which the threshold field is measured at a number of different frequencies at constant temperature. At 100°C the crossover frequency is 395kHz; no variation of the threshold field is seen at frequencies well below the crossover frequency since $\Delta\varepsilon$ is almost constant away from the crossover region. However, at 60°C, where the

ν_c is much lower (35kHz), there is much greater variation. The frequencies at which the threshold field is measured are much closer to ν_c hence the value of $\Delta\varepsilon$ varies more.

a) 100°C

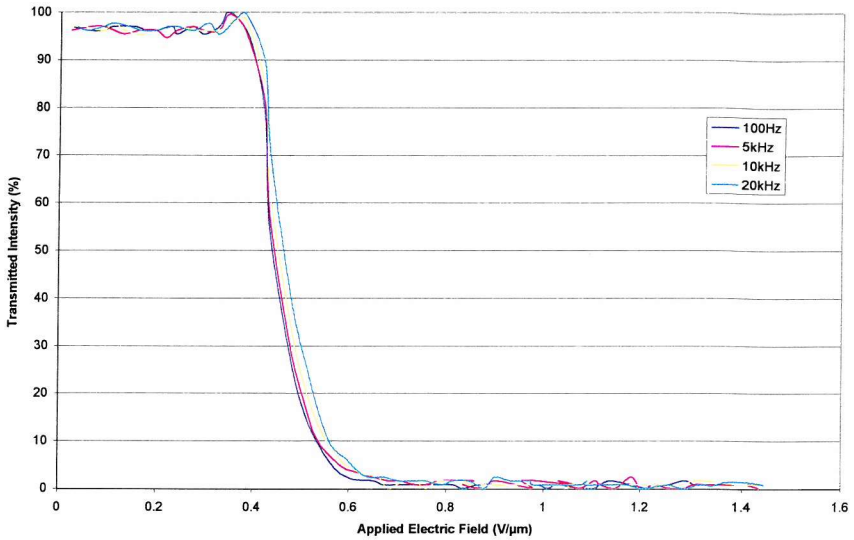

b) 60°C

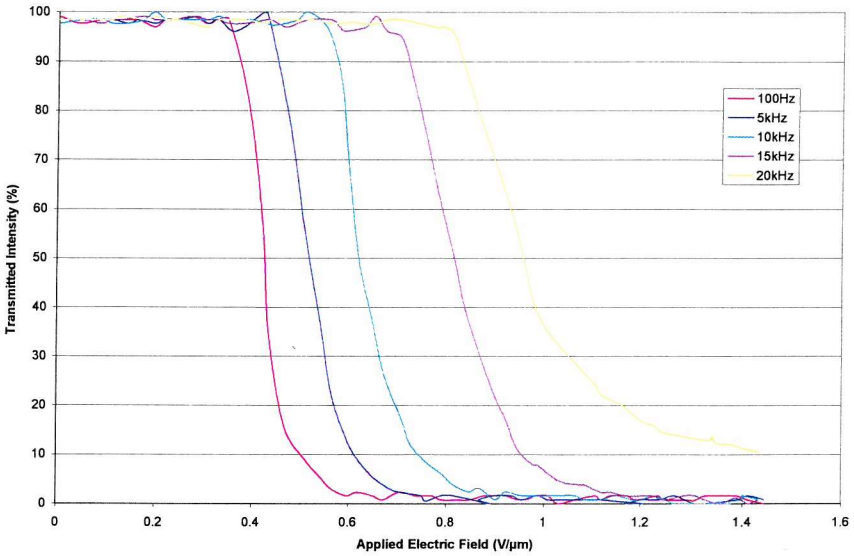

Figure 6.17 The frequency dependence of the threshold fields in pure 5PFP5.

6.3.4.3 Transmission vs Frequency

Measurements of transmission versus frequency were carried out with the TN cell oriented between crossed polarisers such that, with no field applied, the transmission is maximised. The magnitude of the applied field was fixed at the maximum ±2V/μm. It had been

previously verified, Figure 6.16 and Figure 6.17, that this field strength was sufficient to induce a switch. For applied fields of low frequencies the dielectric anisotropy is positive, the molecules therefore couple with the applied field such that the director (i.e. optic axis) is parallel to the field direction. The twist is destroyed and no waveguiding takes place, resulting in a dark state when a twisted nematic cell is placed between crossed polarisers.

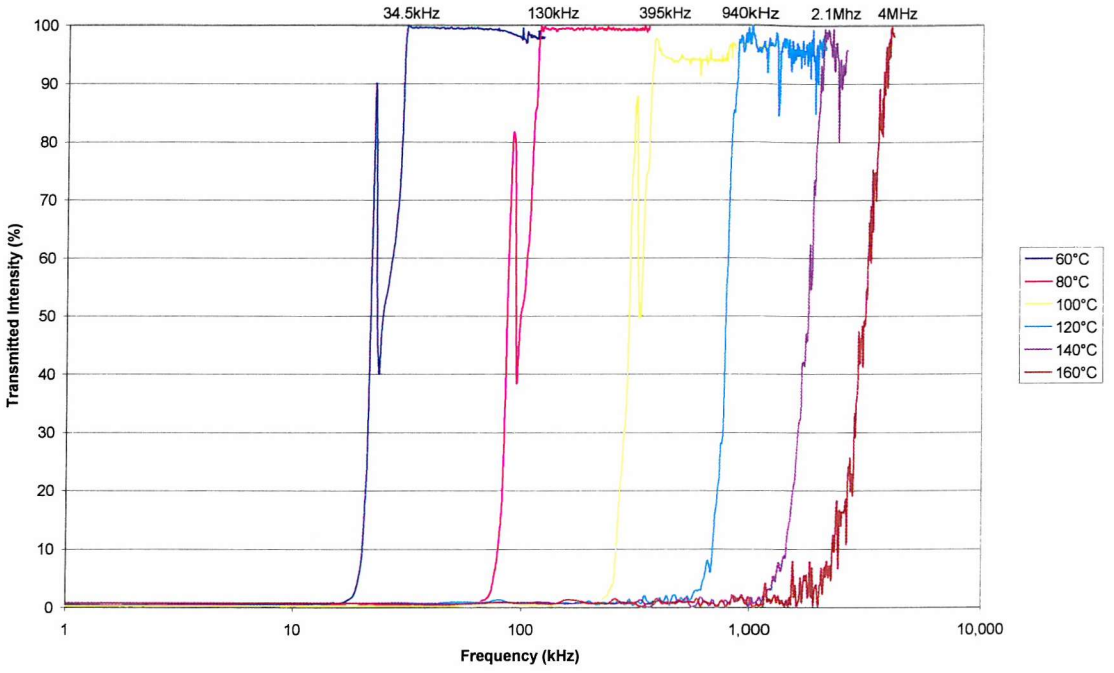

Figure 6.18 The frequency dependence of the transmitted light intensity in pure 5PFP5, applied field ±2V/μm.

Coupling with the applied field at low frequencies due to the positive $\Delta\varepsilon$ destroys the twisted structure resulting in practically zero transmission. The appearance of EHD in the region of ν_c results in erratic transmission.

The temperature dependence of the dispersion frequency is shown in Figure 6.19. When plotted on a logarithmic scale the values of ν_c lie on a straight line, i.e. ν_c varies exponentially as a function of temperature.

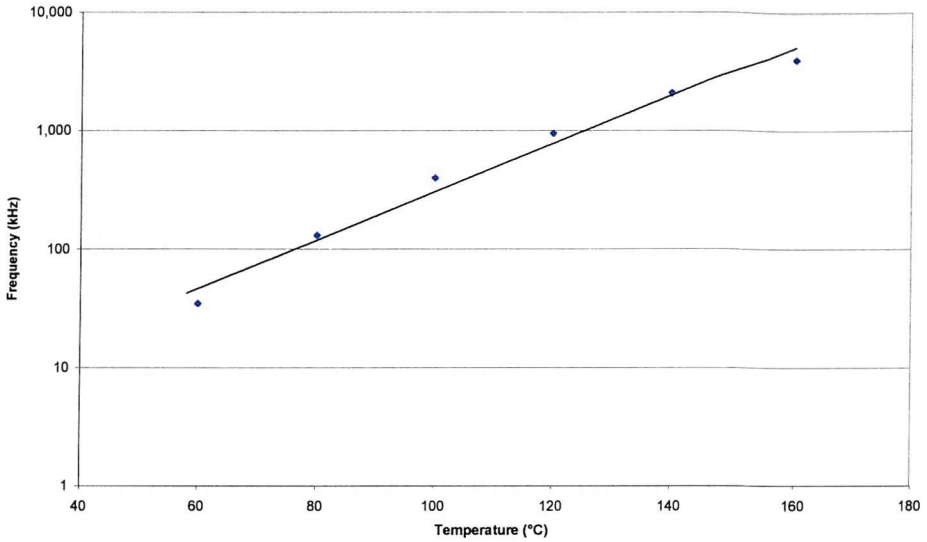

Figure 6.19 The temperature dependence of the dispersion frequency in 5PFP5 (±2V/μm, 5μm cell)

6.3.4.4 Response Time

Measurements of the response time of 5PFP5 as a function of frequency and temperature are shown in Figure 6.20. Fast response times are obtained at high temperatures. There is very weak frequency dependence at frequencies well below ν_c at all temperatures. As ν_c is approached the fall times rapidly increase as a consequence of the reduction of $\Delta\varepsilon$.

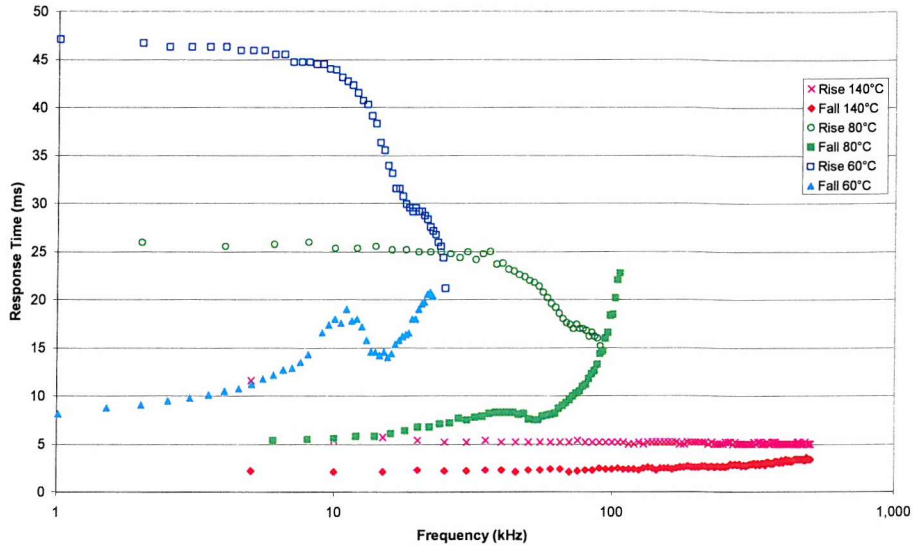

Figure 6.20 Response time measurements of 5PFP5 showing the dependence on the frequency of the applied field and sample temperature, (switching between zero field and xHz, ±2V/μm)

The reduction observed in the rise times as ν_c is approached, particularly noticeable at lower temperatures, is a result of the reduced contrast between the switched states – again a consequence of the reduced $\Delta\varepsilon$. The occurrence of 'optical bounce' distorts the measurement of the 10-90% rise time. This is particularly prevalent at lower temperatures due to the higher viscosity of the material but can be removed by the addition of a chiral dopant. This is discussed in Section 6.3.8.

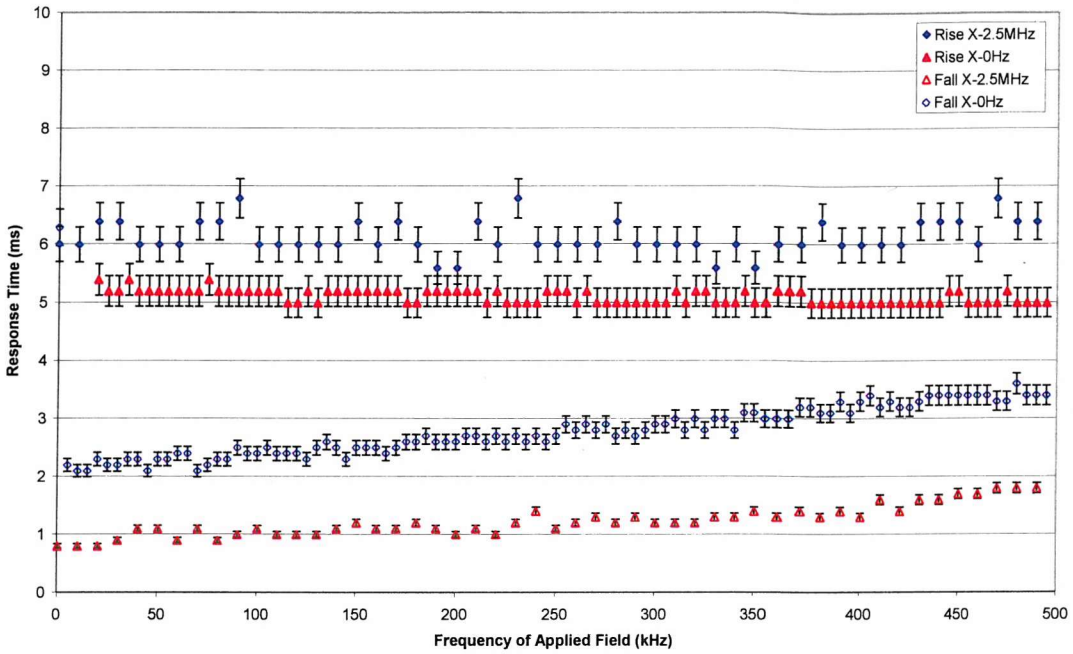

Figure 6.21 Comparison of response times of 5PFP5 when subject to standard and dual frequency driving schemes (±2Vμm, 140°C).

The response time data shown in Figure 6.21 is inconclusive. The perceived advantage of using the dual frequency addressing system is not achieved as the rise time actually increases slightly.

6.3.5 5% and 10% 5PFP5 in MDA

On cooling from the isotropic phase both mixtures undergo a solitary phase transition to the nematic phase. The addition of a small amount of 5PFP5 raises the temperature at which the N-I transition occurs. No crystallisation was observed on cooling to –50°C.

5% 5PFP5	Nematic 60°C Isotropic
10% 5PFP5	Nematic 64°C Isotropic

The low concentration of 5PFP5 is not sufficient for the mixtures to show any apparent switching when addressed by conventional or dual-frequency driving schemes.

6.3.6 18.5% 5PFP5 in MDA

This mixture, 18.5% 5PFP5 in MDA (wt/wt) undergoes a solitary phase transition on cooling from the isotropic phase. The increased concentration of 5PFP5 raises the N-I transition temperature.

Nematic 72°C Isotropic

Electro-optical studies revealed that the concentration of 5PFP5 was sufficient for switching to be observed.

6.3.6.1 Threshold Voltage

The twisted nematic cell is positioned for maximum transmission between crossed polarisers. No change in the transmitted intensity is observed until the electric field overcomes the surface orientation effects. As the director aligns with the field the twist is destroyed resulting in the drop in transmission. If a planar cell is used, the sample is aligned so that the optical axis is at 45° to the axis of each polariser. The transmitted intensity then undergoes a series of maxima and minima due to the sample birefringence changing as the applied field is increased.

a) 100Hz b) 10kHz

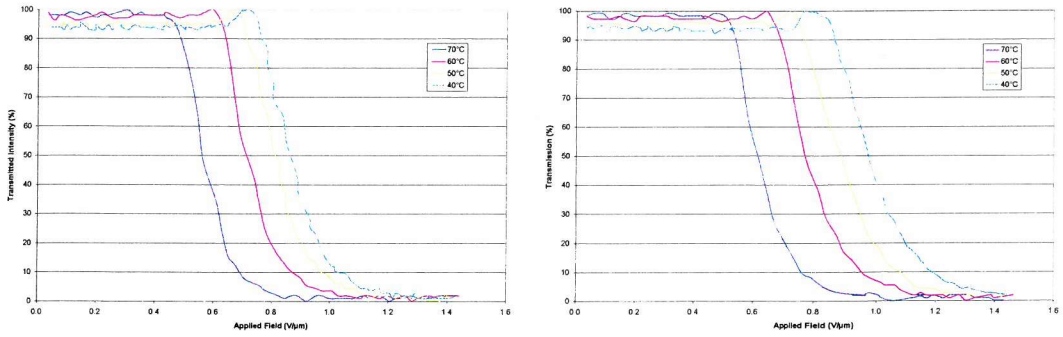

Figure 6.22 The temperature dependence of the threshold voltage in the mixture comprising 18.5% by weight of 5PFP5 in MDA, a) 100Hz and b) 10kHz.

The threshold voltage, V_{th}, increases as the temperature is reduced. This can be explained in terms of the dielectric anisotropy, which decreases as the temperature decreases, see Figure 6.15. When the frequency of the applied field is increased to 10kHz and the experiment repeated it is found that V_{th} increases. This increase is more significant at lower temperatures, see Figure 6.23 a) and b).

At lower temperatures, in this case 40°C, ν_c is much lower (~50kHz), thus, increasing the applied field frequency to 10kHz results in a larger reduction of $\Delta\varepsilon$. At 70°C, ν_c is ~1MHz and increasing the applied field frequency to 10kHz has a much smaller effect on $\Delta\varepsilon$.

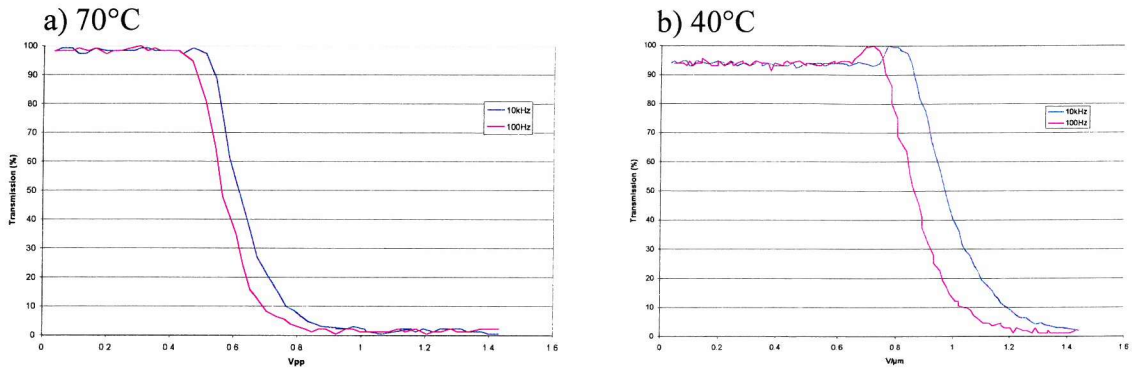

Figure 6.23 The frequency and temperature dependence of the threshold field, V_{TH}, 18.5% 5PFP5 in MDA.

6.3.6.2 Transmission vs Frequency

As previously discussed, the dual frequency material 5PFP5 possesses positive dielectric anisotropy, $\Delta\varepsilon$, at frequencies below a certain crossover frequency, ν_c, above which the dielectric anisotropy becomes negative. Figure 6.18 illustrates this behaviour. The data was obtained from the mixture in a twisted nematic (TN) cell oriented between cross polarisers such that, with no field applied, the transmitted intensity was maximised. A 20Vpp square wave alternating voltage was then applied across the cell and the frequency ramped from low to high frequencies.

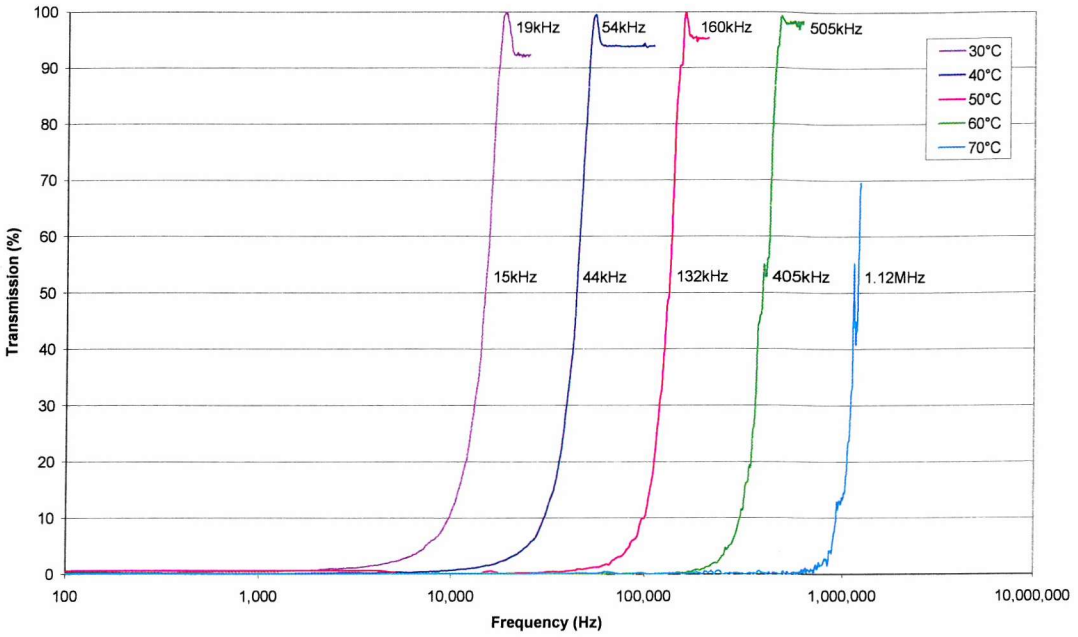

Figure 6.24 The frequency and temperature dependence of the transmitted intensity of the mixture 18.5% 5PFP5 in MDA

Clearly, the data in Figure 6.24 indicates that the value of ν_c is strongly temperature dependent, ν_c increases as the temperature increases. At 70°C the value of ν_c is two orders of magnitude larger than that at 30°C. In the frequency range near ν_c a scattering mode is observed[15], this is particularly prevalent at higher temperatures and results in the transmitted intensity fluctuating significantly rather than smoothly increasing towards a maximum.

[15] W.H.de Jeu, C.J.Gerritsma, P.van Zenten, W.J.A.Goosens, Phys. Lett., **39A**, 355, (1972)

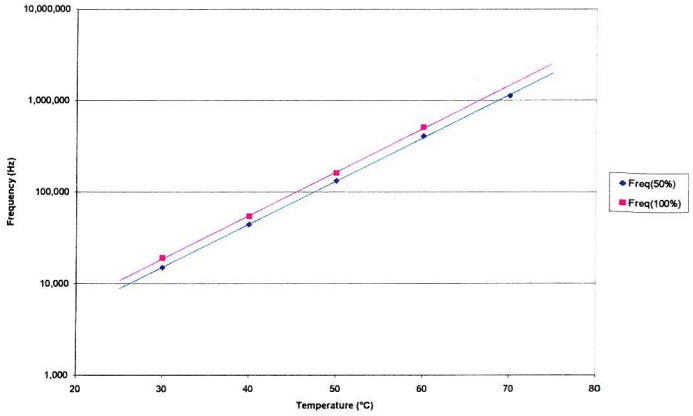

Figure 6.25 The temperature dependence of the dispersion frequency ν_c of the mixture 18.5%5PFP5 in MDA.

Figure 6.25 illustrates the temperature dependence of ν_c, a) uses values of the frequency for which transmission is a maximum ($I_{100\%}$) whilst b) takes the value of the frequency at $I_{50\%}$. The intensity fluctuations due to the formation of the scattering instabilities offset the transmission curve resulting in larger values of ν_c (if taken at $I_{100\%}$) than would otherwise be expected. The log-linear plot illustrates the exponential nature of the temperature dependence. This relationship facilitates the forecast of ν_c for any given temperature.

6.3.6.3 Response Time

Figure 6.26 illustrates the frequency dependent nature of the response time of 18.5% 5PFP5 in MDA to the application of an applied electric field. A TN cell containing the mixture was situated between crossed polarisers and orientated for maximum transmission of light. The response time was measured as the time taken for the transmission to change from 90% to 10% of the maximum intensity, i.e. the rise time or T_{on}. The response times dramatically increase as the frequency of the applied field increases towards the dispersion frequency due to the reduction of $\Delta\varepsilon$. If the frequency of the applied field is fixed then the response time decreases with increasing temperature. At higher temperatures the frequency of the applied field is further away from the dispersion frequency, i.e. $\Delta\varepsilon$ is larger and, secondly, the viscosity is reduced.

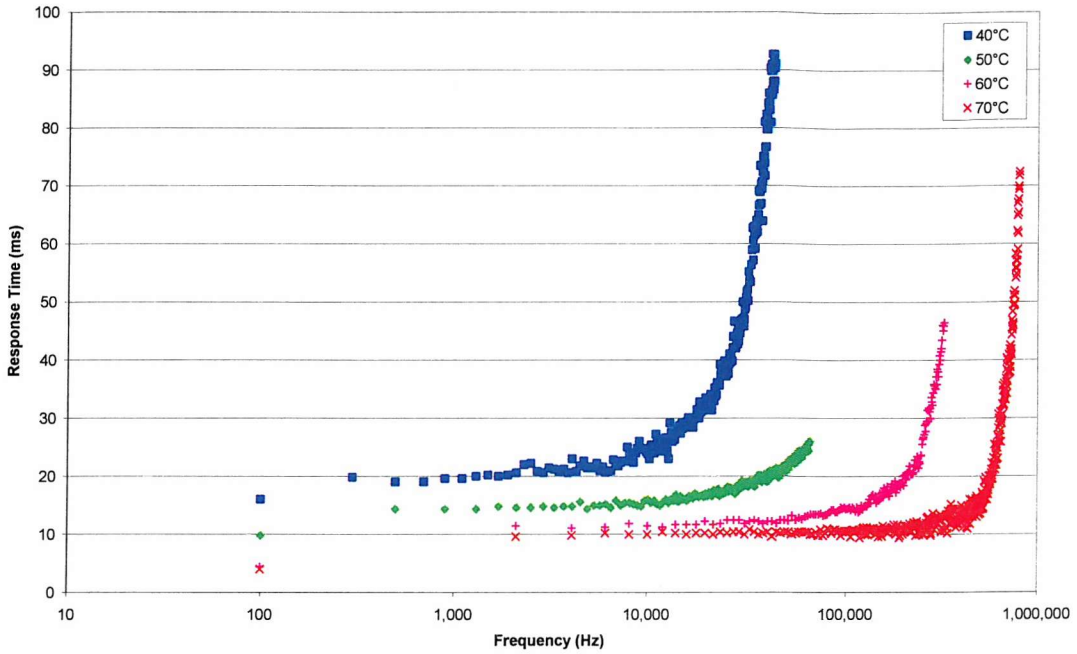

Figure 6.26 The frequency dependence of the response time of 18.5% 5PFP5 in MDA to the application of an electric field of frequency xHz (±2V/μm)

In the low frequency regime (frequencies of less than 1kHz) EHD instabilities result in increased response times. This effect is more pronounced at lower temperatures and is illustrated by the data in Figure 6.27.

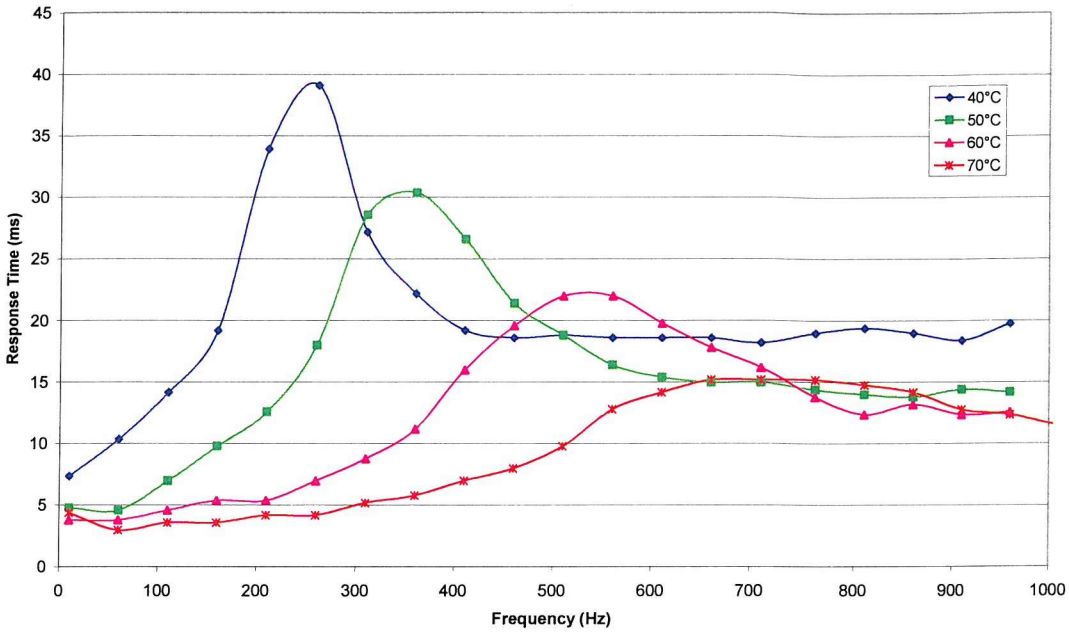

Figure 6.27 The low frequency dependence of the response time of 18.5% 5PFP5 in MDA to the application of an electric field of frequency xHz (±2V/μm)

The data presented in Figure 6.28, measured whilst applying a conventional TN device driving scheme, illustrates the difference between response times measured as the time taken for the transmitted intensity to change from 10-90% and 0-100%. The 0-100% measurement is the time taken from the field application to the maximum intensity

a) T_{on}: Zero Field -1kHz b) T_{off}: 1kHz – Zero Field

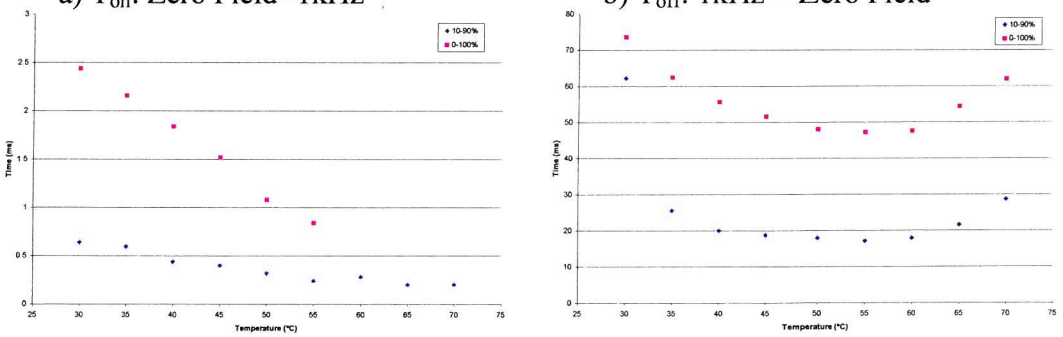

Figure 6.28 Response Times of 18.5% 5PFP5 in MDA as a function of temperature (± 7V/μm)

The temperature dependence is strong, particularly at low temperatures. T_{off} is much slower than T_{on}, as shown in Figure 6.29, due to the reliance on the material properties and surface alignment forces to restore the 'field off' state. In comparison to the T_{on} 0-100%

response times, the 10-90% response times are almost temperature independent. The strong temperature dependence of the 0-100% time is due to the measurement encompassing the 'delay time' between the field application and the 'optical bounce' reorientation of the director, this delay becomes shorter as the temperature increases and the viscosity reduces.

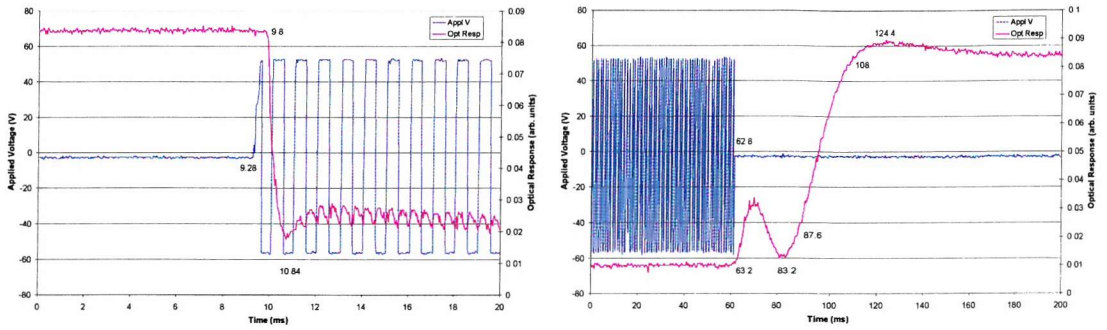

Figure 6.29 The optical response of 18.5% 5PFP5 in MDA.

The variation of optical response times against the frequency of the applied field for a dual frequency driving scheme where the high frequency is held constant at 1MHz whilst the low frequency is varied is shown for the 18% mixture in Figure 6.30 and Figure 6.31. In all cases the optical response time measured was the 10-90% response time of the mixture

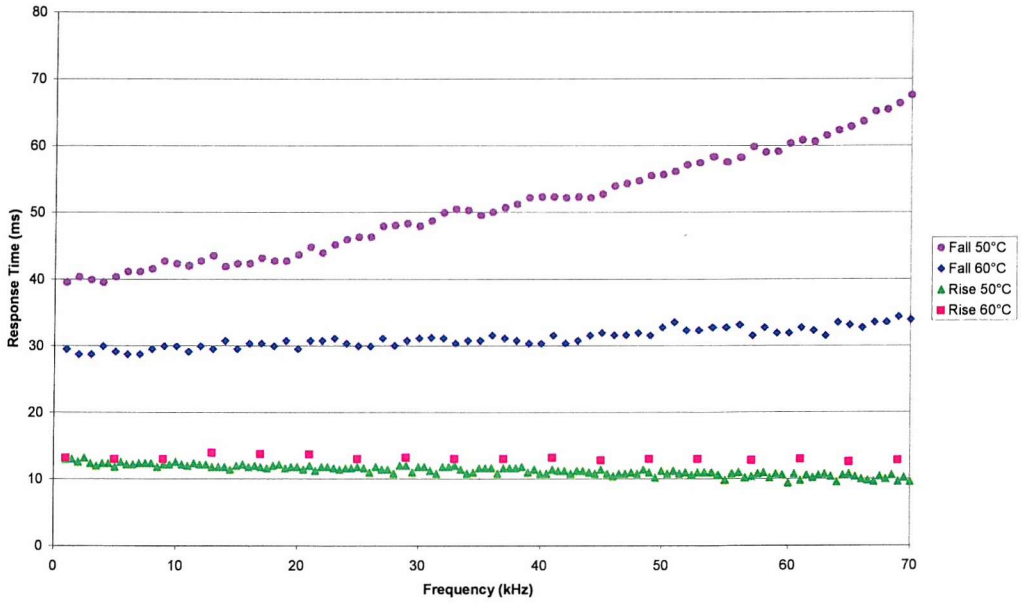

Figure 6.30 The 'dual frequency' response times of 18% 5PFP5 in MDA x-1MHz

The frequency dependence of the fall time is unchanged, with increasing frequency resulting in a longer response time due to the associated reduction in $\Delta\varepsilon$. The fall time also exhibits the same temperature dependence as observed when the mixture is subject to a conventional driving scheme. The main difference to a conventional driving scheme is that the response times of each mechanism have reversed. As expected, dual frequency addressing reduces the $I_{10\%} - I_{90\%}$ response time. However, the $I_{90\%} - I_{10\%}$ response time is markedly increased.

Due to the increase in the fall time response time a study of the dependence on the high frequency was undertaken.

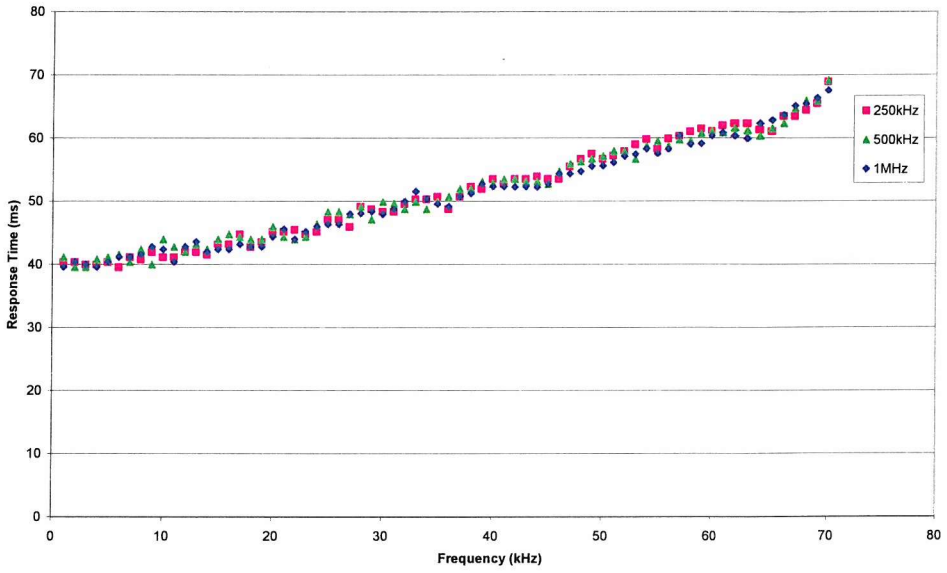

Figure 6.31 The frequency dependence of the fall time of the mixture comprising 18% 5PFP5 in MDA. The frequency of the high frequency applied field remains fixed as the low frequency (displayed on the x-axis) is varied. The optical switching occurs as the frequency of the applied signal is switched from high to low. (±2V/μm, 50°C)

The data in Figure 6.31 shows that the fall time was independent of the high frequency – As the frequency of the low frequency field is increased, $\Delta\varepsilon$ decreases and the weaker coupling between the director and the applied field results in a smaller torque and slower realignment.

6.3.7 50% 5PFP5 in MDA

On cooling from the isotropic phase a transition to the nematic phase is observed at 110°C. The nematic phase exists down to 15°C, at which crystallisation occurs.

Crystal 15°C Nematic 110°C Isotropic

6.3.7.1 Threshold Voltage

Threshold voltage measurements were undertaken using the previously described methodology. The temperature dependence, shown in Figure 6.32, is similar to that exhibited by the 18.5% mixture. Due to the higher concentration of 5PFP5, and hence a larger dielectric anisotropy, V_{th} is reduced in the 50% mixture.

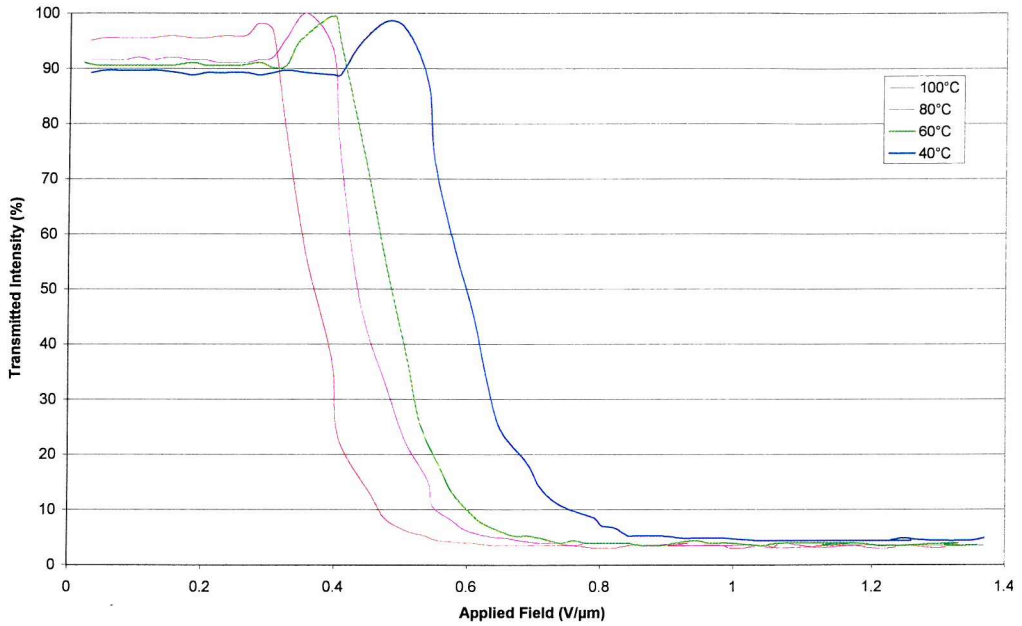

Figure 6.32 The temperature dependence of the threshold voltage of 50% 5PFP5 in MDA (10kHz)

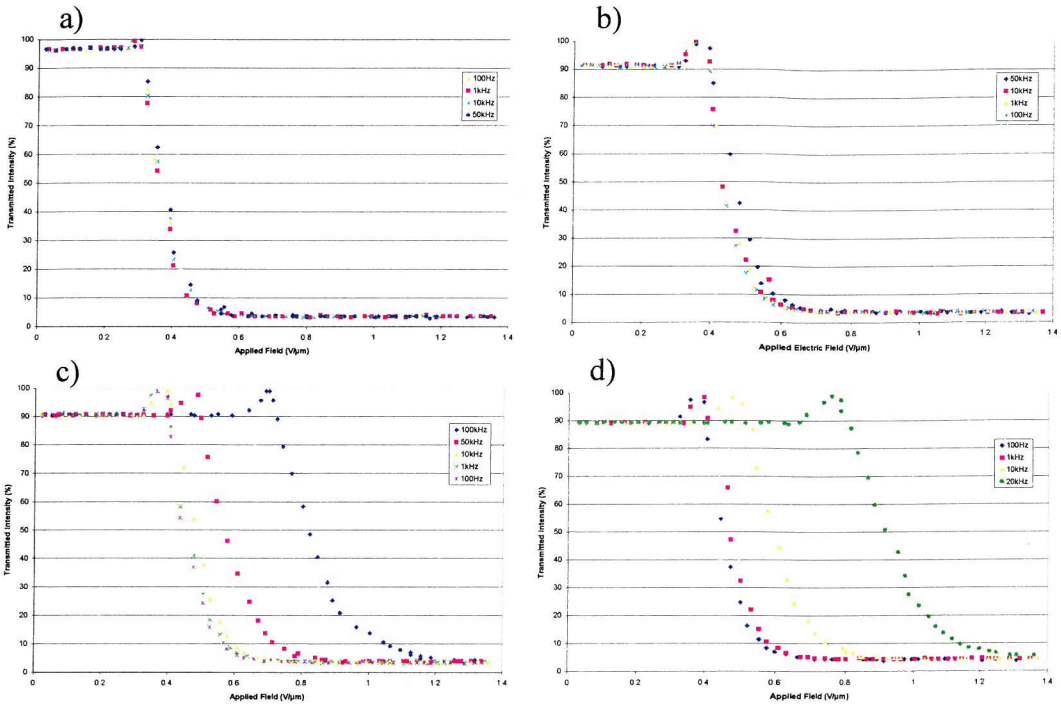

Figure 6.33 The temperature and frequency dependence of the threshold field, V_{th} in the mixture of 50% 5PFP5 in MDA, a) 100°C, b) 80°C, c) 60°C and d) 40°C.

6.3.7.2 Transmission vs Frequency

Measurements of transmitted intensity versus frequency of the applied field yielded similar dependencies to those exhibited by both the pure 5PFP5 and the mixture comprising 18% 5PFP5 in MDA (wt/wt), as shown in Figure 6.34 and Figure 6.35.

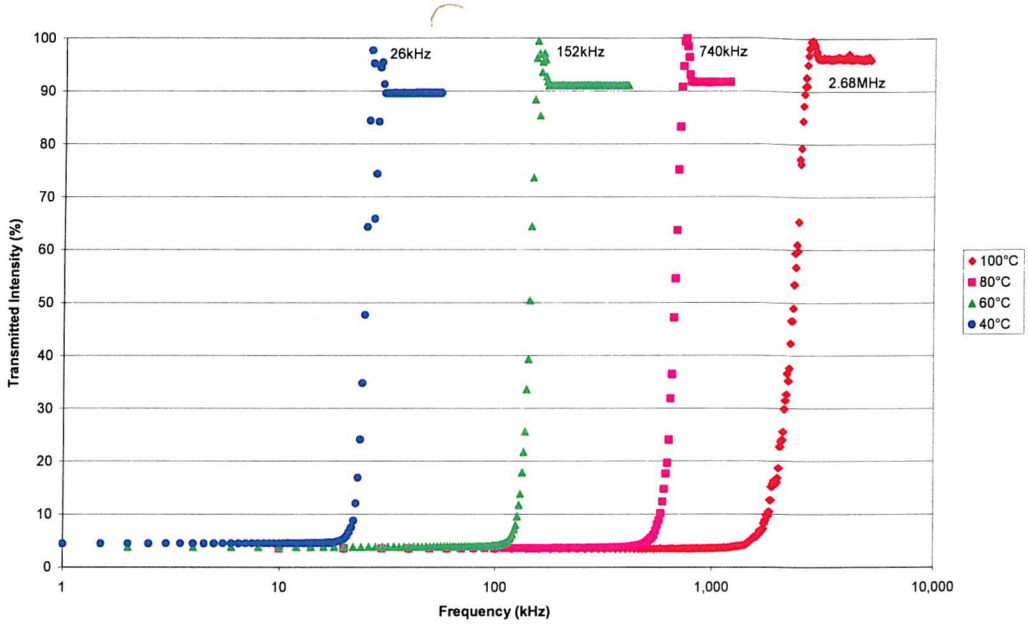

Figure 6.34 The frequency dependence of the transmitted light intensity in the mixture comprising 50% 5PFP5 in MDA(wt/wt).

As observed with the 18% 5PFP5 in MDA mixture (wt/wt), the critical frequency follows an exponential trend and thus a log-linear plot (Figure 6.35) is again appropriate.

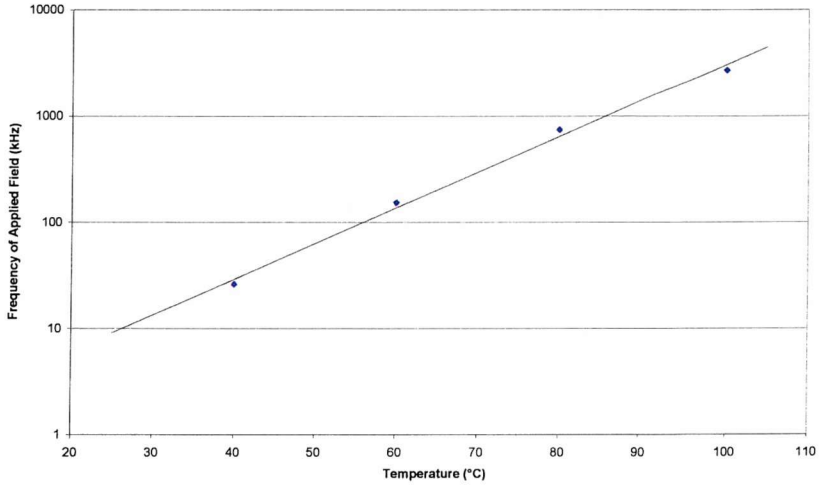

Figure 6.35 Critical frequency measurements from Figure 6.34 re-plotted on a semi-log scale.

6.3.7.3 Response Time

The response times were measured by applying a 2V/μm square wave driving field across the sample and are shown in Figure 6.36. The response times demonstrate similar temperature and frequency dependencies to the 18% 5PFP5 in MDA mixture.

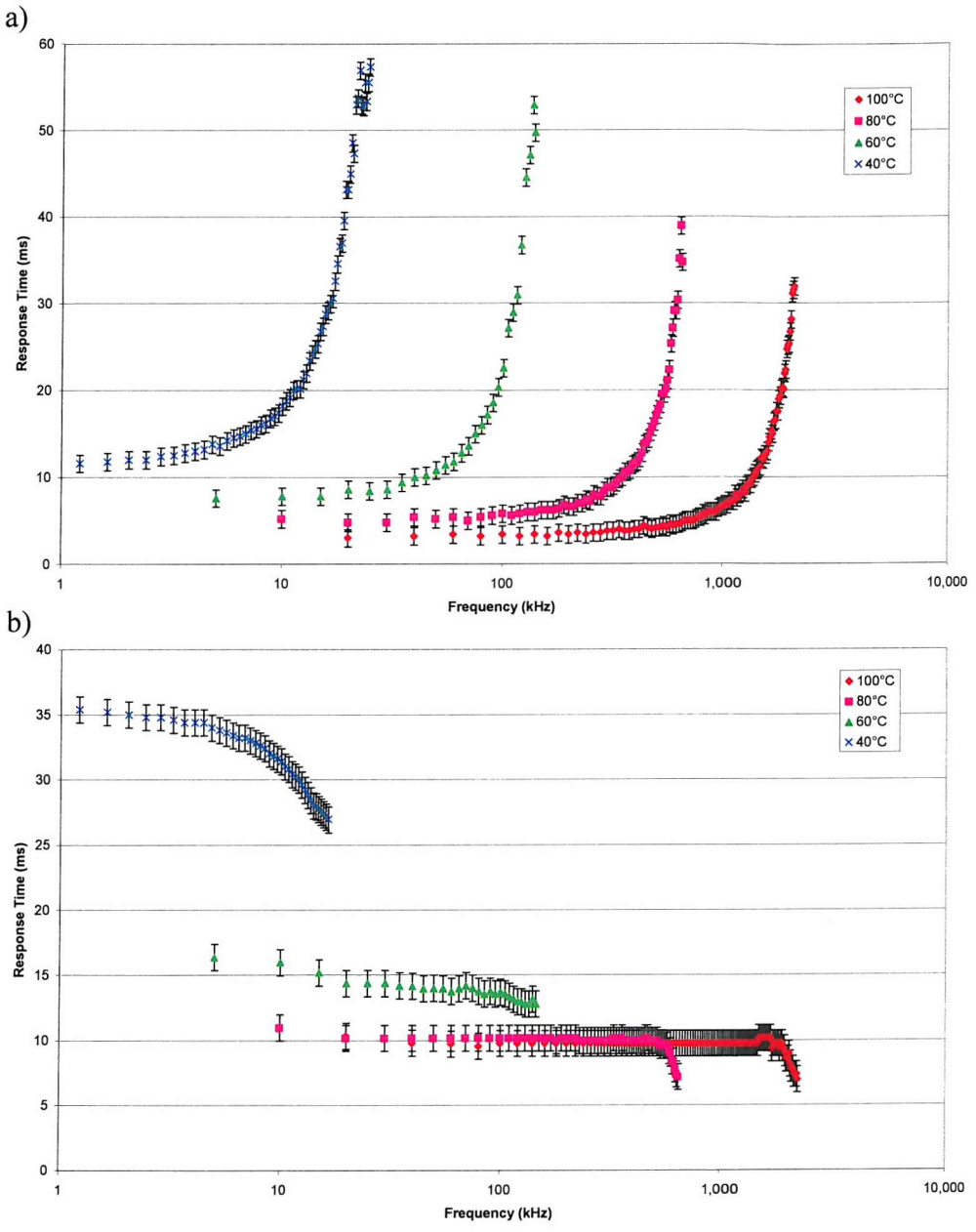

Figure 6.36 Response time measurements of the 50% wt/wt 5PFP5 in MDA mixture, a) Rise time: 0-xHz Response Time, b) Fall time: x-0Hz Response Time (±2V/μm).

A comparison of the optical response times against the frequency of the applied field for conventional and dual frequency driving schemes where the high frequency is held constant at 4MHz whilst the low frequency is varied is shown for the 50% 5PFP5 in MDA mixture Figure 6.37. In all cases the optical response time measured was the 10-90% response time of the mixture.

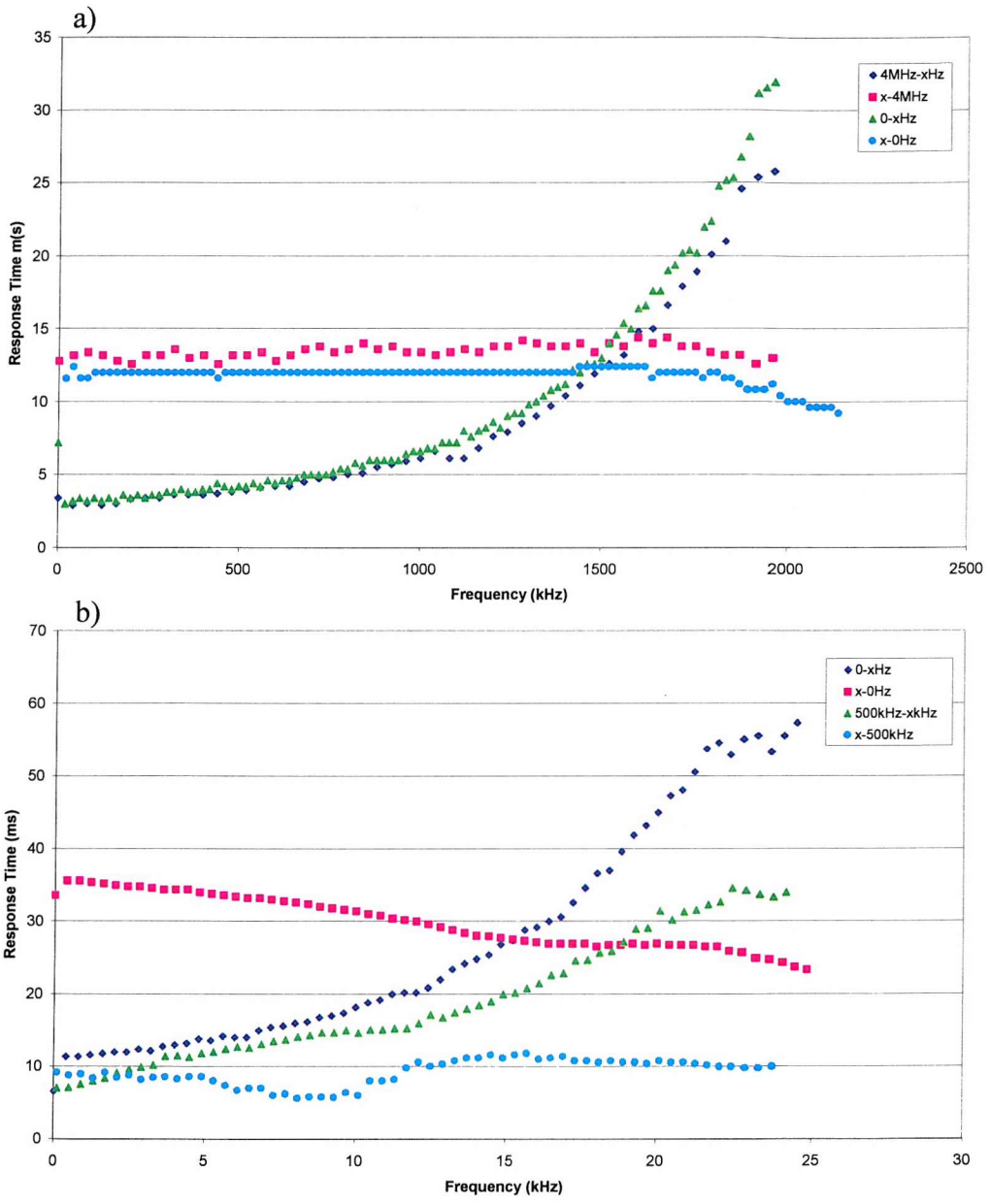

Figure 6.37 Comparison of dual frequency and conventional address schemes in 50% 5PFP5 in MDA (wt/wt), a) 100°C and b) 40°C, (±2V/μm). The error bars have been removed for clarity.

At 100°C the dual frequency addressing scheme does not provide any advantage over the conventional (field on – field off) driving scheme. At 40°C both the rise and fall times are improved by the dual frequency driving scheme. For a given frequency above the critical frequency the dielectric anisotropy is more negative at lower temperatures, thus, the coupling to the field will be stronger at lower temperatures, resulting in a faster reorientation back to the homogenous alignment.

6.3.8 CB15 - Chiral Dopant

This chiral dopant induces a right handed (clockwise) twist. CB15 undergoes a solitary phase transition at 4°C between the crystalline and isotropic phases.

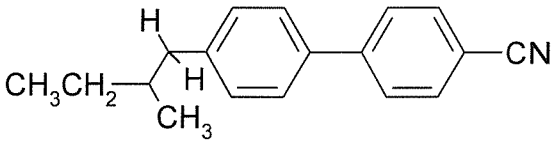

Figure 6.38 The molecular strucure of the chiral dopant CB15.

It was hoped that the addition of a small amount of this material to the mixtures of 5PFP5 and MDA would further reduce the response times, particularly the rise time, by the removal of the 'optical bounce'. The optical bounce or backflow is a result of shear stresses caused by the inhomogenous director rotation in the bulk of the sample due to the fixed director orientation at the surfaces of the sample cell and the torque of the externally applied field.

A small amount, 3% wt/wt, of CB15 was added to the 50% 5PFP5 in MDA mixture. The effect of the CB15 chiral dopant on the rise time is shown in Figure 6.39. The driving signal was a 2V/μm square wave and the high frequency was kept constant at 4MHz. The response time measurements clearly show that the addition of CB15 and the consequent removal of the bounce from the optical response results in a reduction of the rise time.

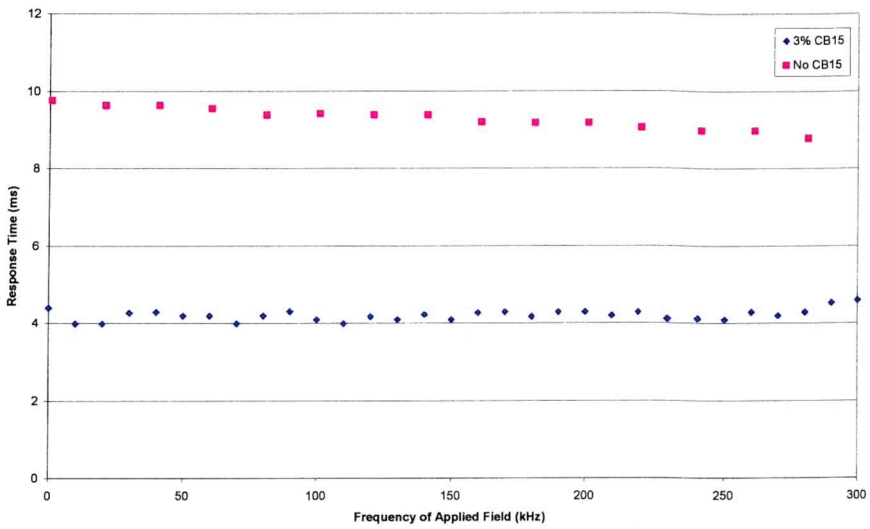

Figure 6.39 The effect of the chiral dopant CB15 on the response time of the 50% 5PFP5 in MDA (wt/wt) mixture.

6.4 Summary

The motivation for the work presented in this chapter was the supposed benefit that could be gained from employing dual frequency addressing in the operation of TN LCD's, namely, faster response times. The Merck mixture TX2A was used to illustrate this point.

A new dual frequency nematic liquid crystal, 5PFP5, was synthesised in Southampton and a series of mixtures of this and a low viscosity host, MDA, have been examined to determine their physical and electrooptic properties. All mixtures exhibit a single nematic mesophase, which crystallised when a high concentration of 5PFP5 was present. In concentrations of 10% and less in MDA, the addition of 5PFP5 did not result in any observable electro-optic switching.

All the physical properties characterised during the course of these studies exhibited a pronounced dependence on the frequency of the applied field. The dispersion frequency showed very strong temperature dependence.

Response time measurements were inconclusive with respect to the advantages of dual frequency addressing although response times of ~5ms were achieved for an applied field of ±2V/μm. Dual frequency addressing was shown to be advantageous at low temperatures, with response times decreasing by a factor of two.

Fast response times allow for larger, higher resolution TFT (thin-film transistor) displays but two frequency materials also have advantages for passive multiplexing by removing the crosstalk inherent in the addressing scheme that causes low contrast between switched states[16]. Passively multiplexed displays do not have separate connections to each pixel; instead the rows are addressed in sequence and only one at a time. The 'data' waveforms applied to the columns are then determined so that each pixel that should be selected experiences the same rms voltage V_s and each pixel that should be off experiences a lower voltage V_{ns}. The voltage selection ratio is defined by Alt and Pleschko[17]

$$\frac{V_s}{V_{ns}} = \sqrt{\frac{\left(\sqrt{N}+1\right)}{\left(\sqrt{N}-1\right)}}, \qquad (6\text{-}1)$$

where V_s and V_{ns} are the voltages of the selected and non-selected states respectively and N is the number of rows multiplexed. For a display consisting of 200 lines the ratio between the voltages of the selected and non-selected states is only 7%. By simultaneously applying both high and low frequency voltages[18] it is possible to achieve lower values of the V_s/V_{ns} ratio than for single frequency addressing and negating the need for a liquid crystal material with a steep transmission-voltage characteristic.

[16] M.G.Clark, *Displays*, **2**, 169 (1981)
[17] P.M.Alt and P.Pleschko, *IEEE Trans. Electron. Devices*, **21**, 146 (1974)
[18] M.Hosokawa, S.Kanbe, M.Nagata, H.Nakamura, *SID Int.Symp.Dig.*, **10**, 116 (1979)

Chapter Seven

CONCLUSIONS

7.1 INTRODUCTION

The work in this thesis has been, primarily, concerned with the search for fast response liquid crystal materials for optical devices. The materials studied have come from across the range of thermotropic liquid crystals and have comprised nematic, chiral nematic, ferroelectric and antiferroelectric systems. Both monomesogens and bimesogens have been studied during the course of this work and a full characterisation of the materials investigated has been presented.

The objective of this chapter is to discuss the progress made so far and outline the potential paths further studies might take.

7.2 SUPPLEMENTARY RESEARCH

This section presents some additional work that was also undertaken during the course of this thesis.

7.2.1 Static Rotator

This work is devoted to the idea of utilising both the physical and optical properties of liquid crystal materials in order to develop and produce a specific device that can be incorporated into the optical system behind a three-dimensional (stereoscopic) display. The motivation for this research was provided by Dr. G. Street of Surgical Vision Ltd. who was developing a stereoscopic display for medical applications.

The 'static rotator' is a device to combine two images, encoded by polarisation, from the output of an optical system, allowing the use of a single optical network to transmit the two optical signals therefore reducing the size of the endoscope and simplifying its construction.

7.2.1.1 Principle of Operation

Two laterally displaced optical images encoded with orthogonal polarisations for propagation through a relay network can be combined using the birefringent nature of calcite. The ordinary and extraordinary rays propagating through calcite will have different path lengths resulting in two different focal image planes as shown in Figure 7.1, (the path length difference is approximately 10%). For practical applications the path lengths should be identical so that both images are reproduced on the same focal plane.

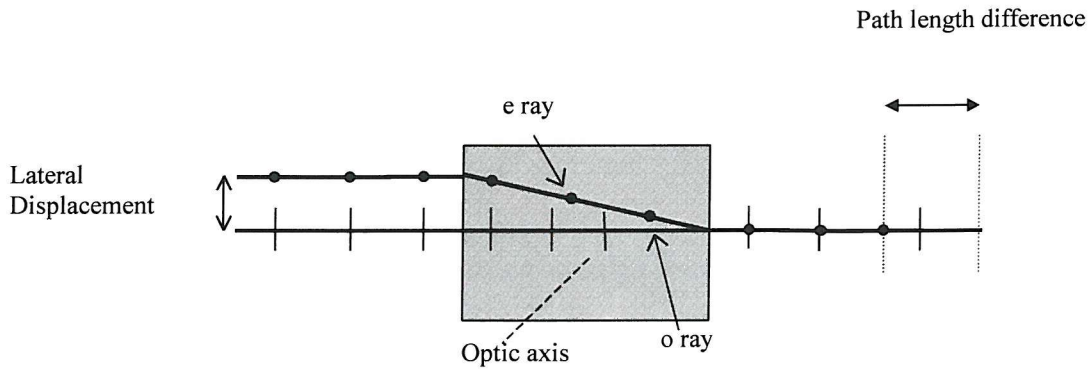

Figure 7.1 The propagation of polarised light through a birefringent crystal.

A device was therefore required to equalise the two path lengths. This could be achieved by positioning a half wave plate between two identical pieces of calcite with their optical axis mirrored about the original axis of the field of view. The half wave plate rotates the planes of polarisation by 90° so that the o-ray in the first calcite block becomes the e-ray in the second and the e-ray in the first becomes the o-ray in the second, as shown in Figure 7.2.

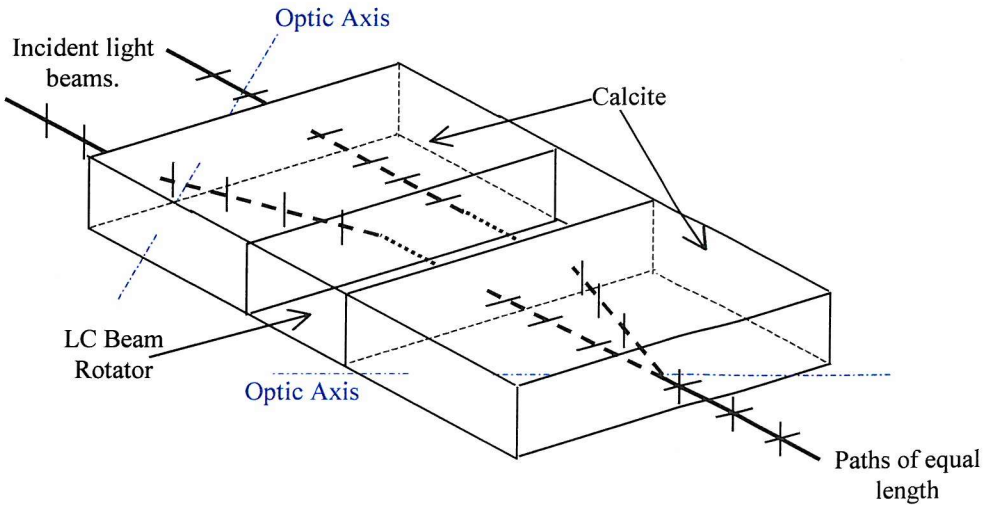

Figure 7.2 Schematic diagram of the in situ operation of the static rotator.

7.2.1.2 Requirements

The device also needed to be achromatic, as any chromatic problems would result in degradation of the final image. Once fabricated, the device would need to be fashioned to the desired shape. The physical dimensions must be small, as shown in Figure 7.3, since the device needed to fit inside an endoscope tube, and dead space needed to be kept to a minimum to maximise the light transmission of the system.

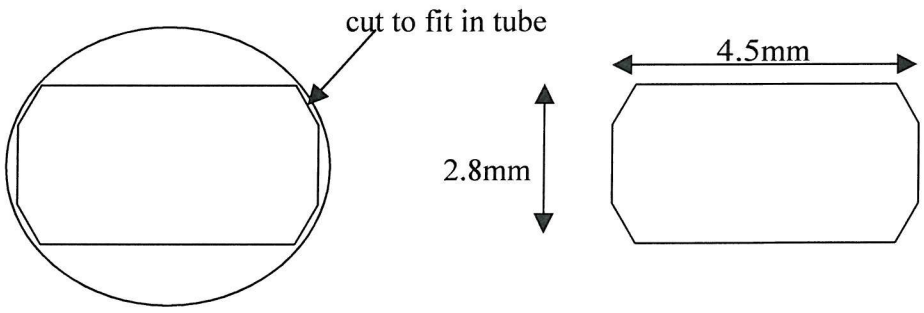

Figure 7.3 Physical dimensions of the static rotator device.

For medical applications the instrument will have to undergo an autoclaving sterilisation process and therefore have to withstand temperatures of approximately 150°C. It is of

paramount importance for the performance of the device that, after being raised to these temperatures, the liquid crystal retains its alignment.

The device was realised by utilising the twisted nematic structure. The material that was chosen to realise the device was C4 Acrylate[1]. C4 Acrylate possesses practical phase ranges; it is glassy below 42°C, allowing the device to be easily shaped at room temperature using a diamond tipped saw, and on cooling from the isotropic phase it enters the nematic phase at 112°C easily adopting any surface induced alignment.

Glass 42°C Nematic 112°C Isotropic

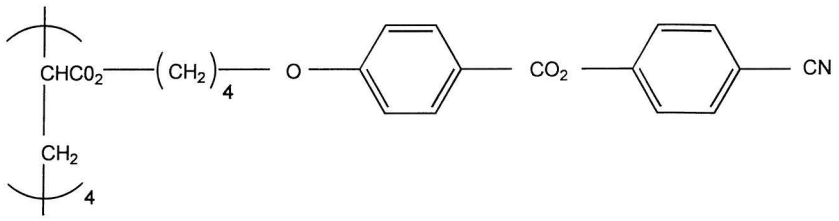

Figure 7.4 Molecular structure of C4 Acrylate

7.2.1.3 Device Evaluation

To assess the device performance a TN cell filled with C4 Acrylate was positioned on the rotating stage of the polarising microscope. The cell was rotated between both crossed and parallel polarisers. The transmission profile is shown in Figure 7.5.

The data in Figure 7.5 and Figure 7.6 shows that maximum transmission occurs at 90° intervals, indicating the device is rotating polarisations that are both parallel and perpendicular to the director on the initial surface as desired. The incident light is only experiencing one refractive index, either n_o or n_e, which remains constant as the light is wave guided. This white state indicates that the device is also achromatic. The intensity of the maximum transmission varies slightly from cell to cell due to a number of reasons, such as the number of chopped optical fibre spacers and small defects in the alignment, but is always around the expected 90% (approximately 10% is reflected from the glass surfaces).

[1] Polymer 85670/32, 3M Corporation, http://www.3m.com

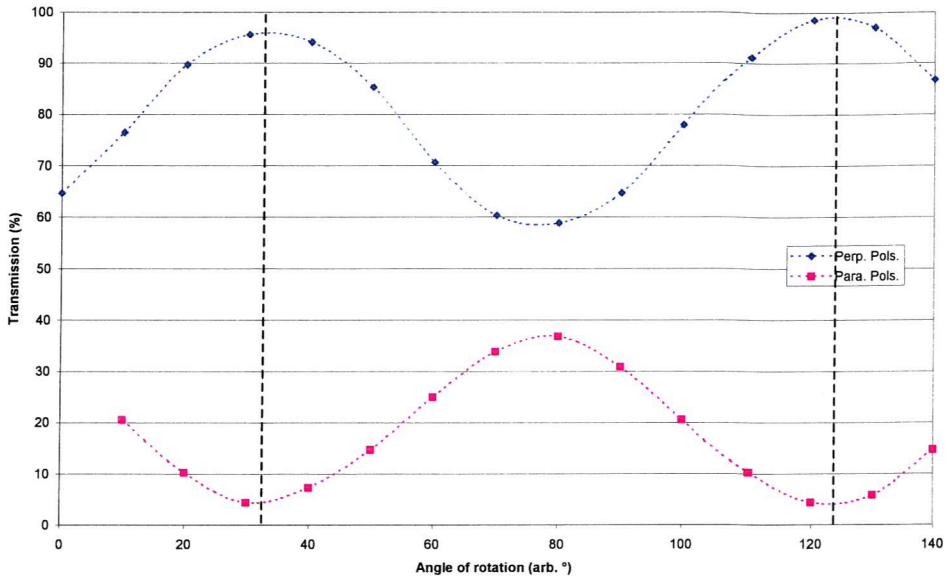

Figure 7.5 Light transmission through a TN cell containing C4 Acrylate positioned between parallel and crossed polarisers. Maximum transmission occurs at 90° intervals, corresponding to the molecular director on the initial surface being parallel, or perpendicular, to the polarisation plane of the incident linearly polarised light.

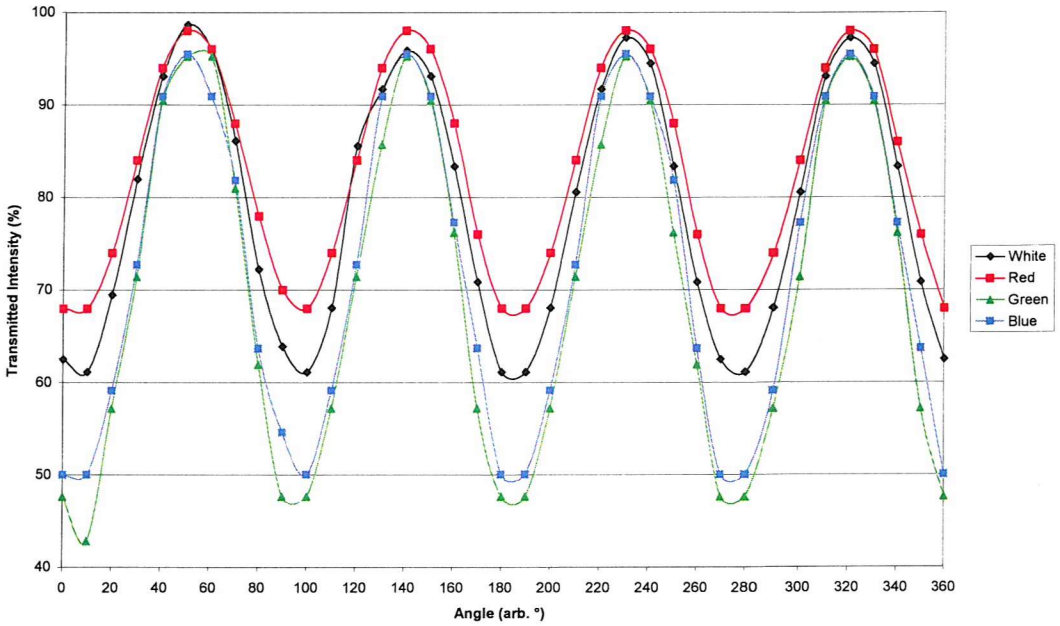

Figure 7.6 Light transmission through a TN cell containing C4 Acrylate positioned between crossed polarisers. Colour filters were used to examine the chromatic effects of the birefringence in the non-waveguiding regime.

However, away from this parallel or perpendicular alignment to the molecular axis, we observe some birefringence effects resulting in a coloured state, as shown in Figure 7.7. This is a result of the linearly polarised incident light experiencing a combination of the two refractive indices; resulting in elliptical polarisation. No waveguiding occurs but light still passes through the crossed polarisers due to it being elliptically polarised.

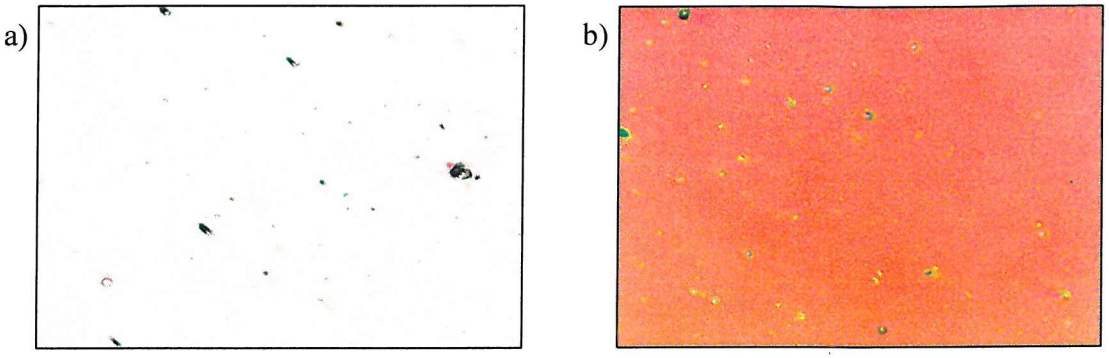

Figure 7.7 The a) white maximum transmission state and b) coloured minimium transmission state of the 'static rotator', as shown in Figure 7.6.

The transmission of the realised device, positioned between crossed polarisers, is shown in Figure 7.8.

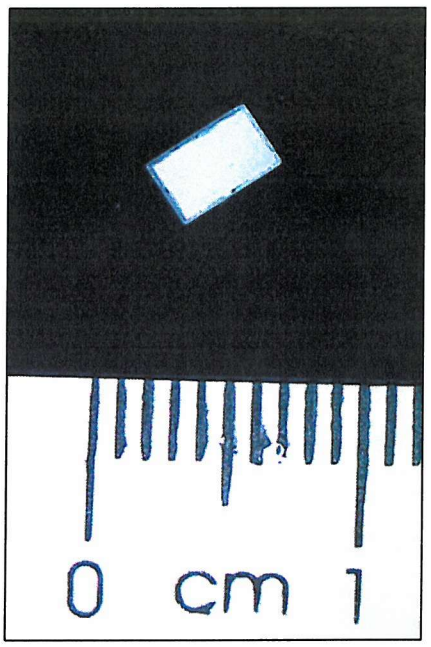

Figure 7.8 The transmission of the realised 'static rotator' positioned between crossed polarisers.

7.3 SYNOPSIS

This section contains an overview of the work presented in this thesis and the important results arising from it. The work undertaken in this thesis has provided an insight into future areas of research and development and these are also discussed.

7.3.1 Chapters 1 & 2 – Introduction & Theory

The first chapter provided the reader with a brief introduction to the liquid crystalline phase. The classification of thermotropic liquid crystals into nematic, chiral nematic and smectic mesophases was described in terms of the order parameter. The motivation for the experimental results presented in later chapters was discussed with respect to the current market for liquid crystal displays and optical devices.

The theory chapter built on the introduction to the liquid crystal phase given in Chapter 1. Landau theory was used to describe first and second order phase transitions. The optical and dielectric properties of liquid crystal materials were then introduced. As a precursor to the work in the following chapters a detailed description of the ferroelectric SmC* and antiferroelectric SmC_A* phases was then given and the flexoelectric effect was described. Finally, the liquid crystal phases described in the preceding sections were discussed in terms of their use in display applications.

7.3.2 Chapter 3 – Experimental Techniques

The basic experimental apparatus and procedures used for the characterisation of the liquid crystalline materials studied in this thesis were introduced. Techniques used for determining the materials phase sequence were discussed. Details of the sample preparation and cell fabrication processes were then outlined. A detailed description of the analytical methods employed in the measurement of spontaneous polarisation, tilt angle and response time was given, with reference to the theories provided in Chapter 2. The design and operation of the 'rotating analyser' technique for measurement of optical tilt angles was also described in detail.

7.3.3 Chapter 4 – Low Molar Mass Organosiloxanes

The compounds studied in this chapter consisted of a laterally substituted halogenic biphenyl benzoate mesogen joined to an organosiloxane core by an eleven length alkyl chain. All the compounds exhibited high, and largely temperature independent, spontaneous polarisation, P_s, and optical tilt angles, θ. Response times of the order of 100μs were readily achievable.

Two series of low molar mass organosiloxane materials were investigated. The mono-mesogenic compounds exhibited the ferroelectric SmC* phase, whilst the phase behaviour of the bi-mesogens was influenced by the length of the siloxane group. The tri- and penta-siloxane bi-mesogenic compounds were antiferroelectric whilst Cl11-4-11Cl was ferroelectric. The antiferroelectric state of the penta-siloxane derivatives is not as stable as the tri-siloxane since less energy is required to change the conformation of the longer siloxane chain.

On cooling from the isotropic phase the mono-mesogens undergo a first order phase transition to the SmC* phase and display ferroelectric properties over a 50°C temperature range. The lack of a less ordered preceding phase makes alignment difficult, although uniform alignment could be obtained by annealing the sample in the presence of an electric field. All mono-mesogenic compounds exhibit P_s of ~100nC/cm^2 with the P_s depending on the concentration and size of the dipoles. Response times of ~50μs are observed and were shown to be inversely proportional to the applied electric field. In contrast, the tilt angles, of ~45°, were shown to be field independent above very small applied electric fields.

All the bimesogenic materials possessed mesophases over a 70°C temperature range. With the exception of Cl11-4-11Cl, the bimesogenic materials exhibited the antiferroelectric behaviour of the SmC_A*. Cl11-4-11Cl displayed ferroelectric behaviour of the SmC* phase. The dependence of the electrical and optical response of the SmC_A* materials to the frequency and magnitude of the applied electric field and sample temperature was examined resulting in the conclusion that the ferroelectric state becomes increasingly

stable as the magnitude and frequency of the applied field is increased. The magnitude of the P_s was larger than that observed in the monomesogens due to the increased dipole concentration.

7.3.3.1 Further Research

The low molar mass organosiloxanes have great potential for use in displays. The tristable switching exhibited by antiferroelectric materials and the threshold field for switching makes large-scale matrix addressing a possibility. Utilisation of the field induced antiferroelectric-to-ferroelectric phase transition allows grey scale AF liquid crystal devices to be realised. The 45° tilt angle results in the maximum contrast being achieved. The high (~45°) tilt angles of the organosiloxanes studied in this chapter allow single polariser dye-guest-host[2] (DGH) displays to be fabricated. The work of de Hondt[3] builds on the research of Shoosmith[4] in this area. However, for such materials to become successful the problems of alignment need to be overcome.

7.3.4 Chapter 5 –Hypertwsited Chiral Nematic Liquid Crystals

The work presented in this chapter examines the flexoelectro-optic effect in eutectic mixtures of a series of achiral nematic bimesogens and small quantities of chiral dopant. The mixtures all possess a room temperature chiral nematic phase and good alignment of the ULH texture can be achieved by combining surface forces and applied AC fields whilst cooling through the isotropic – nematic transition. The temperature dependence of the critical field for unwinding the helix has also been examined.

Investigations into the behaviour of the flexoelectro-optic properties yielded some very promising results. Switching times of the order of 500μs and contrast ratios of 90:1 were readily achieved and, for the first time, a switching angle of 90° is attainable with the flexoelectro-optic effect at room temperature. The constancy of the tilt angle, indicating constant pitch, is particularly useful for fixing the optical contrast as a function of

---

[2] G.H.Heilmeier, L.A.Zanoni, *Appl.Phys.Lett.*, **13**(3), 91 (1968)
[3] P.de Hondt, *Ph.D. Thesis (in preparation)*, University of Southampton, UK
[4] D.E. Shoosmith, *Ph.D. Thesis*, University of Southampton, UK (2001)

temperature as the direction of external polarisers can be optimised and fixed during device fabrication.

Tilt angles of 22.5°, the optimum for birefringence displays, were obtained with moderate applied fields and allow the material to be utilised in double polariser devices. Higher fields yielded tilt angles of 45°, providing optimal contrast ratios for single polariser devices such as dye-guest host displays.

7.3.4.1 Further Research

The work presented in Chapter 5 on a new series of hypertwisted nematic bimesogens opens many avenues of research into the flexoelectro optic effect. The materials presented show great potential for use in commercial applications. Further research into the molecular structure – material property relationship would allow properties such as low dielectric anisotropy, high tilt angle and fast response times to be further enhanced.

The optimisation of the flexoelectric effect requires short and temperature independent helical pitch, large flexoelectric coefficients and small dielectric anisotropy. Enhanced flexoelectric behaviour can be obtained by using symmetric dimer molecules with low molecular dielectric anisotropy. Research into the physical properties of the bimesogens within the liquid crystal group in Southampton has revealed the temperature dependence of the dielectric anisotropy. C.Schott[5] has shown that $\Delta\varepsilon$ is positive at temperatures just below T_{NI} and decreases such that it changes sign at temperatures approximately 15°C below T_{NI}. This temperature dependent behaviour has a number of advantages for the flexoelectric effect. The uniformly lying helix texture can easily be obtained by the application of an electric field whilst cooling the sample from the isotropic phase. Large tilt angles can be measured since $\Delta\varepsilon \approx 0$ at lower temperatures, allowing higher fields to be applied without the helix unwinding.

One current drawback is that the uniform lying helix alignment required to observe the flexoelectro-optic effect requires a shear force and an applied field for it to be stabilised.

The ULH texture is unstable with respect to the Grandjean alignment, in which the helix axis is perpendicular to the alignment surfaces. Research into the stabilisation of the ULH texture by methods such as polymer stabilisation and patterned alignment layers with a view to volume production would enable commercial devices to be developed.

7.3.5 Chapter 6 – Dual Frequency Nematic Liquid Crystals

The motivation for the work presented in this chapter was the benefit that could be gained from employing dual frequency addressing in the operation of TN LCD's, namely, faster response times. The Merck mixture TX2A was used to illustrate this point.

A new dual frequency nematic liquid crystal, 5PFP5, was synthesised in Southampton and a series of mixtures of this and a low viscosity host, MDA, were examined to determine their physical and electro-optic properties. All of the mixtures exhibited a single nematic mesophase that crystallised when a high concentration of 5PFP5 was present. In concentrations of less than 10% wt/wt in MDA, the addition of 5PFP5 did not result in any observable electro-optic switching.

The behaviour of all the properties characterised exhibited a pronounced dependence on the frequency of the applied field. The dispersion frequency showed very strong temperature dependence.

Response time measurements at temperatures close to the nematic-isotropic transition were inconclusive with respect to the advantages of dual frequency addressing although response times of ~5ms were achieved for an applied field of ±2V/μm. Dual frequency addressing was shown to be advantageous at low temperatures, with response times decreasing by a factor of two.

---

[5] C.Schott, *Ph.D. Thesis*, University of Southampton, UK (2002)

7.3.5.1 Further Research

The results presented in Chapter 6 have shown that dual frequency addressing can result in a significant improvement of the response times, particularly at temperatures far below T_{NI}. Further improvement of the response times could be achieved by increasing the dielectric anisotropy via additional fluorination, or by further reduction of the viscosity.

The optical response is complicated by the occurrence of 'optical bounce'. It was demonstrated that the removal of this effect, by the addition of a small quantity of chiral dopant resulted in a faster response. Further studies on mixtures with other chiral additives and on different alignment layers could yield further reductions of the response time.

7.4 CONCLUSION

This thesis has presented the electro-optic properties of a number of liquid crystalline materials with a view to their application in optical devices and displays. The displays market has been driving the research into thermotropic liquid crystal materials for almost 30 years but with the recent advance of optical communications there is great potential for liquid crystal technology to be utilised in many other optical devices such as spatial light modulators, wave plates and waveguides. It is hoped, and envisaged, that materials based on those discussed in this thesis will be employed in such devices in the near future.